



**A University of Sussex DPhil thesis**

Available online via Sussex Research Online:

<http://sro.sussex.ac.uk/>

This thesis is protected by copyright which belongs to the author.

This thesis cannot be reproduced or quoted extensively from without first obtaining permission in writing from the Author

The content must not be changed in any way or sold commercially in any format or medium without the formal permission of the Author

When referring to this work, full bibliographic details including the author, title, awarding institution and date of the thesis must be given

Please visit Sussex Research Online for more information and further details

APPLICATION OF PHOTOACTIVATED  
LOCALISATION MICROSCOPY TO  
VISUALISING EUKARYOTIC DNA  
REPLICATION PROCESSES

By

Thomas James Etheridge

SUBMITTED FOR THE DEGREE OF  
DOCTOR OF PHILOSOPHY

The University of Sussex  
September 2015

## **Declaration**

I hereby declare that this thesis has not been and will not be, submitted in whole or in part to another University for the award of any other degree.

Signature:.....

Date:.....

*“...it’s just a ride.”*

*Bill Hicks*

*This thesis is dedicated to my family and friends.*

## Publications

### Publications related to this thesis:

**Etheridge, T.J.**, Boulineau, R., Herbert, A., Watson, A., Daigaku, Y., Tucker, J., George, S., Jönsson, P., Palayret, M., Lando, D., Laue, E., Osborne, M., Klenerman, D., Lee, S., Carr, A (2014). *Quantification of DNA-associated proteins inside eukaryotic cells using single-molecule localization microscopy*. Nucleic Acids Research. gku726

Daigaku, Y., **Etheridge, T.**, Nakazawa, Y., Watson, A., Miyabe, I., Ogi, T., Osborne, A., and Carr, AM. *PCNA ubiquitylation contributes to unperturbed DNA replication*. (In submission).

### Publications unrelated to this thesis:

Palayret, M., Armes, H., Basu, S., Watson, A., Herbert, A., Lando, D., **Etheridge, T.**, Endesfelder, U., Heilemann, M., Laue, E., Carr, A., Klenerman, D., and Lee, S (2015). *Virtual-'light-sheet' single-molecule localisation microscopy enables quantitative optical sectioning for super-resolution imaging*. PLoS ONE, 10 (4). e0125438. ISSN 1932-6203

Gwang Hyeon Gwon, Youngran Kim, Yaqi Liu, Adam T. Watson, Aera Jo, **Thomas J. Etheridge**, Fenghua Yuan, Yanbin Zhang, YoungChang Kim, Antony M. Carr, and Yunje Cho (2014). *Crystal structure of a Fanconi anemia-associated nuclease homolog bound to 5' flap DNA: basis of interstrand cross-link repair by FAN1*. Genes and Development. 28: 2276-2290

Watson, A.T., Daigaku, Y., Mohebi, S., **Etheridge, T.J.**, Chahwan, C., Murray, J.M., Carr, A.M (2013). *Optimisation of the Schizosaccharomyces pombe urg1 Expression System*. PloS one 8, e83800.

Fontebasso, Y., **Etheridge, T. J.**, Oliver, A. W., Murray, J. M. & Carr, A. M (2013). *The conserved Fanconi anemia nuclease Fan1 and the SUMO E3 ligase Pli1 act in two novel Pso2-independent pathways of DNA interstrand crosslink repair in yeast*. DNA Repair **12** (12), 1011-1023

## Acknowledgements

Taking a risk of sounding a bit of a cliché, this PhD has been a hell of a journey for me. There are many people that have supported me in different ways. Thus, I owe each and every one an acknowledgement for their help in getting me this far.

Firstly, thanks go to the team of people I have worked with over the last 4 years. I would like to thank Tony for trusting me with such an expensive and adventurous project! I could not think of a better boss and mentor to work for and I have enjoyed every minute of working in the lab. Massive thanks also go to the lab guru Adam Watson, who has been there for me every single step of the way. To him I may owe the most, without his god-like patience, support and willingness to teach, I may have not made it. I am also grateful to Jo Murray for her continued support, proofreading and listening to my crazy Smc5/6 ideas.

As this thesis was a cross-disciplinary project, I have relied heavily on those who know what I do not. Massive thanks go to Steve Lee who made the biophysical world seem less scary and almost understandable. Thanks for the support through those initial experiments and tackling SBS, my mathematical incompetence and red room induced insanity. Thanks to 'Magic' Alex Herbert, creator of the mighty PeakFit, for the hours and hours of troubleshooting and patience. One day I will learn how to access the Matrix just like you. Huge thanks also go to Rémi Boulineau for showing me how to use the microscope, helping with development of the methodology and keeping me sane during the many, many hours of imaging. I also received great support and tutoring from Mark Osborne and Mani Maiti, for which I am immensely grateful. I am also very thankful to all of the members of the collaboration between the Carr, Klenerman and Laue labs. Finally, on the science side of things, all of the members of the Carr and Murray labs that I have worked beside over the years, especially Yasukazu Daigaku for the great mentoring and pub nights, Chris Wardlaw for the consistent banter, Kate Doust for the expert thesis proof reading and Sophie George for all the technical support.

Outside of the scientific bubble I have lived in the last 4 years, I have been extremely grateful for the support of my friends. Of greatest importance is Charlotte Knights, thank you for your support and belief in my abilities, I would have never have got this far

without you. Secondly, thanks to Gabby Ferguson for the life coaching and reinforcing a positive mental attitude when I needed it the most. Huge thanks also go to Alex Calder, Alastair White, Hannah Richardson, Rafaella Ferraz Ziegert, Charlotte Fennell, and the Knights family. I am truly sorry for the four years of stress and complaining you have endured, you all handled it very well!

I would like to thank all my family, who never let me stop believing in myself. Mum and Steve, thanks for all the positivity and belief during the tough times. Thanks to Dad and Kelly for reminding me to chill out and always remember the bigger picture. To my grandparents, who have been a constant inspiration in my life, thank you for the continued support in everything I do and the Nature subscription! Sophie, Ben, Thomas, Ian, Valerie, Juliette and Alistair, thanks for the laughs and jokes on my trips home and family holidays.

Finally, thank you to anyone who has ever given me a moment of their time to listen to an idea, a problem or a solution that I may have had.

UNIVERSITY OF SUSSEX

Thomas James Etheridge

A thesis submitted for the degree of Doctor of Philosophy

APPLICATION OF PHOTOACTIVATED LOCALISATION MICROSCOPY TO  
VISUALISING EUKARYOTIC DNA REPLICATION PROCESSES**Summary**

DNA replication is a crucial process that ensures duplication of the genome prior to cellular division. The fidelity of this process is of utmost importance for ensuring genomic stability and the integrity of subsequent generations. Obstruction of the replication machinery by DNA damage, protein barriers or other impediments can cause replication stress, a phenotype often observed in cancer cells. Studying the underlying molecular mechanisms of DNA replication and the repair processes involved during replication arrest is thus critical to ensure a complete understanding of the process and the role it plays in cancer development and progression. A key technique used to study DNA replication and repair proteins is fluorescence microscopy, which allows researchers to visualise the expression and spatial organisation of cellular components. Until recently, the information that could be extracted from fluorescence images was restricted by limited resolution, a consequence of the diffraction of light. Recent advancements in fluorescence microscopy have yielded techniques that can break this diffraction barrier and achieve nanometre scale resolution. One such technique is Photoactivated Localisation Microscopy (PALM), which relies on the detection and high precision localisation of single fluorescent molecules. The work presented in this thesis outlines the development of an adaptation to PALM that can be used to study the chromatin association of proteins inside unfixed cells. This technique was subsequently used to study the role of ubiquitination of the replication-sliding clamp during unperturbed DNA synthesis and characterise the global DNA binding of the Smc5/6 complex during replication stress.

# Table of Contents

Declaration .....	2
Publications .....	5
Acknowledgements .....	6
Summary .....	8
Table of Contents .....	9
Table of Figures .....	15
List of Tables.....	17
List of Abbreviations.....	18
Chapter 1 .....	20
Introduction .....	20
1.1. General introduction and thesis aims.....	20
1.2. DNA replication and cancer development.....	21
1.3. The molecular mechanisms of eukaryotic DNA replication .....	24
1.3.1 Cell cycle progression: entry into S-phase .....	24
1.3.2 Origins of replication.....	26
1.3.3 Origin licensing: forming the Pre-RC .....	27
1.3.4 Origin firing.....	31
1.3.5 DNA synthesis.....	33
1.3.6 Replisome progression complex .....	37
1.3.7 Replication termination .....	38
1.4. Cellular mechanisms to cope with replication stress .....	38
1.4.1 Causes of replication stress .....	38
1.4.2 Replication fork stalling and activation of the intra-S checkpoint .....	40
1.4.3 Intra-S checkpoint response .....	43
1.4.4 The role of PCNA in DNA damage bypass.....	46
1.4.5 Restart and rescue of stalled forks.....	50
1.4.6 Actions of the Smc5/6 complex in maintaining genomic stability .....	53
1.5. Fluorescence microscopy.....	58
1.5.1 Development of fluorescence microscopy .....	58
1.5.2 Basic principles of fluorescence .....	59
1.5.3 Fluorophore properties .....	60

1.5.4	Resolution limits in microscopy .....	63
1.5.5	Extending resolution in fluorescence microscopy.....	66
1.5.6	Single molecule localisation microscopy: PALM and STORM .....	68
1.5.7	Limiting factors of PALM and STORM .....	73
1.5.8	Summary statement .....	75
Chapter 2	.....	77
Materials and Methods	.....	77
2.1.	Growth Media.....	77
2.1.1	Yeast Growth Media .....	77
2.1.2	Bacterial Growth Media .....	79
2.2.	Drugs Used for Genetic Selection .....	79
2.3.	Genotoxic Agents .....	79
2.4.	General Molecular Cloning Techniques .....	80
2.4.1	PCR for amplification of DNA fragments .....	80
2.4.2	Site-directed mutagenesis PCR .....	81
2.4.3	Restriction Digest .....	81
2.4.4	DNA ligation .....	81
2.5.	General <i>E. coli</i> Techniques.....	82
2.5.1	<i>E. coli</i> transformation .....	82
2.5.2	Extraction of Plasmid DNA from <i>E. coli</i> .....	82
2.6.	General <i>S. pombe</i> cell biology techniques.....	83
2.6.1	Crossing of <i>S. pombe</i> strains and random spore analysis.....	83
2.6.2	Tetrad dissection.....	83
2.6.3	<i>S. pombe</i> transformation.....	83
2.6.4	Recombination Mediated Cassette Exchange (RMCE) .....	84
2.6.5	Lactose gradient synchronisation .....	84
2.6.6	Extraction of <i>S. pombe</i> genomic DNA .....	84
2.6.7	Whole cell protein extracts.....	85
2.6.8	Western blot: SDS PAGE and immunostaining.....	85
2.7.	<i>S. pombe</i> strain creation .....	87
2.7.1	Recombination mediated cassette exchange overview .....	87

2.7.2	Creating <i>pcn1</i> gene replacement base strain .....	87
2.7.3	Creating pAW8- <i>mEos3.1-pcn1</i> plasmid.....	88
2.7.4	Creating <i>mEos3.1-pcn1 his3::pcn1<sup>+</sup></i> strain.....	89
2.7.5	Creating C-terminally tagged strains using RMCE.....	89
2.8.	<i>S. pombe</i> sample preparation for single-molecule fluorescence microscopy	91
2.8.1	Formaldehyde fixation of cells for single-molecule microscopy.....	91
2.8.2	Preparation of unfixed cells for single-molecule microscopy.....	91
2.8.3	Slide preparation for single-molecule imaging .....	92
2.9.	PALM Microscopy .....	92
2.9.1	Sample mounting on microscope .....	92
2.9.2	Motion Blur PALM image acquisition.....	93
2.9.3	sptPALM imaging .....	93
2.9.4	Raw image processing for motion blur PALM experiments.....	93
2.9.5	Raw image processing for single particle tracking PALM .....	94
2.9.6	Single particle diffusion simulations and recall analysis .....	95
2.9.7	List of custom microscope components .....	95
2.10.	Human Cell techniques.....	96
2.10.1	Human Cell Culture.....	96
2.10.2	pCCC Chromobody construct creation.....	96
2.10.3	Transfection .....	96
2.10.4	U2OS whole cell protein extraction.....	97
Chapter 3	.....	99
Implementation of Photoactivated Localisation Microscopy for Use in Fission Yeast.	.....	99
3.1.	Introduction.....	99
3.2.	Custom Microscope Design.....	100
3.3.	PeakFit – A single-molecule localisation microscopy image processing program .....	103
3.4.	Assessing custom microscope stability.....	105
3.5.	An optimised fission yeast sample preparation protocol for PALM imaging	107
3.6.	Assessing the impact of cellular autofluorescence on PALM experiments in <i>S. pombe</i> .....	109

3.7. Assessing the effect of 580/14nm emission filter on mEos3.1 detection in <i>S. pombe</i> .....	111
3.8. Summary.....	113
Chapter 4 .....	116
Methodological development for the visualisation of DNA bound proteins in unfixed fission yeast.....	116
4.1. Introduction.....	116
4.2. Effect of cross-linking on PALM experiments focussing on DNA bound proteins.....	118
4.3. Methodological hypothesis .....	120
4.4. Extending camera exposure time enables selective detection of chromatin-associated proteins in unfixed fission yeast .....	122
4.5. Optimisation of camera exposure time via modelling of molecular diffusion 124	
4.6. Application of optimised imaging routine to visualising MCM chromatin association in unfixed cells .....	131
4.7. Quantification of chromatin-associated replication sliding clamp PCNA in differing cell cycle stages and genetic backgrounds .....	133
4.8. Conclusions and Discussion .....	137
Chapter 5 .....	140
Investigating the role of ubiquitylation of the replication sliding clamp during DNA synthesis using photoactivated localisation microscopy.....	140
5.1. Introduction.....	140
5.2. Summary of collaboration .....	141
5.3. Ubiquitylation of PCNA promotes its stable association with DNA.....	145
5.4. Investigating the effect of PCNA ubiquitylation on the DNA-association of the replicative polymerases .....	148
5.4.1 Polymerase $\epsilon$ .....	149
5.4.2 Polymerase $\delta$ .....	151
5.5. Single-particle tracking of polymerases in live fission yeast .....	154
5.5.1 Optimising Pol $\delta$ tracking in live <i>S. pombe</i> .....	155
5.5.2 Comparing dynamics of Pol $\delta$ in G2 and S-phase.....	156

5.5.3	Investigating the effect of <i>rhp18Δ</i> on Pol $\delta$ dynamics .....	159
5.5.4	Limitations of the sptPALM approach in <i>S. pombe</i> .....	161
5.6.	Creation of a stable human cell line for visualising endogenous PCNA via PALM.....	163
5.7.	Discussion and conclusion.....	165
5.7.1	PCNA ubiquitylation prevents PCNA unloading during Okazaki fragment synthesis.....	166
5.7.2	Chromatin association and ubiquitylation status of PCNA effects its interaction with the lagging strand polymerase .....	168
5.7.3	Model: Ubiquitin, a signal for loaded PCNA? .....	170
5.7.4	Species variation.....	173
5.7.5	Conclusion.....	174
Chapter 6	.....	176
Characterisation of factors effecting global chromatin association of the Smc5/6 complex	.....	176
6.1.	Introduction.....	176
6.2.	Smc5/6 chromatin association in an unperturbed cell cycle.....	179
6.3.	Global levels of Smc5/6 chromatin association are unchanged in response to replication fork stalling or DNA damage.....	181
6.4.	Nse1 ubiquitin ligase activity is not required for chromosomal association of Smc5/6 during DNA replication or in response to replication stress.....	182
6.5.	Rad52 chromatin association is increased during unperturbed DNA replication.....	185
6.6.	Discussion and conclusion.....	187
Chapter 7	.....	191
Discussion	.....	191
7	.....	191
7.1.	Overview.....	191
7.2.	Motion Blur PALM .....	191
7.3.	S-phase dependant PCNA ubiquitylation .....	193
7.4.	Smc5/6 chromatin association .....	194
References	.....	196



## Table of Figures

Figure 1-1. Cell cycle fluctuations in CDK-cyclin activity in <i>S. pombe</i> . .....	25
Figure 1-2. Cell cycle regulation of Cdc2 activity in <i>S. pombe</i> . .....	26
Figure 1-3. Initiation of DNA replication at replication origins. ....	30
Figure 1-4. Activation of the intra-S-phase checkpoint. ....	42
Figure 1-5. The <i>S. pombe</i> Smc5/6 complex. ....	54
Figure 1-6. Simplified Jablonski diagram. ....	60
Figure 1-7. Example excitation/emission spectra. ....	61
Figure 1-8. The diffraction limit to resolution. ....	64
Figure 1-9. Single molecule localisation. ....	72
Figure 1-10. Different illumination schemes for single molecule detection. ....	74
Figure 3-1. Schematic representation of custom built PALM microscope. ....	101
Figure 3-2. Preventing axial drift using C-focus system. ....	106
Figure 3-3. Increasing lateral stability of the PALM microscope. ....	107
Figure 3-4. Schematic representation of <i>S. pombe</i> sample preparation for PALM imaging. ....	109
Figure 3-5. Detection and removal of autofluorescent localisations during PALM imaging of fission yeast. ....	110
Figure 3-6. The effect of a 580/14nm band pass on mEos3.1 localisation. ....	113
Figure 4-1. Visualising Mcm4 in fixed cells using PALM. ....	119
Figure 4-2. Selecting for chromatin associated proteins using long exposure times. ...	121
Figure 4-3. PALM imaging with increasing camera exposure times. ....	123
Figure 4-4. Extracting Mcm4-mEos3.1 diffusion coefficient using sptPALM. ....	126
Figure 4-5. Determination of 3D diffusion of Mcm4-mEos3.1. ....	128
Figure 4-6. Simulating Mcm4-mEos3.1 diffusion to optimise camera exposure time. ....	129
Figure 4-7. Fluorophore behaviour dictates optimal camera frame rate choice. ....	131
Figure 4-8. Visualisation of chromatin-associated Mcm4 in unfixed fission yeast. ....	132
Figure 4-9. Creation of <i>S. pombe</i> strains expressing mEos3.1-pcn1. ....	134
Figure 4-10. Visualisation of chromatin associated PCNA using PALM. ....	136
Figure 5-1. Summary of data collected prior to collaboration. ....	143
Figure 5-2. Visualising the influence of PCNA ubiquitination on its DNA-loading status. ....	146

Figure 5-3. Tagging catalytic subunits of the major DNA polymerases for PALM imaging.....	149
Figure 5-4. Visualising the effect of PCNA loading status on Pol $\epsilon$ chromatin association.....	151
Figure 5-5. Measuring the effect of PCNA-loading on Pol $\delta$ chromatin association. ..	153
Figure 5-6. Optimisation of post-acquisition image processing for sptPALM analysis. ....	156
Figure 5-7. sptPALM analysis of Pol $\delta$ in G2 and S-phase cells. ....	158
Figure 5-8. sptPALM analysis of the effect of <i>rhp18<math>\Delta</math></i> on Pol $\delta$ dynamics. ....	160
Figure 5-9. Limitations during application of the sptPALM approach in <i>S. pombe</i> . ...	162
Figure 5-10. Creation of stable human cell line expressing an intracellular nanobody to PCNA.....	165
Figure 5-11. Proposed model for the role of PCNA ubiquitination at the replication fork. ....	171
Figure 6-1. Chromatin association of Smc5/6 is enriched in S-phase. ....	180
Figure 6-2. Smc5/6 chromatin association in response to hydroxyurea and MMS treatment.....	181
Figure 6-3. Mutation of Nse1 ubiquitin ligase domain does not impair chromatin association of Smc5/6. ....	183
Figure 6-4. Smc5/6 chromatin association in response to replication stress is independent of Nse1 ubiquitin liagse activity. ....	185
Figure 6-5. Rad52 chromatin association increases during S-phase.....	187

## List of Tables

Table 2-1- Drugs used for genetic selection .....	79
Table 2-2. Chemicals used as genotoxic agents.....	79
Table 2-3. SDS-PAGE resolving gel recipe.....	86
Table 2-4. SDS-PAGE stacking gel recipe .....	86
Table 2-5. Antibodies used in this thesis. ....	86
Table 2-6. Table of strains used in this study.....	90
Table 2-7. Primers used in the creation of TJE211 .....	91
Table 2-8. Table of specific microscope components used in this study.....	95

## List of Abbreviations

ATP	Adenosine triphosphate
DDR	DNA damage response
DNA	Deoxyribonucleic Acid
dsDNA	Double stranded deoxyribonucleic Acid
HCL	Hydrochloric acid
HR	Homologous recombination
HU	Hydroxyurea
MSD	Mean squared displacement
MMS	Methylmethane sulfonate
PALM	Photoactivated localisation microscopy
PBS	Phosphate buffered saline
SDS	Sodium dodecyl sulfate
SIM	Structured illumination microscopy
ssDNA	Single stranded deoxyribonucleic Acid
STORM	Stochastic optical reconstruction microscopy
STED	Stimulated emission depletion
SUMO	Small Ubiquitin-like modifier
UV	Ultraviolet



# Chapter 1

## Introduction

### 1.1. General introduction and thesis aims

Each living cell possesses a genome that contains hereditary information for the basis of life. This information is stored in the form of deoxyribonucleic acid (DNA) that encodes for the production of all subcellular components required for cell function. Many human diseases, including cancer, are a result of changes to the genomic information, called mutations. Mutations within the DNA code can alter cellular processes by changing the way individual proteins behave within the cell. During each cell cycle, the entire genome must be duplicated in order to transmit this information to successive generations. This process, termed DNA replication, is thus key to ensuring proliferation and survival of daughter cells.

The genome is particularly vulnerable to mutagenesis during DNA replication: either by unfaithful replication of the DNA code or due to the presence of DNA damage, which can prevent progression of replicative enzymes or lead to erroneous repair. Cells have evolved a wide variety of mechanisms designed to ensure that genome stability is maintained, from tight regulation of protein function, to repair of damaged DNA. Studying such processes provides insight into the development of disease, especially if these mechanisms are compromised. Thus, a wide field of research surrounding DNA replication and repair has emerged in recent decades.

Advanced methodologies are necessary to study such intricate and complex mechanisms and fluorescence microscopy is one such technique that has revolutionised the field of molecular cell biology. The use of fluorescent proteins and dyes has allowed researchers to understand protein function by studying their subcellular localisation and dynamics. Extracting such information has been critical in the advancement of our understanding of cellular proliferation and disease development. However, as with all methodologies fluorescence imaging has limitations, most notably the limited resolution of the final

images. Due to the diffraction of light, these techniques have been limited to resolutions of 250-300nm. The spatial organisation and interactions of proteins often occur on much smaller scales and therefore such a limitation can often prevent full understanding the processes being studied. Efforts to improve microscopy resolution brought about the development of adaptations to existing fluorescent techniques, such as confocal microscopy and image deconvolution. These developments ultimately resulted in sharper definition of fluorescence images but have not yielded significant improvements in resolution.

In the last decade, researchers have developed ways to increase image resolution of fluorescence microscopy on orders of 2-10 fold. These techniques have been termed “super-resolution” microscopies, which ultimately break the resolution barrier caused by the diffraction of light. These specialised techniques are starting to become accessible to molecular cell biologists and thus have the potential to facilitate further understanding of biological phenomena and maybe result in new discoveries.

The overarching aim of the work presented in this thesis was to investigate the potential of applying a super-resolution microscopy technique to studying DNA replication processes in the fission yeast *Schizosaccharomyces pombe*. There were three main objectives to achieve during the project. Firstly, it was important to develop an understanding of the methodology, termed photoactivated localisation microscopy (PALM), and how to maintain the custom built equipment required to perform such experiments. Secondly, this project aimed to understand the capabilities of the equipment, and design and establish experimental procedures within the Carr lab that enable the study of the dynamics of DNA replication and repair proteins. Finally, these procedures were applied to existing projects within the lab with the intention of demonstrating how PALM can be used to complement and support results acquired through standard molecular biology techniques.

## **1.2. DNA replication and cancer development**

Cancer is a collection of diseases that occur as a consequence of uncontrolled cellular proliferation. In 2012, cancer was the leading cause of death worldwide and mortality rates have been predicted to rise to 23.6 million cases per year by 2030 (Ferlay *et al* 2013).

Although it is a collection of diseases, which are known to differ in certain aspects, all cancers share certain phenotypes referred to as hallmarks. In 2000, Hanahan and Weinberg described six essential hallmarks of cancer cell physiology, which if acquired would ultimately result in the manifestation of cancerous tumours. The development of cancer is analogous to Darwinian evolution, as positive selection favours each trait that promotes cell proliferation. Research efforts have been focussed on understanding the processes that underlie acquisition of each of these traits, and understanding mechanistically how they promote tumour development.

Cancer is considered a genetic disease, as the underlying mechanisms are a result of genomic mutations that lead to altered gene expression and/or protein function. Although the mutational spectrum of different cancers varies considerably, there are two major classes of genes that contribute to disease progression. The first class, termed oncogenes, are considered to have the potential to cause cancer if activated or highly expressed. These genes usually help to regulate cell growth or differentiation. The second class are known as tumour suppressors. These genes function to tightly regulate cell proliferation to prevent tumour development. Mutations that render the products of these genes non-functional prevent them from suppressing cell growth, which can be a driving factor of carcinogenesis. One of the most well known tumour suppressors is the gene *TP53* that encodes the protein p53. This protein acts to induce cellular senescence and/or apoptosis in response to DNA damage and a recent study highlighted that *TP53* was mutated in 42% of all cancer samples tested (Kandoth 2014).

As the underlying cause to cancer is alterations to genomic information, it is important to understand how these changes arise. As research into cancer development has progressed, the number of hallmarks associated with the disease has increased since they were first described (Hanahan and Weinberg 2011). One of these is genomic instability, which was proposed as an enabling characteristic of tumour development. Genomic instability refers to a state of mutagenesis whereby erroneous DNA replication or DNA damage that is not/incorrectly repaired results in permanent changes to the genetic code. This damage can arise from both endogenous (e.g. reactive oxygen species, ROS) and exogenous (e.g. UV radiation, genotoxic chemicals) sources and poses a threat to cell survival. Thus, cells have evolved a variety of mechanisms designed to maintain genomic stability, either by repairing the damaged DNA or by preventing compromised cells from dividing and

passing erroneous hereditary information to successive generations. Consequently, mutation rates are usually very low during the course of each generation (reviewed in Salk 2010), in spite of approximately  $10^5$  DNA lesions generated per day in each cell (Collins 1999). In response to genomic insult, cells activate specific pathways collectively known as the DNA damage response (DDR), which prevent cell cycle progression and initiate repair procedures. Notably, in pre-cancerous lesions DDR pathways are constitutively active, inducing cellular senescence and apoptosis, thus demonstrating the natural barrier to tumorigenesis (Gorgoulis 2005).

During the progression of cancer, cells often display increased mutagenesis rates, known as a 'mutator phenotype', which further enable chance acquisitions of mutant genotypes (Loeb 2008). Driven by sustained proliferation signals from oncogenes or mutated tumour suppressor genes, cells are forced to replicate their DNA and divide at uncontrolled rates often with reduced replication capacity, and/or in the presence of DNA damage. As previously described, this can be due to loss of p53 function, preventing cells from initiating programmed cell death (Kandoth *et al* 2013, reviewed in Biegging 2014). Studies have shown that over-expression of a variety of oncogenes in normal cells causes cells to enter a senescent state, whereas oncogene overexpression in cells that harbour dysfunctional DNA damage response factors does not (Bartkova 2006, Micco 2006). Consistent with this, inhibition of the DDR in mice injected with a tumour cell line resulted in larger and more invasive tumours (Bartkova 2006).

DNA replication is the stage of the cell cycle where DNA is most vulnerable and further genetic instability is generated by impediments to replication. Obstructions to the replication machinery are known to result in breakage, re-arrangement and under-replicated regions that cause missegregation of chromosomes during mitosis. This phenomenon has been referred to as replication stress, and has been recently proposed as an additional hallmark of cancer and a driving force behind its progression (Macheret and Halazonetis 2015). Central to this proposal is the fact that oncogene expression is a major cause of replication stress, which leads to the further accumulation of DNA damage.

It is clear that replicative stress is thus linked to the promotion of tumorigenesis, especially in the absence of functioning DDR pathways. In fact, many human syndromes that are inherently cancer-prone have been shown to exhibit phenotypes associated with

replicative stress, for example Fanconi anaemia and Werner syndrome (reviewed in Jackson 2013). A detailed understanding of the molecular mechanisms underlying DNA replication, replication stress and its contributions to tumorigenesis is important for future diagnostics and treatment. Thus, I will now discuss the molecular basis of DNA replication and the specific cellular responses that work to protect the fidelity of the genome.

### **1.3. The molecular mechanisms of eukaryotic DNA replication**

#### **1.3.1 Cell cycle progression: entry into S-phase**

Progression through the mitotic cell cycle is tightly regulated to ensure cells accurately replicate their DNA and divide with correctly segregated chromosomes. Transition between different stages of the cell cycle is controlled by two classes of molecules, known as cyclins and cyclin dependent kinases (CDKs). These regulatory proteins are conserved across species; however both fission and budding yeasts possess only one cell cycle CDK, whereas in human cells seven CDKs have been discovered. CDKs regulate cellular processes by phosphorylating specific targets, altering their functionality. As their name suggests, CDKs are only active when complexed with a partner cyclin. The levels of the catalytic subunit stays constant throughout the cell cycle, thus the activity of the kinase is regulated in two ways. Firstly, fluctuations in cyclin levels occur, controlling the formation of the cyclin/kinase complex (Figure 1-1). This is driven by changes in cyclin expression as well as ubiquitin-mediated destruction. CDK activity is also regulated by phosphorylation of regulatory elements in the kinase domain. In *S. pombe*, the cyclin/kinase complex Cdc13-Cdc2 is phosphorylated at Tyr15 on the ATP binding loop of Cdc2 by Wee1 kinase (Gould and Nurse 1989). This phosphorylation keeps CDK inactive, preventing G2-M cell cycle progression. In order to ensure that the cell eventually progresses to mitosis, this inhibitory phosphorylation is counteracted by the activity of Cdc25 phosphatase that removes the Tyr15 phosphate (Figure 1-2) (Russell and Nurse 1986). Cdc25 and Wee1 are themselves regulated in order to ensure they are only active at the appropriate stages of the cell cycle.

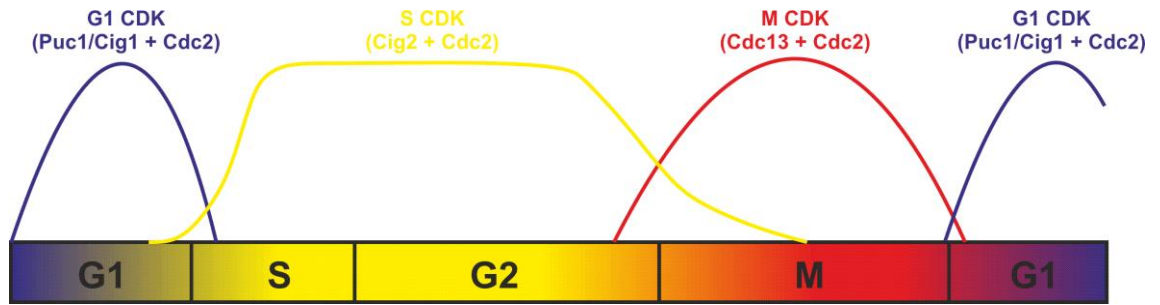


**Figure 1-1. Cell cycle fluctuations in CDK-cyclin activity in *S. pombe*.**

Schematic representation of CDK activity throughout the fission yeast cell cycle. *S. pombe* possess only one catalytic CDK subunit, Cdc2, which is bound by different cyclins throughout the cell cycle. The main two cyclins are Cig2 (yellow) and Cdc13 (red), which when complexed with Cdc2 promote G1-S and G2-M transitions respectively. Cyclins Puc1 and Cig1 play a minor role during G1.

Cells start to prepare for DNA replication during the late stages of mitosis. Replication must be restricted to once per cell cycle and this is achieved by limiting the time in which essential replication licensing complexes can be assembled. Active CDK is inhibitory to replication complex assembly, and thus this process can only occur from late mitosis through G1 where CDK activity is very low. CDKs are kept inactive during this period by the destruction of cyclins by the anaphase promoting complex (APC) and cyclin dependent kinase inhibitors (CKIs) (Diffley 2004). The APC is an E3-ubiquitin ligase that functions to trigger metaphase to anaphase progression by marking various substrates for degradation. S- and M-cyclins are known to be targeted by the APC when bound to its regulatory activator subunit Cdh1 (Sudakin 1995, Schwab 1997, reviewed in Peters 2006). CKI's are small proteins that bind to and inhibit any remaining CDK-cyclin complexes. In *S. pombe*, the CKI Rum1 is known to bind and inhibit Cdc13-Cdc2 (Correa-Bordes and Nurse 1995) (Figure 1-2).

Once the licensing complexes have been established towards the end of G1, cells commit to entry into S-phase by inactivating  $APC^{Cdh1}$  through the activation of G1-CDK. This stage in the yeast cell cycle is known as 'START', coined by Leland Hartwell (1974) as the point in which a budding yeast cell commits to cell division rather than mating. G1-CDKs also target CKIs for degradation by an alternative E3-ubiquitin ligase called SCF (Nash 2001). Inactivation of APC and degradation of CKIs promotes activation of S-phase CDK (S-CDK). S-CDK plays two important roles in initiation of DNA replication. Firstly, it inhibits re-assembly of replication initiation complexes after the G1/S-phase

transition thus preventing re-replication, and secondly it is required for assembly of the replication machinery (discussed in ‘1.3.3 Origin licensing: forming the Pre-RC’).

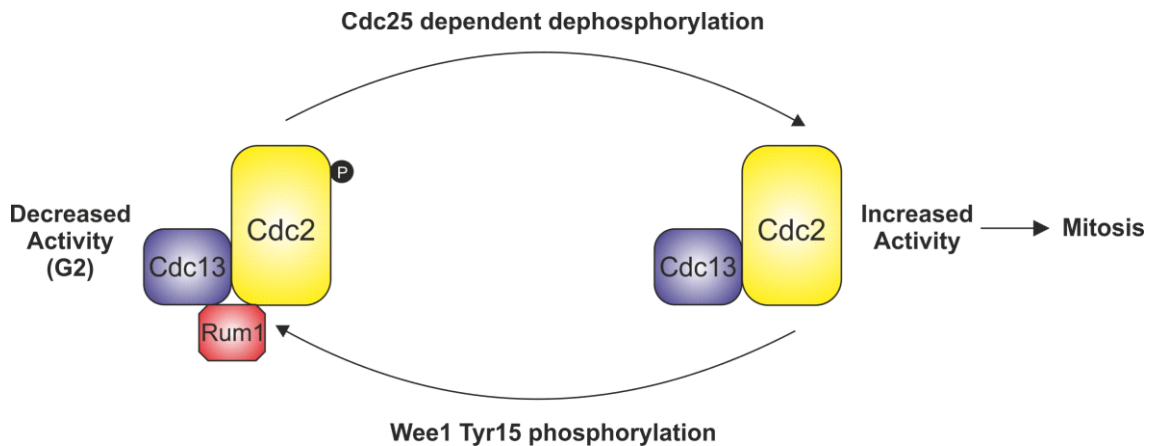


**Figure 1-2. Cell cycle regulation of Cdc2 activity in *S. pombe*.**

Cdc2-Cdc13 activity is restricted during late-S/G2 to prevent premature entry into mitosis. Cdc2 kinase activity is inhibited by Wee1 dependant phosphorylation of Cdc2 on Tyr15 and by binding of Rum1. On the onset of mitosis, Cdc25 phosphatase counteracts Wee1 dependant inhibition of Cdc2 by removing the Tyr15 phosphate, thus restoring its kinase activity.

### 1.3.2 Origins of replication

At the onset of DNA replication, cells recruit the required proteins to a collection of chromosomal locations. This process must be ordered and efficient in order to ensure that each chromosome is replicated entirely before cell division. In 1963, it was hypothesised that the building of replication machinery prior to synthesis must occur at *cis*-acting DNA regions called replication origins (Jacob 1963). Since then, many studies have highlighted the existence of DNA sequences or regions of the genome from which DNA replication is initiated every cell cycle, known as replication origins.

Unlike bacteria, which often possess only one origin of replication, eukaryotic cells assemble replicative complexes at multiple origins within each chromosome. The number of origins per genome is due in part to chromosome size. Whilst bacteria possess one relatively small circular chromosome, higher eukaryotes have multiple linear chromosomes, which are often much larger in size. Possessing multiple origins allows eukaryotic cells to replicate large chromosomes quicker than if only one was present. Origins of replication differ between species; some are sequence specific whereas others lack such definition. In the budding yeast *Saccharomyces cerevisiae*, it has been shown that replication initiates from conserved regions within the genome containing an 11 or 17 base pair consensus sequence (Stinchcomb *et al* 1979, Palzkill and Newlon 1988).

These loci were originally termed “Autonomously Replicating Sequences” (ARS), due to their ability to autonomously stimulate replication of plasmid DNA *in vivo*. Through similar approaches, along with 2-D gel electrophoresis, replication origins were determined within the fission yeast genome (Wohlgenuth *et al* 1994, Dubey *et al* 1994).

It has become apparent that origin definition is not consistent between the two yeasts, as origins within *S. pombe* do not have a consensus motif, but are A-T rich sequences. A lack of sequence specificity is also the case in metazoan cells; however, replication initiation occurs within the same genomic regions in each cell cycle. Early *in vitro* experiments suggested that instead of a specific predictor sequence, origins might be defined by epigenetic marks and DNA topology (Vashee *et al* 2003, Remus *et al* 2004). Recent advancements in genome-wide analyses have indicated that origins in mouse and *Drosophila* cells exhibit a preference for CpG islands and a bias towards transcriptionally active regions (Sequeira-Mendes 2009, Cayrou 2011). This suggests that metazoan origins may differ significantly to those of lower eukaryotes and further experimental evidence is required to elucidate precisely how metazoan origins are defined.

### **1.3.3 Origin licensing: forming the Pre-RC**

Assembly of replication factors at origins is dependent on recognition by an initiator protein that binds and ‘defines’ the position as an origin. In bacteria, this protein was found to be DnaA, a member of the AAA+ ATPase family that binds origin sequences as a monomer before oligomerising to promote strand separation (Messer 2002, Erzberger 2006). In eukaryotic cells origins are first bound by a multi-subunit protein complex called the Origin of Replication Complex (ORC) which consists of 5/6 proteins (ORC 1-6) (Bell and Stillman 1992). Of these six proteins, five are members of the AAA+ ATPase family similar to bacterial DnaA, however Orc1 is the only sub-unit to retain ATPase functionality (Speck 2005). ORC requires ATP to bind to DNA but in contrast to bacterial DnaA, it does not promote DNA melting at origins by itself. Instead, it acts as a recognition platform for the recruitment and loading of the replicative DNA helicase to form what is known as a “Pre-Replicative Complex” (Pre-RC) (Diffley *et al* 1994).

In both bacteria and eukaryotes DNA is unwound during replication by a six-subunit helicase. In eukaryotic cells, this helicase is a heterohexameric complex called the

minichromosome maintenance (MCM) complex, formed from proteins MCM2, 3, 4, 5, 6 and 7 (Mcm2-7). Structural studies of Mcm2-7 via electron microscopy have demonstrated that the sub-units are arranged in a defined order and form a ring-like structure (Davey 2003, Remus 2009). Loading of the MCM complex onto the DNA constitutes origin licensing and defines formation of a pre-RC and thus has been extensively characterised both *in vivo* and *in vitro* (Diffley 2011). Loading of MCM at origins of replication requires two additional components of the pre-RC called Cdc6 (*SpCdc18*) and Cdt1. Cdc6 is an ATPase that recognises and binds the ORC complex at origins of replication. It is essential for DNA replication initiation as it allows for MCM loading and thus pre-RC formation (Cocker *et al* 1996, Donovan 1997). ORC-bound Cdc6 interacts with Cdt1, a protein that directly facilitates the loading of Mcm2-7 (Maiorano *et al* 2000, Nishitani *et al* 2000). Cdt1 was shown to interact with the MCM complex *in vivo* (Tanaka and Diffley 2002) and increase the DNA binding activity of the complex *in vitro* (You and Masai 2008). Loading of the MCM complex in the absence of Cdt1 is prevented by an auto-inhibitory domain in Mcm6 (Fernandez-Cid 2013). In the presence of Cdc6 and Cdt1, Mcm2-7 is loaded onto DNA as a head-to-head double hexamer, wrapped around double stranded DNA (Evrin 2009, Remus 2009). A recent study has demonstrated that loading of Mcm2-7 is achieved by inserting DNA into the hexamer via an entry gate between MCM2 and MCM5 (Samel 2014). Loading of a second MCM hexamer at the site of the OCM complex results in completion of pre-RC formation (Evrin 2013) (Figure 1-3A).

Formation of the pre-RC is known to be dependent on ATP hydrolysis by ORC, Cdc6 and Mcm2-7, however the exact sequence of events is still not entirely understood. Disruption of ORC ATPase (*Orc4-RA* mutant) activity was shown to prevent repeated rounds of MCM loading (Bowers 2004), whereas mutations in the ATP binding domain of Cdc6 (*Cdc6-EG* mutant) leads to a defective protein, which is lethal when overexpressed (Perkins and Diffley 1998). When combined these two mutants abolished ATPase activity *in vitro* (Randell 2006). It was predicted that hydrolysis of ATP by ORC followed by Cdc6 is essential, leading to the release of Cdt1 and the successful formation of a pre-RC intermediate comprised of ORC-Cdc6-MCM (OCM complex) (Fernandez-Cid 2013). However, a recent study found contradictory evidence proposing that these two activities may not be entirely essential for pre-RC formation (Coster 2014). The authors suggest that Cdc6 ATPase is required to release non-productive intermediates and

that MCM ATP binding and hydrolysis are essential for formation of pre-RCs, by stabilising Mcm2-7 and forming the OCM complex respectively.

Origin licensing and pre-RC formation is strictly controlled in order to prevent re-licensing in the same cell cycle. In fission yeast, the levels of *SpCdc6* are regulated by CDK-mediated phosphorylation, which results in its degradation (Baum 1998). Similarly, Cdt1 levels also decline upon entry to S-phase as it is targeted for proteolysis by interacting with DNA-bound PCNA (Guarino 2011). In both cases, expression of *SpCdc6* and Cdt1 is dependent on the G1/S transcription factor Cdc10, which also diminishes in activity on entry to S-phase, helping to reduce levels of the two proteins (Hofman and Beach 1994, Baum 1998). These regulatory mechanisms reduce the amount of functional Cdc6 and Cdt1 and exist in both yeast and metazoans; however, higher eukaryotes possess an extra Cdt1 inhibition mechanism in the form of Geminin. This protein acts as a direct inhibitor of the Cdt1-MCM interaction by binding remaining Cdt1 during S, G2 and M-phase preventing it from loading the helicase outside of G1 (Wohlschlegel 2000, Lee 2004). It is clear that cells have evolved multiple mechanisms to ensure that licensing only occurs once per cell cycle. In fission yeast, Cdc18 (*SpCdc6*) and Cdt1 are essential but over-expression of either will result in pre-RC formation outside of G1 and re-replication of DNA (Falconi 1996, Yanow 2001). Re-replication is considered a form of replication stress and a threat to genomic stability (Gaillard 2015). Consistent with this, abnormal expression of these proteins has been observed in the early stages of epithelial cancers and has been shown to drive tumour development in mice (Liontos 2007).

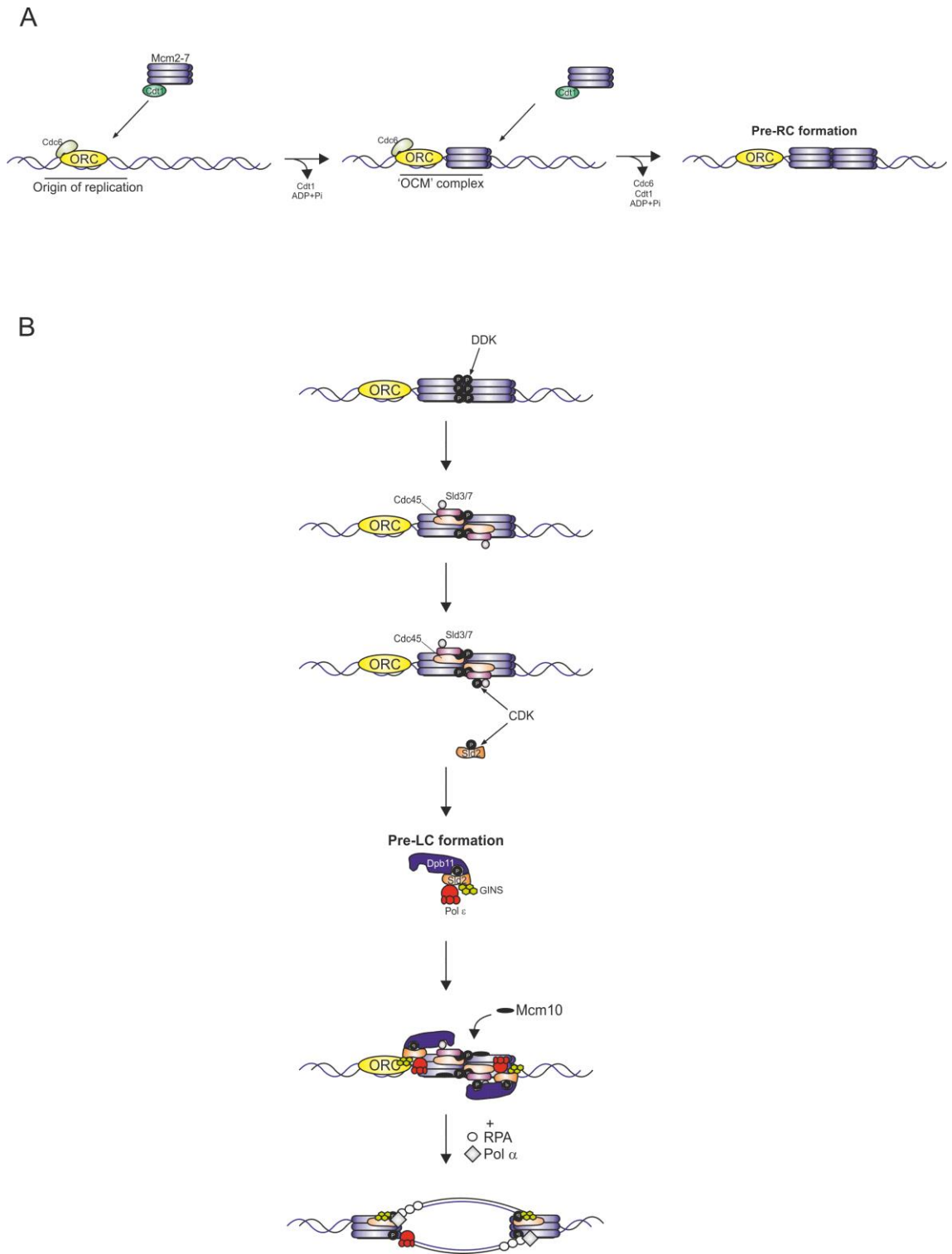


**Figure 1-3. Initiation of DNA replication at replication origins.**

**A)** Schematic representation of Pre-RC formation. Origins of replication are marked by ORC, which together with Cdc6 and Cdt1 recruits the Mcm2-7 helicase. Two MCM helicase complexes are recruited sequentially to origins, resulting in of head-to-head double hexamers, defining the Pre-RC. **B)** Schematic representation of DDK- and CDK-dependent origin firing. DDK phosphorylation promotes binding of Cdc45-Sld3/7. CDK phosphorylation of Sld2 and Sld3 promotes Pre-LC association with origins via the BRCT domain containing Dpb11 (*SpRad4*). Binding of Mcm10 initiates DNA unwinding by the CMG helicase, exposing ssDNA, which is bound by RPA. DNA synthesis is initiated by the binding of polymerase alpha (Pol  $\alpha$ ) that synthesises an RNA:DNA primer. Adapted from Yeeles (2015).

### 1.3.4 Origin firing

Activation of DNA replication in eukaryotes is a two-step process and the loading of the Mcm2-7 subunits at a replication origin does not solely support DNA synthesis. The loaded double hexamers at origins are considered inactive and do not possess any DNA helicase activity this stage. Thus, recruitment of further factors is required to initiate DNA unwinding and promote synthesis. This second step involves formation of the ‘pre-initiation complex’ (pre-IC), which was defined as a complex of proteins that is formed just prior to the initiation of DNA synthesis (Zou and Stillman 1998). The initiation reaction has been widely studied in budding yeast and more recently, the pre-IC was shown to contain at least seven further factors compared to the pre-RC (Muramatsu 2010). Recruitment of these factors and the eventual firing of replication origins has been linked to the activities of two protein kinases: CDK and Dbf4-dependent kinase (DDK). Regulation by these kinases helps to ensure that DNA replication is only initiated at the correct stage of the cell cycle.

The first proteins that associate with the pre-RC at origins are a complex of Cdc45-Sld3-Sld7. Recruitment of Cdc45 is important as it binds to Mcm2-7 along with another protein complex called GINS (Go-Ichi-Ni-San), which together constitute the active form of the replicative helicase known as the CMG complex (Gambus 2006, Moyer 2006). Sld3-Sld7 form a tight complex that loosely associates with Cdc45 (Tanaka 2011a). Whereas Cdc45 and Sld3 are mutually dependent on each other for association with origins, Sld7 is dispensable (Kamimura 2001, Tanaka 2011a). The recruitment of Cdc45-Sld3-Sld7 is considered to be dependant on DDK activity (Tanaka 2011b, Yeeles 2015). DDK possess a catalytic subunit (Cdc7) and a regulatory subunit (Dbf4). The kinase is activated by increased expression at the G1/S boundary and is kept active throughout S-phase (Cheng 1999). The main phosphorylation targets of DDK are believed to be N-terminal domains of MCM proteins loaded at origins. Mcm2, 4 and 6 were shown to possess large unstructured amino termini that are rich in serine and threonine. These non-structured domains (NSD) became heavily phosphorylated when incubated with DDK *in vitro* (Lei 1997, Randell 2010). Further *in vitro* analysis of replication factor recruitment demonstrated DDK activity was required for Cdc45 association with pre-RCs (Heller 2011). The exact mechanism by which DDK phosphorylation of MCM recruits Cdc45 is

unknown. Although structural analysis by cryo-electron microscopy (cryo-EM) has failed to demonstrate gross structural changes in the double hexamer (On 2014), genetic analysis suggests that DDK activity may alleviate auto-inhibitory functions of the NSD of Mcm4 (Sheu and Stillman 2010).

The next step in pre-IC formation is recruitment of the GINS complex in order to form a functional CMG replicative helicase. GINS was first discovered in *Xenopus laevis* egg extracts and later shown to complex with MCM and other replication proteins at replication forks in budding yeast (Kubota *et al* 2003, Gambus *et al* 2006). The association of GINS with pre-RCs containing Cdc45-Sld3-Sld7 is CDK-dependent. At the onset of S-phase, CDK phosphorylates the essential proteins Sld2 and Sld3 (Matsumoto 2002, Tanaka 2007, Zegerman and Diffley 2007). These phosphorylation events have recently been shown to be the minimal requirement of CDK to support replication *in vitro* (Yeeles 2015). Once phosphorylated, Sld2/3 promote the recruitment of the GINS complex via interaction with the BRCT (BRAC1 carboxy-terminal) domain containing protein Dbp11 (*spRad4*, *hTOPBP1*). Phosphorylation of Sld2 stimulates formation of a sub-complex of the pre-IC, termed the pre-loading complex (pre-LC), which is comprised of Sld2, Dpb11, GINS and polymerase  $\epsilon$  (Pol  $\epsilon$ ) (Muramatsu 2010). Once CDK phosphorylates Sld2/3, the pre-LC is bound to the pre-IC, which in turn stabilises the binding of Cdc45 (Yeeles 2015). The recruitment of the pre-IC is mediated by Dbp11, which binds and bridges between Sld3 and Sld2, with two amino- and carboxy-terminal BRCT pairs (Tanaka 2007, Zegerman and Diffley 2007).

Association of the pre-LC with origins almost completes the recruitment of known proteins required to initiate DNA unwinding at origins or replication. In fact, a recent study has shown that only one extra factor, Mcm10, is required in addition to those described above to fire origins and initiate leading strand DNA synthesis with purified *S. cerevisiae* proteins *in vitro* (Yeeles 2015). Mcm10 is a conserved component of eukaryotic replication forks (Gambus 2006) and was recently implicated in initiating unwinding of DNA (van Deursen 2012, Kanke 2012, Watase 2012). Absence of Mcm10 *in vitro* abrogated DNA unwinding by CMG, suggesting it is required for origin firing after formation of the pre-IC (Yeeles 2015). Demonstration of origin firing with purified proteins *in vitro* indicates all the minimal factors required have been identified. In accord, mass spectrometry analysis of proteins recruited from S-phase cell extracts to pre-

assembled pre-RCs yielded no previously unknown components of the reaction (On 2014).

One key mechanism yet to be elucidated, with respect to origin firing, is the remodelling of the Mcm2-7 helicase around ssDNA. As previously mentioned, when the MCM complex is loaded at origins of replication, it encircles the dsDNA. However, evidence from *Xenopus* egg extracts has revealed that the CMG helicase translocates along one of the two DNA strands, suggesting that at some point during pre-IC formation the Mcm2-7 hexamer must be repositioned (Fu 2011). More evidence is required to fully elucidate the exact mechanism behind MCM helicase activation and its subsequent unwinding of origin DNA.

### 1.3.5 DNA synthesis

After origin firing, the CMG helicase unwinds the DNA to create what is termed a 'replication fork'. Two forks are created at each origin due to the loading of two Mcm2-7 hexamers, which travel bi-directionally upon origin firing. As the helicase progresses, ssDNA is produced and must be protected from nuclease degradation, secondary structure formation and re-annealing. This is achieved by coating the ssDNA section with the heterotrimeric replication protein A (RPA) complex, which binds specifically to ssDNA and is recruited to DNA after origin firing (Yeeles 2015). Following ssDNA generation, semi-conservative DNA synthesis is initiated, to create two new daughter molecules. DNA polymerases use ssDNA as a template by incorporating complementary nucleotides opposite the exposed bases. However, DNA polymerases cannot synthesise a new molecule *de novo* and require a 3' terminal hydroxyl group to initiate synthesis, which is provided in the form of an RNA/DNA primer. Thus, all cells have evolved to possess an enzyme called Pol  $\alpha$ /primase, which is recruited to replication forks to initiate DNA synthesis (Kutcha and Stengel 2010). As its name suggests, this protein complex possesses both RNA priming and DNA polymerase activities. The complex initiates DNA synthesis by creating an RNA primer (primase) before switching to DNA polymerase activity and synthesising a short DNA section (Pol  $\alpha$ ). After forming the initiator primer, cells can recruit the major DNA polymerases to continue DNA synthesis. There have been reports that RPA interacts with Pol  $\alpha$ /primase suggesting it may recruit the

primase/polymerase to unwind origins, however DNA synthesis can occur at origins *in vitro* in the absence of RPA (Nasheuer 1992, Yeeles 2015).

The antiparallel nature of DNA and the 3' extension requirements of DNA polymerases determine the way in which the two new strands are synthesised. One strand can be created continuously, since the direction of DNA polymerisation matches that of helicase movement, this is known as the leading strand. In contrast, the other strand must be synthesised in the opposite direction to the helicase movement due to its polarity. Synthesis of this strand can therefore only occur discontinuously, otherwise it will become uncoupled from DNA unwinding. This strand is known as the lagging strand, and its synthesis requires additional specialised enzymatic processing (discussed later). Two main DNA polymerases are known to carry out the bulk of DNA synthesis. Mutational spectra analysis in mutator polymerase genetic backgrounds has led to the demonstration of polymerase strand specificity. Pol  $\epsilon$  was been shown to function as the leading strand polymerase in both budding and fission yeast (Pursell 2007, Miyabe 2011). Whereas the lagging strand is replicated by the other major DNA polymerase, polymerase delta (Pol  $\delta$ ) (McElhinny 2007, Miyabe 2011). Recent data from deep-sequencing experiments agrees with these results, but has highlighted areas in the genome that exhibit a bias for either Pol  $\epsilon$ :Pol  $\epsilon$  or Pol  $\delta$ :Pol  $\delta$  replication (Daigaku 2015).

Upon synthesis of the initiator primer by Pol  $\alpha$ /primase, the major polymerases can be loaded onto the 3' end of the DNA to commence DNA synthesis. However, in all forms of life, replicative polymerases require a ring-like processivity factor known as a replication clamp. In eukaryotic cells, the clamp is called proliferating cell nuclear antigen (PCNA): a homotrimeric ring-like complex with a central cavity that can accommodate dsDNA (Krishna 1994). From crystal structures, it is apparent that PCNA monomers have a positively charged inner surface consisting of  $\alpha$  helices and an outer surface composed of  $\beta$  sheets. Each monomer possesses two globular domains connected by a loop structure termed the interdomain connecting loop (IDL). The main role of PCNA at the replication fork is to act as a platform for polymerases to bind, tethering them to the DNA. *In vitro* evidence has demonstrated that the presence of DNA-loaded PCNA increases polymerase processivity (Langston and O'Donnell 2008, Georgescu 2014). PCNA is loaded around DNA at the 3' end of primer template junctions (PTJs) by a clamp-loading complex known as replication factor C (RFC). RFC is a multi-subunit complex formed of five

proteins RFC1-5, which belong to the AAA+ ATPase family. RFC specifically recognises and binds PTJs, before using DNA-dependent ATPase activity to open the PCNA ring, allowing DNA to enter the central cavity (Gomes and Burgers 2001, Bowman 2004, reviewed in Indiani and O'Donnell 2006). PCNA is loaded onto DNA with its C-terminal face positioned towards the direction of elongation, as this is the side of the protein in which polymerases will bind (Nishida 2009, Moldovan 2007).

The mechanism by which the polymerases achieve strand specificity, whilst both requiring binding to PCNA, is currently an area of interest. Recent work from the O'Donnell lab has shed light on how the two polymerases are recruited to the correct strand at a replication fork. *In vitro* reconstruction of leading strand synthesis, using purified budding yeast CMG helicase and polymerases, highlighted that CMG 'selects' Pol  $\epsilon$  on the leading strand (Georgescu 2014). Pol  $\delta$  proved inefficient and distributive on the leading strand, and Pol  $\epsilon$  was able to take over Pol  $\delta$  leading strand synthesis even when Pol  $\delta$  was eight times more concentrated. Removal of PCNA in this reaction halved the processivity of Pol  $\epsilon$ , but did not completely abolish synthesis, as was the case with Pol  $\delta$ . This is consistent with the notion that Pol  $\epsilon$  is not entirely dependent on PCNA. It was recently shown that Pol  $\epsilon$  is physically linked to the CMG helicase through its Dbp2 subunit and Psf1 of the GINS complex (Sengupta 2013). This suggests that although Pol  $\epsilon$  interacts with PCNA, it is stabilised by the presence of the CMG helicase. When the two polymerases were compared in a model lagging-strand synthesis reaction they both assembled with PCNA, however Pol  $\delta$  synthesis was three times faster and was able to out-compete Pol  $\epsilon$  for PCNA binding (Georgescu 2014). Thus, the replicative polymerases are recruited to the correct strands by differences in affinity to PCNA and the replicative helicase.

Whereas the leading strand is continuously synthesised by Pol  $\epsilon$ , the lagging strand is synthesised in a discontinuous manner by creation of short segments called Okazaki fragments (Sakabe and Okazaki 1966, Okazaki 1968). Each Okazaki fragment is created by extension from a Pol  $\alpha$ /primase primer by the PCNA-Pol  $\delta$  holoenzyme. Due to continuous priming by Pol  $\alpha$ /primase, Pol  $\delta$  recurrently encounters previously synthesised Okazaki fragments downstream. It is important that the RNA section of Okazaki fragments are removed from the DNA and that the fragment are ligated to form a continuous polymer. This process is known as Okazaki fragment maturation, and requires

a specific set of enzymatic activities belonging to two pathways. Firstly, upon collision with a downstream fragment, Pol  $\delta$  displaces the RNA primed section into a 5' flap structure (Maga 2001). The cell must then remove this flap structure in order to complete Okazaki fragment maturation. Flap removal is performed by two enzymatic pathways, known as: short flap and long flap processing (Balakrishnan and Bambara 2011). Short flap processing of Okazaki fragments requires the processing of the displaced DNA/RNA by flap endonuclease 1 (Fen1, *spRad2*). This enzyme recognises the 5' flap and cleaves it at the base, leaving a substrate viable for ligation (Harrington and Leiber 1994, Kao 2002, Gloor 2010). For efficient cleavage of the flap, Fen1 requires interaction with PCNA (Li 1995) probably via interaction with the interdomain connecting loop and its C-terminal face (Jonsson 1998). Research with budding yeast proteins *in vitro* has suggested that the length of short flaps is usually <10 nucleotides (nt) (Ayyagari 2003).

The long flap maturation pathway was proposed from the observation that some fragments are displaced by Pol $\delta$  to lengths exceeding around 25-30nt which are subsequently coated in RPA (Bae 2001). RPA coating of ssDNA flaps inhibited Fen1 cleavage, but was found to stimulate another nuclease, Dna2. These nucleases were shown to work sequentially *in vitro* in processing long flap structures into a ligatable nick (Bae 2001). Further *in vitro* work demonstrated that Fen1 could acquire flap structures before RPA can bind and inhibit cleavage (Rossi and Bambara 2006), this led to a search for a mechanistic explanation for long flap generation. Genetic analysis in budding yeast led to the prediction that the helicase Pif1 (*spPfh1*) is involved in the long flap pathway (Budd 2006). *In vitro* analysis demonstrated that Pif1 could lengthen flap structures at a sufficient rate to promote RPA binding and Fen1 inhibition (Rossi 2008). Further work has predicted that Pif1 plays a role in lengthening flaps in regions that can create secondary hairpin structures (Pike 2010).

After the removal of the displaced flap by either processing pathway, the two adjacent Okazaki fragments need to be ligated in order to form a functional continuous DNA helix. This ligation is performed by DNA ligase I in eukaryotes (*spCdc17*), which seals the nick substrate left after Fen1 cleavage. DNA ligase activity has been shown to be stimulated by the presence of PCNA *in vitro*, thus further highlighting the importance for the sliding clamp during replication, particularly in lagging strand synthesis (Tom 2001).

### 1.3.6 Replisome progression complex

The proteins that act at the replication fork during DNA synthesis are known collectively as the replisome. In addition to Mcm2-7, Cdc45 and GINS a selection of other factors can be isolated when components of the CMG helicase are purified from cell extracts. These factors have been shown to form a salt-stable complex in budding yeast termed the replisome progression complex (RPC) (Gambus 2006). The RPC was shown to contain CMG, Mrc1, Ctf4, Tof1, Csm3, FACT, Topoisomerase 1 and Mcm10. Under low salt conditions, the Pol  $\alpha$ /primase complex was shown to associate with the RPC as well (Gambus 2009).

Recent evidence has led to suggestion that some of the RPC-associated factors provide a physical link between the replicative polymerases and the CMG helicase. Specifically, Ctf4 (*spMcl1*) has been suggested to recruit Pol  $\alpha$  to the chromatin upon origin firing (Zhu 2007), and then to link the primase/polymerase to the CMG helicase by interaction with GINS (Gambus 2009). In an analogous manner on the leading strand, Mrc1 has been shown to associate with both CMG components and Pol  $\epsilon$  during S-phase, leading to a prediction that it links the leading strand polymerase to the CMG (Lou 2008). Although cells in both budding and fission yeast are viable with Ctf4 or Mrc1 deletions, DNA replication is slow and cells often exhibit signs of genomic instability (Alvaro 2005, Szyjka 2005). Furthermore, the combination of Ctf4 and Mrc1 deletions in budding yeast is synthetically lethal due to chronic replication stress (Warren 2004, Gambus 2009).

The other identified RPC components have also been shown to be required for maintaining correct replisome structure and progression. Tof1 and Csm3 (*spSwi1* and *spSwi3*) appear to act together to promote replisome progression, as well as stabilising replication forks at pause sites and activating the replication stress signalling pathways (Noguchi 2003, Noguchi 2004, Tourriere 2005, Calzada 2005). Recent evidence in budding yeast suggests that Tof1/Csm3 specifically acts to prevent replication fork rotation, thus preventing formation of double stranded intertwinings behind the progressing fork. (Schalbetter 2015). Topoisomerase I (Top1) and the FACT complex were also isolated as part of the RPC (Gambus 2006). Top1 is required to remove positive supercoiling tension in the DNA helix as a result of CMG-dependent unwinding (Bermejo 2007, Yeeles 2015) and the FACT complex acts as a histone chaperone required for

nucleosome repositioning during replisome progression (Tan 2006, Han 2010, Abe 2011).

### **1.3.7 Replication termination**

As cells initiate DNA replication at multiple sites across the genome, it is inevitable that two forks will encounter each other head on. This ultimately leads to the termination of replication in that region of the genome, as the sections behind both forks will have been fully replicated. Recent data from the Labib laboratory have elucidated the mechanism by which eukaryotic cells dismantle replisomes from the chromatin (Maric 2014). Using budding yeast cells, the authors demonstrated that a subunit of the CMG helicase, Mcm7, becomes ubiquitinated by the Skp-, Cullin-, F-box complex (SCF) that contains the F-box protein Dia2. This ubiquitylation acts as a signal for the Cdc48 segregase protein, which directly interacts with ubiquitylated CMG and promotes its dissolution. Preventing ubiquitylation of Mcm7 or degradation of the Cdc48 protein *in vivo* lead to retention of CMG complexes on chromatin after S-phase. This informative study highlights that fact that the removal of CMG at regions of replication termination is a regulated process, and that cells may possess further mechanisms of recognising terminated replisomes.

## **1.4. Cellular mechanisms to cope with replication stress**

Replication stress is currently defined as any point during DNA replication in which the cell encounters an obstruction to replication fork progression, by either slowing its speed or causing a complete stall. If the cell fails to deal with such an event, it can have severe consequences for genomic stability as DNA breaks, rearrangements and missegregation of chromosomes can all occur. Thus, the cell has developed mechanisms designed to detect and respond to replication stress, a number of which I will now outline below.

### **1.4.1 Causes of replication stress**

Replication stress can arise from many different sources, since a variety of obstacles can lead to replication fork perturbation. The most commonly studied is the presence of unrepaired DNA lesions, which either arise as a result of environmental or endogenous sources. These lesions can be vastly different in the way they affect the DNA. For example, endogenous reactive oxygen species (ROS) can oxidise DNA bases, whilst

ultraviolet light from the sun can result in pyrimidine dimers and 6-4 photoproducts (reviewed in Ciccia and Elledge 2010). The various different types of DNA lesion can either prevent unwinding of the DNA template by the CMG helicase or result in stalling of the polymerases, both of which prevent replication progression. Another alteration to the DNA helix that can cause replication stress is the misincorporation of ribonucleotides (rNTPs) into the DNA, which if not processed by the cell can stall the replicative polymerases (Nick McElhinny 2010, Lazzaro 2012).

In addition to changes to the chemical structure of DNA, the progression of replication can be obstructed by proteins tightly associated with the DNA. For example, it is inevitable that the replication and transcription machinery may occasionally collide, as they both work from the same template (Helmrich 2013). Such collisions have been shown to create fragility in highly transcribed regions of the mammalian genome, leading to DNA breaks (Barlow 2013). Other protein barriers that can perturb replisome progression include topoisomerase-DNA complexes and natural replication fork barriers in the rDNA (Brewer and Fangman 1988, Hsiang 1989).

Intriguingly, DNA sequences themselves can be challenging for the replisome to progress through. Some sequences are known to form secondary structures and recent research has focussed on structures that form in GC-rich regions of the genome known as G-quadruplexes (Bochman 2012). Replicating through such structures has been shown to require recruitment of additional helicases to the replisome to preserve genomic stability (Paeschke 2013). Regions within the human genome that have enhanced susceptibility to breakage during replication stress are known as common fragile sites (CFS). Whether these regions cause replicative stress or are a readout of replication stress is still under debate, however aberrant replication intermediates arise at CFS and require enzymatic processing in order to preserve genomic integrity (Naim 2013, Ying 2013).

With respect to the development and progression of cancer, oncogene-induced replication stress is emerging as a key source of genetic instability. As discussed earlier, the deregulation of oncogene expression/activity can lead to accelerated cell proliferation. This upregulated cellular division can have several effects on the licensing of origins of replication and their subsequent firing. If cells are driven into S-phase too early via deregulated CDK activity, a common attribute in cancer cells (Asghar 2015), this can

result in initiation of DNA replication with reduced numbers of functional replication origins. Reducing the number of licensed origins in yeast causes increased genomic instability (Tanaka and Diffley 2002) and depleting the amount of Mcm2-7 complexes available for origin licensing in human cells renders them extremely sensitive to genomic insult (Ge 2007). Thus, entering rounds of DNA replication without sufficient number of licensed origins promotes replication stress. The mechanistic cause underlying the subsequent replicative stress is not fully understood, however it is predicted to be as a result of fewer late-firing/dormant origins available to rescue slow/stalled forks.

In contrast, over-use of origins can also result in replication stress. Overexpression of the ordinarily limited firing factors in cells can cause increased origin usage and reduced proliferation (Mantiero 2011, Srinivasan 2013). Excessive origin firing may promote replication stress in two ways. Firstly, firing too many origins could potentially exhaust dNTP levels in the cell causing forks to slow and even stall, much like the situation when cells are exposed to the ribonucleotide reductase inhibitor, hydroxyurea (HU). Secondly, and not mutually exclusive, is the fact that excess origin usage may deplete cellular levels of RPA and due to increased levels of ssDNA being produced by active CMG complexes. Global exhaustion of RPA was recently shown to be a consequence of unscheduled origin firing and was catastrophic for cell survival (Toledo 2013).

#### **1.4.2 Replication fork stalling and activation of the intra-S checkpoint**

A stalled replication fork is defined as a fork that has stopped progressing but is still associated with the major components of the replisome (reviewed in Lambert and Carr 2013). Cells have developed sophisticated mechanisms of sensing perturbed forks, ensuring their stabilisation and delaying cell cycle progression to provide additional time for resolution of the obstruction (Tercero and Diffley 2001). This response is known as the Intra-S checkpoint pathway and is activated by exposure of excess ssDNA and the presence of a primer-template junction (Figure 1-4). When the fork encounters a DNA lesion it causes the helicase and polymerase to become uncoupled, leading to further unwinding of the DNA without synthesis (Byun 2005). Uncoupled progression of the DNA helicase increases the amount of ssDNA exposed at the fork (Sogo 2002). The exposed ssDNA is immediately coated by RPA, and this ssDNA-RPA complex leads in part to sensing of the stalled fork (Zou and Elledge 2003).

Central to the S-phase checkpoint is the phosphatidylinositol 3 kinase-like kinase (PIKK) ATR (Ataxia Telangiectasia and Rad3-related). This signalling kinase is at the top of the checkpoint-signalling cascade, along with its binding partner ATRIP (ATR interacting protein). These two proteins are evolutionarily conserved between humans and yeast (*spRad3<sup>ATR</sup>*, *spRad26<sup>ATRIP</sup>* and *scMec1<sup>ATR</sup>*, *scDdc2<sup>ATRIP</sup>*), and are found in complex with each other (Edwards 1999, Paciotti 2000). ATRIP acts to sense long stretches of RPA-coated ssDNA and recruit ATR to stalled replication forks (Zou and Elledge 2003, Ball 2005). Once ATR is present at a stalled fork, it requires a secondary sensing and signalling mechanism, which is known as the 9-1-1 complex, in order to activate the checkpoint. This complex consists of three proteins Rad9, Hus1 and Rad1 in *S. pombe*. The 9-1-1 complex forms a PCNA-like ring structure that is loaded onto primer-template junctions at stalled forks (Venclovas and Thelen 2000, Dore 2009). Such a structure would form at a stalled fork when one of the polymerases becomes obstructed (MacDougall 2007). The loading of the 9-1-1 complex is achieved in a similar manner to PCNA, as the RFC clamp loader subunits 2-5 are required along with *spRad17* in place of Rfc1. Rad17-RFC detects the primer-template junction and facilitates the loading of 9-1-1 via ATP hydrolysis, whose ring-like structure then encircles the DNA (Bermudez 2003). *In vitro* analyses have suggested that Rad17-RFC prefers to load 9-1-1 at the 5' end of DNA and is directed by RPA (Majka 2006, MacDougall 2007).

Loading of the 9-1-1 complex and recruitment of ATR is sufficient to begin checkpoint activation. ATR possesses basal kinase activity, which in fission yeast was demonstrated to phosphorylate a C-terminal tail on Rad9, an important action for checkpoint activation (Furuya 2004). Similar phosphorylation occurs in human cells albeit via a different kinase (Takeshi 2010). Phosphorylation of Rad9 allows for recruitment of downstream checkpoint mediator proteins that further stimulate ATR activity and lead to activation of the effector kinase. In the case of the DNA damage checkpoint, the BRCT domain containing TopBP1 (*spRad4*) is important for activation of ATR. TopBP1 binds phospho-Rad9 (Furuya 2004, Delacroix 2007, Puddu 2008) and promotes ATR activation via an ATR-activation domain (Kumagi 2006, Lin 2012, reviewed in Wardlaw 2014). However, with regards to the replication checkpoint the role of Rad4<sup>TOPBP1</sup> is still unclear. Recent evidence in budding yeast has suggested that ATR (*scMec1*) becomes fully activated in response to replication stress by interaction with the nuclease/helicase Dna2 (Kumar and

Burgers 2013). As described earlier, Dna2 is associated with the replication fork during elongation, as it required for maturation of Okazaki fragments in the long-flap pathway. Further evidence is required to establish whether Dna2 is a key player in full-ATR activation in fission yeast and mammalian systems.

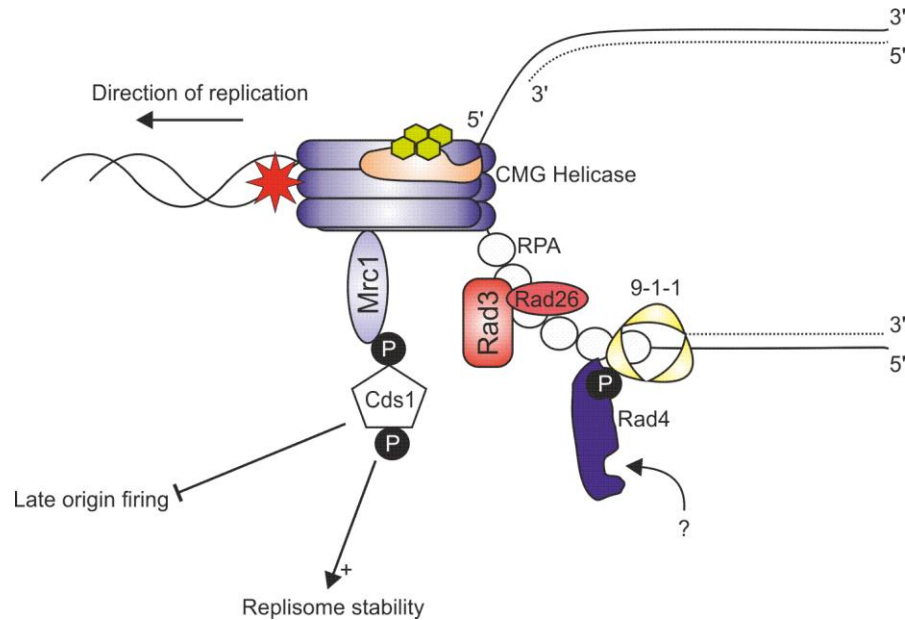


**Figure 1-4. Activation of the intra-S-phase checkpoint.**

Replication forks can stall upon nucleotide depletion or encountering a DNA lesion/tightly bound protein, replication. Exposure of long ssDNA bound by RPA and primer template junctions can lead to checkpoint signalling and activation. Rad3<sup>ATR</sup> is recruited to RPA by Rad26<sup>ATRIP</sup> and the 9-1-1 complex is loaded at exposed ssDNA-dsDNA junctions. Rad3-dependent Rad9 phosphorylation recruits Rad4. Rad3 also phosphorylates Mrc1, which acts as a mediator protein to recruit the effector kinase Cds1. Rad3 phosphorylation of Cds1 leads to Cds1 autophosphorylation and activation. The effector kinase then acts locally to ensure replisome stability and globally to inhibit late origin firing. Adapted from Carr (2002)

Once the ATR kinase is fully activated, it serves to ensure activation of an effector kinase specific to the intra-S checkpoint. In fission yeast, this kinase is known as Cds1 (Lindsay 1998) (*hCHK2*, *scRad53*). Cds1 is recruited to stalled forks in the yeasts via interaction with the mediator protein Mrc1 (*hClaspin*), an action that is dependent on ATR phosphorylation of Mrc1 (Zhao 2003, Xu 2006). Cds1 binds to phosphorylated Mrc1 via a forkhead-associated (FHA) domain, after which Cds1 is phosphorylated on Threonine 11 (T11) by Rad3<sup>ATR</sup>. This priming phosphorylation event of Cds1 promotes FHA-dependent dimerization with another primed Cds1 molecule, before trans-autophosphorylation between the two monomers on T328 results in full activation of their kinase domains (Xu 2006, Yue 2011). The activated checkpoint effector kinase can then proceed to phosphorylate downstream targets required to inhibit new origin firing,

regulate replication fork progression, arrest cell cycle progression and stabilise the stalled replisome.

### 1.4.3 Intra-S checkpoint response

Once activated the intra-S checkpoint serves to guarantee genomic stability by ensuring stalled replication forks are correctly processed and the cell does not initiate mitosis with unreplicated regions of DNA. This response includes a reduction in the rate of DNA synthesis and the stabilisation of stalled replication forks. The outcomes of replication checkpoint activation can be divided into two types of response: local and global.

Local responses of checkpoint activation refer to the actions taken at a single stalled replication fork. The activities of both ATR and the effector kinase are suggested to revolve around stabilisation of the replisome, preventing the occurrence of pathological structures at stalled forks and slowing the rate of DNA synthesis. Early work in *S. cerevisiae* showed that the homologue of Cds1, Rad53, is important for replication fork progression after HU arrest since cells defective for the checkpoint kinase accumulated abnormal DNA structures (Lopes 2001). Importantly, these abnormal structures were similar to those observed in strains harbouring defective replication proteins. This accumulation of irregular structures was thus predicted to be due to replication fork 'collapse', suggesting that Rad53 acts to stabilise the replisome at stalled replication forks to prevent such an occurrence. Since this study, research has intensified around elucidating the mechanisms by which the checkpoint promotes stabilisation of stalled forks.

Chromatin immunoprecipitation (ChIP) experiments in *S. cerevisiae* suggested that in the absence of Rad53, replisome components dissociate from the fork (Cobb 2003, Luca 2004). Checkpoint mutants in *S. pombe* have also demonstrated increased levels of fork breakage and DNA repair foci formation during HU arrest (Noguchi 2003, Meister 2005). This led to the proposal that the checkpoint prevents fork collapse specifically by stabilising the replisome machinery on the DNA (reviewed in Branzei and Foiani 2010). In agreement with this hypothesis, replisome associated components have been identified as Cds1/Rad53 substrates in the two model species of yeast. For example, in *S. pombe* Dna2 is phosphorylated by Cds1 in response to HU treatment, maintaining its association

with the replisome and preventing formation of reversed fork structures (Hu 2012). In contrasting outcomes both the endonuclease Mus81 and the recombination protein Rad60 are phosphorylated by Cds1, promoting their exclusion from the nucleus (Boddy 2000, Miyabe 2009). In budding yeast, Rad53 has been implicated in stabilising replication forks by preventing Exo1-dependent nuclease activity (Cotta-Ramusino 2005, Segurado and Diffley 2008).

Phosphorylation of replisome components by ATR has been reported in higher eukaryotes. Mcm2 was shown to be a substrate of ATR in response to replication fork stalling in both human cells and frog extracts (Cortez 2004, Yoo 2004). The role of MCM phosphorylation by ATR is not fully understood, but a recent study implicated phosphorylated MCM proteins in the recruitment of FANCD2 to the CMG helicase, where it acts to 'slow' replication progression (Lossaint 2013). Without FANCD2 human fibroblast cells accumulated replication-associated DNA lesions. These findings all suggest that, in the absence of the checkpoint kinases stalled replication forks are destabilised, leading to eventual collapse of the replisome and subsequent DNA damage due to unregulated DNA processing.

Although evidence exists of direct checkpoint regulation at the fork, recent studies have suggested that the stability of the replisome at stalled forks is independent of the S-phase checkpoint kinases. Specifically, the Labib laboratory demonstrated that isolated chromatin-associated replisomes did not change in composition or frequency with or without checkpoint kinase activity in response to fork stalling (De Piccoli 2012). Strand-specific analysis of DNA-bound PCNA has also suggested the checkpoint in fact promotes its unloading rather than its stabilisation (Yu 2014). In light of these data, it has recently been proposed that a collapsed replication fork should be defined as one that has lost the capability to continue DNA synthesis, which may or may not be due to loss of replisome components (Cortez 2015). Thus, the overall direct mechanism of checkpoint kinase action on replisome function and the progression of replication forks remains to be fully elucidated.

The checkpoint has also been shown to carry out a global response to stalled replication forks, which appears to modulate the kinetics of DNA synthesis by inhibition of late origin firing. This ensures that the replication process slows as a whole in the presence of

replicative stress, extending S-phase and thus allowing for time to cope with stalled forks. Deletion of Cds1 in HU treated cells is known to alter replication timing and the pattern of replication foci (Kim and Huberman 2001, Meister 2007). Observations in budding yeast show that the Mec1/Rad53 checkpoint prevents replication intermediates occurring at late firing origins during replication stress (Santocanale and Diffley 1998, Lopes 2001). In vertebrates, ATR signalling has also been shown to regulate origin firing in response to replication stress (Feijoo 2001). This may occur through the activation of Chk1 by ATR in response to stalled forks, leading to Cdc25A phosphatase degradation (Mailand 2000). Cdc25A is known to promote dephosphorylation and activation of Cdk2-Cyclin E, which is required for Cdc45 loading at origins (Falck 2002). This mechanism however may not be conserved in fission yeast as the S-phase checkpoint has been shown to be independent of Cdc25 (Kommajosyula and Rhind 2006). Importantly, preventing the regulation of late origin firing in checkpoint deficient fission yeast leads to continued DNA synthesis, creating eventual DNA damage and inability to complete bulk replication (Sabatinos 2012). Likewise, depletion of ATR in human cells leads to replication catastrophe via depletion of RPA levels by unregulated origin firing (Toledo 2013). Thus, global control over the progression of DNA replication is important in response to replicative stress.

Intriguingly, evidence exists to suggest that checkpoint kinases may also regulate origin firing even in the absence of replicative stress. In *Xenopus* egg extracts treated with ATM/ATR inhibitors, replication and the bulk of DNA synthesis occurs faster than normal (Shecter 2004). Fission yeast cells lacking Cds1 show distinct differences in replication foci patterns during normal S-phase when compared to wild type cells (Meister 2007). These results suggest that the checkpoint kinases can act locally during normal replication without initiating a global response, raising an interesting question in the field about the level of intra-S checkpoint signalling required to promote global checkpoint activation. Is there a need to inhibit distant origins if one fork stalls? It may be best to allow origin firing to ensure that the stalled fork could be rescued if it cannot restart. Previously it has been proposed that a threshold must be reached before Rad53 activation is achieved in *S. cerevisiae* (Shimada 2002). More evidence is required to understand the precise effects that different types of replication stress can have on a progressing fork and how the checkpoint kinases operate to protect genomic stability.

#### 1.4.4 The role of PCNA in DNA damage bypass

The exact events that occur at a replication fork upon collision with damaged DNA are not entirely understood. The type of lesion a fork encounters and which strand the damage is on can have substantially different effects on the outcome. Genotoxic agents such as UV light and alkylating agents can induce bulky DNA lesions, which directly block polymerase activity. Cells have developed ways of repairing such lesions before entering S-phase, however some damage will persist during replication. Thus, in order to ensure the completion of bulk synthesis in the presence of such DNA damage the cell possesses a specialised set of components that allow the replication fork to bypass DNA damage (Daigaku 2012). The replication sliding clamp, PCNA is central to the bypass mechanism, and its modification by ubiquitylation directs two major mechanisms that allow cells to tolerate damage in S-phase: translesion synthesis (TLS) and template switching (Moldovan 2007).

Early genetic work in budding yeast led to the identification of an epistatic group of genes, which if mutated conferred sensitivity to UV light. Collectively they are known as the *RAD6* epistasis group and functional analysis has revealed the group consists of two branches; an error-prone pathway consisting of damage tolerant polymerases (reviewed in Lehmann 2007) and a set of ubiquitylation enzymes (reviewed in Ulrich 2009). Two genes were identified as being central to both pathways, *RAD6* and *RAD18*. Rad6 was identified as an E2 ubiquitin-conjugating enzyme that was shown to complex with the E3 Rad18 protein and demonstrated to have ubiquitin ligase activity *in vitro* (Jentsch 1987, Bailly 1994, Bailly 1997). In a similar fashion, Ubc13 and Mms2 (also part of the *RAD6* group) demonstrated E2 conjugating activities as a heterodimer, interacting with the E3 Rad5 (Ulrich and Jentsch 2000). The major target of both of these ubiquitin-conjugating complexes is PCNA, which is ubiquitinated on a highly conserved lysine residue, K164 (Hoege 2002). In response to DNA damage, Rad6- and Rad18-dependent mono-ubiquitylation of PCNA occurs. This mono-ubiquitylation can be extended through lysine 63 (K63) linkage of ubiquitin by Ubc13/Mms2/Rad5. Mutation of PCNA K164 to arginine prevents ubiquitylation and renders yeast and mammalian cells sensitive to DNA damage, thus further linking this modification to DNA damage tolerance (Hoege 2002, Arakawa 2006, Frampton 2006).

PCNA ubiquitylation occurs in all characterised eukaryotic systems and appears to arise as a result of replication fork stalling. Treatment of cells with a variety of genotoxic agents known to inhibit fork progression induces PCNA ubiquitylation, including hydroxyurea, which stalls all forks simultaneously upon nucleotide depletion (Kannouche 2004, Frampton 2006, Davies 2008). As discussed earlier, obstructing polymerase progression can lead to uncoupling with the helicase and generation of ssDNA. Rad18 is known to bind ssDNA *in vitro* (Bailly 1997) and it was predicted from experiments with *Xenopus* egg extracts that ssDNA was required for PCNA ubiquitylation (Chang 2006). In agreement with this hypothesis Rad18-dependent mono-ubiquitylation of PCNA in budding yeast and humans is dependent on RPA-coated ssDNA (Davies 2008, Niimi 2008). Although production of ssDNA is known to elicit a checkpoint response, the ATR-signalling pathway is not required for PCNA ubiquitylation, and *vice versa* suggesting they are two independent responses (Frampton 2006, Chang 2006, Davies 2008). However, one study has highlighted a potential role for Claspin (*spMrc1*) in potentiating PCNA ubiquitylation, which is dependent on Chk1 but not ATR (Yang 2008). Intriguingly, PCNA ubiquitylation has also been detected during unperturbed DNA synthesis in *S. pombe* and *Xenopus* egg extracts (Leach 2005, Frampton 2006), the reason for which has only recently been investigated (see Chapter 5).

The role of PCNA post-translational modification in DNA damage bypass has been studied with great interest. In 2004, two groups highlighted that ubiquitylated PCNA plays a role in the error-prone damage tolerance pathway by guiding specialised polymerases to the site of damage (Kannouche 2004, Watanabe 2004). These polymerases are known as translesion (TLS) polymerases as they possess the ability to incorporate nucleotides opposite damaged bases, thus allowing for the progression of the replication fork. There is a variety of recognised TLS polymerases in eukaryotes, all with different biological roles (reviewed in Waters 2009). The majority of eukaryotic TLS polymerases belong to the Y-family of polymerases: Rev1, Pol $\eta$ , Pol $\kappa$  and Pol $\iota$ . One B-family polymerase, Pol $\zeta$ , is also a recognised TLS polymerase. The current model of how TLS polymerases are recruited to sites of DNA damage and replicate past damage is explained in a ‘two polymerase model’. In this model, one polymerase is required for insertion of nucleotides opposite damaged bases, and another is used to extend from the lesion-nucleotide pairing (Johnson 2000, Shachar 2009). The Rev1 TLS polymerase, whose catalytic activity is dispensable for mutagenesis has been implicated in act to

bridging two such TLS polymerases (Otsuka 2005, Acharya 2006). This model excludes Pol $\eta$ , which is known to solely bypass thymine dimers (Masutani 2000).

Evidence suggests that mono-ubiquitylation of PCNA increases its affinity for Y-family polymerases (Kannouche 2004, Watanabe 2004, Bi 2006), which is ultimately due to their ubiquitin binding domains (Bienko 2005). However, during DNA synthesis the replicative polymerase must be displaced when it stalls, to allow TLS polymerases access to the damaged base. This is known as polymerases switching and the exact underlying mechanism is not fully understood. *In vitro* studies have shown that the presence of mono-ubiquitinated form of PCNA does not negatively affect the processivity of the replicative polymerases, suggesting that the ubiquitin moiety itself does not displace the polymerase (Haracska 2006, Masuda 2010, Dieckman and Washington 2013). It has been suggested recently that replicative polymerase behaviour at the fork is ‘distributive’, i.e. regular disengagement from the DNA occurs during synthesis (Georgescu 2014, reviewed in Georgescu 2015). This disengagement may provide TLS polymerase access to PCNA and the damaged bases. There is some debate in the field as to the timing of TLS relative to the passage of the replication fork. Early models suggested that damage was bypassed ‘on the fly’, i.e. TLS polymerases were recruited to stalled replicative polymerases at the front of the fork. However, such damage tolerance mechanisms have been demonstrated to work independently of the bulk of DNA replication, holding true to its original definition of ‘post-replication repair’ and suggesting that it may operate behind the fork at post-replicative gaps (Daigaku 2010, Karras 2010). Evidence from chicken DT40 cell lines suggests that TLS may occur both ‘on the fly’ and post-replicatively, a balance that may ultimately be determined by the presence of Rev1 (Edmunds 2008).

The alternative *RAD6* DNA damage bypass mechanism relies on the *UBC13*, *MMS2* and *RAD5* genes as part of an error-free damage tolerance pathway (Johnson 1992, Brusky 2000, Torres-Ramos 2002). Hoeye *et al.* (2002) showed that these three genes were required for the poly-ubiquitylation of PCNA, thus linking the multi-ubiquitin species of PCNA to the error-free pathway of DNA damage bypass. The model for poly-ubiquitylation of the sliding clamp suggests that the E2 Mms2-Ubc13 complex is recruited to mono-ubiquitinated PCNA via a Rad5-Ubc13 interaction, which requires the RING finger domain of Rad5. (Ulrich and Jentsch 2000, Hoeye 2002). Rad5 interacts directly with Rad18 at the site of damage, bringing Mms2-Ubc13 into contact with

PCNA. Poly-ubiquitylation of PCNA is suggested to be a cellular signal to initiate the error-free bypass of DNA lesions, however very little is understood about how this occurs.

The underlying mechanism of the error-free pathway was shown to require recombination proteins belonging to the *RAD52* epistasis group (Zhang and Lawrence 2005). This group of genes is required for efficient homologous recombination (HR) and was shown to be required for repair of UV induced DNA damage (Lopes 2006, Gangavarapu 2007). In 1976, Higgins *et al.* proposed a model for replication repair that predicted the use of template switching as a mechanism for bypassing DNA lesions in the template strand. Exposing cells to MMS enabled visualisation of ‘four-pronged’/X-shaped DNA structures in electron microscopy experiments, suggestive of either fork reversal or strand invasion events (Higgins 1976). More recently, the absence of Rad18 and Mms2 was shown to reduce the amount of X-shaped recombination intermediates detected in response to MMS treatment, suggesting that poly-ubiquitylation of PCNA promotes strand exchange in response to fork stalling (Branzei 2008).

The exact mechanism in which the template-switching event occurs in the error-free pathway is not yet fully understood, and neither is the relative contribution of TLS or template-switching tolerance pathways in response to DNA damage. There are two potential factors that may be important when considering which mechanism the cell will use. Firstly, the type of DNA lesion is a contributing factor. For example, bypass of a UV-induced cyclobutane pyrimidine dimer (CPD) can be achieved efficiently and accurately by Pol $\eta$ , whereas a 6,4 T-T photoproduct is estimated to have only a 3% chance of being bypassed by TLS (Gibbs 2005). Thus, in this case it could be predicted that the error-free pathway would be critical for damage tolerance. Secondly, the timing of bypass initiation and the positioning of damage on specific strands could contribute to the choice of mechanism.

There has been debate over the different effects that DNA lesions can have on each of the two template strands. There is a consensus that stalling of the lagging strand polymerase will not affect replication fork progression as much as stalling of the leading strand polymerase, as the discontinuous nature provides a means of re-priming downstream of the damage (reviewed in Yeeles 2013). Re-priming downstream of the damage would result in ssDNA gaps which could be filled in behind the fork and as previously mentioned

damage tolerance mechanisms can operate independently of bulk DNA replication (Daigaku 2010, Karras 2010). In electron microscopy studies, ssDNA regions have been observed in the vicinity of replication forks on both the leading and lagging strands. This suggests that replication fork progression can continue via re-priming on both strands (Lopes 2006), although no evidence of re-priming on the leading strand has been demonstrated. Recently, the structural nature of the template-switching event has been studied by electron microscopy. Results from this study have suggested that template switching is initiated by the presence of ssDNA gaps behind the fork, providing more evidence for leading strand re-priming (Giannattasio 2014).

#### **1.4.5 Restart and rescue of stalled forks**

The DNA damage bypass pathway described above aims to ensure that replication fork progression is not attenuated by the presence of a damaged template. There are however, a wide range of replication fork barriers (RFBs) that threaten fork progression and cannot be overcome by such mechanisms (Lambert and Carr 2013). Thus, it is inevitable that a subset of replication forks will stall during DNA synthesis, and hence require stabilisation through the intra-S checkpoint as previously described. After checkpoint activation, the cell must either resume replication using the stalled fork, or 'rescue' that region of the genome from being left unreplicated if the fork cannot be restarted.

The resumption of replication forks ultimately depends on the stability of the associated replisome, and whether or not the exposed DNA strands are intact. Checkpoint-stabilised forks are predicted to resume synthesis without intervention from other mechanisms: as can be visualised with DNA fibre analysis after cells are released from a HU block (Tourriere 2005, Petermann 2010). Further evidence of replication resumption after fork stalling has been demonstrated at the single loci level in both bacteria and budding yeast, using natural sequence specific fork stalling proteins (Calzada 2005, Possoz 2006). In both cases, replication fork resumption was independent of recombination proteins or DNA breaks. If a stalled replication fork cannot resume, and thus requires additional factors to restart DNA synthesis, it is said to have 'collapsed' (Lambert and Carr 2013). As previously mentioned the fate of the replisome in this situation is still debated, however there is substantial evidence for the formation of DNA structures at the fork in response to fork collapse (Weinert 2009). Electron microscopy and 2-D gel

electrophoresis have allowed for the study of the formation of these structures, and apart from the template switching mechanism described earlier, they appear to result from either fork regression or homologous recombination.

Replication fork regression was originally proposed as a template switching mechanism for error-free DNA damage bypass (Higgins 1976). Although this has not been entirely ruled out, EM analysis suggests that bypass may initiate behind the fork (Giannattasio 2014). Instead, early analysis of replication intermediates in checkpoint-deficient yeast cells suggested that fork regression could be a pathological consequence of failure to stabilise the replisome (Sogo 2002). The role of the intra-S checkpoint in preventing the formation of such structures was reinforced by demonstration that *S. pombe* Cds1 promotes the chromatin association of Dna2 in response to HU, and disrupting this regulation dramatically increases the formation of regressed forks (Hu 2012). Thus, for the last decade fork reversal has been viewed as a form of genetic instability caused by replisome disassociation and fork collapse. However, recent evidence in human cells has led to the hypothesis that regressed forks may be a dynamic cellular response to various types of replication stress (Zellweger 2015, reviewed in Neelsen and Lopes 2015). Zellweger *et al.* demonstrated that, in response to different chemotherapeutic agents at sub-lethal doses, reversed replication forks could be detected at significantly high levels. This phenotype was modulated by poly-ADP ribose polymerase (PARP) and RECQ1 helicase. Interestingly the authors also demonstrated that the reversal of replication forks was strictly dependent on the recombination protein RAD51, which is loaded at forks in response to replication stress (Zellweger 2015). In a parallel study, Thangavel *et al.* showed that an alternative pathway of reversed fork processing exists which is dependent on DNA2 and the WRN helicase, which act to resect the nascent DNA strands to facilitate fork restart (Thangavel 2015). Thus, regression of DNA replication forks could act as a cellular mechanism to promote genomic stability and fork resumption.

The role of recombination proteins in the restart of collapsed replication forks has been predicted from early work in bacterial systems. In *E. coli* restart of the replication forks requires origin-independent reloading of the DnaB helicase at D-loops formed by HR machinery (reviewed in Michel 2007). The recent development of site-specific stalling systems in yeast and human cells has allowed for the study of similar mechanisms in eukaryotes (Lambert 2005, Willis 2014). As of yet, the exact role of the HR machinery

in restarting replication forks in eukaryotic systems remains to be elucidated. However two leading hypotheses exist and depend on the presence or absence of a DSB at the fork. The formation of a one-ended DSB at the fork can theoretically arise via single-strand gaps in template strand or via nucleolytic cleavage of ssDNA region at stalled forks. Studies have suggested that in such cases replication can be restarted via HR-mediated strand invasion of the sister chromatid and recruitment of replisome components (Davis and Symington 2004, Lydeard 2010, Hashimoto 2011). This mechanism is referred to as break-induced replication (BIR).

As prolonged replication stress results in the formation of DSBs, many studies have focused on restart in their presence. However, evidence from human cells suggests that the HR component RAD51 plays two temporally-separated roles in stalled fork restart, depending on the length of time over which replication stress occurs (Petermann 2010). Cells that were subjected to short periods of replication stress restart forks in a RAD51-dependent DSB-independent manner. In fission yeast, analysis of fork restart at a site-specific fork barrier system also demonstrated restart in the absence of DSB formation (Mizuno 2009, Lambert 2010). In this system, restart of a single replication fork at the polar *RTS1* fork barrier is dependent on homologous recombination proteins and cell viability is diminished in their absence (Lambert 2005). Considering the role highlighted for RAD51 in reversal of replication forks (Zellweger 2015), and its requirement for the restart of forks stalled following short periods of replication stress (Petermann 2010), in the absence of DSBs it is possible that Rad51 possess 'fork protection' capabilities, as well as functioning in HR-dependent restart (Carr and Lambert 2013).

This prediction is supported by evidence that RAD51 nucleofilament stability is critical for protecting stalled forks from degradation. RAD51 is known to be loaded onto RPA-bound ssDNA, a process stimulated by the BRCA2 protein (Liu 2010, Jensen 2010). Evidence from the Jasin group demonstrated that BRCA2 is required to prevent nucleolytic degradation of DNA at stalled replication forks, which was attributed to the MRE11 nuclease (Schlacher 2011). Further work from this group highlighted a role for the Fanconi Anaemia (FA) pathway proteins in protecting stalled replication forks from degradation in a repair-independent manner (Schlacher 2012). These studies suggest that stalled forks are stabilised by coating ssDNA with RAD51 and then protecting these nucleofilaments from degradation by 'protection' proteins that consist of BRCA2 and the

FA complex. Recent evidence has uncovered a novel factor of this protection complex, BOD1L, which was shown to be required to stabilise RAD51 on chromatin downstream of BRCA2 activity by preventing the anti-recombinogenic functions of the BLM and FBH1 helicases (Higgs 2015).

Regardless of the precise manner by which HR components promote the restart of replication forks, be it through BIR or DSB-independent mechanisms, evidence suggests that HR-directed synthesis is error prone. In the *RTS1* fork barrier system, restarting collapsed replication forks in the presence of local template homology can result in gross chromosomal rearrangements (Lambert 2005). Further investigation led to the demonstration that recombination-restarted replication forks can cause chromosome fusions at inverted repeat sequences, and are liable to undergo replication slippage at regions of micro-homology (Iraqi 2012, Mizuno 2013). These observations led to the prediction that HR-restarted forks are unstable and intrinsically error-prone. This hypothesis could be explained by the fact that the canonical replication machinery during HR-mediated restart is not present. This has been shown to be the case during BIR as studies in *S. cerevisiae* demonstrated that polymerases  $\alpha$  and  $\delta$  perform a substantial proportion of the initial synthesis, and this requires a Pol  $\delta$  accessory subunit that is dispensable during normal bulk synthesis (Lydeard 2007). More recently, it has been shown that BIR in budding yeast consists of a bubble-like replication fork driven by Pol  $\delta$  and Pif1 (*spPfh1*) helicase (Wilson 2013, Saini 2013).

It is evident from the wealth of data collected that HR proteins play a role at replication forks, by either stabilising stalled forks or restarting collapsed forks. The way in which HR proteins, especially Rad51, are recruited to perturbed replication forks and how their activities directed is now of great interest. As well as the aforementioned BRAC2, FA complex and BOD1L, evidence from the yeasts suggests that the Smc5/6 complex may also be involved in directing HR activities at perturbed replication forks.

#### **1.4.6 Actions of the Smc5/6 complex in maintaining genomic stability**

Structural Maintenance of Chromosomes (SMC) complexes are found in all domains of life and regulate higher order chromosome structure during different cell cycle stages or cellular processes. In eukaryotes, each complex is built around two heterologous SMC

subunits that have extensive coiled coil (~50nm) regions separating a globular head domain and a hinge domain. The subunits associate at the hinge domain and are bridged at the globular heads by accessory subunits, forming a ring like structure (Figure 1-5, reviewed in Murray and Carr 2008). The three major SMC complexes in eukaryotes are cohesin, condensin and Smc5/6. Cohesin and condensin act to maintain sister chromatid cohesion and compact chromatin in mitosis, respectively. The role of the Smc5/6 complex is yet to be fully elucidated but has been linked to both DNA replication and repair events.

The Smc5/6 complex was originally identified in *S. pombe* by genetic complementation of a DNA damage sensitive mutant, *rad18-X* (now referred to as *smc6-X*) (Lehmann 1995). In this study, *smc6* was shown to work in the same DNA repair pathway in response to gamma or UV irradiation as *rhp51*, encoding the recombination protein Rad51(*spRhp51*). Smc5 and Smc6 form the main structural arms of the complex, similar to Smc1/3 and Smc2/4 of cohesin and condensin. Associated with Smc5/6 are six non-SMC element (Nse) subunits, Nse1-6. Of these, Nse1-4 are essential, whereas Nse5-6 are only essential in budding yeast, not in *S. pombe* (Figure 1-5).

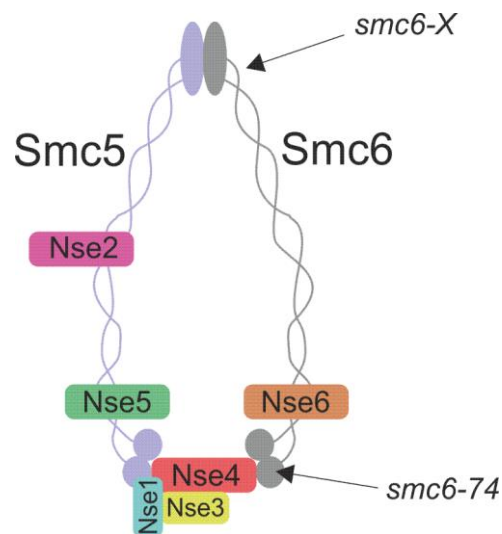


**Figure 1-5. The *S. pombe* Smc5/6 complex.**

Diagram of the Smc5/6 complex and the positions of the *smc6-X* and *smc6-74* mutations

Research into the functional role of the Smc5/6 complex has been mainly focussed on DNA repair due to the damage sensitivity of isolated hypomorphic mutants. However, the essential requirement for the complex in unperturbed cycling cells remains ambiguous. Genetic studies have clearly defined Smc5/6 as operational in HR following DNA damage; hypomorphic mutants demonstrate unrepaired chromosomes in response

to radiation and fail to separate their chromosomes during mitosis after replication perturbation (Verkade 1999, Perbernard 2006, Lindroos 2006). Deletion of HR components, such as Rad51, rescues HU sensitivity of Smc5/6 mutants, suggesting that defective HR is lethal in these backgrounds (Ampatzidou 2006). Although loss of HR capabilities is not lethal, deletion of Smc5/6 is and the essential requirement for Smc5/6 and its subunits is not alleviated by concomitant loss of both Smc5/6 and HR in budding yeast (Cost and Cozzarelli 2006). Thus, the essential role of Smc5/6 does not appear to be due to defective HR processes during DNA replication. Further understanding of the specific functioning of each of the subunits of the complex will be required to fully understand the role it plays in both replication and repair.

The Nse1, 3 and 4 subunits are known to form a sub-complex that acts to link the heads of the Smc proteins (Palecek 2006). Nse1 possesses a RING finger-like motif that was predicted to mediate ubiquitin ligase activity (McDonald 2003), but so far reports are mixed as to whether the holocomplex exhibits such activity (Perbernard 2008a, Doyle 2010). However, mutation or deletion of the domain renders cells sensitive to DNA damage and is important for the stability of the Nse1-3-4 sub-complex (Perbernard 2008a). Intriguingly, mutation of cysteine 216 to serine in Nse1 RING finger domain in fission yeast was able to rescue hypomorphic *smc6* alleles in response to DNA damage (Tapia-Alveal and O'Connell 2011). This was suggested to be due to mis-localisation of the Smc5/6 complex in the C216S mutant background, thus preventing aberrant HR processing by the complex.

The Nse2 subunit also displays a variant RING finger motif that has been demonstrated to possess SUMO ligase activity (Andrews 2005). In budding yeast, Mms21 (*S.p*Nse2), interacts with Smc5 independently of any other Nse subunits by binding to a region of the coiled-coil arm (Duan 2009a). This interaction along with ATP binding by Smc5 activates Nse2 SUMO ligase activity (Bermudez-Lopez 2015). This activity is not required for normal cell growth, but becomes critical in response to DNA damage in S-phase (Andrews 2005). The role of the SUMO-ligase activity of Nse2 is not fully understood, however when exposed to MMS fission yeast cells SUMOylate Nse4 in a Nse2-dependent manner, promoting sub-telomeric localisation (Pebernard 2008b). This suggests Nse2 has a role in recruitment, ensuring the localisation of Smc5/6 to damaged telomeres.

The remaining Nse subunits, Nse5 and Nse6, are HEAT repeat proteins which form a heterodimeric complex that facilitates DNA repair as part of the Smc5/6 complex. They were first discovered in *S. cerevisiae* (Hazbun 2003) and were later shown to bind to Smc5 and Smc6 specifically at the hinge region (Duan 2009b). Nse5 and Nse6 have also been identified in *S. pombe* but show little sequence homology. Unlike in *S. cerevisiae*, the sub-complex is not essential in fission yeast (Perbernard 2006). However, deletion of either components renders fission yeast cells sensitive to DNA damaging agents (Perbernard 2006). Genetic analysis suggests that the heterodimer is required for efficient HR as both *nse5* $\Delta$  and *nse6* $\Delta$  mutants are dependent on Mus81 endonuclease and Rqh1 DNA helicase for proliferation, two proteins known to process HR intermediates (Perbernard 2006). Concordantly, Nse6 is required for efficient chromosome disjunction during meiosis by driving resolution of joint molecules (Wehrkamp-Richter 2012). Functional orthologues of Nse5 have recently been discovered in human and *Xenopus* cells. The two proteins, Smc5/6 localisation factors 1 and 2 (SFL1/2), are involved in recruitment of Smc5/6 to DNA damage. In this study, the authors demonstrate that SFL1/2, along with RAD18, are responsible for the chromatin association of the Smc5/6 complex in response to DNA damage (Raschle 2015). Nse5-6 has been demonstrated to be required for recruitment of Smc5/6 to stalled forks in budding yeast (Bustard 2012) and Rtt107, which contains similar BRCT repeat motifs to SFL1, is required to recruit Smc5/6 to DSBs in budding yeast (Leung 2011). Thus, functional similarities in Smc5/6 recruitment between yeast and higher eukaryotes exist but require further study.

With a view to elucidating Smc5/6 function, many studies have focussed on its positioning on the chromatin during S-phase and in response to DNA damage. CHIP-based studies from the Sjogren lab performed in budding yeast have shown that Smc5/6 associates with telomeric regions and is deposited on chromatin during S-phase (Lindroos 2006). The chromatin association of the complex and its positioning within the genome was in part dependent on cohesin and its loader *ScScc2*, as well as being recruited to double strand breaks and increasing in frequency on longer chromosomes (Lindroos 2006). Increased Smc5/6 association with longer chromosomes was predicted to be due to replication-induced sister chromatid intertwines (SCIs), which led them to conclude that the cell requires Smc5/6 to sequester SCIs (Kegel 2011). More recently, high-

resolution chip data from this lab have reinforced the prediction that Smc5/6 chromatin association is dependent on cohesin and SCIs (Jeppsson 2014). Smc5/6 association is perturbed in cohesin mutants, which the authors suggest is due to lack of sister chromatid cohesion. Consistent with this prediction inactivation of Topoisomerase II, which is known to resolve SCIs, increased the level of Smc5/6 binding to chromosome arms, and this required passage through S-phase and cohesin (Jeppsson 2014). Mechanistic evidence to support a role for Smc5/6 at SCIs and a demonstration that a similar requirement for Smc5/6 at long chromosomes in higher eukaryotes is required to establish this theory.

The requirement for Smc5/6 in response to replication stress has been studied in fission yeast using two mutants, *smc6-X* and *smc6-74*. *smc6-X* (R706C) mutation maps close to the hinge region where Smc5 and Smc6 interact. *smc6-74* (A151T) mutation maps to the ATP binding site in the N-terminal globular domain (Figure 1-5). Both mutants are sensitive to HU arrest of replication forks and are defective in the repair of collapsed forks in *cds1Δ* cells (Ampatzidou 2006). The accumulation of recombination intermediates in *cds1Δ smc6-X/74* double mutants is consistent with a similar role at damaged replication forks in budding yeast (Branzei 2008). Further investigation with these two mutants has suggested an additional early role for the complex in response to replication fork stalling. ChIP analysis of the recombination mediator protein Rad52 in wild type and the *smc6* mutants highlighted that cells harbouring the *smc6-74* mutation are defective in the loading of Rad52 onto chromatin in response to dNTP depletion (Irmisch 2009). This defect was manifested most strongly at loci situated in the rDNA, a known hotspot for recombination in the absence of Smc5/6 (Irmisch 2009, Torres-Rosell 2007). This defect in Rad52 loading is a consequence of reduced RPA loading in *smc6-74* mutants, suggesting that Smc5/6 plays a role in maintaining stalled fork conformation that allows proficient restart and is recombination-competent (Irmisch 2009).

As with most aspects of the Smc5/6 complex, the exact role at stalled and collapsed forks is still not understood. Mechanistic studies of the activities of individual subunits, and the holocomplex are needed. The answers may lie in biochemical reconstitution of the process using purified proteins. A recent study used purified Smc5/6 from budding yeast to show that the complex regulates fork regression ability of the Mph1 (*spFml1*) helicase by Smc5-dependent inhibition of Mph1 oligomer formation at DNA junctions (Xue

2014). This regulation had been previously predicted from genetic and 2D gel electrophoresis and can now be mechanistically explained (Chen 2009, Chavez 2011). The prevention of Mph1-dependent fork reversal is intriguing in light of the recent data from human cells suggesting that fork regression is a cellular response that guards genome integrity (Neelsen and Lopes 2015). Regulating the activities of the plethora of DNA helicases at stalled/collapsed forks seems to be crucial, thus Smc5/6 may play a role in orchestrating such processes.

## **1.5. Fluorescence microscopy**

The aim of the work presented in this thesis was to establish a single-molecule super-resolution microscopy methodology in the Carr lab for studying DNA replication processes. In this section of the introduction, I will introduce the basics of fluorescence and fluorescence based microscopy, as well as the concept of diffraction-limited resolution. I aim to briefly describe a variety of methods that have been developed to increase resolution of fluorescence microscopy images before concluding this introduction by focussing on the development of single-molecule super-resolution techniques, PALM and STORM.

### **1.5.1 Development of fluorescence microscopy**

The advent of fluorescence microscopy revolutionised the molecular cell biology field and in combination with biochemical and genetic approaches has helped to further our understanding of cellular functioning. The first fluorescence microscopes were originally designed to observe cellular autofluorescence emitted from bacterial and eukaryotic cells (Heimstadt 1911, Lehmann 1913). However, further developments in microscope construction allowed for efficient separation of incident light and sample fluorescence leading to the use of fluorescent dyes for labelling biological samples.

The use of fluorescence based microscopes in molecular cell biology gained momentum with the development of fluorescently labelled antibodies and the discovery of fluorescent proteins. Albert Coons and colleagues demonstrated that coupling fluorescent molecules such as fluorescein to antibodies, allowed for the detection of specific antigens in cells

(Coons 1942). This work ultimately gave rise to the era of immunofluorescence, a technique which molecular cell biologists still rely on heavily today (Coons 1961). A discovery of similar importance was that of the extraction and cloning of Green Fluorescent Protein (GFP) from the jellyfish *Aequorea victoria*. GFP was first isolated from *A. victoria* by Osamu Shimomura in 1962, before being used as a marker for gene expression in *E. coli* and *C. elegans* by the Martin Chalfie in 1994 (Shimomura 1962, Chalfie 1994). Since this discovery and application, the wild type form of GFP has been heavily modified by mutagenesis to create variant forms with more desirable properties. Most important was the single point mutation S65T reported by Roger Tsien and colleagues in 1995 which increased the fluorescence and photostability of the protein (Heim 1995). Together, these developments won Shimomura, Chalfie and Tsien the Nobel Prize in Chemistry in 2008. A range of fluorescent proteins (FP) now exists, derived from original GFP or other fluorescent proteins that have been discovered since.

The use of either immunofluorescence or fluorescent proteins depends on the type of experiment being performed, as each have their strengths and weaknesses. Immunofluorescence allows the targeted detection of specific proteins without the need for genetic manipulation, thus is a popular method for use in higher eukaryotic model organisms. However, immunofluorescence is mainly limited to fixed samples as the labelling procedures are often very perturbative. The use of fluorescent proteins allows researchers to visualise protein expression and localisation without the need for such intrusive procedures, by expressing the protein of interest fused directly to an FP. This also removes any off target effects that can arise from non-specific binding of antibodies. Importantly, endogenously expressed FPs also allow biologists to perform live cell experiments whereby protein expression and localisation can be monitored over time.

### **1.5.2 Basic principles of fluorescence**

The phenomenon of non-incandescent production of light is known as photoluminescence, which describes the emission of light from matter after the absorption of photons. Photoluminescence is usually divided into two categories: fluorescence and phosphorescence. Fluorescence is the ability of some molecules, known as fluorophores, to absorb light energy of a particular wavelength and subsequently emit light of a longer wavelength. The process of absorption and radiative emission of a fluorophore can be

described in a simplified Jablonski diagram (Figure 1-6). Upon absorption of a photon, electrons of the fluorophore are excited from a ground state ( $S_0$ ) to an excited state ( $S_1$ ). The molecule exists in the excited state in the order of nanoseconds before relaxing back down to the ground state. Relaxation resulting in spontaneous emission of a photon is known as fluorescence. Electrons in the excited state may also undergo intersystem crossing into a triplet state ( $T_1$ ), before relaxing back down to the ground state resulting in delayed fluorescence, relative to  $S_1 - S_0$  relaxation. Non-radiative relaxation pathways also exist but will not be discussed for simplicity.

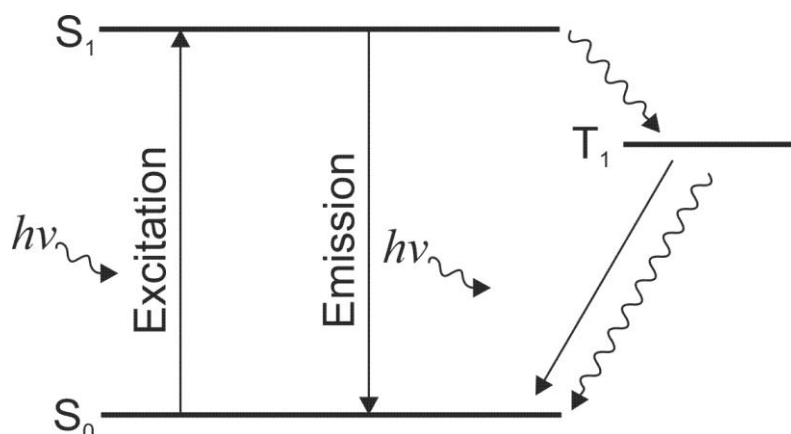


**Figure 1-6. Simplified Jablonski diagram.**

$S_0$  represents the ground state,  $S_1$  the excited state and  $T_1$  the triplet state. Excitation of electrons from  $S_0$  to  $S_1$  occurs by absorption of a photon ( $h\nu$ ). Relaxation back to the ground state releases energy usually by a photon of less energy than that which was absorbed, i.e. fluorescence. Non-radiative transitions can occur (wavy line) from  $S_1$  to the triplet state causing delayed fluorescence. Relaxation from  $T_1$  to the ground state can either occur via fluorescence or can be quenched by oxygen or reactive thiols.

### 1.5.3 Fluorophore properties

There now exists a wide range of molecules that can be used in fluorescence microscopy experiments. The two main classes are organic dyes and fluorescent proteins. Organic dye molecules are typically much brighter than fluorescent proteins, emitting  $10^5$ - $10^6$  photons per molecule and thus provide more fluorescent signal. However, these molecules need to be delivered to the target of interest, and are thus usually coupled to antibodies in immunofluorescence assays. Fluorescent proteins, such as GFP, provide a means of directly labelling a protein of interest via genetic manipulation. Insertion of the GFP DNA coding sequence downstream of an open reading frame results in production of a fusion protein, a process referred to as 'tagging'. Functionality of this protein must be assessed to ensure it confers no deleterious phenotype. Fluorescent proteins usually possess an 11-stranded beta-barrel tertiary structure that houses the fluorophore (known

as a chromophore) which is formed from amino acid residues. In fact, alignment of 202 different fluorescent protein structures highlighted the extreme similarity in structure and chromophore formation (Dedecker 2013). When considering which fluorescent markers to use in an experiment there are a few standard properties should be considered.

Firstly, the wavelengths at which a fluorophore absorbs and subsequently emits photons are important when considering what fluorescent markers to use in an experiment, as they must match the filter sets installed in the microscope. Furthermore, when performing dual colour experiments, fluorophores must be spectrally distinct in order to be able to identify them individually. The excitation and emission of fluorescent molecules can be measured and displayed by an excitation/emission spectrum (Figure 1-7). The peak absorption and emission wavelengths of a fluorophore differ, as the emission wavelength is longer, i.e. it is shifted towards the red end of the visible spectrum. This is due to energy losses via pathways other than fluorescence during relaxation of excited electrons, and is known as Stokes shift.

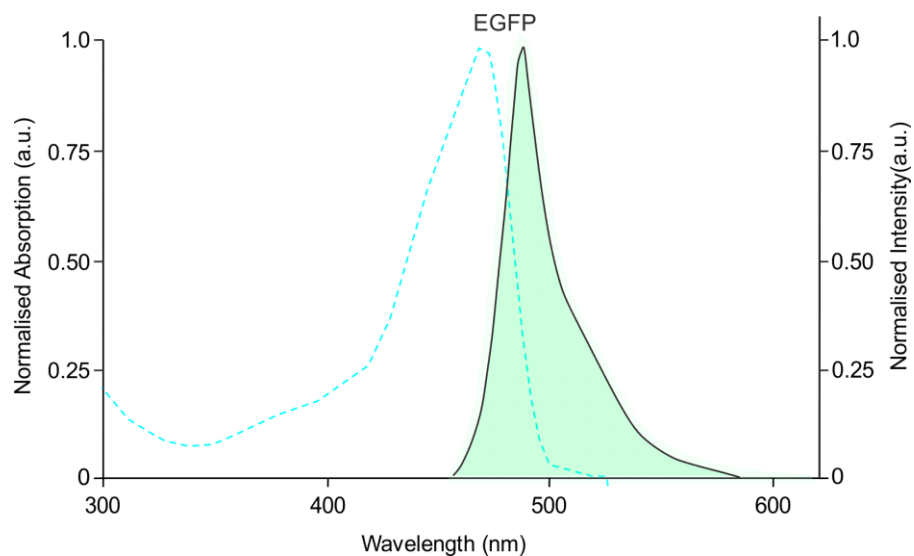


**Figure 1-7. Example excitation/emission spectra.**

Excitation and emission spectra for enhanced GFP. The dotted line represents the probability of absorption of a photon of a certain wavelength, black solid line represents the spectrum of photon emission from the fluorophore. Data taken from ThermoFisher SepctraViewer.

The ability to detect fluorescent emission of molecules above background is dependent on the brightness of a fluorophore, and is thus an important criterion in most fluorescent microscopy experiments. A fluorophores brightness is a measure of the number of

photons that it can release in a given time, a rate that depends on the excitation and emission efficiencies. These efficiencies can vary depending on the environment in which a fluorophore resides as factors such as temperature and pH can affect the overall performance. The amount of photons released from single fluorophores is an important factor in single molecule localisation microscopies, as will be described later.

The number of photons released from a fluorophore, and thus its brightness, will be dependent on its resistance to photobleaching. Photobleaching is the phenomenon by which a fluorophore permanently loses its ability to fluoresce upon excitation. It occurs when the excited fluorophore reacts with oxygen to create a covalent bond. Photobleaching is often a major limitation in fluorescence imaging and high photobleaching resistance is often a desirable feature of fluorescent markers. Efforts have been made to increase the lifetime of fluorophores by enzymatically controlling the level of oxygen in the sample (Rasnik 2006) and now many commercially available products have been created to help reduce photobleaching rates. Although photobleaching is often a restraint in fluorescence microscopy, it has also proved beneficial in studying the dynamics of protein behaviour in techniques such as Fluorescence Recovery After Photobleaching (FRAP) and Fluorescence Loss In Photobleaching (FLIP) (Axelrod 1976, Lippincott-Schwartz 2003).

Finally, it is well characterised that the fluorescence emission from fluorophores can vary considerably overtime, prior to photobleaching. Although this phenomenon does not necessarily affect standard ensemble fluorescence experiments, it is an important consideration when designing single molecule assays. Generally, intensity variation over time is known as 'blinking' and can arise via a multitude of pathways (reviewed in Ha and Tinnefield 2012). Blinking can be a limitation in single molecule tracking studies as periods of reduced/no fluorescence can prevent localisation of molecules and thus accurate calculation of molecular displacement (discussed in Chapter 5). Such transitions from non-fluorescent to fluorescent states have however been utilised in the development of super-resolution techniques such as direct stochastic optical reconstruction microscopy (dSTORM) as a way of temporally separating single molecule fluorescence (discussed below)

#### **1.5.4 Resolution limits in microscopy**

Fluorescence microscopy has provided a means of visualising molecule-specific expression, localisation and dynamics within cells making it a powerful tool for molecular cell biologists. However, as with most techniques, it has its limitations of which resolution is the most notable. Resolution is often described as the ability of an instrument, be it the eye, a telescope or a microscope, to produce an image of two closely spaced objects allowing one to distinguish them as separate entities. In the case of fluorescence microscopy, this would be the ability to visualise and identify two or more fluorescently labelled molecules within a cell. The resolving power of fluorescent microscopes is limited by the wave-like behaviour of light and its subsequent diffraction, and is thus often referred to as the ‘diffraction limit’.

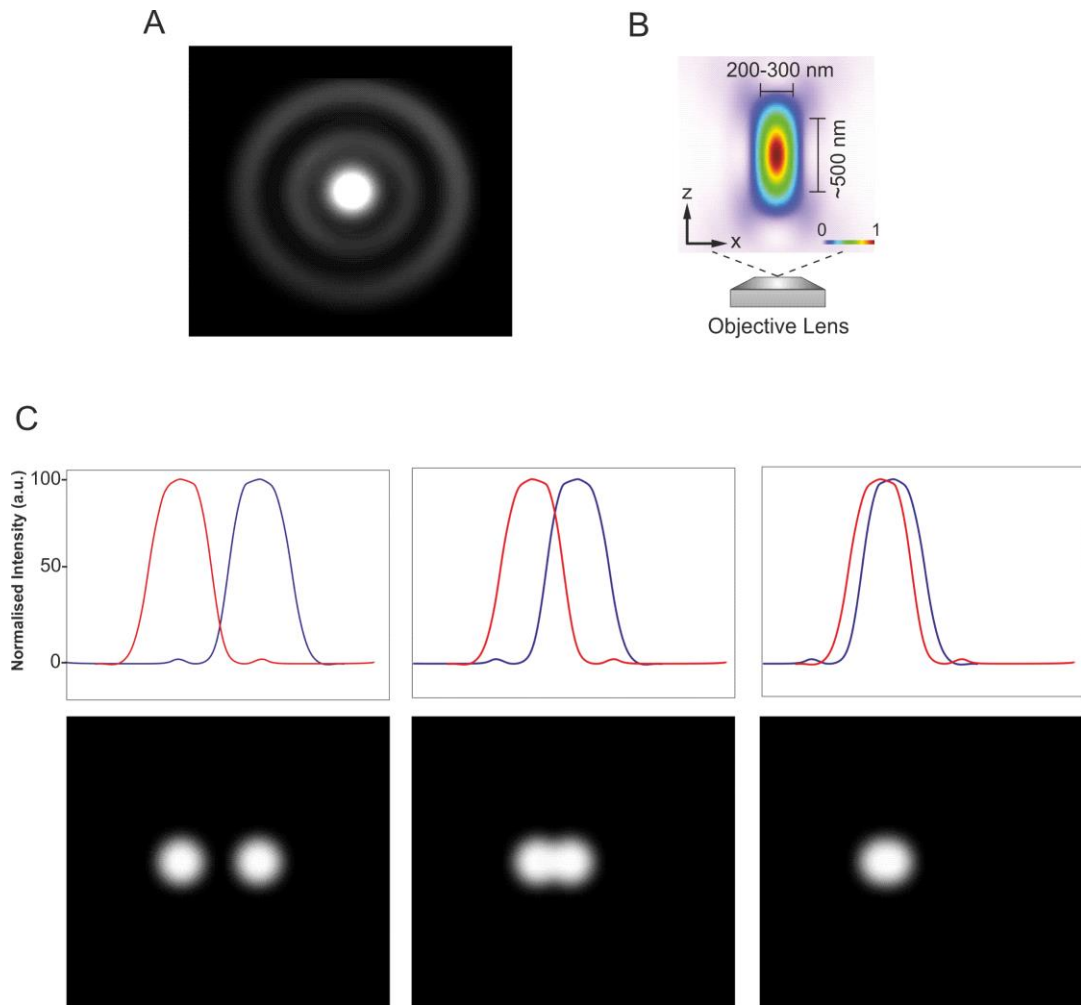


**Figure 1-8. The diffraction limit to resolution.**

**A)** Schematic representation of an Airy disk, the central bright central region, with concentric rings emanating out from the centre forming the Airy pattern. **B)** Diagram of the average dimensions of point spread function in standard microscopes. The lateral dimensions (200-300nm) correspond to the width of the Airy disk. Adapted from Huang 2009. **C)** Schematic representation of the effect of spatial separation on image resolution in fluorescence microscopy. Top panels intensity distributions of the Airy disks (bottom panels). Left, two emitters separated by a distance greater than the diffraction limit can be seen as separate entities. Middle, the Rayleigh limit of resolution whereby the maxima of one Airy disk overlaps with the first minima of another. Right, emitters closer than the Rayleigh limit cannot be distinguished as separate. Adapted from R. Boulineau

In order to understand how the diffraction limit prevents high resolution in fluorescence imaging one must understand the effect of diffraction on the final image. A microscope is a lens-based system that acts to produce a magnified image of a small object and focus that light onto an image plane. However, diffraction of light by the circular aperture of the objective lens prevents it being focused into a sharp point, instead causing it to blur. This can be explained better when considering imaging a point source of light such as a single GFP protein, which is around 4nm in size. The resulting image produced from a standard microscope system has dimensions often around 200-300nm in the focal plane,

much larger than the fluorophore. This finite size spot when projected onto a 2D imaging plane is referred to as the Airy disk (Figure 1-8A). In 3-dimensions, this diffraction pattern is known as the Point Spread Function (PSF), and is the image response of a microscope to a point source of light (Figure 1-8B). It is ultimately the dimensions of the PSF that limits the resolution of fluorescence microscopy.

The limit of resolution was described in 1873 by Ernst Abbe and later refined by Lord Rayleigh in 1896, to quantify the amount of spatial separation required to distinguish two Airy disks as separate (Abbe 1873, Rayleigh 1896). Abbe demonstrated that the size of the Airy disk at full width at half maximum (FWHM) is dependent on the numerical aperture (NA) of the objective lens and the wavelength of light:

$$FWHM = \frac{\lambda}{2NA}$$

This approximates the smallest point that light can be focussed to in a microscope system. Lord Rayleigh further defined the limit of resolution by diffraction as the distance between the centres of two Airy discs when the maxima of one overlaps with the first minima of the other (Figure 1-8C). If the objects are closer than this distance then the Airy discs merge and cannot be resolved. This distance can be approximated for a microscope with the following equation:

$$d_{x,y} = \frac{0.61\lambda}{NA}$$

Although the limit of resolution calculated by these two equations vary depending on the wavelength of light and numerical aperture of the objective lens, the diffraction limit usually ranges between 200-300nm for a standard fluorescence microscope. Whereas the lateral dimensions of the PSF defines spatial resolution in two dimensions, the axial dimensions further constrain the resolution available in three dimensions. The axial width of the PSF is generally around twice as large as the lateral width, ~500nm, giving it an elliptical appearance (Huang 2009) (Figure 1-8B).

The standard resolution of fluorescence microscopes, although sufficient to resolve subcellular structures on a micrometre scale, will render any ultrafine detail undetectable.

Interactions between proteins within a cell occur on a scale of nanometres to tens of nanometres, and sub-cellular components can be formed of hundreds to thousands of proteins within the dimensions of an Airy disk. Thus, when studying a fluorescently labelled protein within the cell, diffraction of light causes overlapping of fluorescent signal from each protein, ultimately causing a loss of high frequency spatial information.

### **1.5.5 Extending resolution in fluorescence microscopy**

Extending the spatial resolution of fluorescent microscopes has been of great interest to the biophysical community for a number of decades. A variety of techniques have thus been developed to overcome the diffraction barrier to improve image quality. Early attempts focussed on purely optical approaches to increase image resolution, whereas recent advancements involve manipulation of fluorophore photophysics.

Most specimen samples in microscopy are axially thicker than the microscopes depth of field of the focal plane, which can vary based on the NA of the objective used. In widefield excitation regimes, this can result in out of focus light reducing the final image quality. The development of laser scanning confocal microscopes increased the contrast of fluorescence images by coupling a tightly focused laser beam with a pinhole prior to the camera. Focussing the laser to a diffraction limited volume reduces the excitation field within the cell, whilst the pinhole ensures only light from the focal plane reaches the camera. This provided the ability to perform ‘optical sectioning’ of thick specimens and in principle can provide a 1.4-fold increase in resolution (Amos and White 2003). Confocal setups can be further coupled to a multi-photon excitation scheme to further restrict the excitation field. Although confocal microscopes provide increased image quality, they are still limited in resolution by the diffraction of light and are thus mainly used for their advantages of optical sectioning and background reduction.

Other optical approaches to increasing resolution involve implementation of multiple objective lenses or structured illumination of excitation light. Techniques such as 4Pi and I<sup>5</sup>M microscopy use two opposing objectives for excitation and/or detection (Hell 1992, Gustafsson 1999). These approaches aim to reduce the elliptical appearance of the PSF in the axial direction by collecting light from an almost spherical angle. This increases axial resolution to around 100nm and only moderately boosts lateral resolution.

Structured illumination microscopy (SIM) aims to increase spatial resolution by modulating the widefield illumination pattern. Introduction of diffraction gratings into the excitation beam induces a periodic incident pattern, creating regions of maximal and minimal intensities. Multiple images are collected for different translations and rotations of the excitation pattern, before high resolution images (~100nm) can be reconstructed (Gustafsson 2000, Schermelleh 2008). One notable benefit of SIM is that it can be used with fluorescent proteins, allowing for live cell imaging (Shao 2011).

Although using purely optical approaches to increasing image resolution has been achieved, these techniques are still ultimately limited by diffraction of light. In order to achieve much higher resolution, techniques have been developed that involve manipulation of fluorophore photophysics and photochemistry to break the diffraction limit. A group of techniques known collectively as reversible saturable optical fluorescence transition (RESOLFT) microscopy have achieved resolution at the scale of tens of nanometres by controlling the fluorescent states of fluorophores using high intensity lasers. These approaches rely on holding the vast majority of fluorophores in a non-fluorescent state, such that time-sequential readout of emitters can be achieved within the diffraction-limited region (reviewed in Hell 2007).

The first RESOLFT concept based methodology to be developed was stimulated emission depletion (STED) microscopy. Simply, STED microscopy utilises two lasers, the first acts as a conventional imaging source whereas the second (known as the STED laser) acts to deplete the number of fluorescent molecules in the excited state. The STED laser is red-shifted compared to the excitation source, and is set at a very high intensity. This acts to suppress fluorescence from fluorophores by depopulating the excited state via stimulated emission (Hell and Wichmann 1994, Klar and Hell 1999). The STED beam is passed through a phase mask to achieve a doughnut shaped pattern with zero intensity at the centre. This beam is co-linearised with the excitation beam, thus sharpening and reducing the size of the excitation PSF. STED has been used successfully to achieve ~20nm resolution of fluorescently labelled subcellular structures (Goffert 2013). Other similar RESOLFT approaches exist, such as ground state depletion (GSD) which utilises the triplet state as the non-fluorescent state and thus requires less laser intensity than STED (Hell and Kroug 1995, Bretschneider 2007).

While the RESOLFT-based techniques rely on reducing the PSF size by actively depleting the number of excited molecules in the excitation region, other techniques exist which employ non-fluorescent states of fluorophores on a more stochastic basis in order to determine the positions of single molecules. These techniques rely on providing temporal separation of fluorescence emission from individual closely spaced molecules and are discussed in detail below.

### **1.5.6 Single molecule localisation microscopy: PALM and STORM**

Simultaneous emission from closely spaced fluorescent molecules results in overlapping of the Airy disks produced from each individual emitter. This merging of fluorescent signals causes a blurring of the image, preventing any underlying structure from being resolved. In 2006, three individual groups published similar methodologies that demonstrated a ten-fold increase in resolution of fluorescence microscopy images by exciting individual spatially separated emitters and localising their positions to greater accuracy than the size of the Airy disk. From these localisations, super-resolution images can be reconstructed, depicting the positions of individual molecules thus retaining some of the high frequency spatial information lost in diffraction-limited approaches. These techniques are known as photoactivated localisation microscopy (PALM), stochastic optical reconstruction microscopy (STORM) and fluorescence photoactivation localisation microscopy (FPALM) (Betzig 2006, Rust 2006, Hess 2006).

The major principle behind these three techniques is the ability to detect fluorescence from a single fluorophore. Single molecule detection was first demonstrated in 1989 by Moerner and Kador, a finding that subsequently led to the expansion of the field of single molecule biophysics (Moerner and Kador 1989, Moerner 2007). Visualising single molecule fluorescence requires an enhanced level of detection sensitivity due to the inherently small signal produced by each fluorophore. In principle, this is achieved by maximising the optical collection efficiency of the microscope and the sensitivity of the detector. High collection efficiency is achieved by using oil immersion objectives with high numerical apertures. The rise in single molecule studies has led to the development of detectors with increased sensitivity and efficiency. Currently the most common form of detector for such studies is the electron multiplying charge-coupled device (EMCCD)

which acts to amplify the minimal signal received from the sample and produce a digitised pixel based image.

Detection of single molecules permits for the observation of molecular behaviour that may be otherwise obscured by ensemble averaging. Previous to the development of PALM/STORM, single molecule experiments were still however constrained by the diffraction limit of light. Thus, experiments were performed *in vitro* with low concentrations of purified proteins or by reducing the number of fluorescent molecules by inducible promoters (Kim 2006, Lee 2006). The PALM and STORM based approaches however demonstrated that single molecule detection could be achieved at endogenous expression levels within cells by reducing the number of fluorescently active fluorophores at any given time. PALM and FPALM (referred to from here on as simply PALM) were developed by Eric Betzig and Harald Hess who realised that single molecules could be detected in densely packed regions of the cell by using photoactivatable or photoconvertible fluorescent proteins. These proteins are non-fluorescent when irradiated with excitation light unless they have been previously exposed to an ‘activating’ laser of a shorter wavelength (Ando 2002, Patterson and Lippencott-Schwartz 2002). This provides temporal control over the emission from such proteins and the photoconversion rates can be tailored to single molecule regime by reducing the activating laser intensity (Betzig 2006, Hess 2006). Irradiation of a sample with low intensity activation laser light and the same time as the excitation laser leads to stochastic activation, fluorescence and photobleaching of molecules. The activating laser is tuned such that the intensity is low enough so that no more than one fluorescent molecule is active within a diffraction limited region at any one time.

A similar concept is applied in STORM, developed by Xiaowei Zhuang, however this technique uses a photoswitchable dye pair of Cy3-Cy5 (Rust 2006). Cy5 had been previously shown to enter a stable dark state from which the dye could be recovered by irradiation with green laser light, a process that is more efficient when in proximity of a Cy3 molecule (Bates 2005). Rust and colleagues utilised this photoswitching mechanism in a similar manner to photoactivation in PALM, recording single molecule fluorescent events in a diffraction-limited region. Further development of the STORM technique showed that switching between dark and fluorescent states could be achieved with a single fluorescent dye in the presence of an oxygen scavenging system and a thiol (e.g.

betamercaptoethanol). The oxygen scavenging system reduces the concentration of oxygen in the sample and stabilises the triplet state of excited fluorophores. Removing oxygen from the sample prevents excited electrons from returning to the ground state and subsequently becoming excited again. This results in the majority of fluorophores occupying the non-fluorescent triplet state upon initial irradiance with high power excitation light. Quenching of the triplet state can then be achieved by the addition of a reducing thiol, the concentration of which will determine the rate at which molecules return to the ground state. This adaptation, known as direct STORM (dSTORM), and has become a popular super-resolution method, as it is compatible with most existing immunofluorescence protocols (Heilemann 2008, van de Linde 2011)

Sequential detection of closely spaced fluorophores does not instantly provide greater resolution; the sum of all of the fluorescent events would still yield a diffraction-limited image. To break the diffraction barrier, each single molecule must be localised to a higher precision than the width of the Airy disk using post-acquisition image processing. This is achieved by locating the central point of the Airy disk from the fluorescence distribution. Measuring the fluorescence counts in cross section through an image of a single fluorophore shows that it approximates a normal distribution (Figure 1-9). This can be fit with a two-dimensional Gaussian, which is a good approximation of the central maxima region of the Airy disk:

$$U(u, v) = A \exp\left[-\frac{(u - \mu_x)^2}{2s_x^2}\right] \exp\left[-\frac{(v - \mu_y)^2}{2s_y^2}\right] + B$$

where  $u$  and  $v$  are the coordinates in the image plane,  $A$  is the amplitude of the function,  $\mu_x$  and  $\mu_y$  are the two dimensional positions of the molecule and  $s_x$  and  $s_y$  are the standard deviations in the  $x$  and  $y$  directions. In order to ensure an accurate approximation the function is usually fit with the least-squares method of parameter estimation (Thompson 2002). From this fit, the centroid of the distribution can be found, thus localising the centre position of the molecule within the Airy disk. Multiple sequential images of the same fluorophore can be used to sample its position several times, thus generating a new distribution of centre positions that will have a substantially reduced standard deviation than the diffraction-limited image (Thompson 2012).

In the case of PALM and STORM, it is not possible to obtain enough sequential images of every fluorophore, as the photobleaching rate is too fast. Thus, the position of the molecule within the Airy disk must be localised from one single image. A 2D Gaussian fit is still applied to the molecule image, however the uncertainty of localisation must be calculated in a different manner. An expression for the calculation of localisation precision (the variance of the estimate  $\mu_x$  of the x coordinate centre) was developed by Thompson *et al.* before later refinement by Mortenson *et al.*:

$$Precision^2 = Variance(\mu_x) = F \frac{\sigma_a^2}{N} \left( \frac{16}{9} + \frac{8\pi\sigma_a^2 b^2}{Na^2} \right)$$

where  $F$  is an EMCCD adjustment factor,  $a$  is the pixel dimension in nanometres,  $b$  is the background image noise,  $\sigma_a^2$  is adjusted standard deviation of the Gaussian and  $N$  is the number of photons detected from the molecule. This approach is now used in the majority of single molecule based super-resolution studies (Thompson 2002, Mortensen 2010). The number of photons collected for each molecule has a large effect on the precision of localisation. Each photon collected can be thought of as a measure of the molecules position, and thus the more photons detected the better the precision of localisation. For example, bright Cy3 fluorophores have been used to achieve 1.5nm localisation of Myosin V moving on actin fibres (Yildiz 2003).

The localised position of a molecule derived from Gaussian fitting is used along with the calculated precision of localisation in PALM and STORM to reconstruct a final image. Each single molecule that is detected in an experiment is localised and then the new position is plotted on a new image. The precision of localisation can then be used to blur the point in the image. Eventually at the end of the experiment, each molecule has been super-localised and a pointillist ‘map’ of molecule positions is created which forms the final super-resolution image (Betzig 2006, Hess 2006, Rust 2006) (Figure 1-9C).

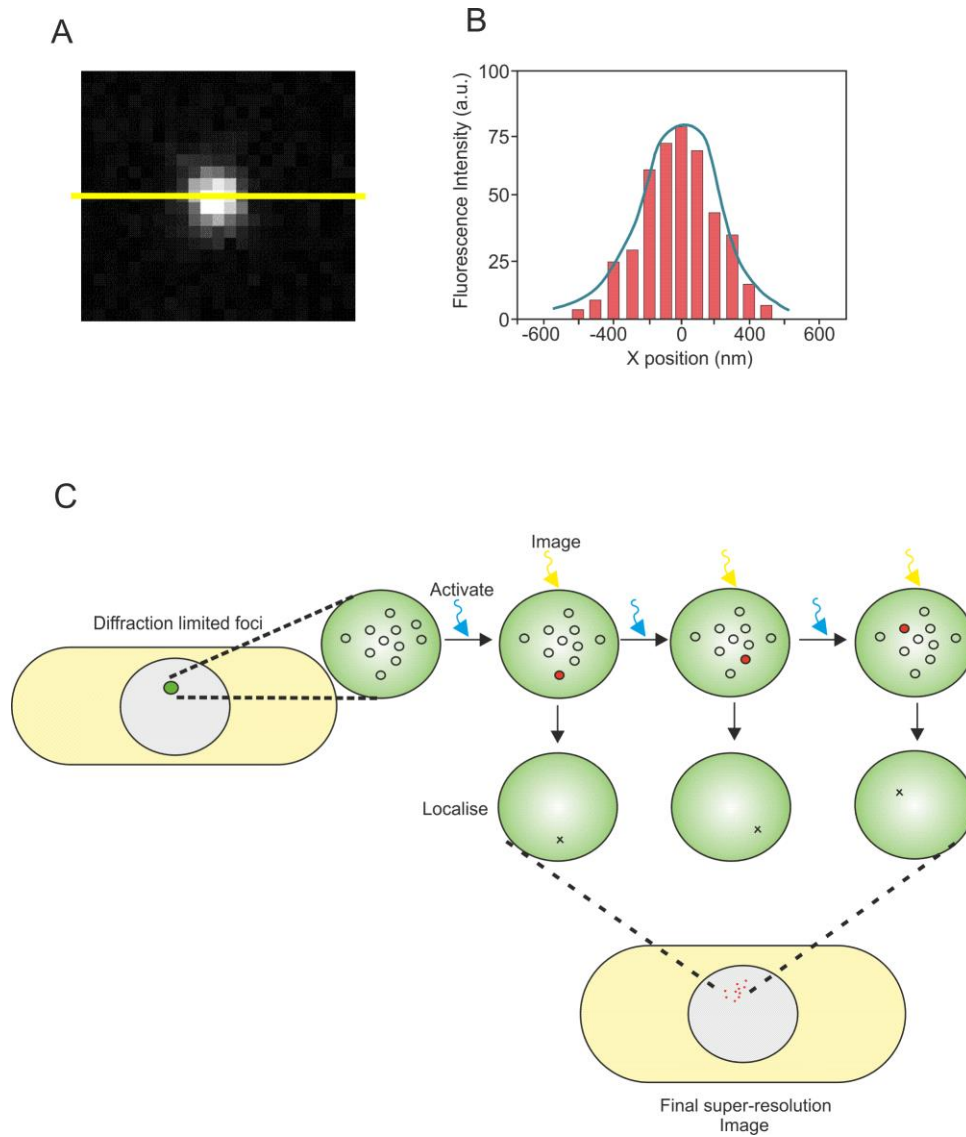


**Figure 1-9. Single molecule localisation.**

**A)** Airy disk generated from a single fluorescent bead imaged on SR-1. Yellow line indicates a cross section through the pixel image to measure the intensity distribution. **B)** Schematic representation of an intensity distribution through an Airy disk fit with a Gaussian function. **C)** Diagram depicting sequential activation of single photoactivatable fluorophores in a diffraction limited region within a *S. pombe* nucleus, as performed in PALM. Detection of single molecule fluorescence allows for the localisation of each molecule to high precision and the reconstruction of a pointillist super-resolution image. Note: the activation laser can either be pulsed or set as continuous at a low intensity.

### 1.5.7 Limiting factors of PALM and STORM

Due to the increased level of sensitivity in single molecule experiments, background fluorescence can become a major limiting factor reducing the signal to background ratio. This can be controlled to a certain extent by good sample preparation, however further steps may need to be taken to reduce the effect of cellular autofluorescence. Autofluorescence from cells can reduce the signal to background ratio of single fluorescent events such that they cannot ultimately be distinguished from background or are poorly localised. This problem is compounded with a widefield excitation regime as autofluorescence from outside the focal plane can add to the background level of fluorescence. Techniques exist to reduce the amount of a sample that is illuminated by modulating the way the excitation beam enters the sample. The most common method is total internal reflection fluorescence (TIRF) microscopy, which utilises an evanescent wave formed when the excitation laser beam with an incident angle larger than the critical angle is completely reflected at the glass sample slide (Axelrod 1981). The evanescent wave decays as it penetrates the sample, such that only fluorescent molecules <200nm from the surface are excited reducing the influence of out-of-focus fluorophores. This method has a highly restricted illumination range and is thus usually limited to investigations either on the glass/cell surface. To study thicker samples, such as the cell nucleus, technique has been developed which selectively illuminate regions deeper than the axial depth of TIRF. For example, both highly inclined and laminated optical sheet (HILO) and variants of light-sheet microscopy have been employed to study single molecule fluorescence deep in mammalian cells (Tokunaga 2008, Gao 2012, Chen 2014) (Figure 1-10).

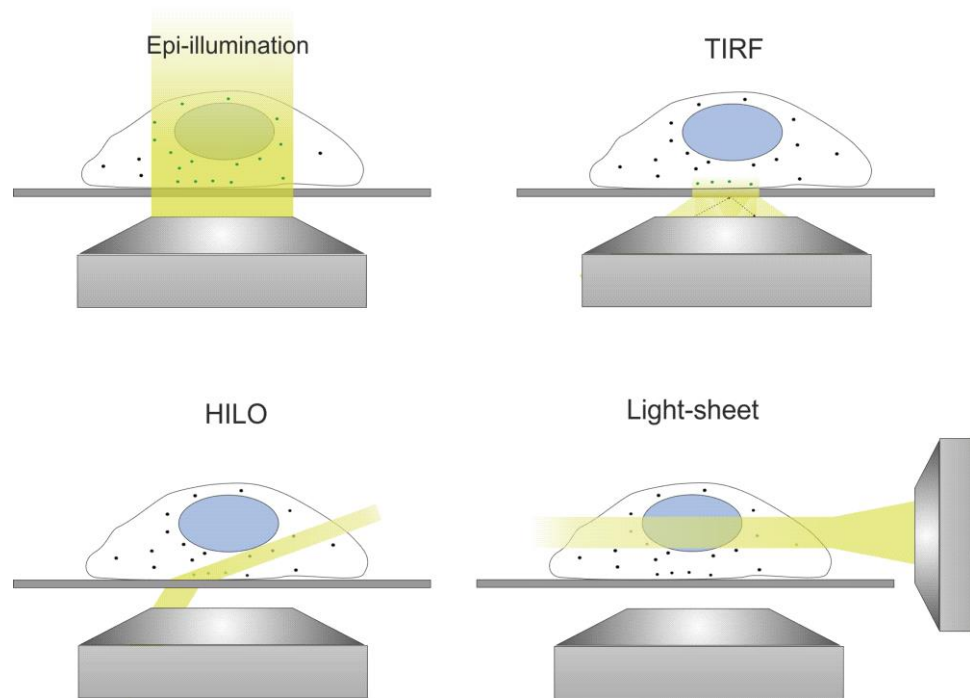


**Figure 1-10. Different illumination schemes for single molecule detection.**

Standard epi-illumination excites molecules above and below the focal plane, increasing background fluorescence counts and reducing the ability for 3D sectioning. TIRF allows excitation of only molecules close to the glass coverslip, reducing the amount of out of focus light collected during imaging. HILO uses a highly inclined beam to create a thin excitation beam that reduces the amount of illuminated area in the specimen and thus out of focus emission. Light-sheet techniques use a secondary illumination objective to generate a sheet of light that selectively illuminates a portion of the sample. Single-molecule detection has been demonstrated with each of these excitation schemes. Adapted from Liu (2015).

The first PALM and STORM experiments also lacked any 3D spatial information, this is due to several reasons. Firstly, the high numerical aperture of the objective lens limits the focal depth of the microscope. Thus, any light received from outside of this region will be out of focus and the fitting routine will fail to fit a 2D-Gaussian. Furthermore, due to the widefield activation regime, optical sectioning is not possible as molecules above and below the focal plane will be stochastically activated and photobleached during the acquisition of a single plane. Thus, since the first publication of both methods, efforts have been directed at adapting them to provide 3D information. Axial information in single-molecule localisation was first described using a cylindrical lens to induce an astigmatism during STORM (Huang 2008a). This results in the image of a single molecule being focussed differently depending on where it resides axially. This has the effect of creating an elliptical Airy disk, from which it is possible to extract a molecules position within the focal plane via a previously generated look up table. This method boasts ~25nm lateral localisation precision and ~50nm axial precision. Another method

that employs PSF engineering is known as the Double-helix. This technique uses further optics to split the PSF into two maxima that rotate around each other depending on the axial depth of the molecule, providing  $\sim 20\text{nm}$  localisation precision over a  $1\text{-}3\mu\text{m}$  axial distance (Pavani 2009). Further methods include, confocal-like scanning of a focussed activation beam (Huang 2008b, York 2011), dual-objective based detection (Schtengel 2009) and multiplane imaging (Hajj 2014).

Single molecule localisation based super-resolution techniques are substantially limited by the time taken to acquire the data. Visualising an entire population of molecules one at a time can take tens of minutes to achieve, depending on the number of molecules in a cell. This does not present significant problems in fixed samples other than sample drift over time, yet it severely limits the application to live-cell imaging. However, live cell PALM has been demonstrated to a certain extent by studying focal adhesion complexes in live hamster (CHO) and human (3T3 fibroblasts) cells, using photoconvertible fluorophore EosFP and separating molecule position data into subgroups at specific intervals (Schroff 2008). PALM has also been used in live cells to track single molecule diffusion, known as single particle tracking PALM (sptPALM) (Manley 2008). Temporal control provided by photoactivation overcomes the diffraction limit to single particle tracking and allows for the observation of single-molecule dynamics at endogenous levels of protein expression.

### **1.5.8 Summary statement**

The technical development of super-resolution techniques still continues in order to achieve better labelling (Kiuchi 2015), time resolution (Holden 2014) and axial information (Jia 2014). However, the application of such techniques to biological phenomena by molecular cell biologists is only just beginning. The commercialisation of super-resolution microscope set-ups and/or collaboration between biophysicists and biologists will help to implement the techniques as standard procedures in research institutes. The work presented from here on in this thesis is a demonstration of such efforts.



# Chapter 2

## Materials and Methods

### 2.1. Growth Media

#### 2.1.1 Yeast Growth Media

##### Yeast Extract (YE), Rich Media

5.0 g/l	Yeast Extract
30 g/l	Glucose
0.2 g/l	Adenine
0.1 g/l	Uracil
0.1 g/l	Histidine
0.1 g/l	Leucine
0.1 g/l	Arginine

##### YE Agar (YEA) Plates

YE plus:

12.5 g/l	Difco Bacto Agar
----------	------------------

##### Edinburgh Minimal Media (EMM)

50.0 ml/l	20x EMM2 salts
25.0 ml/l	20% NH <sub>4</sub> Cl
25.0 ml/l	0.4M Na <sub>2</sub> HPO <sub>4</sub>
50.0 ml/l	40% Glucose
1.0 ml/l	1000x Vitamins
0.1 ml/l	10000x Trace elements

*EMM2 Salts:*

61.20 g/l	Potassium hydrogen phthallate
20.00 g/l	KCl
21.40 g/l	MgCl <sub>2</sub> .6H <sub>2</sub> O
0.20 g/l	Na <sub>2</sub> SO <sub>4</sub>
0.26 g/l	CaCl <sub>2</sub> .2H <sub>2</sub> O

*1000x Vitamins:*

1.0 g/l	Pantothenic acid
10.0 g/l	Nicotinic acid
10.0 g/l	Inositol
0.01 g/l	d-Biotin

*10000x Trace Elements:*

5.0 g/l	H <sub>3</sub> BO <sub>3</sub>
4.0 g/l	MnSO <sub>4</sub>
4.0 g/l	ZnSO <sub>4</sub> x 7H <sub>2</sub> O
2.0 g/l	FeCl <sub>3</sub> x 6H <sub>2</sub> O
1.5 g/l	Na <sub>2</sub> MoO <sub>4</sub>
1.0 g/l	KI
0.4 g/l	CuSO <sub>4</sub> x 5H <sub>2</sub> O
10.0 g/l	Citric acid

EMM Agar Plates

For 400 ml:

10.0 g	Formedium Bacto Agar
300 ml	Double Distilled H <sub>2</sub> O
100 ml	4x EMM

*EMM plates were then supplemented as required per experiment*

### 2.1.2 Bacterial Growth Media

#### Luria-Bertani (LB)

10.0 g/l	Tryptone
5.0 g/l	Yeast Extract
5.0 g/l	Sodium Chloride

#### LB Agar (LA)

LB plus:

12.0 g/l	Difco Bacto Agar
----------	------------------

### 2.2. Drugs Used for Genetic Selection

<u>Drug</u>	<u>Final Concentration</u>
Nourseothricin sulphate (NAT)	100 µg/ml
Geneticin disulphite (G-418)	200 µg/ml
5-Fluoroorotic acid (5-FOA)	1 mg/ml
Kanamycin monosulfate (KAN)	50 µg/ml
Ampicillin sodium salt (AMP)	100 µg/ml

*Table 2-1- Drugs used for genetic selection*

### 2.3. Genotoxic Agents

<u>Chemical</u>
Hydroxyurea (HU)
Methyl methanesulfonate (MMS)

*Table 2-2. Chemicals used as genotoxic agents*

## 2.4. General Molecular Cloning Techniques

### 2.4.1 PCR for amplification of DNA fragments

From plasmid DNA: To amplify DNA fragments from plasmid DNA, a KOD Hot-start polymerase kit was used (Novagen). A standard 50 $\mu$ l reaction consisted of: 5 $\mu$ l 10x KOD buffer, 5 $\mu$ l dNTP mix (2 mM each), 4 $\mu$ l 25 mM MgSO<sub>4</sub>, 1 $\mu$ l of 10 $\mu$ M forward primer, 1 $\mu$ l of 10 $\mu$ M reverse primer, 1 $\mu$ l KOD Hot-start polymerase, 10ng plasmid DNA and ddH<sub>2</sub>O up to 50 $\mu$ l.

From genomic DNA: To amplify DNA fragments from *S. pombe* genomic DNA, 50-100 ng of genomic DNA was added to the above 50  $\mu$ l reaction instead of plasmid DNA.

Standard thermocycling conditions were:

1. 95°C                      3mins
2. 95°C                      15sec
3. 57°C                      30sec
4. 72°C                      20sec/kilobase

*Reactions were cycled from stage 2-4 29x after initial cycle.*

In some rare instances, KOD was unable to produce a PCR product from a specific template. In such cases, the NEB Phusion high fidelity DNA polymerase was used as an alternative. A typical reaction mix consisted of: 10ng plasmid or 100ng genomic DNA, 10 $\mu$ l 5x Phusion GC buffer, 5 $\mu$ l dNTP mix (2mM each), 1 $\mu$ l of 10 $\mu$ M forward primer, 1 $\mu$ l of 10 $\mu$ M reverse primer, 1 $\mu$ l Phusion polymerase and ddH<sub>2</sub>O up to 50 $\mu$ l. The same thermocycling condition used for KOD were applied.

PCR products were run on a 1% (w/v) agarose gel and gel extracted using MacheryNagel Gel extraction and PCR clean up kit.

### **2.4.2 Site-directed mutagenesis PCR**

Single site mutations were introduced into plasmid DNA using single site-directed mutagenesis PCR using a protocol adapted from the Stratagene QuikChange Single Site Mutagenesis Kit.

50ng of each plasmid was amplified with 125ng of both forward and reverse mutagenic primers using Pfu turbo DNA polymerase, as suggested by manufacturer (Stratagene). PCR cycle conditions were: 94°C for 3min and then cycled fifteen times at 94°C for 30 sec, 59°C for 1min and 68°C for 2mins per kilobase. 1µl of DpnI restriction enzyme was added to reactions and incubated at 37°C for 1 hour.

Amplification products were then purified using MacheryNagel Gel Extraction and PCR clean up kit to remove excess primers and the Pfu turbo polymerase. Note: a 1/10 dilution of the NTI buffer provided in the kit was used to prevent retention of the primer DNA. The reaction mixture was then heated to 75°C for 10min to displace primers that had annealed to the end of the PCR product, and then cooled slowly allowing the DNA product ends to anneal and circularise. The annealed PCR product was then transformed into competent *E. coli* DH5α. The removal of excess primers prevents the concentration dependant annealing of the primers to the single strand ends of the desired PCR product, which prevents its circularisation. Removal of the Pfu turbo polymerase during purification also prevents further DNA synthesis that causes blunting of the desired PCR products.

### **2.4.3 Restriction Digest**

Restriction enzymes were purchased from New England Biolabs (NEB). Restriction digests were performed according to the manufacturer's conditions, unless stated otherwise

### **2.4.4 DNA ligation**

Ligation of restriction digested PCR product (Insert) into digested plasmids (vector) was performed using T4 DNA ligase (NEB) as recommended by the manufacturer. Vector (100ng) and insert were incubated in a 1:3 ratio at 16°C overnight.

## 2.5. General *E. coli* Techniques

### 2.5.1 *E. coli* transformation

Competent DH5 $\alpha$  cells were thawed on ice before aliquoting 40 $\mu$ l of cells into pre-chilled Eppendorf tubes containing the DNA mixture. Cells were incubated on ice for 20min before being heat shocked at 42°C for 90sec. After heat shocking, cells were incubated on ice for 5min. 400 $\mu$ l of LB growth media was then added to the cells and they were incubated at 37°C for 30min. Cells were then plated on LB plates containing the relevant selection drug and incubated at 37°C for >16 hours

### 2.5.2 Extraction of Plasmid DNA from *E. coli*

Mini prep: Single *E. coli* colonies were inoculated in 5ml of LB media supplemented with 5 $\mu$ l ampicillin at a final concentration of 10 $\mu$ g/ml and incubated overnight at 37°C. Overnight cultures were centrifuged at 3202 x g for 10 min. Supernatant was discarded and the pellet was re-suspended in 200 $\mu$ l of Qiagen Buffer P1 (50mM Tris.Cl, pH 8.0; 10mM EDTA; 100 $\mu$ g/ml RNase A), 300 $\mu$ l of Qiagen Buffer P2 (200mM NaOH, 1% SDS (w/v)) and 300 $\mu$ l of Qiagen Buffer P3 (3.0M potassium acetate, pH 5.5). The samples were then centrifuged at 22,000 x g for 10 min and the supernatant was transferred into a 1:1 volume of isopropanol. The mixture was then centrifuged at 22,000 x g for 20 min and the pellet was washed in 500 $\mu$ l of 75% (v/v) ethanol. Pellets were then vacuum dried in a SpeedVac for 10 min to remove any remaining ethanol. Finally the pellet was re-suspended in 20 $\mu$ l of double distilled H<sub>2</sub>O and 1 $\mu$ l of RNase A (10mg/ml)

Midi prep: Single *E. coli* colonies were inoculated in 100ml of LB media supplemented with 100 $\mu$ l ampicillin at a final concentration of 10 $\mu$ g/ml and incubated overnight at 37°C. Overnight cultures were centrifuged at 3202 x g for 10 min. The plasmid DNA was then extracted using a Qiagen Midiprep Kit (12145) according to the manufacturer's recommendations.

## 2.6. General *S. pombe* cell biology techniques

### 2.6.1 Crossing of *S. pombe* strains and random spore analysis

*S. pombe* strains of opposite mating types were mixed together in 10µl ddH<sub>2</sub>O on ELN plates and incubated at 25°C for 2-3 days. Crosses which successfully produced asci were then taken and incubated overnight in 1ml of 1:1000 dilution of B-galactosidase from *helix pomentia* (Roche). Spore density was then counted on a heamocytometer before 500 spores were plated on YEA containing relevant selection.

### 2.6.2 Tetrad dissection

Strains were crossed on ELN as described above. A loop of cells was then re-suspended in 100µl H<sub>2</sub>O, before running a drop of cell suspension down the centre of a YEA plate. The plate was incubated overnight at 4°C and for 1 hour at room temperature before dissection. Tetrads were then dissected using the Singer MSM dissection microscope system.

### 2.6.3 *S. pombe* transformation

Respective *S. pombe* strains were grown overnight in culture to a density of  $1 \times 10^7$  cells/ml in YE media. 10ml of cells were used per transformation and centrifuged at 3202 x g for 5min. The pellet was washed with water and then 1ml of LiAc-TE buffer (10mM lithium acetate, 1mM Tris pH 7.5). Cells were then suspended in 100µl LiAc-TE buffer and mixed with 2µl carrier DNA (salmon sperm DNA 10mg/ml) and 500ng of plasmid DNA. After an incubation period of 10 min at room temperature 260µl of 40% (w/v) PEG/LiAc-TE was added and then cells were incubated for a further 30 min at 30°C. 43µl of DMSO was added and then cells were heat shocked at 42°C for 5 min. Following heat shock, cells were washed in 1 ml H<sub>2</sub>O, re-suspended in 500 µl H<sub>2</sub>O and then plated on agar plates containing respective selection supplements.

#### **2.6.4 Recombination Mediated Cassette Exchange (RMCE)**

Cells successfully transformed with an RMCE plasmid, e.g. pAW8 were inoculated in 10ml of YE media and incubated at 30 °C. The overnight culture was then diluted to a concentration of  $10^5$  cells/ml before plating  $10^4$  cells onto YEA+5FOA to select for *ura*<sup>-</sup> cells. Plates were incubated at 30 °C for 3-4days. Colonies which grew on 5FOA plates indicate successful plasmid/chromosome exchange of DNA and loss of *ura4* expression. Single colonies were patched onto YEA+5FOA and then replica plated onto EMM plates supplemented with uracil and adenine to identify leucine auxotrophic cells which had successfully lost the plasmid. Cells which were 5FOA resistant and leucine auxotrophic were then streaked out to single isolates as a final step.

#### **2.6.5 Lactose gradient synchronisation**

Cells were cultured overnight in 100ml of YE media to a density of  $0.5OD^{595}/ml$ . Cells were pelleted by centrifugation at 3500rpm for 3 minutes and re-suspended in 500 $\mu$ l of PBS. Samples were then placed on a lactose gradient (1ml of 30%, 28%, 24%, 21%, 18.5%, 15%, 13%, 10% and 7% lactose) before centrifugation for 8mins at 1000rpm. The top fraction of the separated cells was removed and re-suspended in 1ml of YE. Cells were then incubated at 30°C in an Eppendorf Thermomixer heat block for 2hours to increase the number of S-phase cells in the sample. In some experiments this was done in the presence of HU or MMS.

#### **2.6.6 Extraction of *S. pombe* genomic DNA**

1ml of an overnight culture (approx. 5 ODs) of cells was centrifuged at 22,000 x g for 2mins. Cells were re-suspended in CSE (citrate phosphate buffer pH 5.6 20mM, Sorbitol 1.2M, EDTA 40mM): Zymolyase (20T, Seikagaju Corp.) mix (1mg/ml) and incubated at 37°C for 20 min. Cells were then pelleted and re-suspended in 450 $\mu$ l of 5xTE (pH7.5) and 50 $\mu$ l 10% SDS (v/v) and incubated at room temperature for 5mins. 150 $\mu$ l of 5M potassium acetate was then added to the reaction mixture, which was incubated on ice for 5min and then centrifuged at 22,000 x g for 10min at 4°C. The supernatant was then transferred to 1:1 volume of isopropanol and was centrifuged under the same conditions.

The supernatant was then discarded and the pellet was washed in 500µl of 75% ethanol (v/v) before being dried in a vacuum concentrator. The DNA pellet was re-suspended in 200µl ddH<sub>2</sub>O and 5µl RNase (10mg/ml).

### **2.6.7 Whole cell protein extracts**

Logarithmically growing cells were harvested (5 OD<sup>595</sup>) and pelleted before being re-suspended in 500µl of ddH<sub>2</sub>O. 100µl of 2M NaOH + 7.5% betamercaptoethanol was added to samples and incubated on ice for 15 min. 80µl of 55% trichloroacetic acid (TCA) was then added to the samples and incubated on ice for a further 15mins. Samples were then centrifuged for 10min at 14000rpm after which the supernatant was removed by aspiration. Pellets were re-suspended in 50µl of HU buffer (8M urea, 5% SDS, 200mM Tris-HCl pH6.8, 1mM EDTA, 0.05%(w/v) bromophenol blue and 1.5% DTT) and vortex mixed. Samples were when heated to 65°C for 10min and centrifuged at 8000 rpm prior to electrophoresis.

### **2.6.8 Western blot: SDS PAGE and immunostaining**

Sodium dodecyl sulphate-polyacrylamide gel electrophoresis (SDS-PAGE) was used to separate whole cell protein extracts by size for western blot analysis. For separating PCNA species (tagged/modified) a 4-12% gradient gel was used (Novex NuPage), whereas 8% gels were used for all other experiments (See tables 2-3 and 2-4). Gels were run in 1x SDS running buffer (0.025M Trise Base, 0.25M Glycine, 0.1% SDS) at 80 volts through the stacking gel and 120 volts through the separating gel.

Protein samples were transferred to a Nitrocellulose membrane (GE Healthcare, Nitrocellulose, Hybond RPN3032D) using a wet transfer protocol. Transfer was performed in 1x transfer buffer (20mM Tris Base, 750mM Glycine, 20% Methanol, 0.025% (v/v) SDS) for 2 hours at constant 300mA. Transfer was confirmed by Ponceau-S solution staining (0.2%(w/v) Ponceau, 3% (w/v) TCA) of the membrane.

The membrane was then blocked with 5% milk PBST (Marvel dried skimmed milk, phosphate buffered saline, 0.1% Tween (Sigma P7949)) for one hour. Primary antibodies to the epitope of interest were incubated in 0.5% milk PBST at room temperature. The

membrane was then washed by 3x 10min washes in 0.5 % milk PBST, before being incubated with secondary antibody for 1 hour in 0.5% milk PBST at room temperature. To remove excess secondary antibody, the membrane was then washed 3x10min with PBST. The bound antibody was detected using a standard chemiluminescence technique (ECL Plus Western Lightning, Perkinelmer NEL104001EA) and exposed to light-sensitive film (GE Healthcare Hyperfilm ECL GZ28906837) which was subsequently developed (Xograph Imaging Systems Compact X4).

<b><u>Resolving Gel (8%)</u></b>	
H <sub>2</sub> O	3.3 ml
Acrylamide:Bis (30% Acrylamide, 0.8% Bis, Protogel, National Diagnostics)	4.0 ml
1M Tris (pH 8.8)	2.5 ml
10% SDS	0.1 ml
10% Ammonium persulfate	0.1 ml
TEMED	0.004ml

Table 2-3. SDS-PAGE resolving gel recipe

<b><u>Stacking Gel</u></b>	
H <sub>2</sub> O	3.4ml
Acrylamide:Bis (30% Acrylamide, 0.8% Bis, Protogel, National Diagnostics)	0.83ml
1M Tris (pH 6.8)	0.63ml
10% SDS	0.05ml
10% Ammonium persulfate	0.05ml
TEMED	0.005ml

Table 2-4. SDS-PAGE stacking gel recipe

<b><u>Antibody</u></b>	<b><u>Type</u></b>	<b><u>Supplier</u></b>	<b><u>Dilution</u></b>
Anti-PCNA	Rabbit polyclonal	Custom made	1:2000
Anti-mEos2	Rabbit polyclonal	Custom made	
Swine anti-Rabbit HRP	Swine polyclonal	DakoCytomation	1:2500

Table 2-5. Antibodies used in this thesis.

## 2.7. *S. pombe* strain creation

### 2.7.1 Recombination mediated cassette exchange overview

The recombination mediated cassette exchange (RMCE) system was previously developed in the Carr lab and provides an efficient, site-specific method for gene tagging and gene replacement (Watson 2008). The method relies on creation of a ‘base strain’ whereby two incompatible Cre-recombinase recognition sites, *loxP* and *loxM3*, which are integrated into the genome along with the *ura4* selectable marker creating a ‘cassette’ at a region of interest. The required tag or gene sequence can then be introduced into the genome via introduction of a Cre-expression plasmid containing an equivalent cassette. In this thesis two classes of base strain were used, gene replacement and C-terminal tagging.

In the case of a gene replacement base strain, the *loxP* recognition site is positioned upstream of the gene promoter region, and the *ura4* and *loxM3* are integrated directly downstream of the stop codon (as shown for PCNA in Figure 4-9). C-terminal tagging base strains involve integration of the *loxP-ura4-loxM3* cassette downstream of a gene open reading frame, removing the stop codon in the process.

### 2.7.2 Creating *pcn1* gene replacement base strain

RMCE was used to introduce a copy of the *pcn1* (PCNA) gene fused to the photoactivatable fluorophore mEos3.1. *pcn1* strains were created using the strategy designed for the replacement of an essential gene (Watson, 2008). A *pcn1* “base strain” was constructed by inserting the Cre recognition sequence, *loxP*, upstream of the *pcn1* start codon and *ura4<sup>+</sup>-loxM3* directly downstream of the *pcn1* stop codon. To insert the *loxP* site, Phusion DNA Polymerase (New England Biolabs) was used to amplify the *loxP-ura4<sup>+</sup>-loxP* cassette from plasmid template pAW41(Watson, 2008) using primers P1 and P2. The resulting PCR fragment consisted of *ura4* flanked by *loxP* sites with 80bp stretches of sequence homologous to the *pcn1* locus 927bp upstream of the *pcn1* start codon.

This PCR fragment was used to transform *S. pombe* strain AW310. Following transformation, cells were directly plated onto EMM supplemented with amino acids adenine and leucine plates and grown at 30 °C for 4–5 days until colonies appeared. Transformants were re-streaked onto fresh plates.

In order to remove the *ura4* marker and leave only one loxP site, cells were transformed with the Cre-recombinase expressing plasmid pAW5(Watson, 2008), and were plated onto EMM plates supplemented with uracil (EMM+U) and grown at 30°C. Cassette exchange was then performed using successful transformants. Cells that were leucine and uracil auxotrophic were retained and the insertion of the loxP site was confirmed by DNA sequencing.

Cells containing the loxP site upstream of the start codon were subject to a second integration designed to introduce the *ura4* marker and loxM3 site downstream of the stop codon was then performed. The *ura4-loxM3* cassette from plasmid template pAW12 (Watson, 2008) was amplified using primers P3 and P4. The resulting PCR fragment was flanked with 80bp stretches homologous to sequences directly downstream of the *pcn1* stop codon and was transformed into cells. After transformation, cells were directly plated onto EMM+L+A plates and grown at 30 °C for 4–5 days to allow colony growth. Transformants were re-streaked onto fresh EMM+L+A plates. The resulting *pcn1* base strain TJE47 (*h<sup>-</sup> loxP:pcn1:ura4:loxM3, leu1-32, ura4-D18*) was confirmed by PCR and sequencing.

### 2.7.3 Creating pAW8-*mEos3.1-pcn1* plasmid

To create the *mEos3.1-pcn1* construct the *pcn1* ORF and 927bp of upstream sequence was amplified from wild type *S. pombe* genomic DNA using primers P5 and P6. The product was then cloned into SphI/SpeI restricted plasmid pGEM5fz to create pGEM5fz-*pcn1* and the insert confirmed by sequencing.

In order to N-terminally tag Pcn1 with the mEos3.1 protein, a *Bam*HI restriction site was introduced directly upstream of the *pcn1* start codon by single site mutational PCR using primers P7 and P8. An mEos3.1 coding sequence was commercially synthesised that was codon-optimised for *S. pombe* (Forsburg, 1994), and encoded a C-terminal polythreonine-glycine-serine (TGS) linker (Genscript). This sequence was flanked by *Bam*HI

restriction sites and was subcloned into *Bam*HI restricted pGEM5fz-*pcn1* to create pGEM5fz-*mEos3.1-pcn1*. The *mEos3.1-pcn1* construct was then finally subcloned from pGEM5fz-*mEos3.1-pcn1* into the Cre-expression plasmid pAW8 (Watson *et al* 2008) to create pAW8-*mEos3.1-pcn1*.

#### 2.7.4 Creating *mEos3.1-pcn1 his3::pcn1*<sup>+</sup> strain

It has been previously reported that *pcn1* can be N-terminally tagged in *S. pombe*, however this can cause sensitivity to HU (Meister *et al* 2007). This was also observed in this study as an mEos3.1 N-terminally tagged *pcn1* strain was created by cassette exchanging the pAW8-*mEos3.1-pcn1* into the *pcn1* base strain. This construct was not stable inside cells and was selected against over time resulting in a mixed population of tagged and untagged cells. Therefore, a strain containing one mEos3.1 tagged *pcn1* and one wild type copy of *pcn1* was created. This approach has been previously shown to result in PCNA homotrimers that contain both tagged and un-tagged subunits.

To introduce a wild type copy of the *pcn1* gene we used a *his3* targeting plasmid (Matsuyama, 2008). The promoter-*pcn1* fragment from plasmid pAW8-*pcn1* was PCR amplified by primers P9 and P10. The resulting fragment and plasmid pHIS3K were restricted with *Sph*I and *Sal*I enzymes before the fragment was ligated into the vector to create plasmid pHIS3-*pcn1*. Plasmid pHIS3-*pcn1* was linearised with *Not*I and transformed into the *pcn1* base strain (TJE47). Cells were grown on YEA plates before being replica plated onto YEA+Hygromycin (Melford) to select for successful transformants. Integration was further confirmed by patching cells on EMM+U+L plates to check for histidine auxotrophy. Cells which were Hygromycin resistant and histidine auxotrophic generated strain TJE177. The *mEos3.1-pcn1* construct was introduced into strain TJE177 by RMCE using the plasmid pAW8-*mEos3.1-pcn1*. The resulting strain was TJE211.

#### 2.7.5 Creating C-terminally tagged strains using RMCE

C-terminal tagging RMCE base strains were used to tag Mcm4 and Cdc20 with mEos3.1 for experiments in Chapter 4 and 5 respectively. In both cases, the base strains had been previously created in the Carr lab, and were gifts from Izumi Miyabe. Integration of the mEos3.1 fluorescent tag into both strains was achieved by transformation with plasmid

pAW8-mEos3.1 and RMCE to create the final strains *mcm4-mEos3.1* (TJE148) and *cdc20-mEos3.1* (TJE226).

<b><u>Number</u></b>	<b><u>Genotype</u></b>
AW310	<i>leu1-31 ura4-D18</i>
AW691	<i>loxP-mEos2-cdc6-loxM3 leu1-32 ura4-D18 ade6-704</i>
YDP451	<i>loxP-mEos3.1-pcn1-loxM3 his3::pHIS-pcn1:HphMX6 rhp18::KanMX6 leu1-32 ura4-D18</i>
TJE47	<i>loxP-pcn1-ura4-loxM3 leu1-31 ura4-D18</i>
TJE108	<i>loxP-pcn1-loxM3 leu1-31 ura4-D18</i>
TJE119	<i>loxP-rad52-mEos3.1-loxM3 ura4-D18 leu1-32 ade6-704</i>
TJE148	<i>mcm4-loxP-mEos3.1-loxM3 leu1-32 ura4-D18 ade6-704</i>
TJE177	<i>loxP-pcn1-ura4-loxM3 his3::pHIS-pcn1:HphMX6 leu1-31 ura4-D18</i>
TJE211	<i>loxP-mEos3.1-pcn1-loxM3 his3::pHIS-pcn1:HphMX6 leu1-32 ura4-D18</i>
TJE212	<i>loxP-mEos3.1-pcn1-loxM3 his3::pHIS-pcn1:HphMX6 rhp18::KanMX6 elg1::NatMX6 leu1-32 ura4-D18</i>
TJE214	<i>loxP-mEos3.1-pcn1-loxM3 his3::pHIS-pcn1:HphMX6 elg1::NatMX6 leu1-32 ura4-D18</i>
TJE215	<i>mcm4-loxP-yEGFP-loxM3 leu1-32 ura4-D18 ade6-704</i>
TJE216	<i>mcm4-loxP-ura4-loxM3 leu1-32 ura4-D18 ade6-704</i>
TJE226	<i>cdc20-loxP-mEos3.1-loxM3 leu1-31 ura4-D18 ade6-704</i>
TJE227	<i>cdc20-loxP-mEos3.1-loxM3 rhp18::KanMX6 leu1-31 ura4-D18 ade6-704</i>
TJE228	<i>cdc20-loxP-mEos3.1-loxM3 pcn1-K164R leu1-31 ura4-D18 ade6-704</i>
TJE229	<i>cdc20-loxP-mEos3.1-loxM3 elg1::NatMX6 leu1-31 ura4-D18 ade6-704</i>
TJE302	<i>loxP-mEos2-cdc6-loxM3 elg1::NatMX6 leu1-32 ura4-D18 ade6-704</i>
TJE304	<i>loxP-mEos2-cdc6-loxM3 rhp18::KanMX6 elg1::NatMX6 leu1-32 ura4-D18 ade6-704</i>
TJE316	<i>loxP-mEos2-cdc6-loxM3 rhp18::KanMX6 leu1-32 ura4-D18 ade6-704</i>
TJE323*	<i>nse4-loxP-mEos3.2-loxM3 leu1-32 ura4-D18 ade6-704</i>
TJE340*	<i>nse4-loxP-mEos3.2-loxM3 nse1-R188E leu1-32 ura4-D18 ade6-704</i>

Table 2-6. Table of strains used in this study.

Strains starting with AW were gifts from Adam Watson, strains marked with YDP were gifts from Yasukazu Daigaku and strains marked with \* were created by the Murray lab

<b>Number</b>	<b>Sequence</b>
P1	CATAGTTCTTCTATTACAGAGATTCTAGTCATATTTCCAAGCTATTTCTAAGATAGAGCTCTTACATTACTTATTCTATATAGAATACTCAAGCTTGGAC
P2	TTGGTTTGTGTTAGTTTATAAACCACTATGGTCAAGTAACTAAAGTTCTGTAAATGTCATTACGACGAATAATCGCTACCGTTCACCACCCCGCCGCCCCG
P3	TTCTTGTGGAGTATAAAATGGAATCCGGATTTTTACGATTTTATCTTGCCCCAAAATTGGTGAGGAGGATGAGGAGTAGAAGCTTAGCTACAAATCCCA
P4	AAAAGTAAACAAAAGTATGTTTATAATGATGCTAGCTCGTCAATTGCA AAGAGATTACTAAAAGATATTGATTCCGTAATGAATTCGAGCTCGTTTAAAC
P5	AAAAGCATGCCGGTAGCGATTATTCGTCGTAATGA
P6	AAAACTAGTCTACTCCTCATCCTCCTCACCA
P7	AATTACGACTGGATCCATGCTTGAAGCTAGATTTTCAGCA
P8	TCAAGCATGGATCCAGTCGTAATTATATTTTATACAAGCTAGATAAGAGATATAAAGAATAGC
P9	AAAAGCATGCCGGTAGCGATTATTCGTCGTAATGACATTTA
P10	AAAAGTCGACCTACTCCTCATCCTCCTCACCAATTTTTGG

Table 2-7. Primers used in the creation of TJE211

## 2.8. *S. pombe* sample preparation for single-molecule fluorescence microscopy

### 2.8.1 Formaldehyde fixation of cells for single-molecule microscopy

Cells were cultured overnight to an OD<sup>595nm</sup> of 0.5. Cells were then harvested by centrifugation of 1ml of culture, before being washed once in PBS and re-suspended in 1% (v/v) formaldehyde (Fisher Scientific, 10751395). Cells were incubated in formaldehyde for 20mins at room temperature before being washed three times in PBS, and finally re-suspended in 10-20µl PBS.

### 2.8.2 Preparation of unfixed cells for single-molecule microscopy

To prepare unfixed cells for motion blur based PALM imaging, 10µl of 100x Sodium Azide stock solution (0.1g/ml) was added to 1ml of cell culture (either an asynchronous

overnight culture or lactose gradient synchronised sample). Cells were incubated on ice for 2mins before being harvested by centrifugation and washed three times in ice cold PBS. After washing, cells were pelleted and re-suspended in 10-20 $\mu$ l ice cold PBS.

### **2.8.3 Slide preparation for single-molecule imaging**

In order to prevent cells from moving during imaging, it was necessary to immobilise them on an agarose pad. To create an agarose pad for imaging, a 1% (w/v) agarose (Sigma, A0169) solution was made in PBS. Molten agarose was then prepared by microwaving and 380  $\mu$ l of molten agarose was sandwiched between two 22mm x 40mm coverslips. Prior cleaning of coverslips by ozonation and UV irradiation was critical to achieve minimal background fluorescence (Novascan PSD –UV6.). After the agarose pad had solidified, a small square was cut into the pad onto which 5 $\mu$ l of cell sample was deposited. Once the sample had soaked into the agarose and no surface liquid could be observed, the agarose was sandwiched between one large and one small (22mm x 22mm) coverslip (ozonated). The slide was then sealed with paraffin wax, so to prevent evaporation from the agarose, which can result in sample drift.

## **2.9. PALM Microscopy**

### **2.9.1 Sample mounting on microscope**

In order to reduce sample drift during imaging a simple procedure for mounting the sample slide onto the microscope was followed every time. Firstly, immersion oil was applied to the objective lens up to an hour prior to imaging, which allowed the oil to settle and substantially increased stability during imaging. After the sample slide was prepared, it was placed on the microscope stage and the cells were brought into focus. The C-focus mid-range position was then set according to manufacturer's suggestions. The slide was then fixed to the stage insert by using rare-earth magnets to further prevent drift. Finally, the cells were brought into focus again and the whole system was left to settle for 15-30mins. This settle time was extremely important for ensuring stability throughout the subsequent experiment.

### 2.9.2 Motion Blur PALM image acquisition

Motion blur PALM imaging was performed using continuous wave illumination of 405nm and 561nm laser light. Photoconversion of mEos3.1 was controlled by manually modulating the intensity of the 405nm laser using neutral density filters (0.1-1W/cm<sup>2</sup>). 561nm illumination intensity was continuously set at 1kW/cm<sup>2</sup> for all experiments. Camera exposure settings were set to 350ms via the micromanager control panel. For experiments on SR-2.1 the camera gain was set to '2' and for experiments on both SR-2.1 and SR-2.2 the camera EM Gain set at 250. The number of frames collected for each experiment was dependant on level of protein expression, but ranged between 3000-15000 frames. Experiments were performed in an air-conditioned room ranging from 17-19°C. All motion blur experiments were carried out as described above except in case of Figures 4-1 and 4-3C, which were performed by sequential pulsing of 405nm illumination at powers ranging from 0.1 to 10W/cm<sup>2</sup>. Each activation was followed by imaging of the sample for 500 frames with 561nm laser light (1kW/cm<sup>2</sup>). The continuous wave photoconversion regime was preferred as it reduced experiment duration.

### 2.9.3 sptPALM imaging

Single particle tracking experiments were performed using sequential pulsing of 405nm laser light described above. For experiments in Chapter 4 performed on SR-2.1, a region of interest was cropped around cells in order to achieve 30ms camera exposure time. For later experiments performed on SR-2.2 in Chapter 5, the full camera chip was used at an exposure setting of 25ms.

### 2.9.4 Raw image processing for motion blur PALM experiments

Raw image data from motion blur experiments was processed using the PeakFit plugin (<https://github.com/aherbert/GDSC-SMLM>). Only single molecule PSFs that were in focus and had a high signal to background ratio were retained. To achieve this the 'Peak Filtering' settings were applied as follows:

Shift Factor – 1.5

Signal Strength - 150

Min Photons – 50

Width Factor – 1.5

All other PeakFit settings had been previously optimised by Dr Alex Herbert via computer simulations and were thus remained unchanged.

In order to quantify nuclear single-molecule localisations, images were reconstructed using the ‘Binary Image’ function within peak fit. Localisations in each nuclear region were counted using the ImageJ ‘Measure’ tool with a circular ROI and recording the integrated density measurement. Nuclear regions were identified from maximum projections of raw data as described in Figure 4-3. To reconstruct images of nuclear localisations in Chapter 4, localisations were plotted with the average precision of the experiment of 11nm.

### **2.9.5 Raw image processing for single particle tracking PALM**

Single particle tracking experiments were performed using the PeakFit ‘Trace Diffusion’ tool. Firstly, localisation data sets were generated by fitting single molecules with the following ‘Peak Filtering’ settings:

Shift Factor – 1.5

Signal Strength - 60

Min Photons – 50

Width Factor – 1.5

Precision Threshold – 40

A distance threshold of 800nm and a minimum trace length of 5 were then set as the Trace Diffusion parameters. For experiments in Chapter 5, multiple localisation data sets were loaded into the plugin by using ‘Multiple Inputs’ selection. This allowed for the combining of experimental repeats to generate a larger data set.

### 2.9.6 Single particle diffusion simulations and recall analysis

Simulations of molecular diffusion were performed using the PeakFit ‘Create Data’ plugin. An experimentally derived average 3D PSF was generated using ‘PSF Creator’ from raw image data of fluorescent beads (FluoSpheres, Life Technologies) imaged at 20nm axial intervals. This PSF was then loaded into the Create Data plugin and simulations were performed by simulating a total of 500 molecules, randomly positioned within 2 micron confinements to mimic a fission yeast nucleus. Diffusing molecules were simulated with an axial depth of 2 microns and a speed of  $1.7\mu\text{m}^2$ . In all cases, molecules were simulated with photon emission, background noise and blinking parameters that were provided by Dr Alex Herbert. Simulated data was fitted with the 2D Gaussian fitting settings used for experiments in cells. Recall analysis was then performed using the ‘Results Match Calculator’ that provided a recall percentage for each simulation. Molecules were considered correctly recalled if a localisation was present within a 50nm radius of the true simulated position. Each simulation was performed three times.

### 2.9.7 List of custom microscope components

<u>Component</u>	<u>Manufacturer Details</u>
Inverted Microscope	Olympus IX71/IX83
Motorised stage	Prior H117E114
405nm laser	LaserBoxx Oxxius
561nm laser	Cobalt, Jive
Quarter-wave plates	Thorlabs WPQ05M-405 and -561
Low pass filters	Semrock FF01-417/60-25 and FF01-561/14-25
Beam expander	Thorlabs LC1975 and LA1986
Dichroic mirror	Semrock FF552-Di02-25
Objective Lens	Olympus, UIS2 APON 60× OTIRF
TIRF Lens	Thorlabs LA1253-A
Multi-band dichroic mirror	Semrock Di01-R405/488/561/635-25 36
Long-pass filter	Semrock BLP02-561R-25
Band-pass filter	Semrock FF01-580/14-25
EMCCD Camera	Photometrics Evolve 512/Evolve Delta

Table 2-8. Table of specific microscope components used in this study

## **2.10. Human Cell techniques**

### **2.10.1 Human Cell Culture**

U2OS human cells were cultured in Minimal Essential Media (MEM, Gibco), supplemented with 10% fetal calf serum, 2 mM L-glutamine, 100 U/mL penicillin and 0.1 mg/mL streptomycin (Pen/Strep, Gibco). Cells were incubated in a 37°C, 5% CO<sub>2</sub> incubator. U2OS cells were a gift from Dr Thomas Stiff (Hochegger Lab, Sussex).

### **2.10.2 pCCC Chromobody construct creation**

To create pCCC-mEos3.2, the mEos3.2 sequence was sent for codon optimisation for human cells and gene synthesis by Genscript. Constructs were designed such that the mEos3.2 coding sequence was flanked by HindIII and NotI restriction enzyme sites for integration in the pCCC plasmid. A 4XTGS (Threonine-Glycine-Serine) linker was also engineered directly upstream of the start codon. The mEos3.2 insert was isolated from the gene synthesis plasmid via HindIII/NotI restriction digest and purified away from the plasmid backbone via agarose gel electrophoresis and gel extraction. The pCCC-GFP plasmid was purchased from Chromotek and digested in the same manner before isolating the plasmid backbone. The mEos3.2 insert was ligated into the pCCC plasmid backbone, transformed in competent *E. coli* cells and midi-prepped as described above. Successful ligation was confirmed by HindIII/NotI restriction digest and DNA sequencing.

### **2.10.3 Transfection**

U2OS cells were transfected with linearised plasmid DNA using X-tremeGENE (Roche) transfection reagent as suggested in the manufacturer's instructions. Briefly, X-tremeGENE was added in a 3:1 ratio to the linear DNA, mixed by flicking the tube and left to incubate at room temperature for 15mins. This mixture was then added to 2ml of culture media and placed on cells in a 6 well plate. Cell culture medium contained G418 in a range from 600µg/ml - 1400µg/ml to select for integration of the linearised plasmid. Colonies that grew in the presence of G418 were picked by treatment with 1µl amounts of trypsin-PBS (2.5µg/ml) and transferred to fresh media containing 800µg/ml G418 to

keep selection. Isolated cells that grew to confluence were then retained for western blot analysis.

#### **2.10.4 U2OS whole cell protein extraction**

U2OS cells were isolated from six well plates via trypsin-PBS treatment before being washed in PBS. Pellets were then resuspended in protein extraction buffer (25mM Tris-HCL pH8.0, 150mM NaCl, 0.1% SDS and protease inhibitor tablet (Roche)). Samples were then centrifuged for 5min at 10,000 rpm and the supernatant was collected.



# Chapter 3

## Implementation of Photoactivated Localisation Microscopy for Use in Fission Yeast

### 3.1. Introduction

*Schizosaccharomyces pombe* is a tractable model organism that has been widely used to study the mechanisms underlying cell cycle progression such as DNA replication, DNA repair and cytokinesis. One major advantage of using *S. pombe* is the relative ease in which genetic manipulations such as gene deletions, mutations and protein fusions, can be performed. Studying components of cellular machinery regularly involves investigation by fluorescent microscopy. Such studies often focus on protein spatial distribution (Meister 2007, Miyabe 2009), but can also be used to extract diffusive properties (Grallert 2013) and detect protein-protein interactions (Nestoras 2010).

Although such studies have proved beneficial, fluorescence microscopy in fission yeast is limited in its output by both microscope resolution and cell size. The relatively small dimension of the *S. pombe* compared to larger higher eukaryotes makes it difficult to study the spatial distribution of proteins in any fine detail, as the resolution of standard fluorescence microscopy is not sufficient. These images are usually limited to detecting protein localisation in large organelles or diffraction limited regions within them. Slight enhancements can be made via the use of confocal microscopes or post-acquisition deconvolution of images; however, the underlying features of protein distribution remain indiscernible.

In 2006, three studies were published which demonstrated the use of single-molecule localisation of fluorescent probes to achieve a 10-fold increase in microscopy image resolution, effectively breaking the diffraction limit of light (Betzig 2006, Hess 2006, Rust 2006). Active temporal control of the fluorescent emission of these probes and subsequent detection of the single molecule fluorescence, permitted localisation of single fluorophore positions to nanometre accuracy and construction of ‘super-resolution’

images. Two of these studies used photoactivatable GFP (PA-GFP), highlighting that this technique (FPALM/PALM) was directly compatible with cellular research (Betzig 2006, Hess 2006).

Until the recent development of commercial set-ups, the use of such super-resolution approaches was limited to custom-built microscopes in biophysical research laboratories. It was thus necessary for cell and molecular biologists to initiate collaborative projects with biophysicists in order to utilise these techniques. The study presented in this thesis is a result of such a collaboration, which enabled the implementation of PALM microscopy in a biological research setting.

The aim of this study was to establish photoactivated localisation microscopy as a technique in the Carr lab and to learn how to use PALM to study DNA replication processes, primarily in fission yeast. In this chapter, I will outline the work that was required in order to implement PALM in fission yeast. Initial experiments were aimed at optimising sample preparation and imaging conditions, as well as using *S. pombe* strains expressing the photoconvertible fluorescent protein mEos3 to study basic fluorophore characteristics. In addition, this involved learning to use and maintain a specialised, custom-built PALM microscope and helping to develop single-molecule localisation software.

### **3.2. Custom Microscope Design**

In order to allow for flexibility in experiment design, a custom microscope set-up was used. During this study two similar set ups were used that differ only slightly in their construction. The first set-up was designed by Dr Steven Lee (Cambridge University, UK) and built by Dr Remi Boulineau (Osborne lab, University of Sussex); this will be referred to as ‘SR-2.1’ (Figure3-1A). Further into the project a second microscope set-up was built, referred to from here on as ‘SR-2.2’ (Figure 3-1B). SR-2.2 was built by Dr Manisankar Maiti (Carr Lab, University of Sussex) and myself and was based on the original set-up, but included upgraded and dual colour imaging components. A comprehensive list of components and their manufacturers is given in the Materials and Methods chapter.

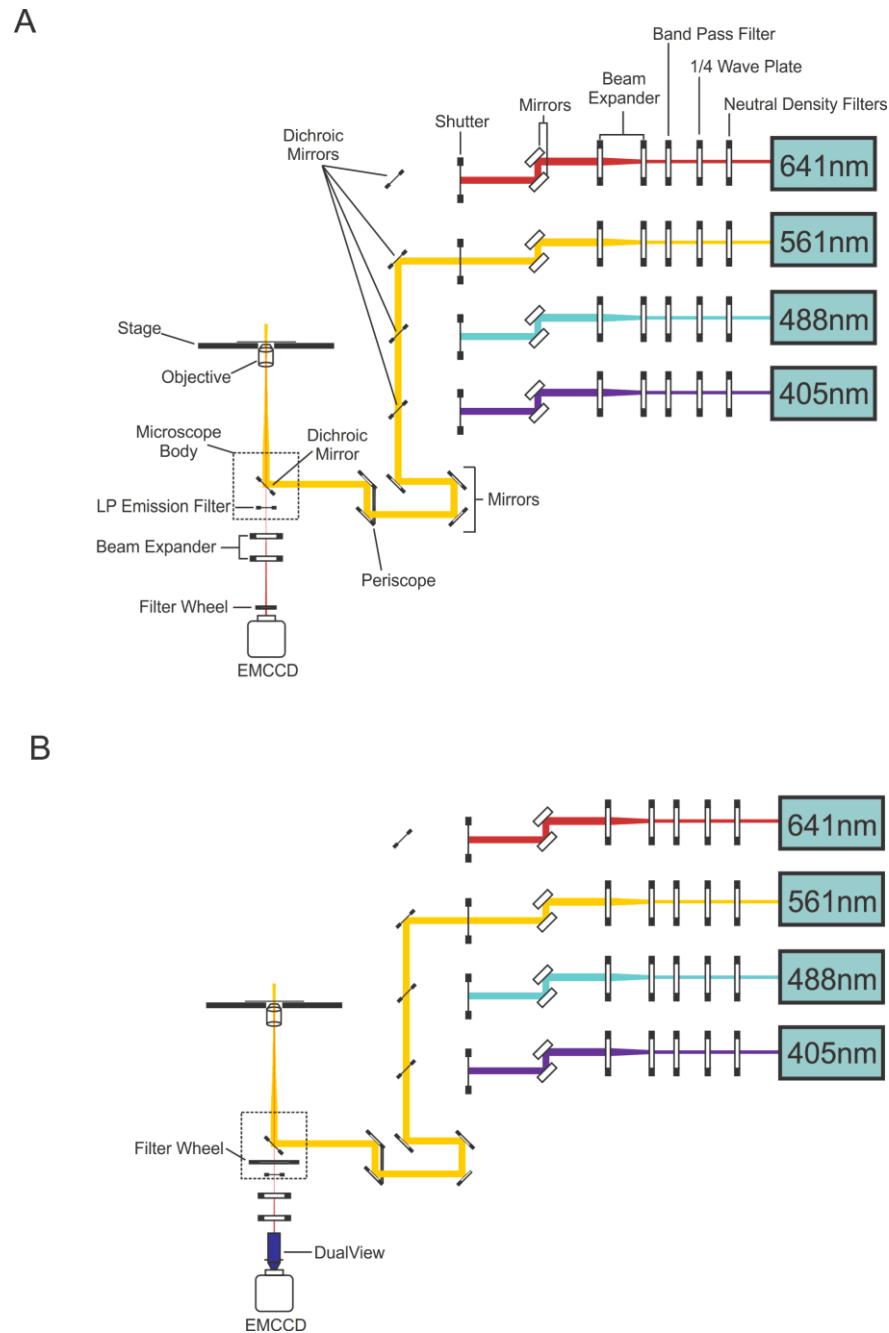


**Figure 3-1. Schematic representation of custom built PALM microscope.**

Outline of A) SR2.1 and B) SR2.2 PALM microscopes. In both cases, all shutters are displayed as closed, except for the 561nm laser line, which depicts the light path into the microscope and onto the sample.

Both microscopes were fitted with four lasers spanning the visible spectrum: 405nm, 488nm, 561nm and 641nm. This allowed for the potential of single colour experiments with different fluorescent probes or dual colour experiments with two spectrally separated fluorophores. After each laser, two sets of neutral density filters were used to control the laser power that reached the sample. This is important in SMLM experiments as laser power can be used to control both the rate of photoconversion/photoswitching of fluorescent proteins as well their brightness. Thereafter, each laser line displayed a

quarter-wave plate in order to convert the linearly polarised laser light into a circularly polarised beam. Circular polarisation of the laser beam is necessary in order to ensure that differentially orientated fluorophores within the sample are excited, rather than just those whose dipole orientations match that of the linearly polarised beam.

The circularly polarised beams were then passed through a band pass filter with bandwidths that match the specified output wavelengths of the lasers. This was to ensure that no wavelengths shorter or longer than that desired reached the sample, helping to prevent potential photobleaching, activation or autofluorescence from extraneous light. Each laser beam was then expanded and collimated with a custom designed Galilean beam expander, using two (plano-concave/convex) matched lenses. Beams were expanded to increase the laser footprint on the sample, and thereby utilise the whole chip on the camera. Collimation was also important to prevent the beams from over expanding or focussing before they reached the sample.

The path of each expanded and collimated beam was opened or closed controlled by individual automated shutters. The beams were then coupled with the use of dichroic mirrors and were co-aligned to ensure spatial overlap of the beam footprints on the sample. Finally, the beams were focussed on to the back focal plane of an apochromatic TIRF objective lens using a plano-convex lens, thus ensuring a widefield illumination regime with a near-collimated beam emergent from the objective lens. The objective lens specification was 60x magnification, a high numerical aperture of 1.45 and was mounted on the objective turret of an Olympus IX71 inverted microscope body for SR-2.1, or in the case of SR-2.2 the upgraded IX-82 inverted body. In both cases a multi-band dichroic (405m/488nm/561nm/635-25nm) was used within the body of both microscopes in order to separate the fluorescence signal from reflected laser emission. Furthermore, both configurations were fitted with motorised stages that possessed custom-built steel inserts to increase microscope stability. Axial stability of the microscope during imaging was maintained by a constant focus device (C-focus, MCL – described later).

The emission path for the sample fluorescence was the major difference between the SR-2.1 and SR-2.2 configurations. Within SR-2.1 the emission was reflected out of the camera side port of the microscope body, where it was expanded by a 2.5x Olympus photo-eyepiece and passed through a motorised filter wheel before reaching the detector.

One major advantage of the IX82 microscope body of SR-2.2 was the ability to insert optical components between the objective lens and the tube lens, in what is known as ‘infinity space’. This space in the microscope is where light is not focussed but propagates as a collimated beam of parallel rays. Any optics that are inserted into this space will therefore not influence the focal plane of the final image. Thus we decided to insert the motorised filter wheel inside the microscope body so that there would be minimal chromatic aberrations when switching colours in future dual colour imaging. After passing through the filter wheel, fluorescence was directed out of the microscope side-port, expanded by a 2.5x photo-eyepiece and finally passed through a Photometrics DualView multichannel imaging system. In ‘bypass mode’, the fluorescence reached the detector without further filtering. The DualView system was installed into the SR-2.2 set-up for future two colour experiments that do not feature in this thesis.

In both configurations, the detectors were back-illuminated cooled EMCCD cameras from Photometrics. SR-2.1 was equipped with the Evolve 512, whereas SR-2.2 was fitted with the newer Evolve 512 Delta. The final image pixel size for both machines was optimised (by the use of the 2.5x photo-eyepiece) to 107nm and 110nm for SR-2.1 and SR-2.2 respectively. This was based on a study that highlighted the importance of having a final pixel size which was the equivalent to 1 standard deviation of the predicted point spread function of the microscope (Thompson 2002).

Finally, the shutters, emission filter wheel, camera and stage were controlled remotely using the open-source software Micro-manager (Edelstein 2010). For data acquisition that required alternating laser illumination, custom routines written for Micro-manager’s script panel were provided by Dr Steven Lee or Dr Remi Boulineau.

### **3.3. PeakFit – A single-molecule localisation microscopy image processing program**

The raw data generated in PALM based experiments and the post-acquisition processing differs significantly from standard fluorescence images. These are often single exposures at different focal depths within a cell, which capture emission from all fluorescent molecules at once. As discussed in the introduction, the aim of SMLM techniques is temporal separation of fluorescence, in order to detect emission from single molecules.

Thus, in contrast to conventional fluorescent images, raw PALM data exists as movies of the sample that have been recorded with a user-defined exposure per frame. Within each frame, there will be areas of intensity, corresponding to emission from single fluorescent molecules. In order to create the final super-resolved image, each molecule that is detected is localised by fitting each PSF with a 2D Gaussian distribution. Further processing can include filtering of molecules based on their intensity, size of PSF or precision of localisation.

Most of the early programs written to handle SMLM data were done so in programming environments such as MatLab and IDL (Betzig 2006, Hess 2006, Manley 2008). Each software package was written for a specific project, in a specific laboratory by a select group of people. This makes these programs difficult to use if one is not familiar with the programming language. Several groups have aimed to release full SMLM program packages that are designed to be easy to use, with graphical user interfaces hiding the background code (Henriques 2010, Wolter 2012). These programs are a good step forward to making SMLM more accessible to researchers who are not familiar with programming. However, during this project a fully customisable software package was desired, to allow flexibility and to ensure accuracy in post-acquisition processing. Thus, as part of this project, I collaborated closely with Dr Alex Herbert (University of Sussex) who created a custom SMLM software package that runs in the ubiquitous image manipulation software ImageJ, called PeakFit.

This software was developed continuously throughout the duration of this project, and in this thesis, I will be referring to PeakFit as the data collected during this project was analysed with it. However, I would like to note that the writing and development of the program was the sole achievement of Dr Alex Herbert. My role in the evolution of the software was suggesting new functionalities, providing test data and as an end-user. PeakFit was recently compared against other SMLM software programs in the Localisation Microscopy Challenge. Published results place PeakFit as third best of 28 tested for low density PALM-like data and fifth best of 16 for high density STORM-like data (Sage 2015). All PeakFit parameters used for each experiment within this study are listed in the Materials and Methods chapter.

### 3.4. Assessing custom microscope stability

The aim of single-molecule super-resolution microscopy is to localise the positions of single fluorophores with nanometre precision. As this involves temporal separation of the emission of fluorophores, data acquisition during such experiments can be lengthy. During data acquisition, the stability of the microscope is of paramount importance in order to provide accurate information regarding molecule positions. Sample drift during imaging could create artefacts in the final reconstructed image and thus it was important to control movement in both lateral and axial dimensions.

In both microscope configurations, axial drift was controlled by the installation of a constant focus device (C-focus®, Mad City Labs). This device is a closed loop system that measures the position of the stage relative to the objective lens during data acquisition. If at any point the distance changes i.e. drift in the  $z$ -plane, the system corrects for this by moving the position of the objective via a piezo nano-positioner. In order to ensure that this equipment was suitable for maintaining axial stability for the time periods require for PALM imaging, the stability was measured by an imaging timecourse of fluorescent beads.

Fluorescent beads (Tetraspeck Microspheres 0.1  $\mu\text{m}$ ) were adsorbed onto a clean coverslip and imaged by excitation with the 561nm laser line once every minute, over a 30 min time period. This experiment was performed either with or without the focus lock of the C-focus engaged (Figure 3-2). Without the focus lock a clear axial drift was observed by the end of the experiment, highlighted by the defocusing of the Airy disk from the fluorescent beads (Figure 3-2A). Conversely, the use of the focus lock resulted in no defocusing, suggesting no axial drift over the time course. This result shows that during the acquisition of a typical PALM data set, no detectable axial stage drift will occur with the C-focus engaged. It is important to note however that this system only corrects for movement of the stage during imaging, any  $z$ -drift of the sample will not be detected. Thus it was important before experiments to let the immersion oil settle for at least 15mins after placing the sample on the microscope. In addition, rare earth magnets were used to prevent the coverslip from moving on the stage.

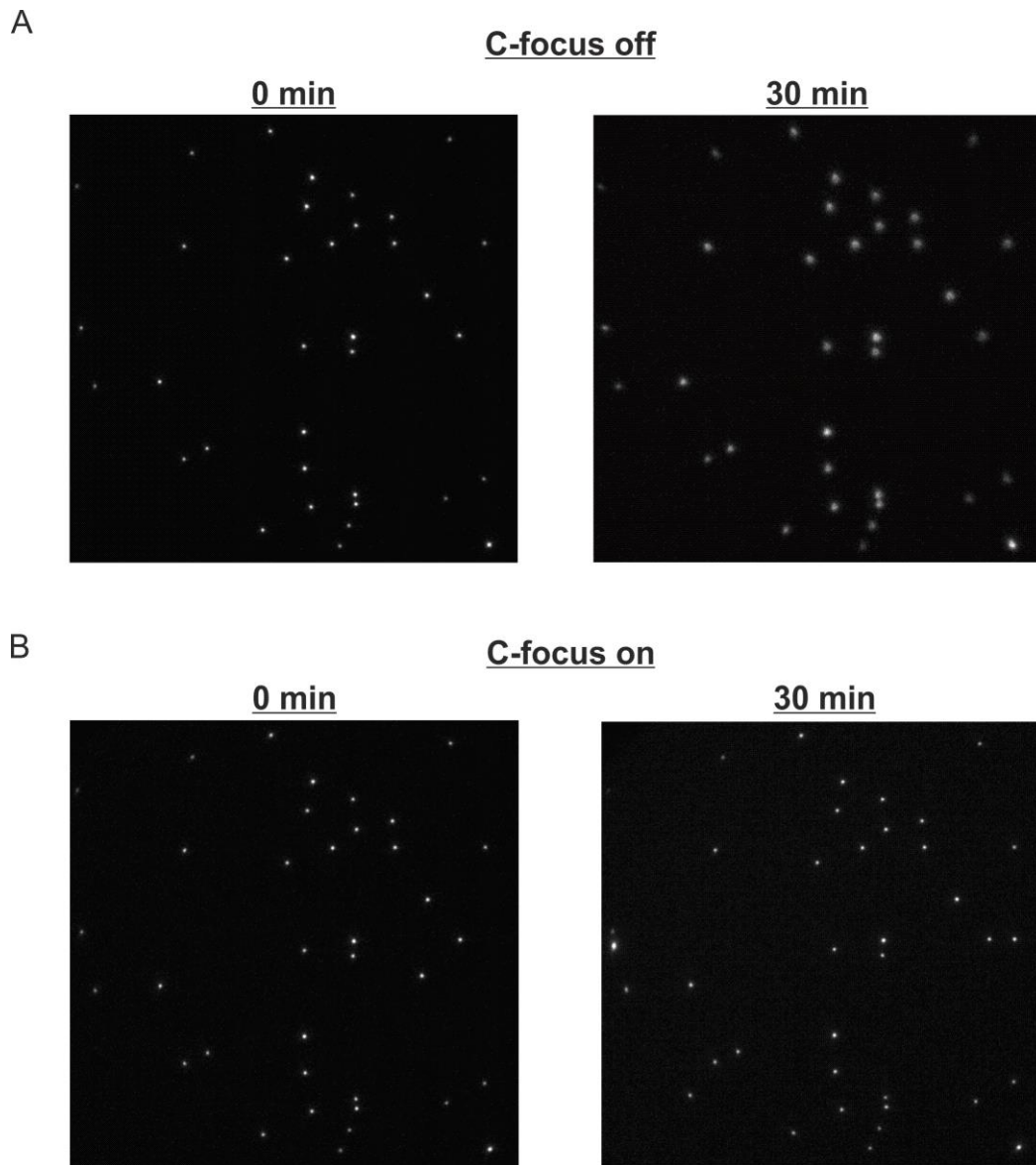


**Figure 3-2. Preventing axial drift using C-focus system.**

Images of fluorescent beads at the beginning '0 min' and end '30 min' of a 30min time period A) without or B) with C-focus focus lock engaged. Beads were excited by 561nm laser and images are 50ms exposures.

Lateral drift in the  $x$ ,  $y$  dimensions may also have potential impact of PALM imaging and the final images created. In order to assess the lateral stability of the microscope, the  $x$ ,  $y$  positions of fluorescent beads were measured over the course of a 30-minute imaging period. With the C-focus focus lock engaged, beads were imaged once every minute for 30 minutes as described before, and were localised by PeakFit software. Positions of the beads in  $x$  and  $y$  were extracted from the PeakFit results table for every time point and plotted as a scatter graph to observe drift (Figure 3-3A). The results from this experiment demonstrate substantial lateral drift during the 30 minutes imaging period. The localisation of the beads revealed both a movement in  $x$  over time of  $\sim 400\text{nm}$ , and a near

oscillating movement in  $y$ . The stability of microscopes can be affected by both temperature changes and air currents. In order to prevent such environmental fluctuations influencing the microscope stability, a custom-built wooden enclosure was built to surround the microscope. Repeating the  $x, y$  stability experiment with the microscope enclosed revealed a substantial increase in stability (Figure 3-3B). As a constant temperature of 18°C was maintained during imaging to prevent any thermal fluctuation in the equipment, the large drift in Figure 3-3A was probably due to air currents from air conditioning equipment. Although the large fluctuations in drift were reduced, small sub-pixel (<107nm) displacements were still noticeable over time which can be corrected for when reconstructing future super-resolution images.

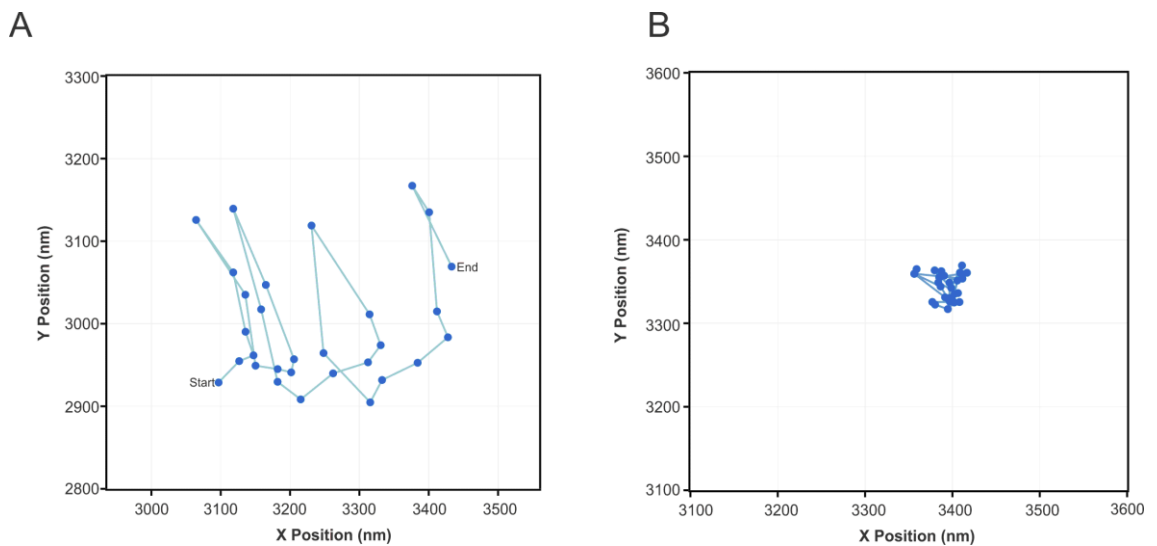


**Figure 3-3. Increasing lateral stability of the PALM microscope.**

Representative  $x, y$  localisation positions of single fluorescent beads over 30 one-minute time points either A) without or with B) custom-built wooden enclosure.

### 3.5. An optimised fission yeast sample preparation protocol for PALM imaging

Fundamental to PALM imaging is the detection of fluorescent events from single fluorophores. Precise localisation of molecules by least squares fitting of the two-dimensional PSF image relies on, amongst other parameters, the number of photons collected per molecule and the number of background photons detected per fitting window (Thompson 2002). The total number of photons released from a molecule cannot be controlled by the experimenter, thus is considered limited. However, the amount of background photons detected can be controlled, to some extent, by careful sample

preparation. Low background fluorescence will ultimately result in better single molecule detection and increased precision of localisation. Thus substantial efforts were made to optimise a sample preparation protocol for imaging fixed *S. pombe* cells, the resulting protocol is described below, specific manufacturer details are described in Material and Methods chapter.

*S. pombe* strains were cultured overnight to a density of  $5 \times 10^6$  cells/ml. The choice of growth media will be discussed in the next section. Cells were then harvested by centrifugation of 1-2ml of liquid culture depending on the number of cells required. Samples were then washed once with PBS before being fixed in formaldehyde solution for 20mins (1% formaldehyde in PBS). Washing cells in double distilled water instead of PBS resulted in increased background fluorescence caused by probable hypotonic lysis of dead cells. After fixation, the sample was then washed three times in PBS before re-suspending cells in 10-20 $\mu$ l PBS. It was important during the washing steps to position the pipette at the surface of the liquid and remove the supernatant slowly from the top, as this is where cell debris accumulates during centrifugation. Failure to remove this cell debris result in high levels of background fluorescence during imaging.

There are several methods which can be employed to prevent fission yeast cells from moving during microscopy experiments such as, poly-l-lysine or concavalin A treated slides. However, in this study it was found that the most reproducibly clean method was immobilisation on agarose. A 1.2% agarose pad was made by sandwiching molten agarose between two coverslips. It was imperative that that coverslips were cleaned prior to making the agarose pad, otherwise this resulted in substantial background fluorescence. Cleaning was performed by ozonation in the presence of UV light. Once set, a small square was cut into the pad to which the sample was placed. Once the liquid from the sample had soaked into the agarose, the square was then sandwiched between long (22mm x 40mm) and small (22mm x 22mm) clean coverslips. In order to prevent any evaporation from the agarose pad and subsequent shrinking during imaging, the sample was sealed around the edges with paraffin wax (Figure 3-4). This protocol reproducibly resulted in samples that possessed minimal background fluorescence.

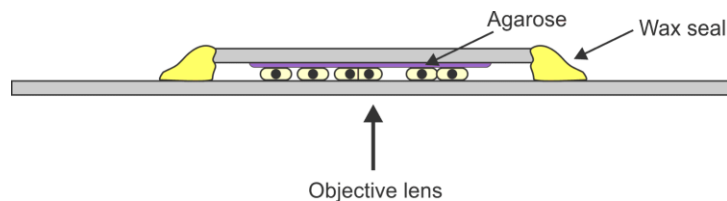


**Figure 3-4. Schematic representation of *S. pombe* sample preparation for PALM imaging.** Fission yeast cells were placed on a 1.2% agarose pad and sandwiched between two pre-cleaned No. 1.5 glass coverslips. The sample was then sealed with molten paraffin wax to prevent evaporation from the agarose.

### 3.6. Assessing the impact of cellular autofluorescence on PALM experiments in *S. pombe*

It is a well-known phenomenon that yeast cells can produce fluorescent emission during fluorescence microscopy experiments, in the absence of a fluorescent marker such as GFP. This ‘autofluorescence’ can make it difficult to image proteins that are expressed at low levels as it may hide the signal from chosen tag. Autofluorescence could potentially limit PALM imaging by preventing detection of fluorescence from single molecules above background. In order to assess whether cellular autofluorescence would have an impact on such sensitive imaging in fission yeast, untagged fixed cells were illuminated with a 561nm laser and continuously increasing levels of 405nm, thus mimicking a standard PALM experiment. Processing of the raw data with PeakFit localisation software revealed substantial numbers of single molecule localisations occurring within the cells (Figure 3-5A).

These autofluorescent events were not limited to the early stages of the experiment as they were detected throughout the imaging period, and thus could not be pre-bleached. This presented a limiting factor for future experiments in the Carr lab, which were focussed on potentially utilising PALM for extracting quantitative information regarding protein complex stoichiometry. Thus, it was beneficial to try to prevent these autofluorescent events from being detected. The most practical possibility was to filter out the ‘false’ localisations spectrally, using optical components within the microscope. SR-2.1 was originally fitted with a 593/40nm band pass filter in order to filter sample emission when imaging with the 561nm laser. In order to prevent as much autofluorescent emission from being detected as possible during mEos3 based PALM imaging, an alternative band-pass filter (580/14nm) was sourced which had a narrower transmission

window, centred on the peak emission of mEos3.1 (Figure 3-5B). Untagged cells were then imaged as before, but this time using the new band-pass filter. The number of localisations detected on average per cell was reduced when imaged with the narrower band-pass (Figure 3-5C). This filter also reduced the total integrated autofluorescence detected from within the cell (Figure 3-5D). This would be potentially beneficial for future experiments that require high localisation precision as the number of background photons detected can be a limiting factor (Thompson 2002).

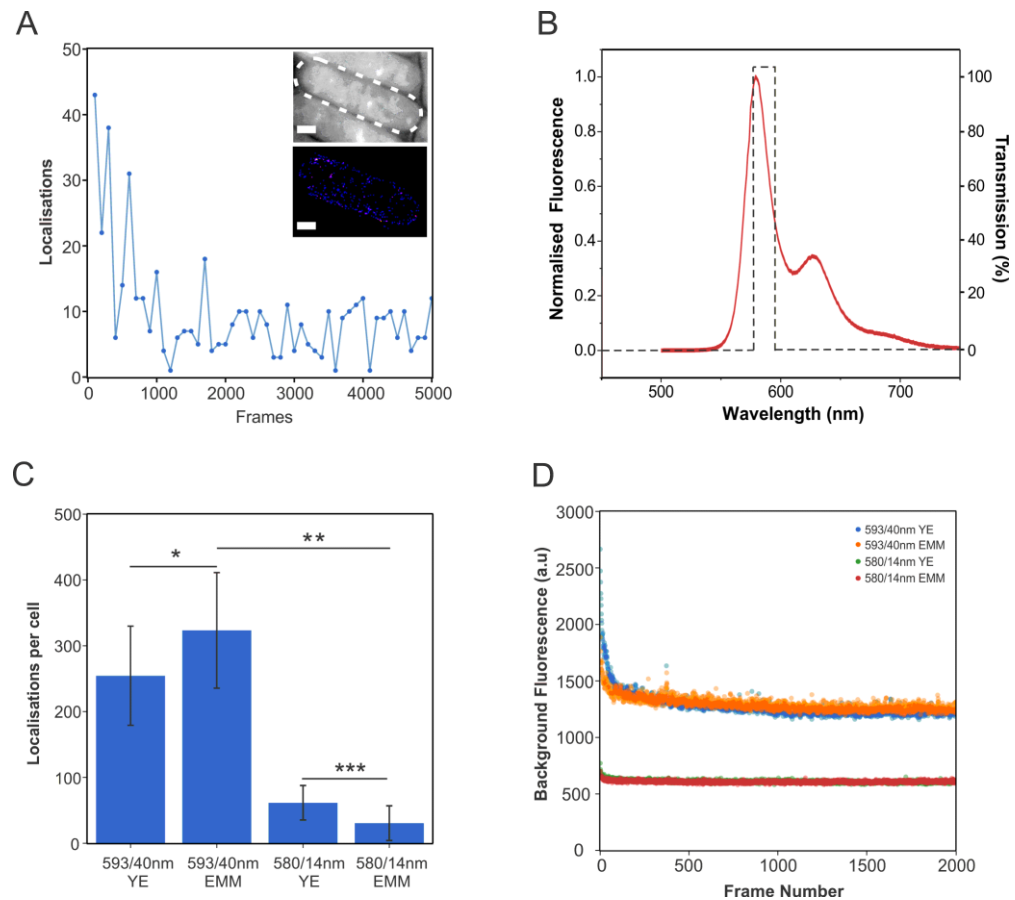


**Figure 3-5. Detection and removal of autofluorescent localisations during PALM imaging of fission yeast.**

A) Detection of single molecule localisations inside a representative untagged fission yeast cell. Cells were imaged for 5000 frames with an exposure time of 100ms. Localisation counts are binned every 100 frames. Inserts: average intensity projection of fission yeast cell and plotted single molecule localisations. Scale bar equal to  $2\mu\text{m}$ . B) Emission spectra for photoconverted mEos3.1 (red) and overlaid fluorescence transmission of the 580/14nm band-pass filter (dashed). Adapted from Zhang 2012. C) Average single molecule localisations detected and D) Integrated fluorescence intensity traces of cellular background fluorescence during PALM imaging of untagged fixed fission yeast. Cells were grown in either YE or EMM media overnight and then imaged using either a 593/40nm or a 580/14nm emission filter. Statistical tests were performed using two-tailed Student's T-test. P values: \* = 0.03, \*\* =  $9.8 \times 10^{-8}$  and \*\*\* = 0.03.

As well as spectral filtering, the effect of different growth media on the presence of autofluorescence was determined. Cells were either grown overnight in yeast extract (YE) or edinburgh minimal media (EMM). Without the 580/14nm bandpass, cells grown in EMM exhibited slightly more autofluorescent localisations than cells grown in YE (Figure 3-5C). The growth media had no effect on total integrated background fluorescence. However, when imaging with the 580/14nm filter, cells grown in EMM showed consistently lower levels of autofluorescent localisations than cells grown in YE. This effect was weakly significant but consistently reproducible. It was also noticed that there was less fluctuation in autofluorescence between experiments when using cells grown in EMM. In conclusion culturing cells in EMM media and imaging with a 580/14nm band-pass filter reduced levels of ‘false’ single molecule localisations, and was subsequently used as the default imaging approach. Further observations were noted during this study that affected autofluorescence levels. Firstly, fresh starting patches of yeast strains prior to inoculation in media resulted in low levels of autofluorescence, as did keeping strains on EMM agar plates. Also, pre-culturing cells two days before imaging and subsequent dilution with fresh media to prevent the culture becoming too dense ( $>1 \times 10^7$  cells/ml), helped keep autofluorescence levels low.

### **3.7. Assessing the effect of 580/14nm emission filter on mEos3.1 detection in *S. pombe***

Photoactivated localisation microscopy requires the use of photoactivatable or photoconvertible fluorophores to provide temporal control of fluorescence emission. PALM was first demonstrated with a range of such fluorescent proteins: PA-GFP, Dronpa, Kaede and EosFP (Betzig 2006). Since this first demonstration, efforts have been focussed on development of new photoactivatable/photoconvertible proteins, and when this study was initiated, the EosFP variants mEos2 and mEos3 (McKinney 2009, Zhuang 2012) were considered optimal for PALM imaging. As mEos2 had been shown to aggregate when expressed at high levels, mEos3 was the chosen fluorophore for this study.

In order to demonstrate PALM in fission yeast and to learn some of the basic characteristics of mEos3 prior to designing future experiments, the fluorophore was expressed in cells from the *urg1* promoter. This promoter had been previously utilised in

the Carr lab as a means of regulating gene expression by insertion of open reading frames at the *urg1* locus (Watson 2011, Watson 2013). Upon addition of uracil to growth media, expression of transcripts from the *urg1* locus are induced resulting in a subsequent increase in protein levels. Previously, mEos3.1 had been positioned under control of the *urg1* promoter by Dr Adam Watson. This strain (AW790) was subsequently used in this study to observe mEos3.1 photoconversion in fission yeast.

The implementation of the 580/14nm emission filter in order to remove autofluorescence could potentially have detrimental effects on the final PALM image quality. From the emission spectrum of photoconverted mEos3.1 it is clear that the narrow filter could prevent a substantial amount of mEos3.1 fluorescence from reaching the detector (Figure 3-5B). As the localisation precision of each molecule is limited by the number of photons detected, it was a concern that the narrow filter could limit the potential for producing super-resolution images. To address this concern, mEos3.1 was imaged in fixed AW790 cells either using the 580/14nm or 593/40nm emission filters and the number of photons per localisation was measured. This experiment showed a clear reduction in the number of photons collected per mEos3.1 localisation when the 580/14nm filter was used (Figure 3-6A). However, this reduction in the number of photons per localisation did not greatly affect the average precision of localisation (Figure 3-6B). In the case of the 593/40nm emission filter, a median of 552 photons resulted in a median localisation precision of 16.5nm. Whereas, a much reduced median of 230 photons per localisation, resulted in 22.6nm average localisation precision for the 580/14nm band pass. The precision of localisation may only change slightly due to the fact that the measured background in the fitting window during localisation is significantly decreased when using the 580/14nm emission filter (Figure 3-6C). Overall, installation of the narrow band pass into the microscope did slightly reduce PALM image quality, however only by 6nm on average, which was seen as a worthwhile compromise for reducing the number of background localisations. However, if future experiments were focussed more on image resolution of well-defined cellular structures rather than quantification of molecules per se, then it could be beneficial to use the 593/40nm filter to achieve higher precision on average.

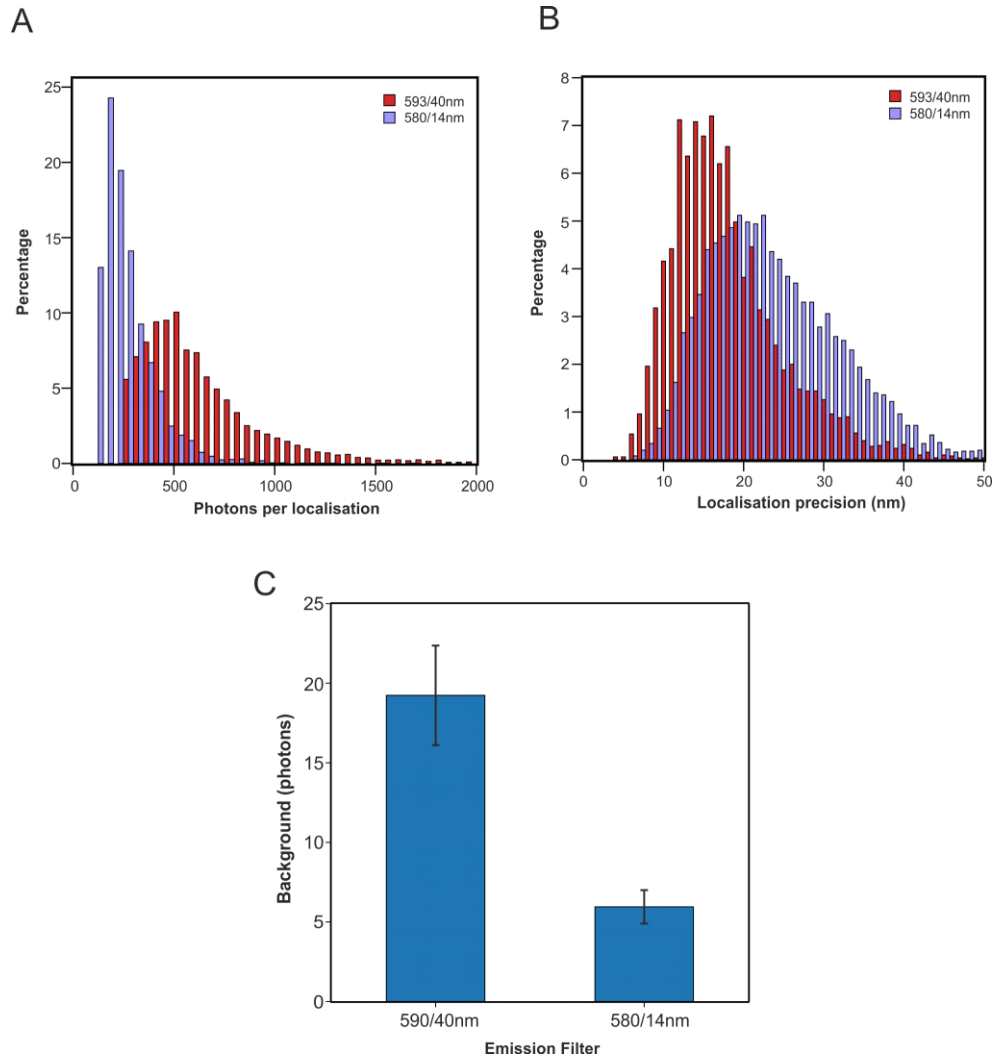


**Figure 3-6. The effect of a 580/14nm band pass on mEos3.1 localisation.**

*urg1-mEos3.1* cells (AW790) were grown in the presence of uracil to induce mEos3.1 expression. Cells were then fixed and PALM microscopy was performed. Data sets of 5000 localisations detected using either the 593/40nm or 580/14nm band-pass filter were compared for **A**) photon count per mEos3.1 localisation, **B**) mEos3.1 localisation precisions and **C**) Background photons calculated for fitting window.

### 3.8. Summary

The data presented in this chapter demonstrate the successful installation of a custom-built PALM microscope in the Carr lab. The main aim of the work presented was to learn the specifics of how the PALM microscope and methodology work, and to successfully demonstrate photoactivation and localisation of mEos3 fluorophores expressed in fission yeast cells.

During the initial stages of this project, efforts were focussed on ensuring microscope operational stability and optimal preparation of samples. Axial stability was of great

importance for future experiments in this thesis due to the size of fission yeast cells. Any variation in the axial position would result in data being recorded from more than one focal plane during an experiment. This axial stability was achieved using the C-focus system, however as noted in the material and methods section this stability also relied on constant room temperature, magnets and a period of sample stabilisation. The accuracy of each experiment relied on the strict adherence to this procedure. As demonstrated in Figure 3-3C, sample drift also occurred in the lateral dimension during data acquisition. This was caused mainly by fluctuations in air currents from conditioning units, and thus was substantially reduced by covering the microscope body (Figure 3-3D). However, localisation of fluorescent beads showed that drift still occurred at a sub-pixel level. Due to the type of future experiments described in the next chapters, this drift did not affect data collection or analysis.

Once a stable microscope system had been built, the most important factor in the success of each experiment is undoubtedly sample preparation. In order to detect single bursts of fluorescence in PALM experiments the background level of fluorescence needs to be much lower than that of a single fluorophore. The two main sources of background fluorescence were from the cell suspension and the agarose pad. Washing cells several times in filtered PBS and carefully removing the supernatant from the meniscus ensured that background from the suspension was negligible. The use of very clean glassware for agarose preparation and making up fresh molten agarose for each pad guaranteed very low background fluorescence. During the optimisation process, we found that ozonation of the coverslips used to make the agarose pad was also of utmost importance.

At the start of this project, the view was to use PALM for super-resolution based studies of protein localisation and oligomerisation. In order to ensure that localisations detected were from actual mEos3 fluorescent events and not autofluorescence, a narrow band pass filter was installed to filter out as much autofluorescence as possible. This successfully reduced the amount of false localisations that were detected in wild type cells, and will be important for future experiments in the Carr lab concerned with absolute quantification of protein number. However, as described in the next chapter, the experiments performed for the rest of the project did not aim to study protein localisation/oligomerisation and instead PALM was used as a semi-quantitative read-out of protein association with the chromatin. In this case the level of autofluorescence detected was not as crucial, but the

580/14nm bandpass was still utilised as it helped reduce the overall integrated autofluorescence from cells, which was beneficial at longer exposure times.

# Chapter 4

## Methodological development for the visualisation of DNA bound proteins in unfixed fission yeast

### 4.1. Introduction

During the course of this project, the main aim was to develop ways of using photoactivated localisation microscopy to study proteins involved in DNA metabolism, specifically DNA replication. This field has particularly benefited from high-end microscopy platforms, including SMLM techniques (discussed in introduction, reviewed in Stracy 2014). However, these studies have largely been performed in prokaryotic model organisms exploiting their physical dimensions as the small axial sizes of bacterial cells match the focal depth of the microscope. This allows researchers to image the whole cell without the need to take multiple images from different  $z$ -planes. This permits the use of techniques such as Total Internal Reflection Fluorescence (TIRF) microscopy and single particle tracking techniques. Experiments in these systems have focussed on detecting individual replication events and attempting to quantify the number of individual proteins at replication forks (Reyes-Lamothe 2010, Su'etsugu and Errington 2011). More recently, DNA repair events have been detected in bacterial cells by using single particle tracking PALM, allowing researchers to probe residency times of repair factors on DNA (Uphoff 2013). There are clear advantages of using SMLM approaches within this field and as previously mentioned there is now a need to develop SMLM protocols that are applicable to larger eukaryotic model organisms, such as *S. pombe*.

PALM was designed to increase the resolution of fluorescence microscopy images, in order to visualise biological structures in detail greater than previously achieved. Furthermore, it has the ability to provide quantitative data on protein stoichiometry as the method relies on seeing one fluorescent molecule at a time. To date many studies using single-molecule based super-resolution approaches have focussed on phenomena paralleled in structural biochemistry which have a repetitive structure or known stoichiometry such as microtubules (Heilemann 2008) or nuclear pores (Szyzborska

2013). This acts as an internal control for such experiments as the researcher already knows what structure/stoichiometry to expect. Such ordered repeating protein structures, are not known to exist in the molecular pathways underlying the major DNA metabolism processes. This presented a challenge in that there was no positive control to certify that observations at this new improved level of resolution were not due to artefacts born from sample preparation or post-acquisition image processing.

Most proteins involved in DNA metabolism are typically localised within the nucleus and only transiently interact with the chromatin. These interactions may involve either direct binding to the DNA via specific domains or they may bind to other proteins that are involved in the same pathway. Moreover, the chromatin association of some proteins is often strictly controlled, occurring only during specific cell cycle stages or in response to DNA damage. Regardless of the mechanism of recruitment to the chromatin, it is this event that we are interested in studying during such processes. PALM microscopy presents opportunities to learn more about such recruitment at greater resolution as well as potentially extracting quantitative information on protein quantity.

Standard fluorescence microscopy protocols for visualising spatial organisation of proteins in fission yeast usually involve chemical fixation of the sample with either an aldehyde or methanol. However, in this chapter I will discuss how the use of such fixation methods when attempting to visualise only chromatin-associated proteins in *S. pombe* is not compatible with PALM. This incompatibility stems from the immobilisation of a freely diffusing sub-population of molecules, thus leading to an inability to distinguish between chromatin bound or un-bound molecules. The realisation of this unsuitability lead to the development of a PALM-based approach that enables the observation and relative quantification of chromatin-associated proteins inside unfixed fission yeast cells. This technique uses motion blurring of fluorescence via increased detector exposure times as a way of filtering out the freely diffusing population of molecules in the nucleus. This adaptation facilitated the observation of chromatin-associated replication proteins and the quantification of levels of association in different cell cycle stages and distinct genetic backgrounds.

## **4.2. Effect of cross-linking on PALM experiments focussing on DNA bound proteins**

In order to study DNA replication proteins via PALM microscopy it was important to understand the type of images that would be generated and to consider the type of data we would be able to extract. With this in mind, a basic PALM experiment was designed aimed at detecting the well-characterised replicative helicase (MCM 2-7) in two distinct cell cycle phases and comparing the observed outcome to previously reported data. The DNA association of the MCM helicase is widely studied and has been shown to be recruited to DNA during late M-phase/early G1 and persists to the end of S-phase (Kearsey 2000, Mendez and Stillman 2000). Upon completion of replication, replisomes are dismantled, MCMs dissociate from the DNA and the cell passes into G2 phase (Maric 2014). Thus it was hypothesised that when comparing G2 and S-phase fission yeast expressing a fluorescently labelled MCM subunit, that there would be distinct differences in the final images. The prediction was that more MCM proteins would be visualised during S-phase and the spatial distribution of single molecule localisations would change.

To demonstrate it is possible to study MCM proteins at super-resolution, a strain expressing the Mcm4 subunit C-terminally tagged with mEos3.1 fluorescent protein was created (Materials and Methods). This strain was cultured in EMM liquid media (for reasons described in the previous chapter), and small G2 cells were isolated by lactose gradient centrifugation. Initially, cells were then chemically fixed with formaldehyde in either G2 or after incubation for a further 120mins to enrich for binuclear septated S-phase cells. Each sample was then subjected to PALM imaging at a standard exposure time of 100ms per frame and the raw data was processed using the PeakFit plugin. Reconstructed images were created, drawing each molecule with the average localisation precision of the experiment (15nm) (Figure 4-1A).

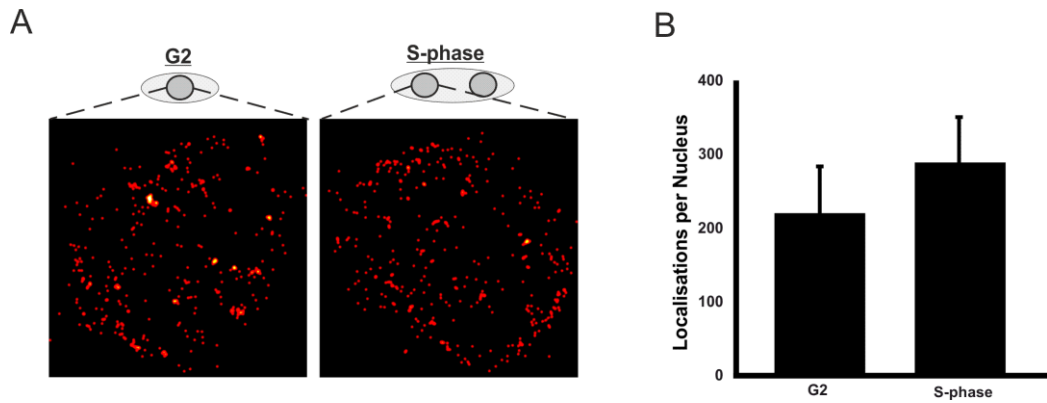


**Figure 4-1. Visualising Mcm4 in fixed cells using PALM.**

A) Representative images of nuclear fluorescent localisations of Mcm4-mEos3.1 visualised in formaldehyde cross-linked G2 and S-phase cells. B) Quantification of the average number of localisations in G2 (219) and S-phase (287) nuclei.

The resulting reconstructed images are very similar, both showing a dispersed pattern with small areas of repeat localisations. The number of localisations per nucleus was also measured and it was found that there were 1.3x more localisations on average in S-phase cells compared to G2 (Figure 4-1B). The reason for the similarity between the two samples was assumed to be due to the chemical fixation of a freely diffusing sub-population of molecules that are not chromatin associated.

Standard fluorescence microscopy experiments designed to study the activity of replication proteins usually consider the formation of bright foci in the nucleus as a marker of activity (Meister 2007). In these experiments, the diffuse unbound sub-species appear as a dull haze, whereas the chromatin-associated molecules in the same diffraction limited area appear as punctate, bright foci. However, the experiment shown in Figure 4-1A demonstrates that increase in resolution is actually a hindrance as one can no longer differentiate between molecules which were diffuse and have become cross-linked to nuclear components or those which were chromatin-associated. Although the increase in the number localisations is a clear difference between the two different cell cycle stages, the presence of such vast number of MCMs detected in G2 and the very similar spatial distribution suggests that it would be very difficult to study changes in protein behaviour with this level of false positives.

Inadvertent crosslinking of freely diffusing molecules is not a novel dilemma and methodologies involving detergent extraction of the soluble proteins have been previously developed. These are mostly used in higher eukaryotic model systems that do not possess a cell wall. However, a similar technique has been demonstrated in *S. pombe*, where the cell wall is partially digested using  $\beta$ -glucanase thus creating spheroplasts, before extracting with Triton X-100 (Kearsey 2000). This technique was attempted in this study; but it was found to be incompatible in our hands as some fluorescent protein remained after detergent extraction, causing single-molecule localisations to appear across the cell. In addition, the methodology resulted in an increase in fluorescent background and inconsistencies in the extent of extraction.

Considering the shortcomings in the approaches above, it was clear that development of a new technique was necessary in order to visualise only the chromatin bound fraction of a protein of interest. The aim of this chapter is to describe an adaptation to PALM imaging developed to enable such experiments.

### **4.3. Methodological hypothesis**

In order to distinguish between chromatin-associated and freely diffusing proteins within a fission yeast nucleus, it was necessary to find a characteristic that allows for their differentiation during image processing. In fixed cells, this is particularly difficult and the only possibility considered was co-localisation with a protein that is known to interact directly with the protein of interest when chromatin bound. This approach would come with its own difficulties, mainly being the potential for false co-localisation due to fixation of freely diffusing proteins. Therefore the direction of the project turned towards unfixed cells as a clear distinction can be made between the subspecies of molecules based on their apparent diffusivity.

The strategy for discriminating between chromatin-bound and unbound molecules was to utilise the effect of motion blurring by extending the camera exposure time during PALM imaging of unfixed cells so as to filter out the diffusing molecules. The reasoning behind this adaptation was that extension of the exposure time would cause the fluorescent signal from the diffusing molecules to become blurred. This blurring would be caused by

diffusing proteins emitting fluorescence from multiple physical locations during the exposure time of one frame. Consequently, the detected fluorescence from a diffusing molecule would no longer approximate the PSF of the microscope and would not be detected in post-acquisition processing (Figure 4-2). In contrast, the diffusion of chromatin-associated molecules will be greatly attenuated by their interaction with the chromatin and thus will be relatively static compared to the diffusing population. In this case, the fluorescence detected from the chromatin-bound molecules will still approximate the PSF and will be detected by the PeakFit program.

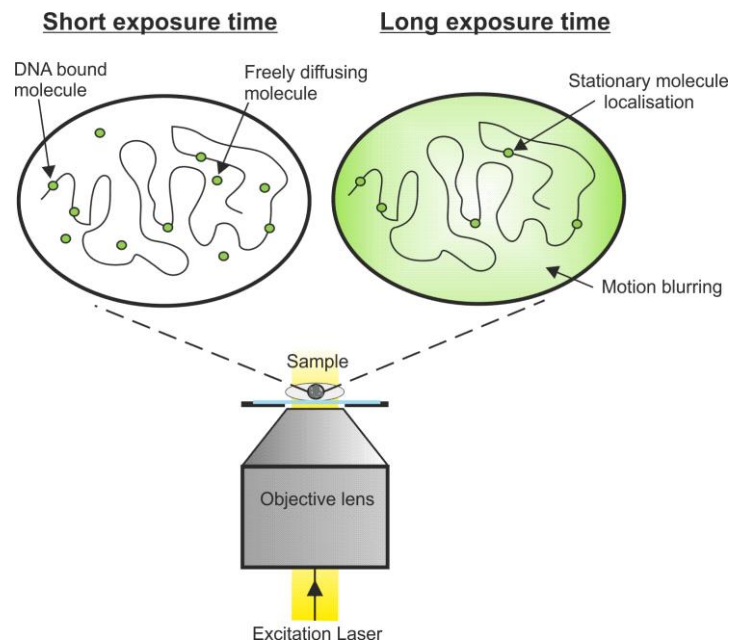


**Figure 4-2. Selecting for chromatin associated proteins using long exposure times.**

A schematic representation of the effect of using extended camera exposure times on the detection of single molecules in unfixed cells. Left: at short exposure times, molecules from both the DNA bound and freely diffusing subpopulations are localised. Right: Longer exposure times cause fluorescence from freely diffusing molecules to blur preventing their detection. Chromatin-associated molecules are relatively static, preventing blurring of the PSF.

The use of long camera exposure times to detect specifically DNA-associated fluorescent molecules has been previously used to great effect in bacterial cells. In these cases, the authors were able to use detection by immobilisation to visualise transcription factor binding (Elf 2007) and more recently DNA-bound repair proteins (Uphoff 2013). Thus, this approach was applied to assess whether it could be used in unfixed *S. pombe* cells as a method for quantifying chromatin associated proteins.

#### **4.4. Extending camera exposure time enables selective detection of chromatin-associated proteins in unfixed fission yeast**

To assess the potential of the proposed approach for detecting chromatin-associated proteins, the Mcm4-mEos3.1 strain described previously was imaged in either G2 or S-phase at different exposure times. The number of single fluorescent localisations detected per nucleus at each exposure time was used as a quantitative read out of the relative amount of chromatin-bound molecules between each sample. In G2 phase, where the majority of MCM proteins have been shown to be freely diffusing (Kuipers 2011), it was hypothesised that as the exposure time of the camera increased, the number of localisations would substantially decrease. However, when the same approach is applied to S-phase cells, the prediction was that the presence of a static chromatin-bound population of Mcm4 would lead to a higher number of localisations per nucleus. It was considered that the blinking and bleaching rates of mEos3.1 would be unchanged between different samples and thus would not bias the results.

The raw data collected from PALM imaging of Mcm4-mEos3.1 was processed using PeakFit and the number of single molecule localisations were counted in the nuclear region of each cell. Nuclear regions were defined by Z-stack projections of the raw data, instead of using a nuclear stain (Figure 4-3A). This was because the standard DNA stain DAPI is excited by ultraviolet wavelengths around 350-400nm, which is also the wavelength required to photoconvert mEos3.1. Thus, excitation with the 405nm laser to find nuclear regions would cause photoconversion of a population of the mEos3.1 molecules prior to imaging. It is also important to note that only nuclei of cells that were considered to have the focal plane focused in the mid-plane of the cell were counted (Figure 4-3B). This was to prevent any bias in the data sets, which could arise from a high proportion of “out of focus” nuclei.

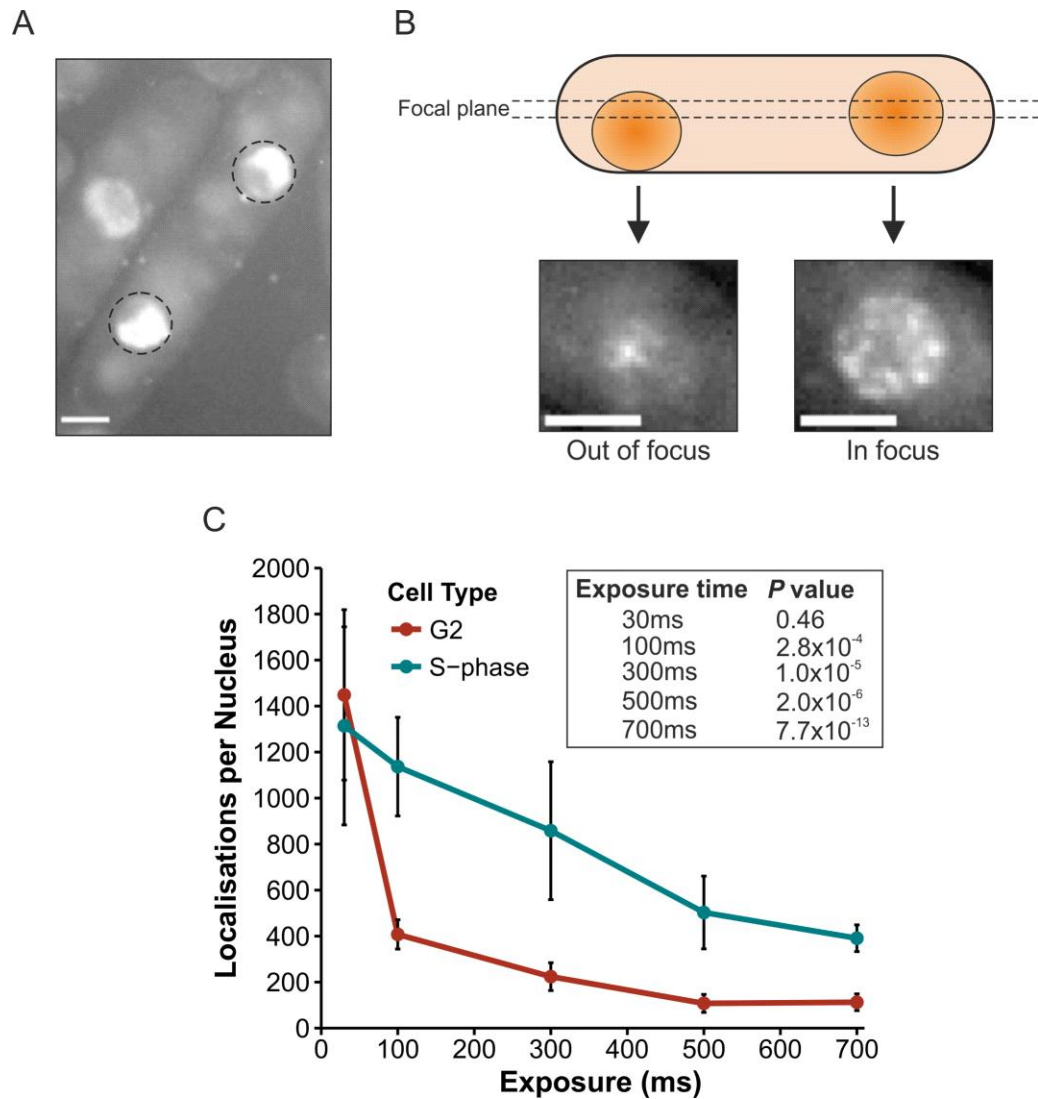


**Figure 4-3. PALM imaging with increasing camera exposure times.**

A) Nuclear regions were detected without DNA staining by Z-projections of fluorescence from Mcm4-mEos3.1, scale =  $2\mu\text{m}$  B) Nucleus positioning within a cell relative to the focal plane. Nuclei deemed to be out of focus (Left) were discarded from processing. Nuclei centered in the focal plane displayed a wide circular appearance. Scale =  $2\mu\text{m}$ . C) Numbers of Mcm4-mEos3.1 fluorescent localisations per nucleus decreases as a function of exposure time. A minimum of 6 nuclei were analysed per data point, error bars = standard deviation. *P* values for each exposure time were calculated as a comparison between G2 and S using a two-tailed Students T-test.

Single molecule localisations were then counted from processed raw data and the average number of localisations was observed as a function of exposure time (Figure 4-3C). At short exposure times (30ms) the extent of exposure is enough to capture diffusing molecules as individual fluorescent puncta that are recognised by the PeakFit program. These fluorescent maxima are indistinguishable from those that arise from chromatin bound proteins. The data from this experiment are consistent with this fact as no significant difference in the average number of localisations per nucleus at 30ms exposure was observed. In accordance with the hypothesis described above, as exposure times were

extended an increasing differentiation between S-phase and G2 cells became evident. Increased exposure time resulted in motion blurring of fluorescence from diffusing molecules preventing them from being detected by the PeakFit localisation software. Whereas, the chromatin-associated molecules in S-phase cells remained relatively static within the exposure time and were not subjected to motion blur effects. This resulted in the number of localisations detected in S-phase cells remaining significantly higher than that of G2 cells as exposure time increased (Figure 4-3C, table of *P* values). The maximum differences between the two cell cycle stages occurred between 100-300ms. These data demonstrate that simply extending the exposure time of the camera allows for the distinction between the chromatin-bound and freely diffusing populations of a protein.

#### **4.5. Optimisation of camera exposure time via modelling of molecular diffusion**

The data shown in the previous section highlight that extending the camera exposure time allows for the removal of localisations from diffusing fluorescent molecules in PALM imaging of unfixed fission yeast, whilst retaining localisations from chromatin-associated molecules. In order to be an efficient protocol the exposure time needed to be optimised and several factors come into play when deciding which exposure time to use. Firstly, reducing the amount of false positive localisations that are detected is of importance. This will depend upon extending the exposure time long enough so that the 3-dimensional diffusion of a single molecule within that time period is enough to cause sufficient blurring of the PSF in 2 dimensions, such that it will not be fit by the PeakFit program. Conversely, over-extending the exposure time could have detrimental effects on the detection of the chromatin bound proteins or true positives, via increasing background fluorescence intensity.

In an attempt to computationally validate the previous observations and determine an optimum camera exposure time such that false positives are reduced and true positives are retained, computer simulation experiments were designed. These simulations aimed to mimic the raw data that would be observed from diffusing Mcm4-mEos3.1 proteins at different camera exposure times. The starting point for these experiments required a robust estimate of the diffusion speed of Mcm4-mEos3.1 proteins inside a fission yeast

nucleus. Thus, a diffusion coefficient was extracted using mean squared displacement (MSD) analysis by performing single particle tracking PALM (sptPALM).

In sptPALM, sparse activation of fluorophores in unfixed cells, coupled with a short camera exposure allows for the tracking of individual diffusing molecules over a series of frames. In this study, a pulsed activation laser regime was adopted whereby a short pulse of the 405nm laser (50ms-500ms) is followed by 500 frames of continuous 561nm excitation (Figure 4-4A). This imaging regime ensured that there was only ~1 molecule active per nucleus during image acquisition. Too many molecules active at any one time could affect the diffusion rate estimation by joining up localisations from multiple molecules to form a molecular track. To build a data set of localisations for sptPALM analysis G2 *S. pombe* cells expressing Mcm4-mEos3.1 were harvested from lactose gradients and were imaged with pulsed activation and molecules were localised post-acquisition using sptPALM PeakFit settings (see Materials and Methods).

After single molecule localisation data sets had been collected, sptPALM and MSD analysis were performed with the help of Dr Rémi Boulineau. This involved firstly grouping single molecule localisations that appear in consecutive frames within a user-defined radius,  $r$  (Figure 4-4B). In the original sptPALM paper by Manley *et al* 2008, the authors implemented a probability distribution to determine accurately the value of  $r$  to set depending on diffusion coefficient,  $D$ . This is given by:

$$P(L, \Delta t) = 1 - \exp\left(-\frac{L^2}{4D\Delta t}\right)$$

which shows the probability of detecting a molecule that has moved by a distance  $L$  during an acquisition time of  $\Delta t$  (0.03s). A threshold of  $r = 800\text{nm}$  was chosen assuming a molecular diffusion of between  $1\mu\text{m}^2/\text{s}$  and  $2\mu\text{m}^2/\text{s}$  (Figure 4-4C). This threshold ensured that the probability of detecting a molecule in the next frame was comprised between 93% and 99%. The radius of 800nm was thus used to join localisations together that appeared in consecutive frames using PeakFit's "Trace Diffusion" plugin. Once a data set of molecular tracks had been achieved, it was filtered such that only tracks that contained a minimum of four steps (5 localisations) were retained for MSD analysis.

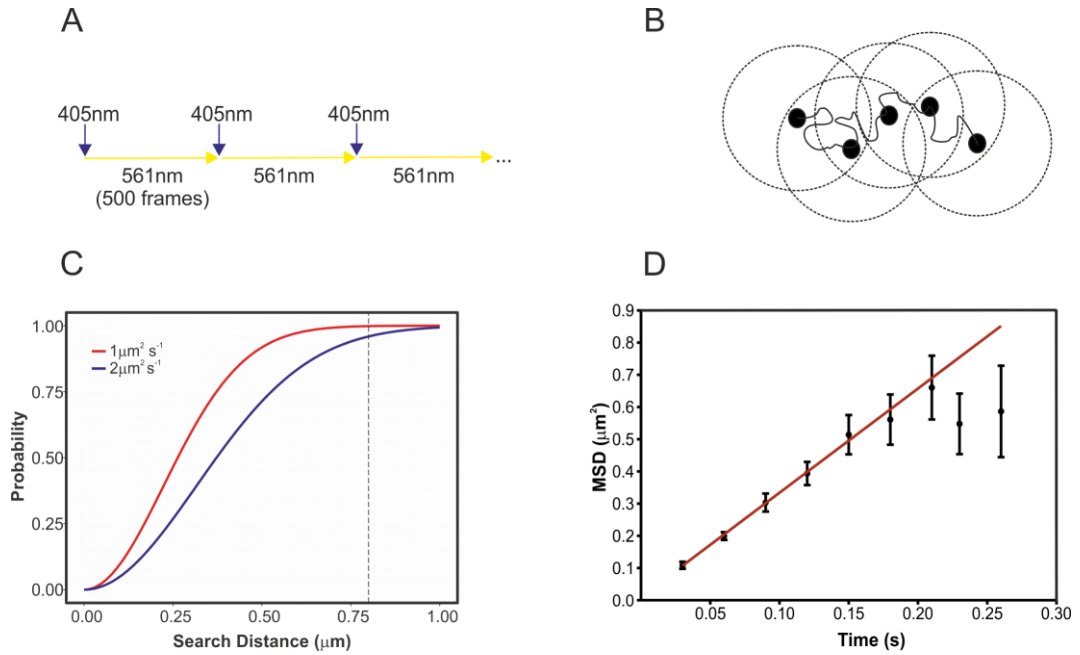


**Figure 4-4. Extracting Mcm4-mEos3.1 diffusion coefficient using sptPALM.**

A) Diagram demonstrating pulsed activation regime used to minimise mEos3.1 photoconversion. B) Diagram representing the use of a user defined search area when tracking single molecules. Black circles denote single molecule localisations, black line represents molecule diffusion path. If a localisation appears with the search area (dotted circles) in a subsequent frame then the localisations are linked. C) Probability distributions for molecules diffusing at  $1 \mu\text{m}^2/\text{s}$  and  $2 \mu\text{m}^2/\text{s}$ . Dotted line represents the selected search distance of 800nm, giving 93-99% probability of detecting a molecule in the next frame. D) Mean squared displacement ( $\pm$ standard error) of Mcm4-mEos3.1 proteins. Linear fit of the first 4 points (red line) leads to extraction of apparent diffusion coefficient of  $D^* = 0.7 \mu\text{m}^2/\text{s}$ . This data was produced with the help of Dr Rémi Boulineau.

Mean squared displacement analysis was performed across all the trajectories by calculating the displacement of each molecule at lag time  $\tau$  relative to the first localisation in the track  $r_i(t)$  using the following expression:

$$MSD(\tau) = \langle [r_i(t + \tau) - r_i(t)]^2 \rangle$$

This analysis was then used to calculate an apparent diffusion coefficient ( $D^*$ ) of freely diffusing Mcm4-mEos3.1 molecules inside the nucleus. This was achieved by linearly fitting point associated with first four lag times of the MSD curve, following the relation:  $MSD = 4D^* \Delta t + 4\sigma^2$  (Figure 4-4C). From the fit, a  $D^*$  value of  $0.7 \mu\text{m}^2/\text{s}$  was extracted from 762 molecular trajectories.

This diffusion coefficient is an underestimation of the real value, due to confinement of the 3D diffusion of Mcm4-mEos3.1 molecules in the nucleus and motion blur effects (Michalet 2012, Uphoff 2013). The displacements between localisations are also 2-dimensional representations of 3-dimensional movements. Thus, in order to estimate the 3D diffusion of Mcm4-mEos3.1 more accurately, computer simulations of particles undergoing 3D Brownian motion were performed using the “Create Data” plugin within the PeakFit analysis suite (performed alongside Dr Rémi Boulineau).

The simulation plugin employs an experimentally derived 3D-PSF thus using a similar PSF profile to that of the microscope. The 3D-PSF was first constructed by imaging 20nm Z-stacks of fluorescent beads and averaging stacks from 9 individual beads (using the “Create PSF” plugin). The simulation plugin then uses this PSF and randomly positions molecules, simulates fluorescent photon emissions based on the characteristics of mEos3 before rendering them to pixels. Attributes for both the camera (such as exposure time and pixel size) and particles (such as diffusion, Z-depth and number of molecules) can be controlled within the plugin.

To simulate 3D Brownian motion within a nucleus, the Create Data plugin was used to simulate molecules in a radius of  $1\mu\text{m}^2$  at a density suitable for single particle tracking. A range of diffusion coefficients between  $1.5\mu\text{m}^2/\text{s}$  and  $2\mu\text{m}^2/\text{s}$  were simulated and then the raw data underwent single molecule localisation and MSD analysis. A 3D diffusion coefficient of  $D = 1.7 \pm 0.3 \mu\text{m}^2/\text{s}$  was found to best match the  $D^*$  derived from the *in vivo* tracking data (Figure 4-5A). This 3D diffusion data was supported by an independent measurement using *in vivo* fluorescence correlation spectroscopy (FCS) data using a strain expressing Mcm4-EGFP. This data was collected by Jem Tucker as part of a Masters degree project run in the Osborne lab. Using FCS a diffusion coefficient of  $D = 1.6 \pm 0.4 \mu\text{m}^2/\text{s}$  was extracted (Figure 4-5B, Etheridge *et al* 2014), which is in agreement with the 3D simulation data.

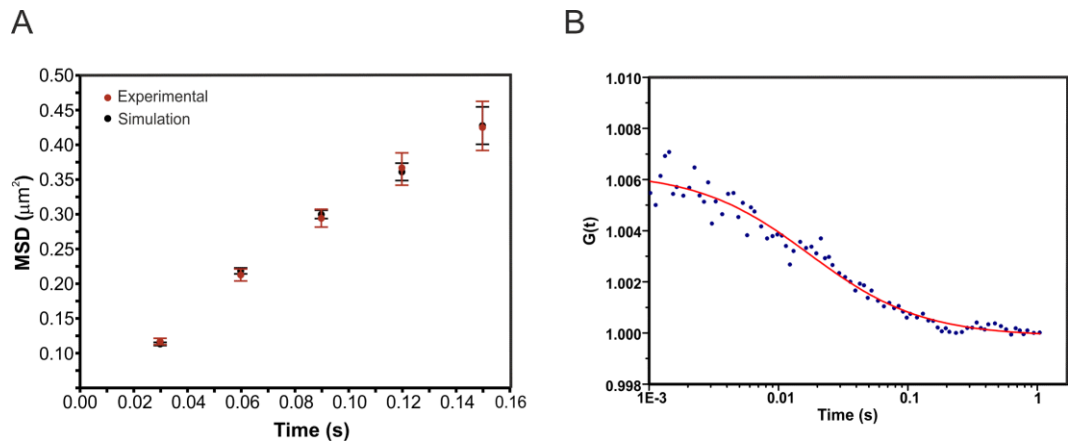


**Figure 4-5. Determination of 3D diffusion of Mcm4-mEos3.1.**

A) Mean squared displacement of experimental (red) and simulated (black) data showing best correspondence of  $1.7 \mu\text{m}^2/\text{s}$ . Simulations of 2D MSD from 3D diffusing molecules inside a sphere of diameter  $2 \mu\text{m}$  ranging from  $1.5$  to  $2.0 \mu\text{m}^2/\text{s}$  ( $n > 1000$  tracks per simulation). This data was collected alongside Dr Rémi Boulineau. B) Representative FCS curve obtained *in vivo* from *S. pombe* cells expressing Mcm4-EGFP. FCS experiments lead to an average diffusion coefficient of  $1.6 \pm 0.4 \mu\text{m}^2/\text{s}$ . This data was kindly provided by Jem Tucker in the Osborne Lab, University of Sussex.

Once a robust 3D diffusion coefficient for Mcm4-mEos3.1 of  $D = 1.7 \mu\text{m}^2/\text{s}$  had been established this enabled for the modelling of diffusing and static molecules at different camera exposure times. The aim of the experiment was to optimise the camera exposure time for imaging chromatin-associated Mcm4-mEos3.1 molecules by observing which exposure time resulted in high true positive recall and low false positive recall. Simulations were performed which mimicked the camera exposure times within a range of 30ms-700ms, similar to the experiment performed *in vivo* in Figure 4-3C. For each simulation, 500 molecules were randomly positioned in confined spherical regions that had a diameter of  $2 \mu\text{m}$ , similar to that of a fission yeast nucleus. Simulations containing diffusing molecules were performed with a Z-depth of 2 microns, mimicking the depth of a nucleus. Whereas, static molecule simulations were performed in two dimensions, simulating chromatin-associated molecules within a focal plane. Raw simulation data was then fitted with the PeakFit localisation software to produce a data set of molecular positions. This data set was then compared to the known positions of the simulated molecules using the “Results Match Calculator” function in PeakFit. Recall of the simulated molecules was measured by calculating the percentage of molecules correctly localised:

$$recall = \frac{tp}{tp + fn}$$

In this calculation, true positives ( $tp$ ) are considered localisations that occur within a 50nm radius of the true position of a simulated molecule. False negatives ( $fn$ ) are considered true positions that do not match with a localisation within 50nm. Using this recall analysis it was clear that exposure times longer than 300ms yielded optimal recall results (Figure 4-6A). At these higher exposure times, recall of static molecules was almost 100%, whereas the recall of diffusing molecules was almost zero. Exposure times greater than 300ms lead to probabilities of localising a diffusing rather than a static molecule of <5% (Figure 4-6B). These results indicate that in order to discriminate maximally between static and diffusing molecules, the longest exposure times are superior, for example at 700ms the probability of localising a diffusing molecule is on average 0.1%.

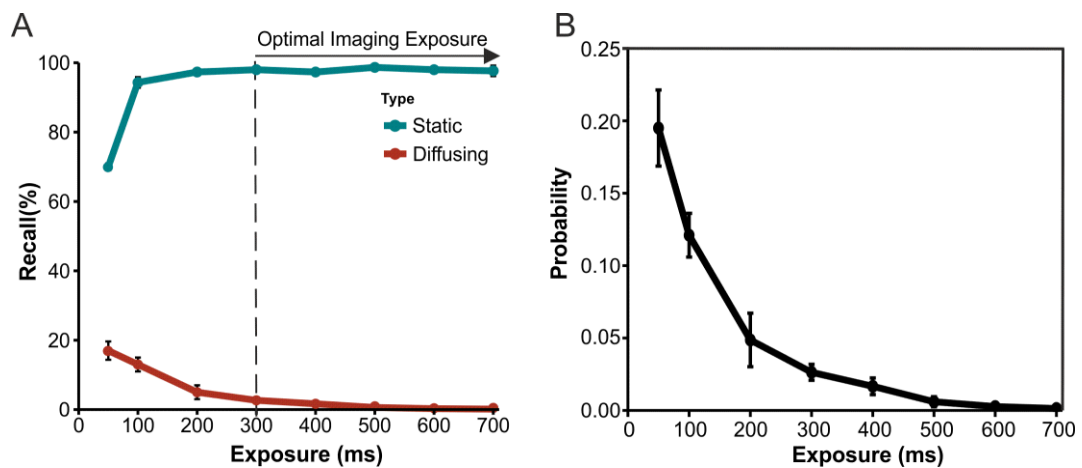


**Figure 4-6. Simulating Mcm4-mEos3.1 diffusion to optimise camera exposure time.**

A) Diffusing ( $1.7 \mu\text{m}^2/\text{s}$ ) and static molecules were simulated with different exposure times and processed using the PeakFit localisation software. The percentage recall of molecules was then analysed by comparing the simulated and localisation data sets. Error bars represent standard deviation calculated from 3 repeats. B) Probabilities of detecting diffusing rather than static molecules at each exposure time. Probabilities were calculated from recall percentages:  $\text{diffusing}/(\text{diffusing}+\text{static})$ . Error bars represent standard deviation calculated from three independent repeats.

However, it was decided that the optimal exposure time to be used for subsequent experiments would be 350ms. The reason behind this decision was based on observations from the *in vivo* experiments in figure 4-3C of a loss of dynamic range at the higher exposure times. This was not seen at the same exposure times in the recall analysis, which is most likely due to shortcomings of the simulations. Firstly as the exposure time

increases so does the amount of background fluorescence from the cell. This can potentially swamp the short-lived fluorophore bursts resulting in them going undetected during fitting. In the case of the simulations, this increase in contribution of cellular autofluorescence is not modelled. To support this hypothesis the average “on-time” for mEos3.1 was measured in fixed cells using a short exposure time of 30ms. Single molecule localisations that appeared in consecutive frames were joined together using the “Trace Molecules” PeakFit plugin. The time for which each single fluorescent burst was detected formed an exponential distribution with a median time of 40ms (Figure 4-7A). These data also showed that the 95<sup>th</sup> percentile of on-times fell at 97ms. Therefore, the loss of dynamic range at high exposure times is likely due to continued integration of background signal, which limits the detection of localisations above background to a small population of long-lived fluorophores.

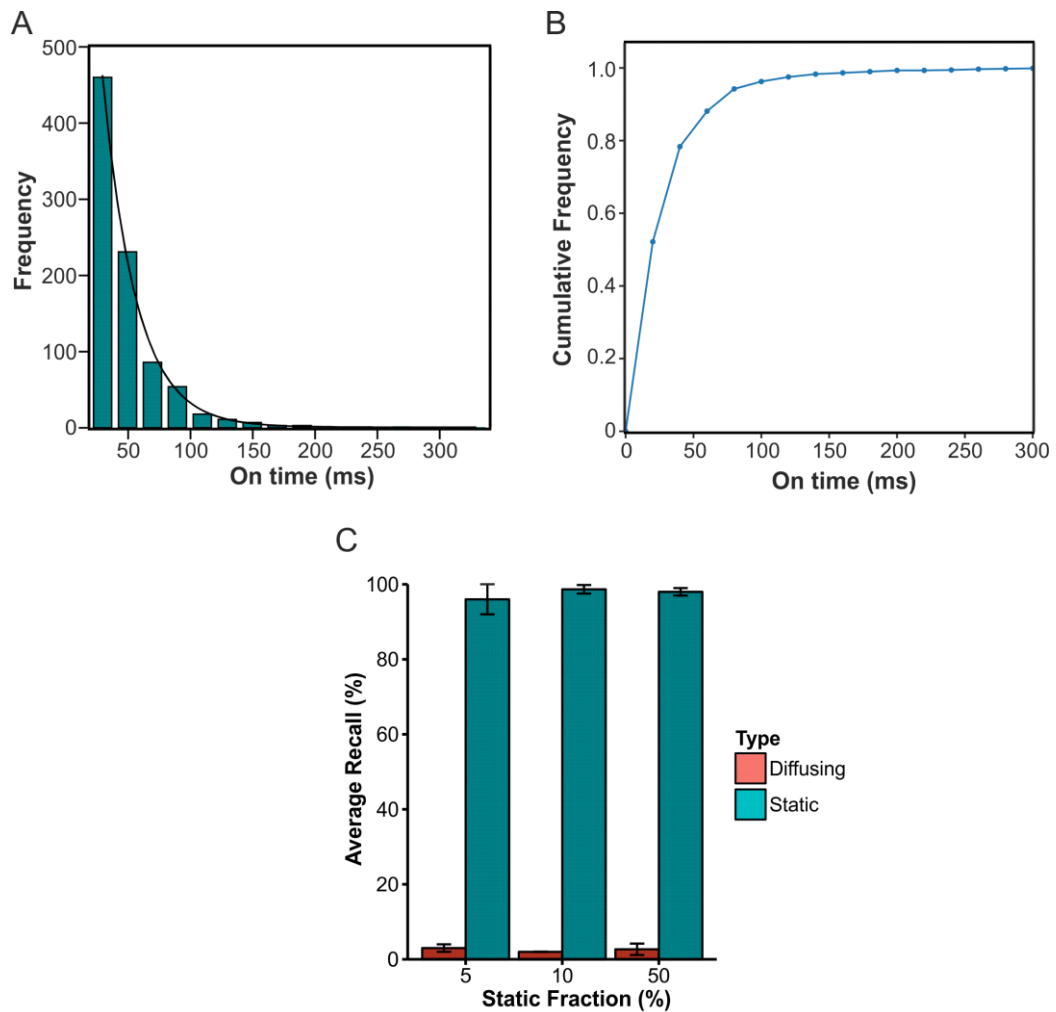


**Figure 4-7. Fluorophore behaviour dictates optimal camera frame rate choice.**

A) Distribution of mEos3.1 on-times measures in Mcm4-mEos3.1 cells fixed with 1% formaldehyde. Cells were imaged with a short exposure time of 30ms to accurately sample fluorescent burst length. Median on-time per burst is 47ms. B) Cumulative histogram of data presented in A. The 95<sup>th</sup> percentile falls at 97ms, demonstrating the short life time of single mEos3.1 fluorescent bursts. C) Recall analysis performed on simulations with optimal exposure time of 350ms containing mixed population of molecules. Varying the fraction of static molecules had no effect on their recall regardless of the high proportion of diffusing species. Error bars represent standard deviation calculated from three independent simulations.

Finally, it was necessary to show that the recall values observed in the simulations were not affected by a mixed population of diffusing and static molecules, which would be the case *in vivo* in the nucleus. To mimic such a situation, simulations were performed as described above but this time different proportions of diffusing and static molecules were modelled. These simulations were run at the optimised exposure time of 350ms and recall analysis was performed on the localisation data set. The result of this experiment showed that the efficiency of static molecule recall was not affected by the proportions of each sub-population, even when 95% of the molecules were diffusive. When performing this experiment in cells, this of course will also depend on the density of activated molecules, which will be down to the experimenter to control.

#### **4.6. Application of optimised imaging routine to visualising MCM chromatin association in unfixed cells**

The development of this PALM imaging routine was driven by the observation in Figure 4-1A, whereby little difference was observed in MCM spatial patterning and quantification, due to cross-linked diffusive molecules. To show the benefit of using the newly optimised motion blur based imaging regime the experiment was repeated, this time in unfixed cells using the optimised camera exposure time.

Using this technique a clear difference in the localisations patterns of Mcm4-mEos3.1 in S-phase and G2 cells was visualised (Figure 4-8A). When the number of localisations was quantified in each nucleus a highly significant difference ( $P = 1.5 \times 10^{-21}$ ) was observed (Figure 4-8B). This result is highly consistent with the expectation that in S-phase nuclei a proportion of the pool of MCM proteins are associated with the chromatin, but not in G2 nuclei. In this experiment S-phase and G2 cells were imaged separately. In order to show that this difference was not due to changing experimental conditions between samples, both cell types were imaged simultaneously. S-phase and G2 cells were

mixed in a 1:1 ratio before being placed on the agarose pad for imaging. Simultaneous imaging reproduced the previous observation of significantly more fluorescent localisations in S-phase nuclei than G2 (Figure 4-8C).

These data suggest that using the motion blurring effect of diffusing molecules that occurs during the longer optimised exposure time, facilitates the visualisation and relative quantification of chromatin-associated molecules.

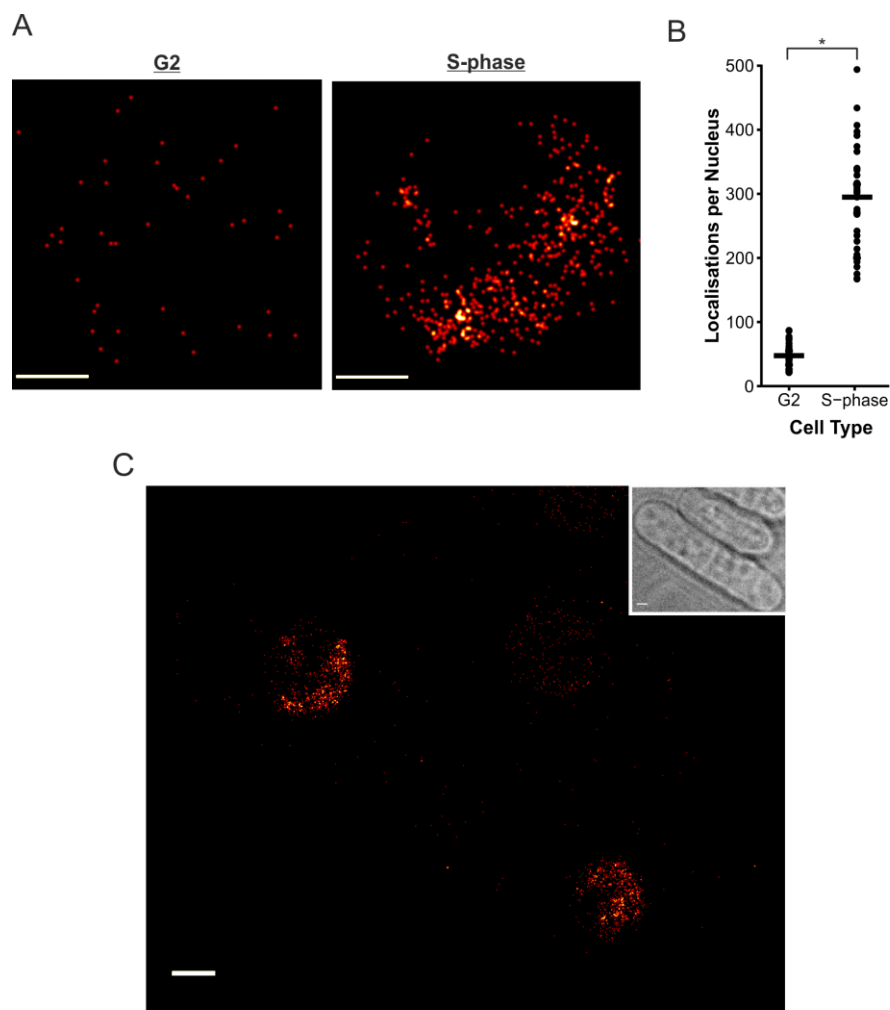


**Figure 4-8. Visualisation of chromatin-associated Mcm4 in unfixed fission yeast.**

A) Typical Mcm4-mEos3.1 reconstructed nuclear localisation patterns from G2 and S-phase cells. Reconstructed single molecule PSFs were drawn with a width matching the experimental average localisation precision of 11nm. Scale bar represents 500nm. B) Quantification of localisations per nucleus from G2 ( $n = 36$ ) and S-phase ( $n = 39$ ) cells imaged at the optimised exposure time of 350ms. Black lines indicate median values (G2 = 47, S-phase = 295).  $P$  value =  $1.5 \times 10^{-21}$ , determined from two-tailed students T-test. C) Reconstructed PALM image of chromatin-associated Mcm4-mEos3.1 molecules in S-phase and G2 cells imaged simultaneously. Localisation patterning is similar to when cell types are imaged separately. Inset = white light image of cells. Scale bars indicated 2  $\mu$ m.

#### 4.7. Quantification of chromatin-associated replication sliding clamp PCNA in differing cell cycle stages and genetic backgrounds

To ensure that the methodology described above was applicable to other replication proteins and not merely a Mcm4 phenomenon, the same imaging routines were applied to visualise chromatin-associated PCNA (Proliferating Cell Nuclear Antigen). PCNA foci are often used as a marker of DNA synthesis in diffraction limited microscopy (Meister et al 2007). In order to perform PALM based microscopy on PCNA it was necessary to create a strain that expressed a mEos3.1-tagged version of the protein. This was achieved by recombinase mediated cassette exchange (RMCE) (described extensively in Materials and Methods). Briefly, the gene encoding the *S. pombe* PCNA homologue, *pcn1*, was marked with *ura4* and flanked by the Cre-recombinase recognition sites *loxP* and *loxM3*, creating a 'base strain' (Figure 4-9A). Previous reports have shown that PCNA can tolerate a fluorescent protein fusion on its N-terminus. Thus, *pcn1*<sup>+</sup> and a small amount of promoter region was cloned into the RMCE plasmid pAW8 and a copy of mEos3.1 was inserted directly upstream of the start codon. This construct was then transformed into the base strain and recombination between the plasmid and the genomic *lox* sites resulted in a strain that expressed mEos3.1-Pcn1 from its endogenous locus (Figure 4-9A).

Although previous reports have suggested that PCNA can tolerate an N-terminal fusion in *S. pombe*, the data also suggested that this causes an increase in HU sensitivity (Meister et al 2007). In this study, a mild HU phenotype was observed for both *mEos3.1-pcn1* but also for a strain whereby the wild type *pcn1* gene has been inserted back into the genome (Figure 4-9C). Such phenotypes can often arise due to alteration in expression levels caused by insertion of the *loxP* and/or *loxM3* sequence upstream/downstream of the gene. Furthermore, the N-terminal mEos3.1-pcn1 fusion strain displayed loss of the fluorescent tag over time. The authors of Meister et al (2007) showed that the HU phenotype could be overcome by introducing a second copy of *pcn1* into the genome that is not tagged, and that both versions are incorporated into the PCNA trimer. In order to prevent loss of the mEos3.1-Pcn1 fusion protein and rescue the HU phenotype, an untagged copy of *pcn1* was introduced into the *his3* locus using a previously described plasmid system (Matsuyama 2008, Material and Methods, Figure 4-9B). The resultant strain displayed wild type growth at 30°C, no temperature or HU sensitivity and no loss of the mEos3.1

fluorescence, and was subsequently used for further experiments (Figure 4-9C). Further attempts were made towards the end of this project to reposition the *loxP* site upstream of *pcn1* were made, however this was not completed due to time restrictions.

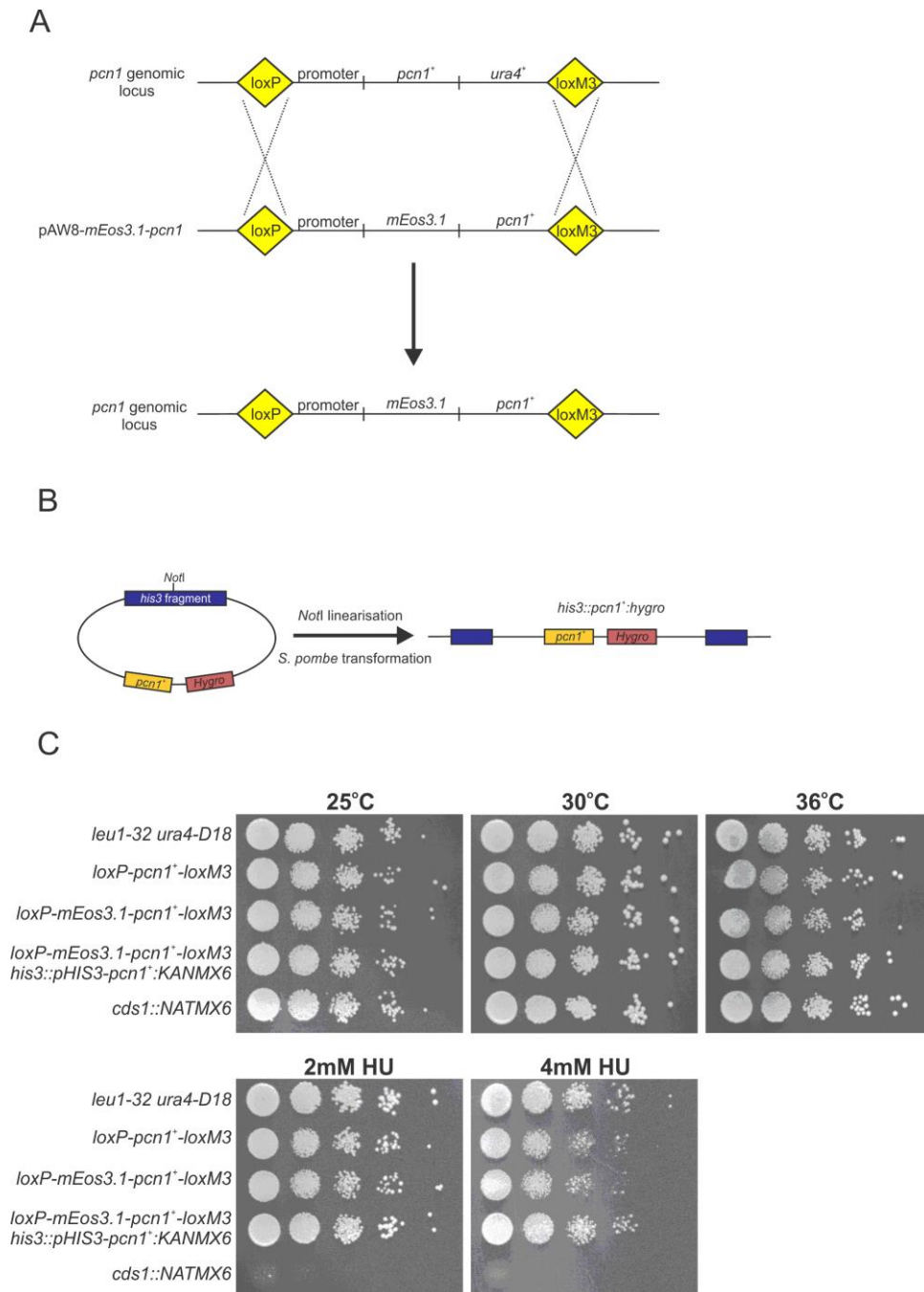


**Figure 4-9. Creation of *S. pombe* strains expressing *mEos3.1-pcn1*.**

**A)** Schematic representation of recombinase mediated cassette exchange between the *pcn1* base strain and the pAW8-*mEos3.1-pcn1* Cre-expression plasmid. Expression of the Cre recombinase from the pAW8 plasmid facilitates *loxP:loxP* and *loxM3:loxM3* recombination resulting in integration of the plasmid based sequence into the genomic locus. **B)** Schematic demonstrating the use of pHIS3K to introduce a wild type *pcn1* copy into the *his3* genomic locus. **C)** Spot assay demonstrating rescue of mild hydroxyurea phenotype by integration of second *pcn1* copy. Ten-fold serial dilutions of cells were spotted on YEA or YEA containing hydroxyurea. Plates were then incubated for 3 days at 30°C unless otherwise stated

PCNA is known to associate with DNA upon entry into S-phase where it serves as a platform for a multitude of enzymes, most importantly for the major DNA polymerases (discussed in depth in Introduction and Chapter 5). To demonstrate that the methodology described above was also applicable to PCNA and that the tagged copy was behaving as expected, mEos3.1-PCNA expressing cells were synchronised into either G2 or S-phase and imaged with the parameters used to study Mcm4. It was reasoned that due to the significantly smaller size of PCNA (28.9 kDa) compared to Mcm4 (101.5 kDa), that the soluble pool of PCNA would be diffusing faster than Mcm4 and thus would not warrant the simulation experiments performed previously. Indeed, when G2 and S-phase cells were compared, there was a visual difference in the number of localisations and their spatial distribution within nuclei (Figure 4-10A). When the number of localisations per nuclei were quantified, an expected significant increase ( $P = 8.1 \times 10^{-7}$ ) in the number of PCNA localisations was observed in S-phase cells compared to G2 cells (Figure 4-10B).

An advantage of using yeast as a model eukaryote is the ability to perform sophisticated genetic experiments with relative ease. This allows for the elucidation of important relationships between gene function and phenotype. To demonstrate that this methodology is sufficiently sensitive enough to detect global changes in the chromatin-association of proteins due to background genetic mutations, the *mEos3.1-pcn1 his3::pcn1* construct was introduced into an *elg1Δ* genetic background. Elg1 has recently been implicated in the unloading of PCNA from the DNA during DNA replication (Kubota 2013, Shiomi 2013). In these studies, removal of Elg1 resulted in the retention of PCNA on the DNA after bulk DNA synthesis. As predicted from this previous biochemical data, using the motion blur PALM methodology we were able to detect a significant increase in the number of localisations detected per nucleus in *elg1Δ* cells compared to *elg1<sup>+</sup>* (Figure 4-10B). This increase is clearly visible in the reconstructed images as areas of dense localisations (Figure 4-10C). These data support previous findings that deletion of *elg1* causes PCNA accumulation on the DNA and further demonstrate that the methodology described above can be used to quantify relative changes of chromatin-associated proteins in different cell cycle stages and genetic backgrounds.

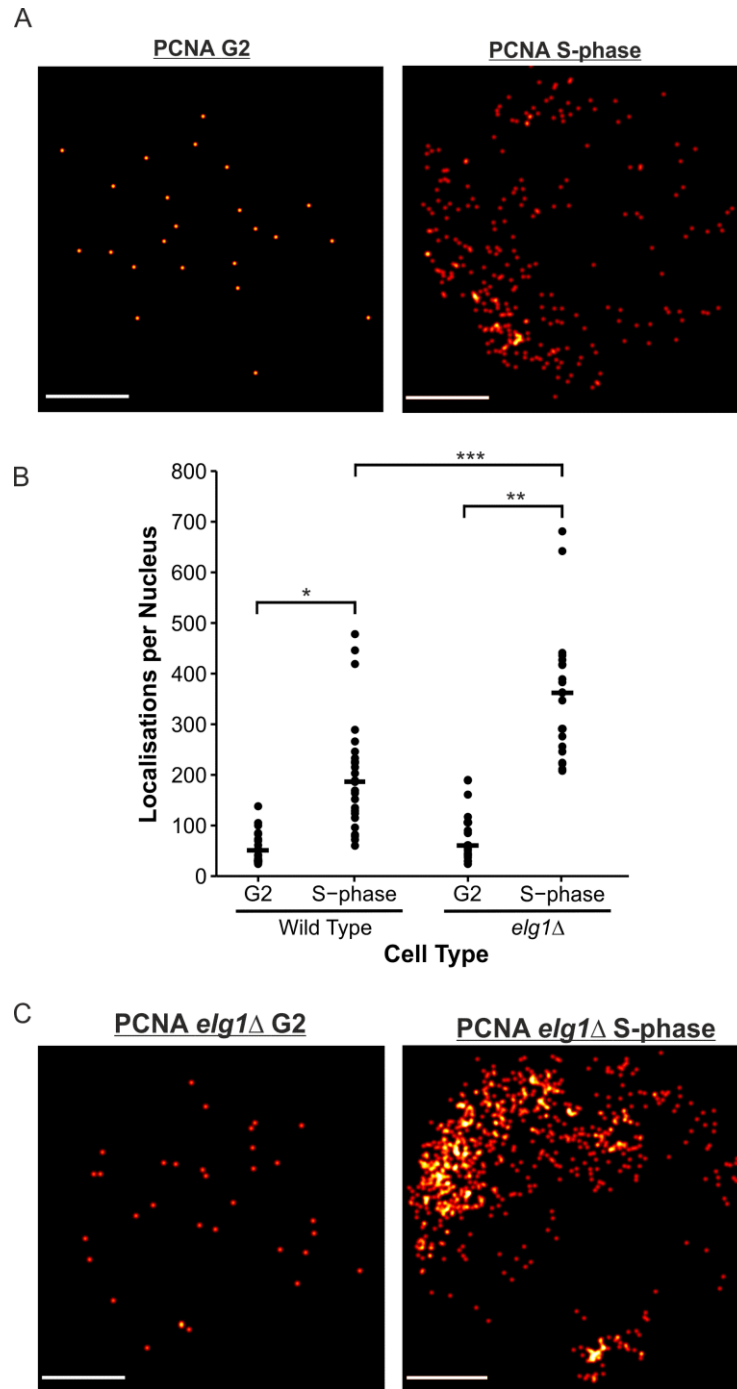


**Figure 4-10. Visualisation of chromatin associated PCNA using PALM.**

**A)** Representative reconstructed images of nuclear mEos3.1-PCNA localisations in G2 and S-phase *S. pombe* cells. **B)** Quantitative analysis of PCNA chromatin association in *elg1+* and *elg1Δ* cells. Cells were imaged with an exposure time of 350ms and the number of single molecule localisations was counted per nucleus ( $n = 19, 26, 21$  and  $20$  nuclei for G2 *elg1+*, S-phase *elg1+*, G2 *elg1Δ* and S-phase *elg1Δ* respectively). Horizontal bar indicates median values (*elg1+* G2 = 51, *elg1+* S-phase = 187, *elg1Δ* G2 = 60, *elg1Δ* S-phase = 362). *P*-values were determined by two-tailed Students T-test: \* $P = 8.1 \times 10^{-7}$ , \*\* $P = 9.4 \times 10^{-10}$ , \*\*\* $P = 5.9 \times 10^{-5}$ . **C)** Reconstructed images of mEos3.1-PCNA localisations in *elg1Δ* nuclei of cells in G2 or S-phase. Note the increase in localisations between WT S-phase in A) and *elg1Δ*.

## 4.8. Conclusions and Discussion

As previously discussed, the single-molecule localisation microscopy has so far shown great promise in the study of DNA replication and repair processes. However, the majority of studies have been limited to prokaryotic model organisms. Extending these methodologies so they can be used in eukaryotic systems has the potential to greatly benefit the field. Application of such technologies will rely on demonstration of their capabilities and development of a robust methodological toolkit that warrants investment in either collaborations or the technology itself.

In this chapter, data demonstrating a methodological adaptation to PALM imaging which enables visualisation and quantification of chromatin-associated proteins in unfixed fission yeast have been presented. The development of this technique stemmed from limitations associated with chemical fixation and detergent extraction approaches, which made it difficult to identify single molecule localisations that arose from chromatin-associated molecules. This methodology utilises long camera exposure times and the subsequent effect of motion blurring to filter out fluorescent localisations from diffusing molecules while retaining those of static chromatin-associated proteins. The exact camera exposure time was optimised via computer simulations and the resulting procedure used to detect changes in DNA binding of replication proteins in distinct cell cycle stages and genetic backgrounds.

This is not the first time that long exposure times have been used to monitor DNA-association of proteins. Previous studies have used a similar approach to monitor transcription factor dynamics and the detection of DNA bound repair proteins in bacteria (Elf 2007, Uphoff 2013). Long exposure times have also been coupled with time-lapse imaging to track single molecules moving extremely slowly along actin filaments (Kim et al 2006). At the time of this study, a group used long exposure times to measure the DNA dissociation kinetics of transcription factors inside live human cells (Chen *et al* 2014). The data presented here demonstrate that this well documented phenomenon can be used slightly differently to study changes in the global association of proteins to the chromatin inside a eukaryotic model organism.

This development is of importance for various reasons. Firstly, this study demonstrates that SMLM approaches can be used to great effect in organisms that present significant challenges for such microscopy approaches. For example, bacterial models are favourable for studies like these due to their small size meaning that majority of the cell, and therefore the fluorophores, are in focus. In the yeast system, this is not the case as the larger cell size means a large proportion of the cell is out of focus. In SMLM techniques, widefield illumination and the stochastic nature of fluorophore activation prevents the user from collecting light from several Z-planes. However, as demonstrated here, although only a section of the cell can be visualised, this is still enough to collect meaningful data. The larger size of yeast cells also has potential effects on sptPALM-based experiments and this will be discussed in the next chapter.

A second benefit of this study is it provides a sensitive assay for measuring changes in chromatin association without disruption to the cell. Current biochemical techniques involve chemical crosslinking and breaking open cells to study chromatin association. Although such techniques are informative, the methodology presented here can be seen as a complementary approach that is much less perturbative. Its ability to quantitatively measure global changes in chromatin association could be potentially crucial in revealing previously unknown protein behaviour.

As with all methodologies, there are limitations and this approach is no exception. The main drawback of this methodology is that it does not provide accurate spatial information on protein localisation. One advantage of SMLM techniques is the ability to create super-resolution images and is one reason that this project was initiated. However, because the cells are not chemically fixed during the procedure it allows for the diffusion of chromatin and potential rotation of the nucleus. Thus, coupled with the fact that the activation of single fluorophores is stochastic, any grouping/clustering of localisations may be an artefact of chromatin diffusion. This therefore limits the output of the approach to the relative measurement of DNA association. Efforts are still ongoing to develop an *S. pombe* extraction technique that is compatible with PALM.

Despite the mobility of the chromatin during imaging, this does not have a significant effect on fitting the PSFs of chromatin-associated molecules. Diffusion of any one chromosomal locus has been shown to lie between  $10^{-4}$  and  $10^{-3}$   $\mu\text{m}^2/\text{s}$  (Dion and Gasser

2013). This movement would equate to a 45nm displacement during a 350ms exposure which is well within the size equating to a single pixel (usually 100-110nm). Although in this study *S. pombe* was the model system chosen to establish this method, there is no reason why this cannot be extended to other eukaryotic systems. In situations where the chromatin is more mobile (such as DNA damage or certain cell types) or the molecule size is greater than 100 kDa, it is recommended that users explore altering exposure times or a localisation procedure that enables fitting slightly enlarged PSFs. In addition, there is no reason why other photoconvertible/photoactivatable fluorescent proteins that are compatible with PALM could be used.

An observation made during this imaging is the presence of a low number of localisations in situations where it would be predicted that there are no chromatin-bound molecules, e.g. Mcm4-mEos3.1 localisations in G2 cells. These localisations could be due to a multitude of reasons. Primarily, random collision with nuclear matrix proteins or indeed the chromatin itself inside the crowded nucleus could render molecules static for a short period of time. Alternatively, molecules that diffuse vertically within the focal plane within the 350ms exposure time could be detected. In the case of Mcm4, the possibility exists that random association with an ORC complex and origins of replication could result in transient association with the DNA. Recent *in vitro* data have shown that association of only one MCM hexamer with an origin can lead to ATP-dependant release of the helicase (Coster 2014). During sample preparation for the experiments in this chapter, sodium azide is added to prevent ATP-dependent DNA loading/unloading of molecules during imaging. Thus, the observed localisations in G2 cells could be MCMs that have transiently associated with ORC complexes and are unable to be released due to the lack of ATP. In the case of PCNA, the G2 localisations detected could well be due to post replicative repair which is known to require PCNA (Daigaku et al 2013)

In conclusion, the simple approach presented in this chapter provides a means to complement biochemical studies of protein chromatin association using PALM based localisation microscopy. In the next chapter, I will describe how this methodology has been used to complement such investigations further demonstrating the potential for its use in future discoveries.

# Chapter 5

## Investigating the role of ubiquitylation of the replication sliding clamp during DNA synthesis using photoactivated localisation microscopy

### 5.1. Introduction

The replication sliding clamp, PCNA, is an essential scaffold protein that is required for many DNA metabolism processes. Most notable, is its role as a processivity factor and docking platform for the replicative polymerases during DNA synthesis. PCNA has also been well studied for its role in DNA damage bypass mechanisms that involve translesion synthesis and template switching. Central to its role in DNA damage tolerance is the post-translational modification of PCNA by addition of one or multiple ubiquitin moieties to lysine 164. This modification of PCNA and its subsequent roles in repair have been studied extensively, and its presence was considered to be solely as a result of the formation of DNA damage (discussed in Introduction).

This chapter focuses on work that was performed as part of a collaboration with Dr Yasukazu Daigaku in the Carr lab. A large amount of biochemical and genetic data had been collected by Dr Daigaku prior to the experiments described in this chapter, which allude to a damage independent role for PCNA ubiquitylation during unperturbed S-phase. These data provide evidence to suggest that ubiquitylation of PCNA promotes a stable association with the DNA. Preventing ubiquitylation by removing the E3 ubiquitin ligase, RAD18 (*S. pombe* Rhp18), had consequences for the progression of replication, predicted to be due to lagging strand synthesis defects. In order to support these observations PALM based imaging was utilised to investigate the role of PCNA ubiquitylation in the chromatin association of PCNA and the replicative polymerases *in vivo*.

## 5.2. Summary of collaboration

In this section, I will briefly outline the data that had been previously collected by Dr Daigaku and colleagues. The initial observation that initiated this project was that in both *S. pombe* and other eukaryotes PCNA ubiquitylation is detectable in the absence of genotoxic agents. To repeat this finding, fission yeast cells were synchronised and released into S-phase whilst monitoring the ubiquitylation status of PCNA by western blotting. This experiment confirmed the presence of damage independent ubiquitylation accumulates as cells progress through S-phase. Cells that were irradiated with UV upon release into S-phase demonstrated no significant increase in the amount of ubiquitinated PCNA detected by western blot analysis. Instead, the ubiquitylation signal persisted for longer, consistent with a slower S-phase progression (Figure 5-1A). This directly contrasts with data collected from *S. cerevisiae* whereby Ub-PCNA is almost exclusively detected in response to exposure to DNA damaging agents (Davies et al 2008). The ubiquitylation detected in fission yeast was dependant on the Rad18 E3 ligase homologue, Rhp18, and is thus a result of the same ubiquitylation pathway that is active in response to DNA damage (Figure 5-1A, Hoege 2002). These data suggested that PCNA ubiquitylation is not just linked to exposure to genotoxic agents and the resulting DNA damage; therefore, it may play a role during normal DNA synthesis. To assess whether this observation had any relevance with respect to human cells, both U2OS and 1BR3hTERT cell lines were synchronised into S-phase with and without the presence of UV damage. Both cell lines exhibited a clear accumulation of Ub-PCNA during unperturbed DNA synthesis (Figure 5-1B). However, there was also a noticeable increase in Ub-PCNA in response to UV damage, dissimilar to what was observed in fission yeast. Nonetheless, the clear phenotype of S-phase dependent PCNA ubiquitylation lead to the further investigation of the role of Ub-PCNA in unperturbed cells.

To investigate whether the PCNA ubiquitylation imposes any influence on the progression of DNA replication; a genome-wide BrdU incorporation assay was employed in *S. pombe*. Deep sequencing of BrdU incorporated DNA fragments at different time points during replication allowed for the observation of local replication rates. This analysis revealed a significant decrease in local rates of replication at late-replicating regions in *rhp18* $\Delta$  cells (Figure 5-1C). This analysis provided further support for an involvement of Ub-PCNA in unperturbed genomic replication.

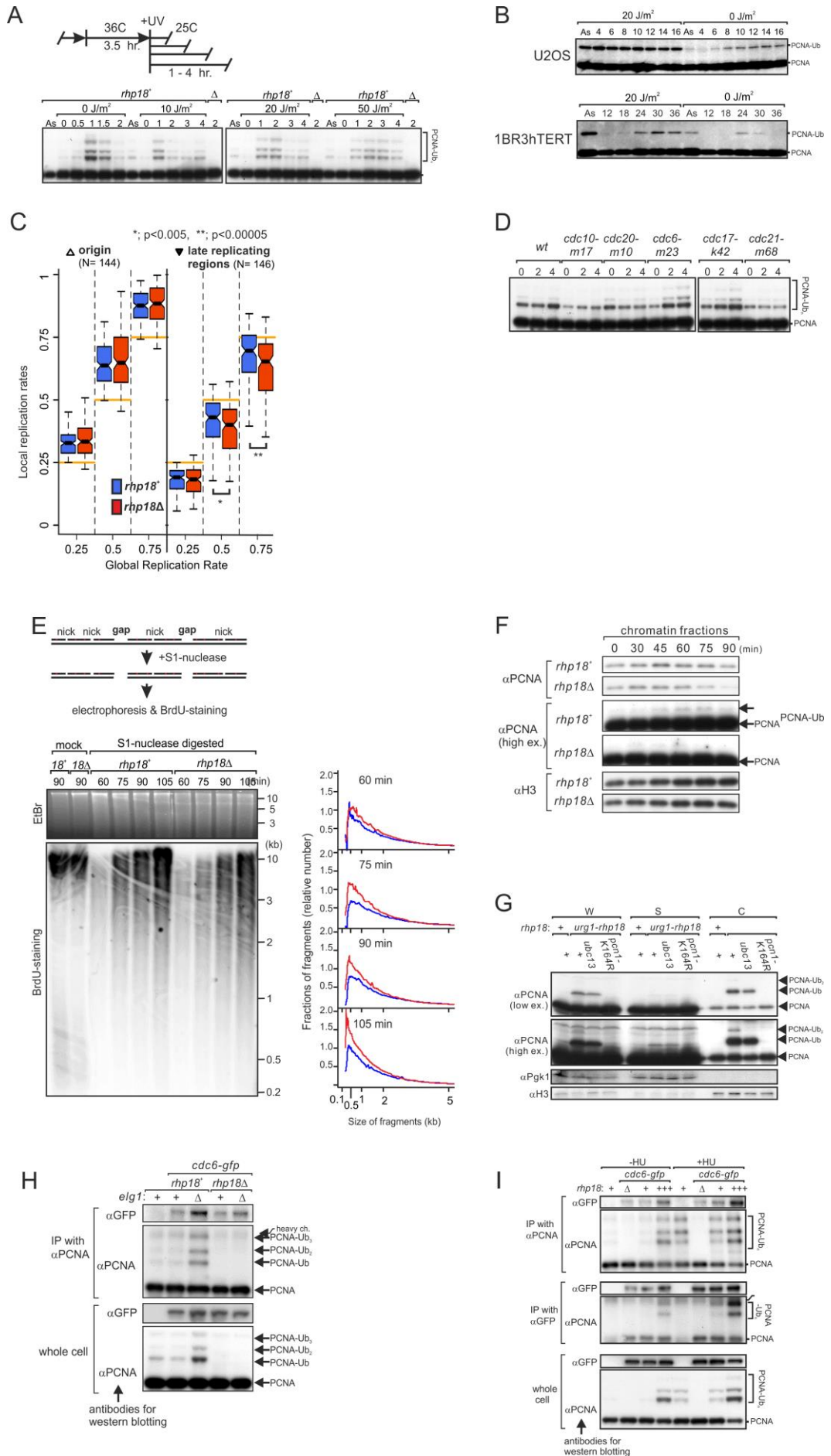


**Figure 5-1. Summary of data collected prior to collaboration.**

**A)** Time course experiment of PCNA ubiquitylation during S-phase in fission yeast. Top panel: experimental scheme. Cells were synchronised at the G1/S boundary by *cdc10-m17* block, UV irradiated and released from block by incubation at 25°C. Bottom panel: PCNA ubiquitylation status was analysed by western blotting. **B)** PCNA ubiquitylation during cell cycle progression in human cells. Top panel: U2OS cells were synchronised with nocodazol, released into fresh media with or without UV irradiation. Cells were harvested at indicated time points and PCNA ubiquitylation was assayed by western blot. Bottom panel: equivalent experiment in 1BR3hTERT immortalised human fibroblasts. Cells were synchronised by serum starvation (15 days), before being released into serum-containing media. Cells were either UV irradiated or untreated. **C)** Analysis of local replication rates determined by BrdU immunoprecipitation and high throughput DNA sequence analysis. Local replication progression was determined in *rhp18<sup>+</sup>* and *rhp18Δ* cells at 300bp bin regions for three time points: when either 25%, 50% or 75% of global genomic replication was completed. The distribution of local replication rates was then examined at early and late replicating regions at each time point in both cell types. Left: early replicating regions, Right: late-replicating regions distal to origins. **D)** PCNA ubiquitylation analysed as a response to specific replication defects. The indicated temperature sensitive mutants were shifted from permissive to restrictive temperature and PCNA ubiquitylation levels were analysed by western blotting of whole cell extracts. **E)** PCNA ubiquitylation mediates repair of ssDNA gaps during S-phase. Top panel: schematic of S1 nuclease specificity to ssDNA gaps. Bottom panel: *cdc25-22* cells were synchronised at G2 phase at the restrictive temperature and then released into the cell cycle in the presence of BrdU. DNA samples were harvested at indicated time points, digested with S1 nuclease and subjected to agarose gel electrophoresis. DNA fragments were visualised by ethidium bromide staining and anti-BrdU antibody. Right panel: Quantification of digested fragments in *rhp18<sup>+</sup>* and *rhp18Δ* cells from BrdU signal intensity. **F)** Chromatin association of PCNA is affected by its ubiquitylation. Cells synchronised at G1/S boundary by *cdc10* block were released into S-phase and the total level of PCNA in the chromatin fraction was analysed by western blotting. **G)** PCNA chromatin association in cells with upregulated levels of Rad18. Overexpression of Rad18 was achieved via control of the rapidly inducible *urg1* promoter. PCNA levels from whole cell, soluble or chromatin fractionations were analysed by western blot. **H)** Co-immunoprecipitation of Polδ with PCNA in *elg1<sup>+</sup>* and *elg1Δ* cells with or without *rhp18*. **I)** PCNA ubiquitylation contributes to its interaction with Polδ. Co-immunoprecipitation experiment whereby soluble extracts were precipitated with either anti-PCNA or anti-GFP in the presence or absence of HU. Expression of *rhp18* was varied: (+) wild-type levels, (++) *urg1-rhp18* overexpression or (Δ) deletion. **Note: The data in this figure were generated and supplied by Dr Yasukazu Daigaku.**

Further analysis revealed that defects in lagging strand DNA synthesis enhance the Ub-PCNA phenotype observed in normal S-phase (Figure 5-1D). Temperature sensitive mutants in the lagging strand polymerase (*cdc6-m23*) and the DNA ligase (*cdc17-K42*) both presented augmented levels of Ub-PCNA during DNA synthesis when incubated at the restrictive temperature. This response was not detected in mutants associated with leading strand synthesis (*cdc20-m10*, polymerase delta) or the replicative helicase (*cdc21-m68*, Mcm4). These results lead to the hypothesis that ubiquitylation of PCNA plays a role in lagging strand synthesis, which is intrinsically dependent on PCNA to act as a platform for polymerase delta during Okazaki fragment synthesis.

To further support this hypothesis, data was collected that demonstrates Ub-PCNA contributes to gap filling during lagging strand synthesis. Detection of single strand gaps can be performed by S1-nuclease digestion of genomic DNA. Treating genomic DNA extracted from *rhp18<sup>+</sup>* and *rhp18Δ* cells with S1-nuclease showed an accumulation of small DNA fragments in the absence of PCNA ubiquitylation (Figure 5-1E). This increase in S1-nuclease sensitivity highlights the fact that Ub-PCNA is required for the efficient

replication of the lagging strand, probably by co-ordinating the enzymatic processes necessary to complete Okazaki fragment synthesis.

In order to uncover a mechanistic role for the presence of Ub-PCNA during normal DNA synthesis, the chromatin-association of PCNA was analysed. It was hypothesised that the ubiquitylation of PCNA could be effecting its loading status on DNA. Thus, levels of DNA-associated PCNA was measured by extraction of chromatin fractions throughout S-phase in synchronised cells. This experiment indicated that the amount of PCNA associated with the chromatin towards the latter stages of S-phase was reduced in the absence of Rhp18 (Figure 5-1F). This is consistent with the previous observation that late replicating regions were effected in *rhp18Δ* cells. Overexpression of Rhp18 resulted in a large amount of Ub-PCNA detected in the chromatin fraction (Figure 5-1G). This accumulation was dependent on the PCNA ubiquitylation site K164. These results indicated that the ubiquitylation of PCNA plays a role in its loading status.

If the loading status of PCNA is dependent on its ubiquitylation by Rhp18, this could have a direct effect on the enzymes that associate with it during replication. Deletion of the unloader of PCNA, Elg1, resulted in higher amounts of PCNA in the chromatin fraction, consistent with previously published data and data presented in Chapter 4. Co-immunoprecipitation experiments of PCNA and polymerase delta found that the increased amount of PCNA on the chromatin in *elg1Δ* cells leads to an increase in the amount of polymerase delta isolated in the pull-downs (Figure 5-1H). This suggested that the level of PCNA on the DNA directly effects its interaction with polymerase delta. Consistent with this was the observation that increasing the amount of Ub-PCNA by overexpressing Rhp18 lead to an increased interaction with polymerase delta (Figure 5-1I).

Overall, the previous data highlights that PCNA ubiquitylation occurs during normal DNA synthesis in fission yeast, and may act to promote stable association of PCNA with the DNA thus promoting the interaction with polymerase delta. This project presented an opportunity to demonstrate how the PALM-based approach described in Chapter 4 can complement standard biochemical techniques as well as test Dr Daigaku's hypothesis. In this chapter, I will present data that contributed to the development of this project by utilising the approach to confirm the ubiquitin-dependent changes in global PCNA DNA-

association as well as investigating any downstream effects Ub-PCNA has on the replicative polymerases.

### **5.3. Ubiquitylation of PCNA promotes its stable association with DNA**

To confirm that the chromatin loading status of PCNA is indeed affected by its ubiquitylation by Rhp18 in *S. pombe*, the *mEos3.1-pcn1 his3::pcn1* strain created in the previous chapter was utilised to study the chromatin-bound fraction of PCNA by PALM. As discussed earlier, previous work in fission yeast demonstrated that fluorescently-tagged PCNA monomers can be incorporated into a PCNA trimer, in a strain expressing both the fusion protein and wild type PCNA (Meister 2007). As this project aimed to study the role of ubiquitylation of PCNA, it was important to ensure that the mEos3.1-labelled Pcn1 protein could be ubiquitinated. Western blotting of wild type and *mEos3.1-pcn1* total cell extracts with an anti-PCNA antibody revealed the two species of PCNA as well as a band that is of the expected molecular weight for Ub-mEos3.1-Pcn1 (Figure5-1A). This strain was therefore used in subsequent experiments in this chapter.

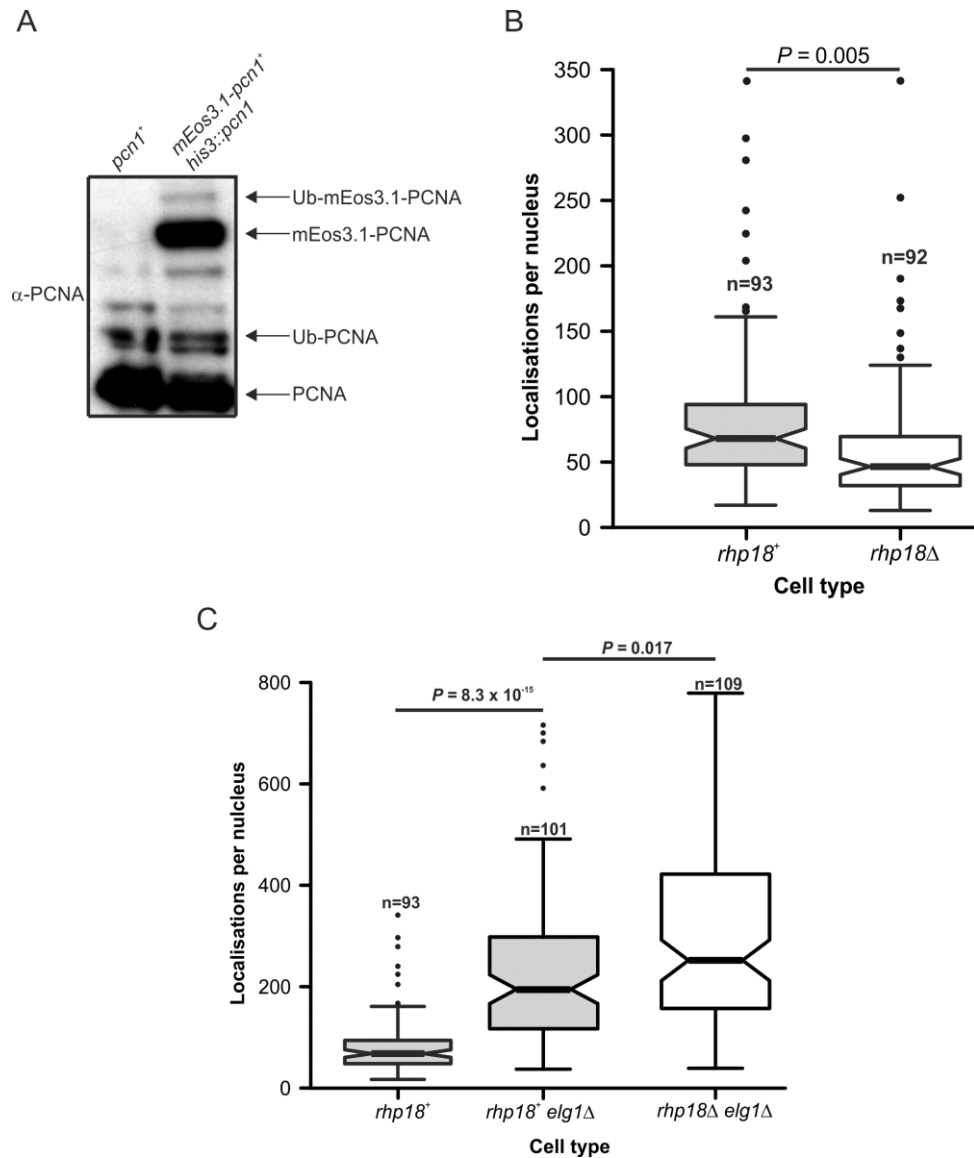


**Figure 5-2. Visualising the influence of PCNA ubiquitination on its DNA-loading status.**

A) Anti-PCNA western blot analysis of *S. pombe* whole cell extracts highlighting the presence of mEos3.1-PCNA and Ub-mEos3.1-PCNA. B) Motion blur based PALM analysis of chromatin-associated PCNA in *rhp18<sup>+</sup>* and *rhp18 $\Delta$*  or C) *rhp18<sup>+</sup> elg1 $\Delta$*  and *rhp18 $\Delta$  elg1 $\Delta$*  cells undergoing DNA synthesis. Single molecule localisations were quantified in nuclear regions of binuclear cells. Data shown were obtained from a minimum of 3 repeats. Boxplot centre lines show median values, notches represent 95% confidence interval of the median and black dots represent outliers.

To assess the effect of PCNA ubiquitylation on its DNA association, *rhp18*, the *S. pombe* orthologue of RAD18 in budding yeast (Verkade 2001), was deleted in the *mEos3.1-pcn1 his3::pcn1<sup>+</sup>* strain. Both strains were then synchronised into S-phase using the lactose gradient method and imaged using the protocol described in the previous chapter. Single molecule localisations from binuclear cells considered to be undergoing DNA synthesis were then quantified. In agreement with the biochemical data collected by Dr Daigaku, there was a statistically significant decrease in single molecule localisations and thus the

amount of chromatin associated PCNA during S-phase (Figure 5-1B). This result provides *in vivo* evidence that supports the hypothesis that ubiquitylation of PCNA promotes its stability when loaded on the DNA.

As the biochemical and motion blurring microscopy data both demonstrated a role for ubiquitylation in stabilising DNA-associated PCNA, the next interesting question to ask was: what is the mechanism behind the increased stability of loaded PCNA once it is ubiquitinated? There are two potential explanations for such a question. Firstly, the addition of a ubiquitin moiety to PCNA could stabilise the PCNA trimer by inducing conformational changes in the tertiary protein structure. However, evidence from overlaying crystal structures of Ub-PCNA and PCNA suggest that the presence of the ubiquitin causes no apparent structural alteration of the protein (Freudenthal *et al* 2010). The second possibility is that addition of ubiquitin acts as a cellular signal to prevent its unloading from the DNA. As previously mentioned, Elg1 has been implicated in the removal of PCNA from DNA during DNA replication. Ub-PCNA could prevent Elg1 from unloading PCNA from the DNA until each Okazaki fragment has been ligated.

To test this hypothesis, an *mEos3.1-pcn1 his3::pcn1<sup>+</sup>* was created which had both *elg1* and *rhp18* deleted and compared to the *elg1Δ* strain described in Chapter 4. If ubiquitylation induces conformational changes which stabilise the PCNA:DNA interaction, then the deletion of *rhp18* would reduce the amount of DNA-associated PCNA detected. However, if Ub-PCNA was preventing Elg1-dependent unloading then the relationship would be epistatic and there would be no difference in loaded PCNA. PALM imaging of *rhp18Δ* and *rhp18Δ elg1Δ* cells in S-phase revealed no decrease in DNA-associated PCNA. In fact, there was a slight, but significant increase ( $P=0.017$ ) in the amount of DNA-bound PCNA detected. This result suggests a potential role for ubiquitylation of PCNA as a negative regulator of its unloading by Elg1 (Figure 5-1C). The slight increase in detected PCNA in the *rhp18Δ elg1Δ* strain was unexpected, but could be due to compounding factors in the double mutant. Cells lacking *elg1* have been shown to have increased levels of genomic instability (Ben-Aroya 2003, Ogiwara 2007) and this coupled to potential *rhp18Δ* lagging strand defects could result in defective S-phase, which requires high levels of loaded PCNA.

#### 5.4. Investigating the effect of PCNA ubiquitylation on the DNA-association of the replicative polymerases

The main role of PCNA during DNA synthesis is to act as a platform for the replicative polymerases, especially on the lagging strand. If the amount of loaded PCNA is compromised in the absence of *rhp18* then this could have consequences for the processivity of the polymerases. As outlined earlier, increasing the amount of PCNA associated with the DNA by either deletion of *elg1* or by overexpression of Rhp18, results in increased amounts of polymerase delta that can be co-immunoprecipitated with PCNA. This suggests that the defects in DNA replication seen in *rhp18* cells could be due to reduced levels of polymerase delta on the DNA caused by premature unloading of PCNA. This hypothesis could not be tested using chromatin fractionation techniques or Co-IPs, due a lack of sensitivity in such assays. Thus, to study the global DNA-association of the replicative polymerases at the more sensitive, single-molecule level, we applied PALM imaging.

Catalytic subunits of both the leading strand (*S.p* Cdc20, Pol $\epsilon$ ) and the lagging strand (*S.p* Cdc6, Pol $\delta$ ) polymerases were tagged with mEos fluorescent proteins. Previously in the Carr lab, RMCE base strains for both of these subunits were created and the genes had previously been tagged with GFP for ChIP experiments. Cdc20 had been previously tagged at its C-terminus using a C-terminal tagging base strain, thus this was used to introduce mEos3.1 at the C-terminus (Figure 5-2A, Materials and Methods). Cdc6 was known to tolerate an N-terminal GFP tag, and had been previously tagged with the older Eos variant mEos2. Although created to be monomeric, mEos2 was shown to cause aggregation of highly expressed proteins in cells, thus was further developed to be truly monomeric in the form of the mEos3.1 and 3.2. (Zhang 2012). Although Cdc6 is not highly expressed (Marguerat 2012), attempts were made to tag the protein with mEos3.1 in order to retain consistency of fluorophores throughout this study. Unfortunately, replacing mEos2 with mEos3.1 resulted in negative effects on imaging the protein. It was noticed that a strain expressing mEos3.1-Cdc6 had a substantial reduction in total fluorescence when imaged compared to mEos2, GFP or mEos3.1-HaloTag-Cdc6 (DL107, acquired from Dr David Lando, Cambridge University, UK). Western blotting demonstrated a considerably reduced amount of mEos3.1 tagged-Cdc6 protein in total cell extracts (Figure 5-2B). Thus, it was decided that Cdc6 experiments would be carried

out using the original mEos2-Cdc6 strain (AW691) previously made by Dr Adam Watson in the Carr lab. This construct, as well as *mEos3.1-cdc20*, was introduced into *rhp18Δ*, *elg1Δ* and *rhp18Δ elg1Δ* genetic backgrounds (Materials and Methods).

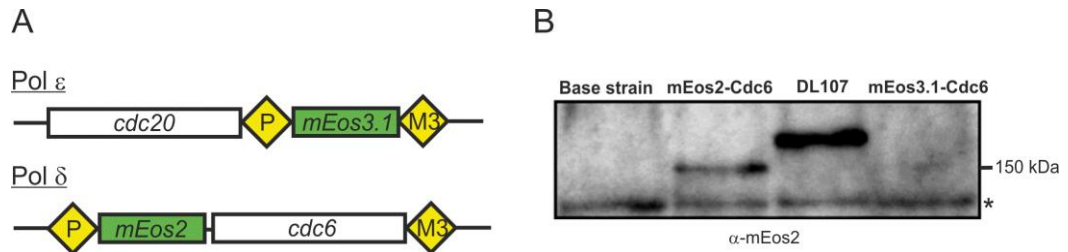


**Figure 5-3. Tagging catalytic subunits of the major DNA polymerases for PALM imaging.**

A) Final tagging constructs for polymerases using recombinase mediated cassette exchange (RMCE). Pol  $\epsilon$  subunit Cdc20 was fused to mEos3.1 via C-terminal RMCE, whilst Pol  $\delta$  subunit Cdc6 was N-terminally fused to mEos2 via gene replacement RMCE. P = *loxP*, M3 = *loxM3*. B) Western blot analysis of *S. pombe* whole cell extracts, probed with anti-mEos2 antibody. Fusing mEos3.1 to Cdc6 caused a reduction in the expression of the fusion protein. \* indicates non-specific band used as loading control.

#### 5.4.1 Polymerase $\epsilon$

Leading strand DNA synthesis is considered less dependent on PCNA compared to the lagging strand. Polymerase epsilon synthesises new DNA continuously unlike the lagging strand and therefore requires only one copy of the PCNA trimer. Recent *in vitro* data from reconstituted leading strand synthesis suggest that Pol  $\epsilon$  is not completely dependent on PCNA, most likely due to a direct interaction with the CMG helicase (Georgescu 2014). Previous data from this collaboration showed that PCNA could not be isolated in co-immunoprecipitation experiments with Pol  $\epsilon$ , and that *rhp18Δ* has no effect in a *cdc20-m10* temperature sensitive genetic background. From these data, it was hypothesised that the chromatin-association of Pol  $\epsilon$  would be unaffected by changing the levels of DNA-bound PCNA either by deletion of *rhp18* or *elg1*.

Quantitative PALM imaging of chromatin-associated Pol  $\epsilon$  revealed that there was indeed no global change in the amount of DNA-bound Pol  $\epsilon$  in either an *rhp18* or *elg1* deletion (Figure 5-4A). However, there was a significant decrease in the amount of leading strand polymerase detected in a *pcn1-K164R* mutant background. The K164R mutant is often used to study the role of PCNA ubiquitylation as removal of the lysine prevents the ligation of a ubiquitin moiety. This mutant also displays a slow growth phenotype as well as reduced levels of BrdU incorporation (Y.Daigaku, data not shown). As well as K164

ubiquitination, PCNA is also known to be SUMOylated at the same position (Hoegge 2002). To investigate whether lack of SUMOylation is the cause of the phenotype observed in the *pcn1-K164R* background, the *cdc20-mEos3.1* construct was introduced a *pli1* $\Delta$  genetic background. Pli1 is known to be responsible for the majority of K164R SUMOylation in *S. pombe*. Deletion of Pli1 showed no significant effect on the chromatin association of Pol  $\epsilon$  compared to *pli1*<sup>+</sup> cells (Figure 5-4B). Thus, as the *pcn1-K164R* mutation behaved differently to *rhp18* and the phenotype was not considered to be due to abolition of SUMOylation, it was considered that maybe it results in an additional phenotype caused by structural alteration of the PCNA molecule. With this in mind, it was removed from future experiments.

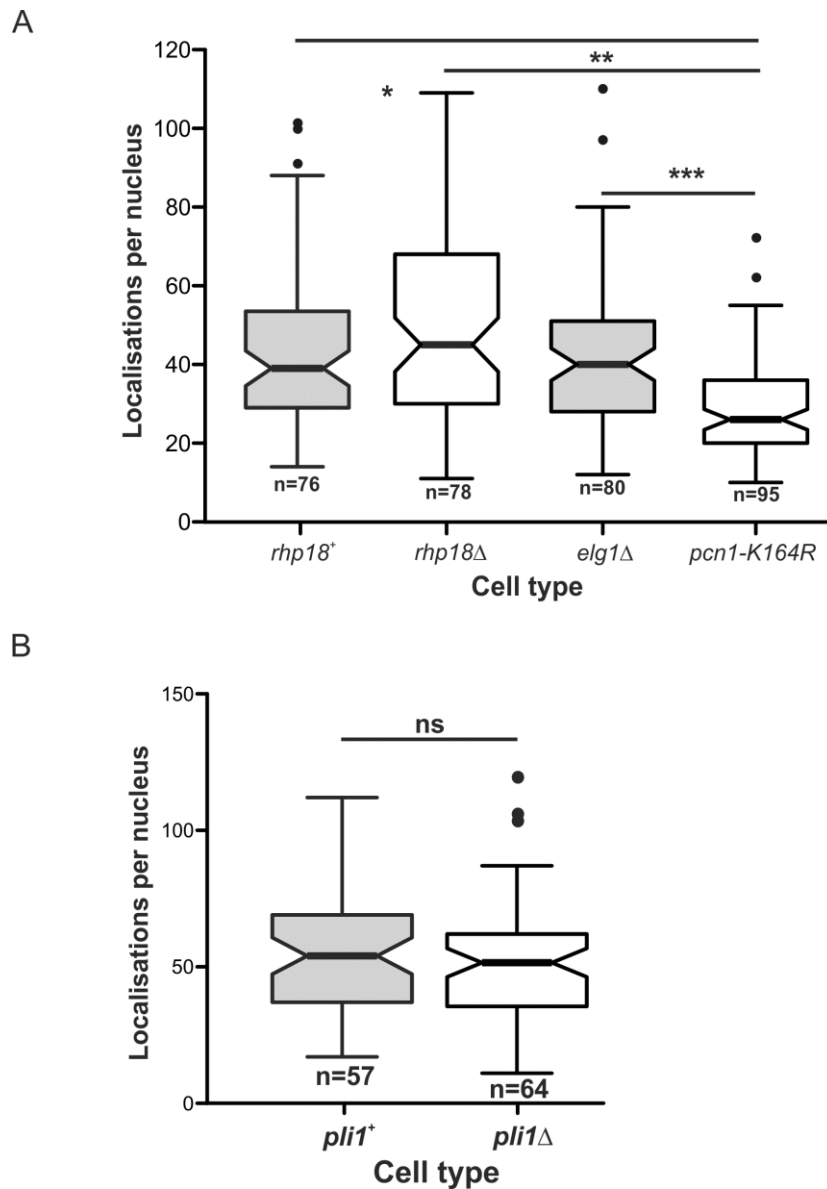


**Figure 5-4. Visualising the effect of PCNA loading status on Pol  $\epsilon$  chromatin association.**

Quantification of nuclear mEos3.1-Cdc20 single-molecule localisations detected during motion blur PALM imaging of binuclear S-phase cells. Data shown were obtained from a minimum of 3 repeats. Boxplot centre lines show median values, notches represent 95% confidence interval of the median and black dots represent outliers. *P* values: \* =  $1.4 \times 10^{-6}$ , \*\* =  $1.6 \times 10^{-9}$  and \*\*\* =  $5.5 \times 10^{-7}$ . *P* values determined from two-tailed Students T-test.

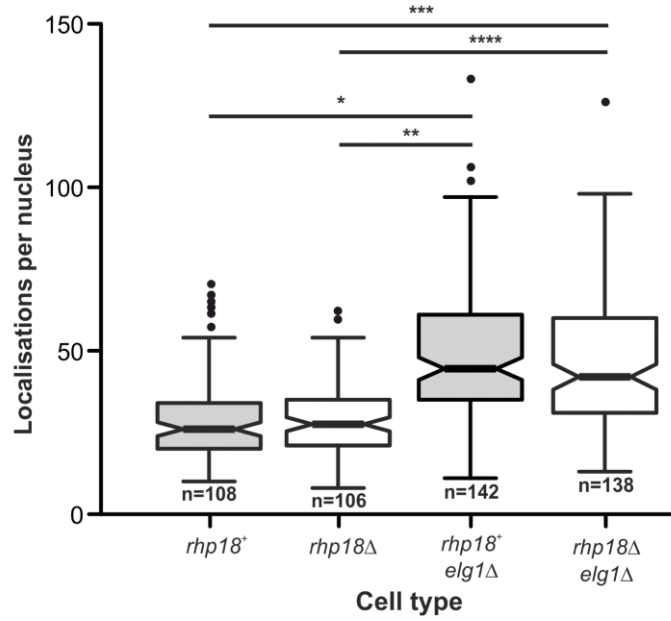
**5.4.2 Polymerase  $\delta$** 

In contrast to the leading strand, lagging strand synthesis relies heavily on PCNA. Polymerase delta processivity is stimulated by PCNA (Dieckman and Washington 2013) and has a high affinity for the sliding clamp (Chilkova 2007). Cross-linking co-IPs in fission yeast demonstrate that Pol  $\delta$  catalytic subunit can be readily isolated with PCNA (Figure 5-1 I and J). Thus, any defects in PCNA-loading or functionality could have profound effects on lagging strand synthesis during S-phase. In light of the data provided from biochemical assays that suggest lagging strand synthesis is impaired in the absence of Ub-PCNA, a hypothesis was formed to explain these phenomena. If ubiquitylation of PCNA is preventing its untimely removal from the DNA, then preventing this modification may also effect the chromatin-association of the lagging strand polymerase. Removing the PCNA:Pol  $\delta$  complex prior to Okazaki fragment completion could result in an increase in ssDNA gaps left behind the fork, consistent with the S1-nuclease digest assays (Figure 5-1E). Thus, in order to investigate the effect of Ub-PCNA on Pol  $\delta$  chromatin association, DNA-bound mEos2-Cdc6 was measured using motion blur based PALM imaging.

Increasing the amount of chromatin associated PCNA by deletion of *elg1* resulted in more Cdc6 localisations detected, suggesting that the amount of PCNA on the DNA directly affects the amount of polymerase delta on the DNA (Figure 5-5A). This result correlates well with the previous biochemical data, demonstrating more polymerase delta was recovered in a Co-IP for PCNA in an *elg1 $\Delta$*  background (Figure 5-1H). However, PALM microscopy analysis was unable to detect a difference in DNA-bound Cdc6 when comparing *rhp18<sup>+</sup>* and *rhp18 $\Delta$*  cells (Figure 5-5A). There was also no significant change in the levels of Cdc6 detected when deleting *rhp18* in an *elg1 $\Delta$*  genetic background, when compared to *elg1 $\Delta$* . The hypothesis that less Cdc6 would be associated with the chromatin in the absence of *rhp18* cannot therefore be accepted from this data.

The inconsistency between PCNA and Cdc6 chromatin association when deleting *rhp18* could be a consequence of the distributive nature of polymerase delta. The lagging strand is replicated discontinuously by the formation of Okazaki fragments, which requires recycling of the polymerase. This distributive nature of the enzyme, coupled with the low amounts of localisations per nucleus (median = 26) could make detecting small changes difficult with this method. Previous data from this project indicate that polymerase delta could interact more readily with the ubiquitinated form of PCNA. Exposure to hydroxyurea is known to increase levels of PCNA ubiquitylation in fission yeast (Frampton 2006) and overexpression of Rhp18 results in increased PCNA ubiquitylation in the absence of DNA damage (Figure 5-1G). In both cases, augmented amounts of ubiquitinated PCNA can be recovered from co-immunoprecipitation with Cdc6 (Figure 5-1I). Thus, with the intention of teasing out any underlying phenotype, both *rhp18<sup>+</sup>* and *rhp18 $\Delta$*  cells were synchronised into S-phase in the presence of hydroxyurea and polymerase delta chromatin-association was quantified using PALM. In wild type cells, the amount of chromatin associated polymerase delta increased when treated with HU, however this increase was not detected in the absence of *rhp18* as DNA-bound levels of Cdc6 remained similar to untreated (Figure 5-5B). When considered alongside the previous biochemical data this result suggests that the polymerase delta:PCNA interaction is strengthened when PCNA is ubiquitinated and that this can increase that amount of Cdc6 associated with the chromatin.

A



B

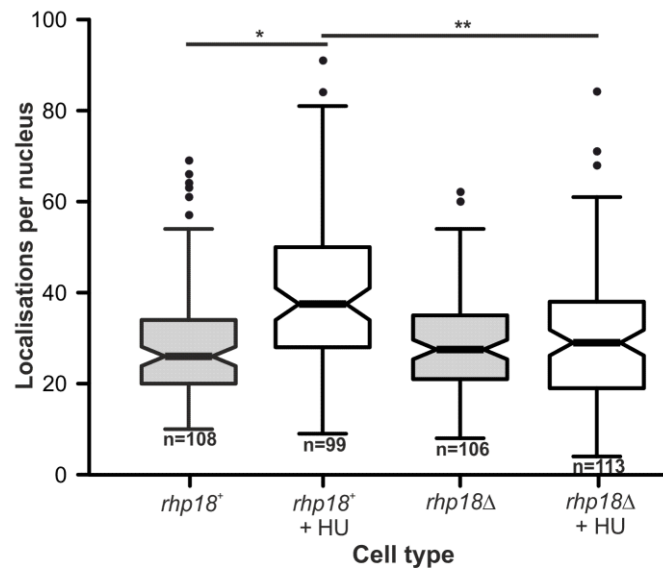


**Figure 5-5. Measuring the effect of PCNA-loading on Pol  $\delta$  chromatin association.**

Quantification of nuclear mEos2-Cdc6 localisations during motion blur PALM imaging. A) Pol  $\delta$  chromatin association in unperturbed S-phase cells. *P* values: \* =  $1.5 \times 10^{-17}$ , \*\* =  $1.8 \times 10^{-19}$ , \*\*\* =  $6.1 \times 10^{-13}$  and \*\*\*\* =  $1.1 \times 10^{-14}$ . B) Pol  $\delta$  chromatin association in response to increase PCNA ubiquitination. G2 cells harvested from lactose gradients were incubated in the presence of 10mM hydroxyurea for 120mins to induce PCNA ubiquitination prior to imaging. *P* values: \* =  $5.8 \times 10^{-8}$  and \*\* =  $8.4 \times 10^{-7}$ . Significance testing in both experiments was from two-tailed student's *t*-test.

## 5.5. Single-particle tracking of polymerases in live fission yeast

One aim of this chapter was to use PALM to test the hypothesis that *rhp18* deletion effects the chromatin association of polymerase delta during unperturbed S-phase. The hypothesis was centred on the reduction of chromatin associated PCNA observed in the *rhp18* $\Delta$  background, suggesting that this may in turn reduce the amount of DNA-bound Pol  $\delta$ . If this prediction were true, then it could explain some of the earlier observations concerning replication delay in late replicating regions and increased S1-nuclease sensitivity.

It is possible that there is no effect in the global chromatin association Pol  $\delta$  in the presence and absence of PCNA ubiquitylation. However, the prediction made from the previous data is that lack of Ub-PCNA leads to lagging strand synthesis defects, specifically a general slowing of replication, which would be best explained by weakened PCNA:Pol $\delta$  interaction. A possible reason why the predicted difference was not observed in Figure 5-4A could be due to weaknesses in the methodology. As explained earlier, lagging strand synthesis is a dynamic process and Pol  $\delta$  is considered a distributive enzyme as each molecule is only required to synthesise one Okazaki fragment before it releases from the chromatin (Hu 2012). The PALM-based approach developed in Chapter 4 requires that the chromatin-associated sub-species of the molecule of interest is stably associated with the DNA for at least the same time as the camera exposure setting. This would result in a well-defined Airy disk that would be recognised by the localisation software. However, if a molecule was DNA-associated for a shorter time than the camera exposure settings and then was released from the chromatin, this could result in a blurring of the PSF, preventing it from being detected. The approach in Chapter 4 was developed using proteins that are assumed to have long DNA residency times, based on their roles. If Pol  $\delta$  activity is shorter than the 350ms exposure time used then this could result in only a fraction of the bound polymerase being detected.

In order to assess whether the dynamics of lagging strand synthesis were preventing detection of polymerase binding events in the motion blur based PALM approach, an experiment using sptPALM in live fission was designed. The aim of this experiment was to try to extract information about the dynamics of Pol  $\delta$  in live cells, in the presence and absence of *rhp18*. Firstly, analysis of the distribution of molecular diffusion coefficients

could potentially reveal any small changes in the diffusivity of Pol  $\delta$  molecules. Also, examination of the amount of time static molecules are detected for could provide an insight into the stability of Pol  $\delta$  chromatin association.

### 5.5.1 Optimising Pol $\delta$ tracking in live *S. pombe*

Single-particle tracking was implemented in the previous chapter to extract a diffusion coefficient for freely diffusing Mcm4-mEos3.1 proteins. This experiment was performed on SR-1 microscope that has an older version of the Photometrics® Evolve™ 512 EM-CCD camera. In order to run the camera chip fast enough to perform sptPALM, the imaging region was cropped to a small ROI which limited the number of cells that could be processed (< 5 cells). After the installation of SR-2, the addition of the Evolve™ 512 Delta allowed for sptPALM experiments using the full chip, and with slightly shorter exposure times (25ms).

To image live cells, samples were synchronised by lactose gradient centrifugation as previously described before being placed on EMM-agarose pads (Materials and Methods). Imaging routines were similar to previous experiments using Mcm4, using pulsed 405nm activation to control molecular density. Localisation analysis was performed in PeakFit to create a raw data set of ‘Total localisations’ (Figure 5-5A). To ensure that any molecular tracks that were detected during sptPALM processing only originated from the nucleus, localisation data sets were filtered. Firstly, maximum intensity projections of the raw data were created to identify nuclear regions based on mEos2-Cdc6 fluorescence (as in Figure 4-3A). Next, a mask of all nuclear regions in the image was created using the ImageJ selection and mask tools. This mask was then used to filter out cytoplasmic and membranous localisations using the PeakFit plugin ‘Filter Results’, creating a final ‘Filtered localisation’ data set (Figure 5-6A)

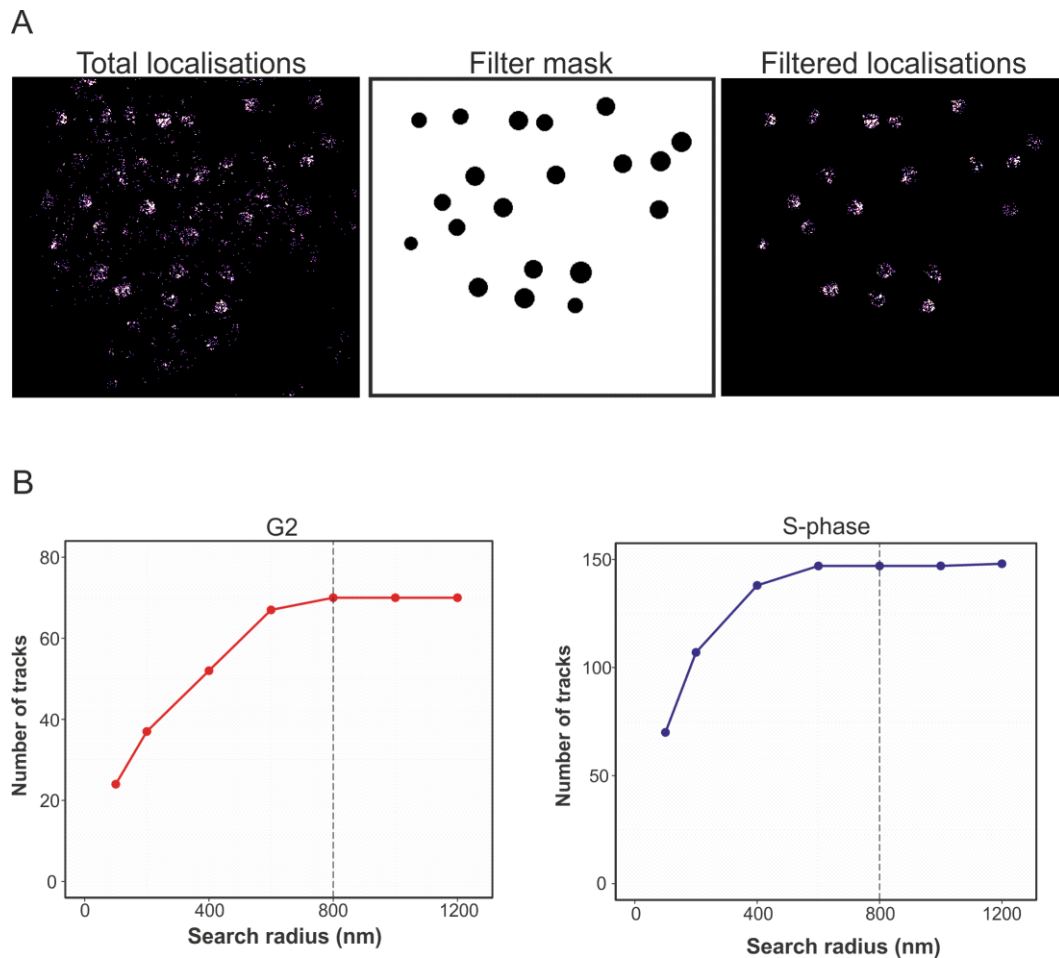


**Figure 5-6. Optimisation of post-acquisition image processing for sptPALM analysis.**

A) Removal of cytoplasmic and membranous localisations prior to sptPALM analysis. Total localisation data sets were filtered by retaining localisations that appeared only within a user-defined mask of nuclear areas. B) Optimising the search radius for single particle tracking of mEos2-Cdc6. The number of molecular tracks with a minimum of 4 steps plotted as a function of search radius in both G2 and S-phase cells. Dotted line represents chosen radius whereby no more tracks can be created. Data was extracted from a minimum of 2 repeats that contained >10 nuclei. Note the small number of tracks obtained from the experiment, this is discussed later in the chapter.

As mEos2-Cdc6 is complexed with other Pol  $\delta$  holoenzyme subunits, similar to Mcm4-mEos3.1 forming part of the Mcm2-7 complex, it was expected that the same search radius of 800nm could be used based on the previously described probability distribution (Figure 4-4C). This radius proved to be optimal as analysis of number of molecular tracks detected as a function of search radius showed that no additional traces longer than four steps could be made after 800nm (Figure 5-6B).

### 5.5.2 Comparing dynamics of Pol $\delta$ in G2 and S-phase

The primary measurement of sptPALM experiments is that of diffusivity. When comparing wild type and *rhp18 $\Delta$*  cells undergoing DNA synthesis our hypothesis was that preventing PCNA ubiquitylation would result in a change in the diffusivity of Pol  $\delta$ .

This was predicted to manifest as an increase in the amount of freely diffusing molecules identified, and a subsequent decrease in static traces.

With the purpose of ensuring that the sptPALM method could be applied in *S. pombe* to visualise changes in diffusivity of molecules between cell types, G2 and S-phase mEos2-Cdc6 cells were compared. The assumption was similar to that of previous experiments in Chapter 4. Cells in G2 would not require Pol  $\delta$  to be DNA-bound, as bulk replication would have been completed therefore; the majority of detected molecular tracks will be diffusive in nature. Conversely, in S-phase cells Pol  $\delta$  will be recruited to the DNA for lagging strand DNA synthesis. The prediction was that a significant proportion of molecule traces would be of a 'static' nature, as the displacement of the polymerase on the DNA will be less than the localisation precision of the experiment.

Both cell cycle stages were imaged using the protocol described above. Experiments were repeated a minimum of three times and the filtered data sets for each repeat were combined and analysed using the PeakFit 'Trace Diffusion' plugin. Mean squared displacement analysis exhibited a clear difference in average diffusivity of the polymerase between cell cycle stages (Figure 5-7A). Cells in G2 exhibited a 2D apparent diffusion coefficient for mEos2-Cdc6 of  $D^*=0.5 \mu\text{m}^2/\text{s}$  whereas in S-phase cells it was slower at  $0.2 \mu\text{m}^2/\text{s}$ . This slower average diffusion is due to the increase in DNA bound species. Surprisingly, when the distribution of apparent diffusion coefficients was examined for both cell types, the percentage of molecular tracks which had extremely low (static) coefficients ( $<0.1 \mu\text{m}^2/\text{s}$ ) was particularly high (47%) in G2 cells (Figure 5-7B). Although there were less static molecules in G2 than S-phase, this result is contradictory to the predicted outcome of very few DNA-bound molecules in G2 cells.

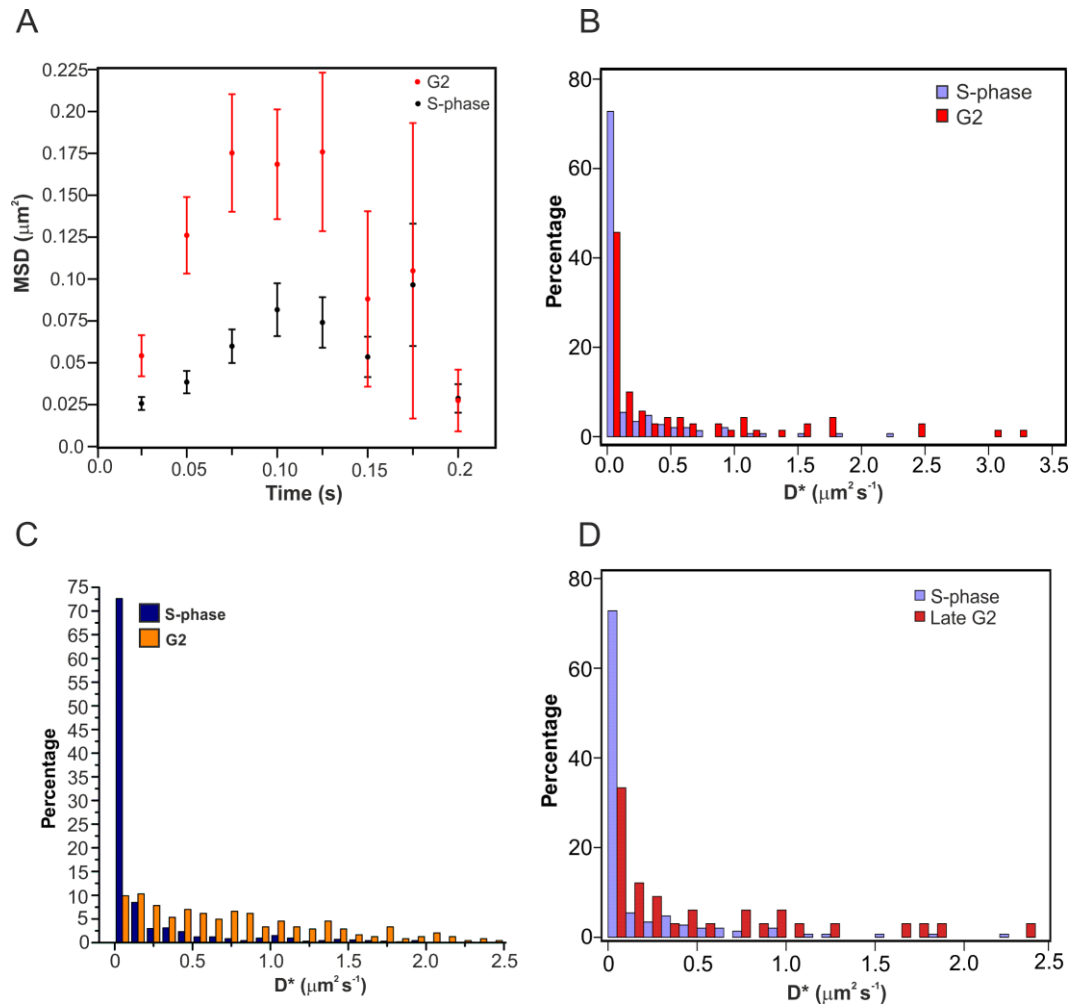


**Figure 5-7. sptPALM analysis of Pol  $\delta$  in G2 and S-phase cells.**

A) Mean squared displacement analysis of mEos2-Cdc6 in both G2 and S-phase fission yeast cells imaged with 25ms exposure time. Tracks containing minimum of 4 steps were retained for analysis. Number of tracks per sample: G2 = 70, S-phase = 147. Linear fitting of the first four data points revealed apparent diffusion coefficients ( $D^*$ ) of  $0.5 \mu\text{m}^2/\text{s}$  and  $0.2 \mu\text{m}^2/\text{s}$  for G2 and S respectively. Data was acquired from multiple imaging repeats (G2 = 5, S = 3). B) Histogram of  $D^*$  values for G2 and S-phase data sets. Bin size =  $0.1 \mu\text{m}^2/\text{s}$ . C) Histogram of  $D^*$  values for Mcm4-mEos3.1 in G2 and S-phase collected from experiment in Figure 4-8. Number of tracks: G2 = 250, S-phase = 750. This data was obtained with the help of Dr Rémi Boulineau. D) Histogram of mEos-Cdc6  $D^*$  values obtained from S-phase and late G2 cells. Number of tracks: S-phase 147 (3 repeats), Late G2 = 34 (3 repeats).

To ensure that the type of analysis was not biased towards static molecular tracks, sptPALM of Mcm4-mEos3.1 from Chapter 4 was analysed in the same manner. A similar prediction was made concerning the diffusivity of Mcm4 in G2 and S-phase as was made for Cdc6, based on previous observations in Figure 4-8. In agreement with the hypothesis, the distribution of G2 and S-phase Mcm4 apparent diffusion coefficients were vastly different (Figure 5-7C). More than 70% of the tracks in S-phase cells had a  $D^*$  value of  $<0.1 \mu\text{m}^2/\text{s}$ , compared to just 10% of G2 tracks. This result suggest that this type of

analysis does not bias towards static molecular tracks indicating that the data regarding Pol  $\delta$  is most likely accurate.

It is possible that the static Pol  $\delta$  species detected in G2 cells are performing DNA synthesis at late replicating regions or are part of gap filling in post-replication repair (PRR) pathways. G2 cells isolated in lactose gradient centrifugation experiments are the small cells produced just after cytokinesis, thus are quite early G2 cells. If Pol  $\delta$  was performing such roles, then one might expect to see a decrease in the amount of active DNA-bound polymerase in mid-late G2 cells. To test this hypothesis, small G2 cells isolated from lactose gradients were incubated for 1 hour at 30°C to progress into mid-late G2. Results from sptPALM analysis showed a slight reduction in the percentage of static traces from 47% (early G2) to 33% (Figure 5-7D). This value is still higher than expected and could potentially indicate that Pol  $\delta$  is involved in DNA synthesis pathways during G2 right up to mitosis.

### 5.5.3 Investigating the effect of *rhp18* $\Delta$ on Pol $\delta$ dynamics

Confident that the sptPALM methodology was applicable for studying Pol  $\delta$  in live cells, mEos2-Cdc6 was imaged using the sptPALM routine in an *rhp18* $\Delta$  genetic background in cells undergoing DNA synthesis. Diffusion analysis revealed no significant difference between the diffusivity of mEos2-Cdc6 molecules in *rhp18*<sup>+</sup> and *rhp18* $\Delta$  cells (Figure 5-8A). Both strains exhibited static track percentages of >70%, indicating that there is no effect on the chromatin association of Pol  $\delta$  in the absence of PCNA ubiquitylation. This result is consistent with data collected using the motion blur approach, suggesting that the observed result in those set of experiments is most likely accurate and that Pol  $\delta$  dynamics do not hinder the measurement of global polymerase chromatin association.

Although both PALM techniques demonstrate that there is no difference in the chromatin binding of polymerase delta in the absence of S-phase dependent PCNA ubiquitylation, the delay in DNA synthesis in late replicating regions could be due to a slower processivity of PCNA:Pol  $\delta$  compared to the Ub-PCNA:Pol  $\delta$  complex. This effect may not manifest itself as a change in the amount of polymerase bound at any one time, rather it could be a result of reduced primer extension before release or merely slower Okazaki fragment synthesis. Studying the speed of a synthesising DNA polymerase using

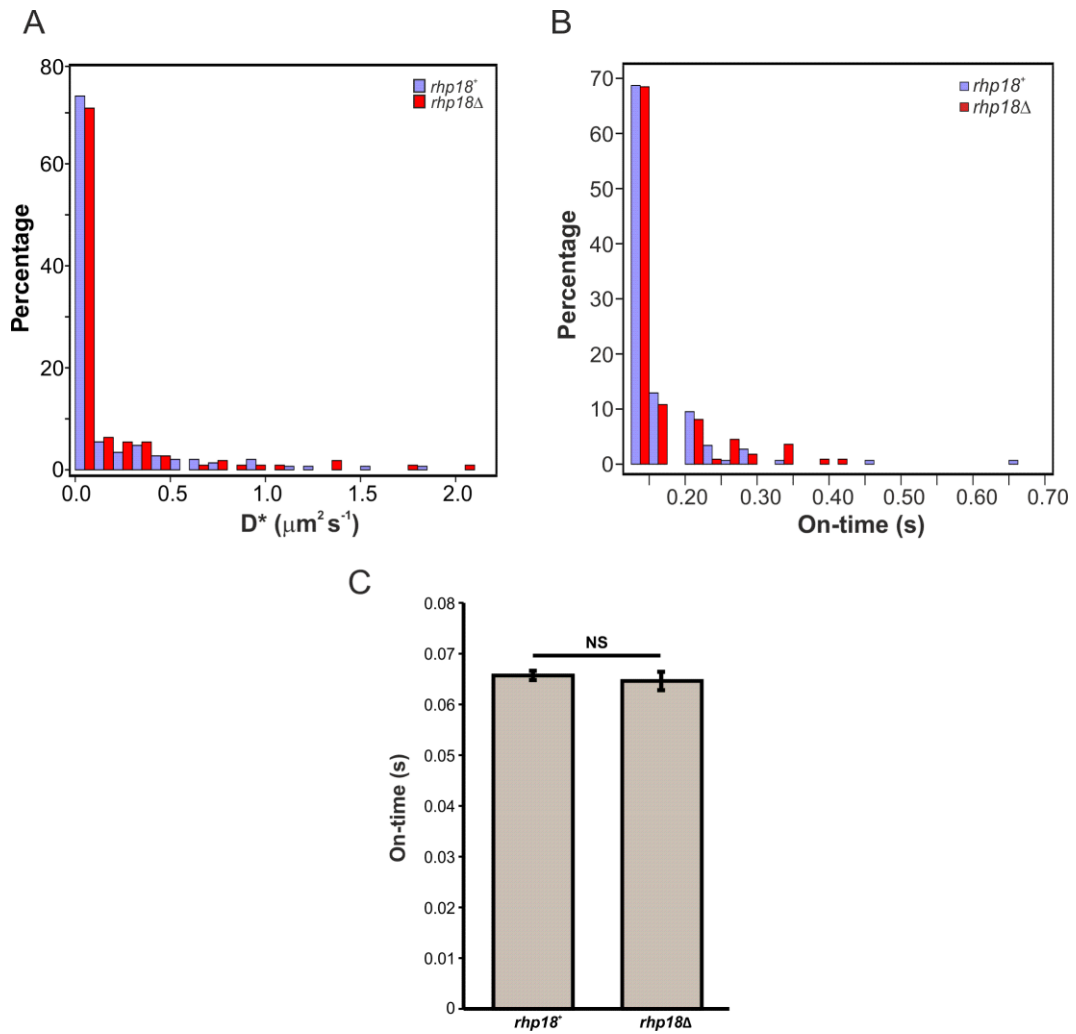


**Figure 5-8. sptPALM analysis of the effect of *rhp18* $\Delta$  on Pol  $\delta$  dynamics.**

A) Histogram of apparent diffusion coefficients collected from *rhp18*<sup>+</sup> and *rhp18* $\Delta$  cells undergoing DNA synthesis. Bin size =  $0.1\mu\text{m}^2/\text{s}$ . Number of molecular tracks: *rhp18*<sup>+</sup> = 147, *rhp18* $\Delta$  = 111. B) mEos2 fluorescent 'on-time' distribution from data present in A). Bin size = 0.05 sec. C) On-time analysis from 'static' tracks. Tracks were comprised from localisations that occurred within 100nm radius for a minimum of 2 consecutive frames. Data presented is the mean value from 3 independent repeats. Error bars denote standard deviation.

sptPALM would be challenging due to the short fluorescent lifetime of the mEos2 fluorophore. The residency time each polymerase spent bound to the DNA could potentially be extracted from tracking data by analysis of the average number of frames mEos2 fluorescence was detected, referred to here as 'on-time'. If lack of Ub-PCNA resulted in instability of the PCNA:Cdc6 complex and thus premature release of the polymerase, it could be predicted that this would be observed as a reduction in the average on-time. Molecular trace on-times were extracted from traced localisation data sets for both cell types. Histograms of on-time distributions reveal no difference between *rhp18*<sup>+</sup> and *rhp18* $\Delta$ , both exhibiting median on-time of 0.15s (Figure 5-7B). This analysis suggests that there is no detectable difference in Pol  $\delta$  residency time in the absence of

Ub-PCNA. However, traced localisation data sets contain only molecule traces that possess a minimum of five consecutive localisations within the defined search radius (800nm). In order to assess whether lack of Ub-PCNA resulted in an increase in the number of static tracks with <5 localisations, which would correlate with a potential premature release from the chromatin, static molecules were traced with a search area of 100nm for a minimum of 2 consecutive frames. Average on-times extracted from this analysis showed no difference when comparing the two cell types (Figure 5-7C), suggesting decreased synthesis in late replicating regions may not be from premature release of the Pol  $\delta$  polymerase in absence of Ub-PCNA. However, the short fluorescence lifetime of mEos2 could be preventing observation of association times. If Pol  $\delta$  were chromatin bound for longer than the lifetime, even in the *rhp18 $\Delta$*  background, then this would give the same result as in Figure 5-7C.

#### 5.5.4 Limitations of the sptPALM approach in *S. pombe*

During this part of the study, several limitations were identified when applying the sptPALM approach in fission yeast. In combination, these limitations prevented the acquisition of large numbers of molecular traces and substantial amount of imaging had to be performed in order to retrieve the small amount of data presented. Typically, experiments involving single particle tracking acquire several hundred to several thousand molecular tracks in order to present significant and reproducible data (Uphoff 2014). In this study, the data was limited to <150 tracks per sample. These tracks were collected from tens of cells across a minimum of three repeats, demonstrating the difficulty in building a large data set.

There are several factors affecting the data collection in fission yeast. Firstly, the large axial depth of *S. pombe* (~2-3  $\mu\text{m}$ ) coupled with the small depth of field of the objective lens (NA = 1.49) results in a substantial amount of molecules going undetected as they were out of focus. This reduced the total number of molecules that could be sampled within each cell. The small focal depth of the microscope also affected the length of the single molecule tracks that could be detected (Figure 5-9A). Freely diffusing molecules can potentially diffuse in and out of the focal plane while they are fluorescing. Moving out of the focal plane results in a defocusing of the single molecule Airy disk and rejection by the localisation software. Thus, the resulting tracks will not contain enough

consecutive localisations to be retained in further analysis (minimum of 4 steps, 100ms). Molecules that are retained will have arisen from either static, DNA bound species (Figure 5-9A, red line) or from molecules that diffuse within the focal plane for  $\geq 5$  consecutive frames (Figure 5-9A, blue line).

A compounding factor that restricts data collection are the characteristics of the mEos2 fluorophore. As demonstrated in previous reports (Annibale 2010, Lando 2012, Lee 2012), the mEos fluorophore variants can transiently enter a non-fluorescent state, with a lifetime of milliseconds to seconds, before returning to the fluorescently ‘competent’ ground state. This phenomena is termed ‘blinking’ and can severely affect the ability to extract single molecule tracks of suitable length. Blinking of a single fluorophore during the window of detection would result in loss of localisations in consecutive frames thus ‘breaking’ a molecular trace (Figure 5-8B).

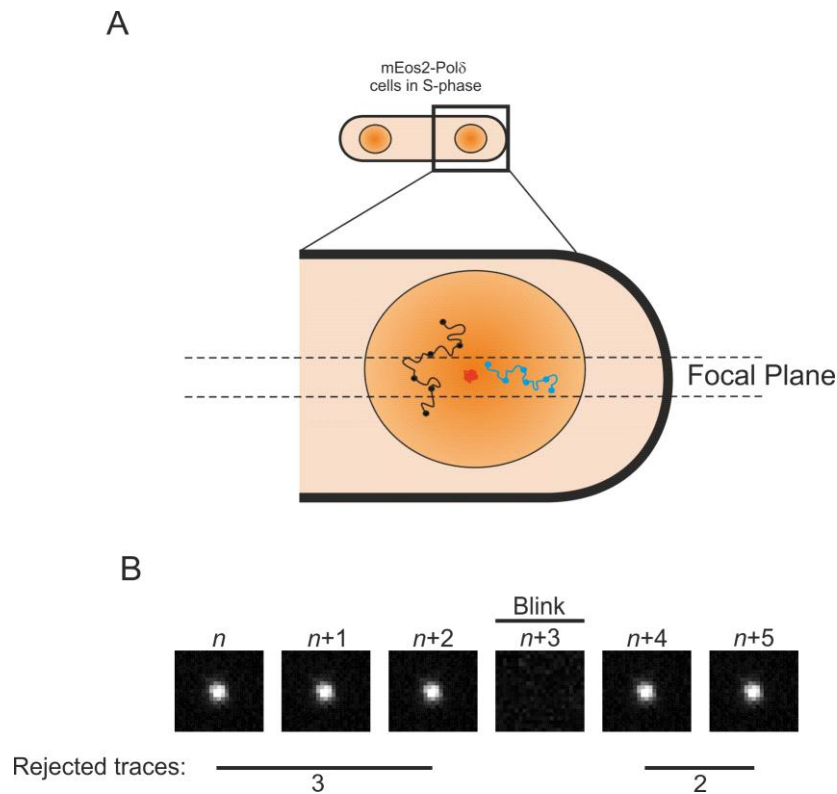


**Figure 5-9. Limitations during application of the sptPALM approach in *S. pombe*.**

A) Schematic representation of the diffusion of single molecules in the focal plane of the microscope. Solid lines represent potential diffusion paths and solid dots indicate localised positions. Freely diffusing proteins could either diffuse in and out of the focal plane (Black line), resulting in  $< 5$  localisations detected. Or, diffusive proteins could reside for long enough within the focal plane to detect  $\geq 5$  localisations if they are chromatin associated (Red line) or diffuse within the focal plane for long enough (Blue line). B) Demonstration of the effect of blinking of the mEos fluorophores on tracing single molecules. In this hypothetical example, a molecule has been detected for 3 frames before it transiently enters a dark state (‘Blink’). Although the molecule re-appears for two more consecutive frames the trace has now been broken into two tracks of 3 and 2 localisations which will be rejected by sptPALM analysis software.

The data presented here highlight these two limitations and must be considered when designing future single-molecule experiments in yeast. A third factor that can affect such an experiment is the level of expression of the protein of interest. This will be experiment specific, but low expression levels will ultimately result in less molecular tracks per experiment. This is considered as one reason for the low amount of data collected in this study, as the level of expression for each polymerase was low.

## **5.6. Creation of a stable human cell line for visualising endogenous PCNA via PALM**

During this study, a collaboration with Dr Tomoo Ogi and Dr Yuka Nakazawa highlighted that PCNA ubiquitylation in unperturbed S-phase is not a fission yeast specific phenomena. Synchronisation and release both osteosarcoma cells (U2OS) and immortalised human fibroblasts (1BR3hTERT) resulted in an increase in mono-ubiquitinated PCNA that appeared concomitantly with an increase in S-phase cells. This observation supports data collected in fission yeast, which highlights a role for Ub-PCNA in normal DNA synthesis. However, no more experiments were performed in human cell lines on the effect of this S-phase dependent ubiquitylation. Thus, for future experiments involving PCNA, a stable cell line was created that allows the study of PCNA localisation in human cells via PALM.

In order to visualise PCNA via fluorescence microscopy there are several conventional techniques that could be employed. Firstly, ectopic expression of a fluorescently-tagged copy of PCNA could be introduced to the cells (as performed in fission yeast) either from a plasmid or integrated into the genome. While this approach has been previously successful in mammalian cells (Leonhardt 2000, Essers 2005, Ge and Blow 2010), a method that did not alter PCNA protein levels or involve direct fusion of the tag to PCNA was desired. Another key approach to visualising PCNA localisation is via immunofluorescence. Targeting PCNA either by direct or indirect immunofluorescence is a standard approach and could be compatible with stochastic optical reconstruction microscopy (STORM) to create super-resolution images. Although this approach may be useful in the future, it requires fixation of the sample and is therefore incompatible with live cells and the motion blur based PALM approach. In light of these restrictions, an

approach was chosen that utilises expression of an intracellular chromobody that targets PCNA.

Previously it has been shown that expression of highly specific, single chain antibodies (nanobodies) generated in *Camelidae* species can be fused to fluorescent proteins, creating 'chromobodies'. These can be expressed in cells to target and highlight a specific antigen for fluorescence microscopy (Rothbauer et al 2006). More recently, a chromobody was developed which specifically targets human PCNA and allows for visualisation of PCNA localisation throughout the cell cycle without influencing PCNA functionality (Burgess 2012, Chromotek®). This chromobody was made commercially available as 'Cell Cycle Chromobody', with either TagGFP or TagRFP as the fluorescent protein.

In order to adapt the Cell Cycle Chromobody (Chromotek) for use with PALM microscopy, the expression plasmid was purchased and the fluorophore was switched from TagGFP to mEos3.2 (Figure 5-10A, Materials and Methods). In order for future experiments to be quantitative, a stable cell line was required whereby expression of the chromobody was at a similar level between cells. To create a stable human cell line the pCCC-mEos3.2 plasmid was linearised by restriction enzyme digestion before transfection into U2OS cell line. U2OS cells were chosen as previous experiments by Dr Ogi and colleagues were performed in U2OS, and stable U2OS cell lines were previously created by Chromotek for the TagGFP/RFP versions. Successful transfectants were screened for by growing cells in the presence of geneticin (G418) and colonies were retained for western blot analysis. Whole cell protein extracts from G418 resistant colonies were probed with anti-mEos2 antibody and extracts that revealed a band at ~40 kDa (mEos3.2 chromobody molecular weight) were retained for microscopy analysis (Figure 5-10B). Unfortunately, due to time restrictions no further experiments were performed on these cells. However, they will be utilised in future studies in the Carr lab to study PCNA spatial distribution and chromatin association during DNA replication.

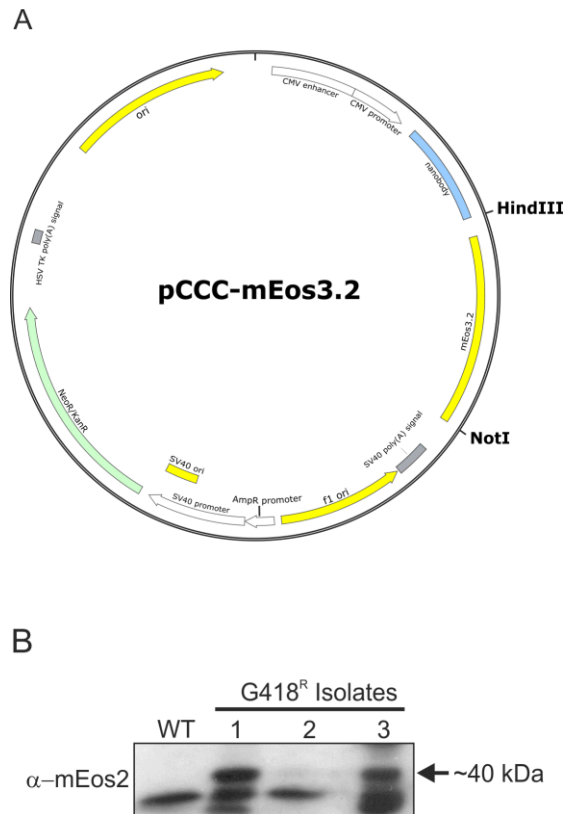


**Figure 5-10. Creation of stable human cell line expressing an intracellular nanobody to PCNA.**

**A)** Plasmid map showing the nanobody-mEos3.2 construct and the Kanamycin/G418 antibiotic resistance gene. mEos3.2 was cloned into the plasmid as a NotI/HindIII fragment and the positions shown. **B)** Anti-mEos western blot of whole cell extracts from G418 resistant colonies. Isolates 1 and 3 possess an extra band at the molecular weight expected for the nanobody.

## 5.7. Discussion and conclusion

The aim of this chapter was to test a previous hypothesis drawn from biochemical data and explore the role of PCNA ubiquitylation during unperturbed DNA synthesis using PALM based experimental approaches. Previous to the experiments described above, a substantial amount of biochemical and genetic data had been collected in the Carr lab that suggests ubiquitylation of PCNA during normal S-phase is linked to its stability once loaded onto the DNA. Furthermore, the DNA-loading and ubiquitylation status of PCNA was suggested to affect its interaction with the lagging strand polymerase, Pol  $\delta$ . The standard biochemical approaches used to generate the previous results involve cellular disruption and often require chemical fixation, both of which could be prone to generating artefacts. Thus, to support these observations using a less-invasive, *in vivo* method, the levels of chromatin associated PCNA and replicative polymerases were measured using motion blur based PALM.

### **5.7.1 PCNA ubiquitylation may prevent PCNA unloading during Okazaki fragment synthesis**

PCNA mono-ubiquitylation has been extensively linked to the recruitment of translesion synthesis (TLS) polymerases during S-phase in response to DNA lesions (Stelter and Ulrich 2003, Kannouche 2004, Watanabe 2004). The basic model involves ubiquitylation of PCNA in response to stalling of the replicative polymerase at a site of DNA damage. This ubiquitylation acts as a signal and recruits TLS polymerases to the damage, whereby they switch places with the stalled polymerase. These enzymes can accommodate bulky lesions in their active sites that enables the cell to synthesise across a DNA lesion. This method of ‘polymerase switching’ almost exclusively requires PCNA ubiquitylation, but the exact mechanism and the resulting effect of Ub-PCNA on the replicative polymerases is still unknown.

Although the presence of Ub-PCNA in *S. cerevisiae* is only observed in response to genotoxic stress, ubiquitylation has been detected during unperturbed growth in other organisms, including fission yeast (Frampton 2006), chicken DT40 (Simpson 2006), frog extract (Leach 2005) and human cells (Niimi 2008). In addition, some studies have reported induction of Ub-PCNA in the presence of replication intermediates (Das-Bradoo 2010, Karras 2010). More specifically, previous data collected by Dr Daigaku and colleagues suggest that ubiquitylation of PCNA occurs upon the onset of DNA replication, in both fission yeast and human cell lines. These observations are significant as Ub-PCNA is thought to act to recruit TLS polymerases; however, these enzymes are considered not to be required during unperturbed S-phase.

In search of a role for Ub-PCNA during S-phase, the loading status of PCNA in wild type and *rhp18Δ* backgrounds was investigated. Previous chromatin fractionation experiments of cells undergoing S-phase indicated a potential reduction in loaded PCNA, especially in mid-late S-phase. In agreement with this observation, PALM imaging of mEos3.1-PCNA during DNA synthesis revealed a significant decrease in the level of chromatin-associated PCNA (Figure 5-1B). This result supports the premise that the ubiquitylation of PCNA plays a role in its chromatin association once loaded onto the DNA. From this data, two hypotheses were formed based on the role of ubiquitin in stabilisation of loaded PCNA. Either, ubiquitin causes a structural alteration to PCNA that creates a more stable

association with the DNA, or the presence of a ubiquitin moiety prevents PCNA from being unloaded.

To examine these possibilities further, the requirement for PCNA ubiquitylation was studied in the absence of RFC-like unloader Elg1 (Figure 5-2C). Retention of PCNA on the DNA in an *elg1* $\Delta$  background was observed as predicted from previous studies (Kubota 2013, Shiomi 2013 and Figure 4-10), however consistent with the second hypothesis, preventing PCNA ubiquitylation by deletion of *rhp18* did not reduce loaded PCNA levels. In fact, the double mutant exhibited slightly higher PCNA retention, the reason for this is unknown but could be a result of compounding genomic instabilities in the absence of *rhp18* and *elg1* leading to a requirement of more PCNA. The statistical significance of this difference is not as strong as other effects observed in this study and thus could be a result of experimental variability. If such a case is true, then this will be important to note for future studies utilising the motion blur PALM method, and greater significance may be required to accurately interpret the data.

Together these data suggest that ubiquitylation of PCNA during DNA synthesis stabilises its association with the chromatin by preventing untimely unloading by Elg1. Consistent with this hypothesis are results from the Carr lab that show accumulation of single-stranded gaps in the genome in *rhp18* $\Delta$  cells during S-phase. These observations could point to incomplete Okazaki fragment maturation caused by premature Elg1-dependent PCNA unloading. However, a recent study in budding yeast concluded from ChIP-seq based studies that less PCNA was unloaded from HU arrested forks in *pcn1-K164R* mutants (Yu 2014). This is in direct conflict with the suggestion that ubiquitylation inhibits unloading. However, these results are in response to fork arrest, which was not tested in this study, and in budding yeast that seems to possess different PCNA based mechanisms (discussed below). In order to investigate this phenomenon further, *in vitro* studies must be performed that assess the ability of Elg1 to remove Ub-PCNA from DNA.

### 5.7.2 Chromatin association and ubiquitylation status of PCNA effects its interaction with the lagging strand polymerase

PCNA is considered to act as a processivity factor for the major replicative polymerases during genomic replication. Recent *in vitro* data have highlighted that this role is most important for lagging strand synthesis. In these experiments, Pol  $\epsilon$  bound weakly to PCNA and was able to perform leading strand synthesis in its absence (Chilkova 2007, Georgescu 2014). In contrast, Pol  $\delta$  demonstrated high binding affinity to PCNA and increased processivity in its presence. In light of the requirement for PCNA during DNA replication, specifically concerning lagging strand synthesis, and considering a new role for Ub-PCNA, the chromatin association of both polymerases was assessed in the absence of S-phase dependant PCNA ubiquitylation.

In the case of the leading strand polymerase, the deletion of *rhp18* resulted in no significant difference in Pol  $\epsilon$  DNA binding in the PALM studies (Figure 5-3). This is consistent with data from Dr Daigaku which suggest that PCNA ubiquitylation is important for lagging strand rather than leading strand synthesis. The small increase localisations detected in the *rhp18 $\Delta$  cell is not significant ( $P = 0.08$ , Student's T-test) and is considered to be due to experimental variability. The interesting observation from this experiment is the highly significant decrease of chromatin-bound Pol  $\epsilon$  observed in the *pcn1-K164R* mutant background. Lysine 164 is considered the major site for ubiquitin conjugation in PCNA and has been used extensively to study the role of PCNA ubiquitylation. The stark contrast between the *rhp18 $\Delta$  and *pcn1-K164R* strains reveals a potential additive hypomorphic effect of the mutation. No PCNA ubiquitylation is detected in the absence of Rhp18 in *S. pombe* (Frampton 2006, Figure 5-1A), thus it would be expected that the K164R mutant should possess a similar phenotype to *rhp18 $\Delta$ . The observed result could suggest either this mutation effects PCNA structure and thus effects DNA synthesis as a whole, or it could reveal a role for an alternative modification. Crystal structures of PCNA would suggest that such a small change would yield no conformational change in PCNA structure as a result of the modification (Freudenthal 2010). Data from the Carr lab show that *pcn1-K164R* possess a more severe phenotype in several assays, including reduced BrdU incorporation during S-phase. Interestingly, it has been shown that PCNA can be modified by the ubiquitin-related modifier SUMO (Small Ubiquitin-like Modifier) at lysine 164 in *S. cerevisiae* and humans (Hoegge 2002,***

Gali 2012). Thus, we tested whether SUMO may play a role at the replication fork with respect to leading strand synthesis. However, preliminary studies in a *pli1Δ* background demonstrated no significant effect on Pol  $\epsilon$  chromatin association (Figure 5-4B). This indicates that a more substantial effect on replication occurs in cells with the *pcn1-K164R* allele compared to *rhp18Δ*, and thus was excluded from further experiments in this study.

The genetic data collected prior to the experiments presented in this chapter implicated Ub-PCNA as having an important role in lagging strand synthesis. Conditional mutants in the lagging strand polymerase (*cdc6-m10*) and the ligase required during Okazaki fragment ligation (*cdc17-m68*) exhibited increased levels of Ub-PCNA at the restrictive temperature. Moreover, deleting *rhp18* in strains that contain defects in PCNA loading or lagging strand synthesis reduced cell viability. Coupled with the instability of loaded PCNA in *rhp18Δ* cells observed in PALM experiments, it was hypothesised that Ub-PCNA was playing a role in lagging strand synthesis by preventing PCNA dissociation from the chromatin. Based on this prediction, instability of loaded PCNA in *rhp18Δ* cells could result in a corresponding dissociation of Pol  $\delta$ . However, levels of chromatin-bound Pol  $\delta$  during DNA synthesis were measured by motion blur based PALM, and results showed no change in the amount of polymerase detected in the absence of *rhp18* compared to wild type cells (Figure 5-4A). This observation was repeated, in albeit limited, sptPALM experiments, that demonstrated no change in the percentage of static tracks detected between the two cell types.

These results appear to disprove the hypothesis that reduced levels of chromatin associated PCNA in an *rhp18Δ* strain causes a reduction in the amount of Pol $\delta$  bound to the DNA. This suggests that changing the levels of loaded PCNA does not directly affect the levels of DNA bound polymerase delta. However, when levels of PCNA were increased by deletion of the Elg1 unloader, an increase in the amount of chromatin associated Pol  $\delta$  was detected, in both biochemical and PALM-based approaches (Figure 5-1I and 5-4A). Pol $\delta$  chromatin association also followed a similar trend to PCNA in the absence of both *elg1 rhp18*, as DNA-bound Pol $\delta$  levels were epistatic with the *elg1* single mutant. The question then remains as to why does Pol  $\delta$  not follow PCNA's trend in the *rhp18Δ* background? One potential explanation for this may be purely a limitation of the motion blur PALM technique when observing highly dynamic processes such a lagging strand synthesis. However, this technique involves treatment of cells with sodium azide

prior to imaging, in order to prevent any ATP-dependent enzymatic loading/unloading of proteins during sample preparation and imaging. Thus, the sample should provide a snapshot of chromatin bound proteins at the time of azide addition without the need for fixation. Nevertheless, the retention of proteins to the DNA during data acquisition could depend on the strength of interaction with the DNA/protein. Application of sptPALM to observing lagging strand dynamic in live cells was made in an attempt to overcome potential pitfalls in the motion blur technique. However, as discussed previously the results agreed with motion blur data and as well as possessing additional limitations.

The slowing of DNA replication observed by BrdU-IP sequencing and the increased appearance of single strand gaps cannot thus be explained by a reduction in total DNA bound polymerase delta. A different explanation could be that Ub-PCNA also acts to increase the strength of interaction between Pol  $\delta$  and PCNA and thus correspondingly the processivity of the holoenzyme. Preventing PCNA ubiquitylation by deletion of *rhp18* could thus reduce the processivity of the polymerase, causing it to disengage with PCNA and the DNA more readily. One could imagine that this would lead to a general slowing in replication progression. Previous *in vitro* studies have focussed on the effect of PCNA ubiquitylation on Pol  $\delta$ . Diekman and Washinton (2013) demonstrated that the processivity of the lagging strand polymerase was increased 10-fold with the addition of PCNA to the reaction and 20-fold with the addition of Ub-PCNA. Another study demonstrated that mono-ubiquitylation of PCNA actually was stimulated when bound to Pol  $\delta$ , indicating that the Pol  $\delta$ :PCNA complex is a potential target for ubiquitylation. Consistent with the idea that replication dependent ubiquitylation of PCNA enhances its association with the polymerase; motion blur PALM imaging detected an increased association of Pol  $\delta$  in response to elevated Ub-PCNA levels in the presence of hydroxyurea (Figure 5-4B). This result is in agreement with IP data from Dr Daigaku (Figure 5-11) and presents an interesting quandary to the field in regards to the precise role of PCNA ubiquitylation.

### **5.7.3 Model: Ubiquitin, a signal for loaded PCNA?**

In light of the data collected previously in the Carr lab and presented here in this chapter, a new model for the role of PCNA ubiquitylation in S-phase is presented. During this project, it became clear that lagging strand synthesis and DNA damage bypass (DDB)

mechanisms appear seemingly very similar. Both processes involve PCNA and a polymerase loaded at a primer template junction. In the case of DDB, the replicative polymerase is stalled by a DNA lesion, which was considered the signal for inducing Rad6-Rad18 dependent PCNA ubiquitylation (Figure 5-11-v). However, as shown in this study, damage is not required for this ubiquitylation to occur in fission yeast. Thus, the most parsimonious explanation for this observation is that PCNA is ubiquitinated when loaded by RFC at a primer template junction at the beginning of each Okazaki fragment synthesis (Figure 5-11-i). This occurs via the Rad6-Rad18 complex, which is potentially recruited to the RPA coated ssDNA at the front of the lagging strand. Rad18 has been previously shown to be recruited by RPA in *S. cerevisiae* in response to MMS treatment, and was required for PCNA ubiquitylation (Davies 2008, Niimi 2008). In this model, Rad18 recruited to RPA at the lagging strand can then ubiquitinate PCNA, which acts as a platform for Pol  $\delta$  to bind. The strength of this association is increased when PCNA is modified compared to unmodified PCNA. Polymerase delta then proceeds to synthesise the new Okazaki fragment, during which the Ub-PCNA acts as a negative signal to prevent Elg1-dependent PCNA unloading (Figure 5-11-ii). Once the fragment is complete, Pol  $\delta$  dissociates and then PCNA is de-ubiquitinated after processing by Fen1 and DNA Ligase, allowing for Elg1-dependent removal (Figure 5-11-iii). It is difficult to determine whether PCNA is ubiquitinated on the leading strand when bound to Pol  $\epsilon$ , however genetic evidence suggests no role of Ub-PCNA on the leading strand (Figure 5-11-iv). Strand specific isolation of PCNA would be a potentially interesting experiment to observe leading strand specific modifications.

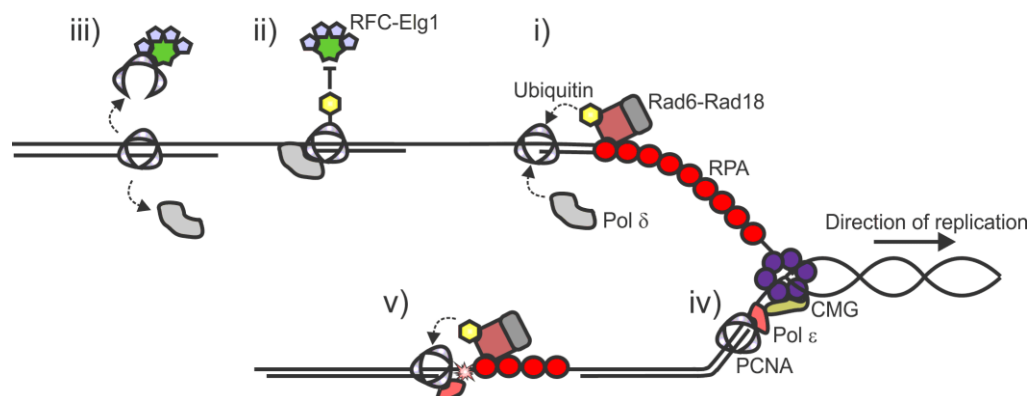


**Figure 5-11. Proposed model for the role of PCNA ubiquitylation at the replication fork.**

i) During unperturbed DNA synthesis, recruitment of RAD6-RAD18 to stretches of ssDNA-RPA on the lagging strand result in ubiquitylation of RFC loaded PCNA at primer template junctions. ii) During Okazaki fragment synthesis ubiquitin may serve to prevent Elg1-dependent unloading. iii) As each Okazaki fragment is completed, removal of ubiquitin (potentially by ubiquitin proteases) allows for Elg1 removal. iv) Polymerase epsilon is physically linked to the CMG helicase and may not be ubiquitinated due to lack of ssDNA-RPA. However upon colliding with DNA lesions v) RPA binds to ssDNA uncovered by the progressing helicase, recruiting RAD6-RAD18, resulting in PCNA ubiquitylation

In this model, ubiquitylation of PCNA is an S-phase dependent phenomena, however it is well documented that damage prior to or during S-phase can lead to induction of PCNA ubiquitylation. Experiments in human cells in the Ogi lab as part of this collaboration showed that UV irradiation induced PCNA ubiquitylation to levels greater than detected in normal S-phase. This could be explained by accumulated levels of PCNA at primer template junctions caused by global replication fork stalling, particularly from leading strand lesions. In this instance, single stranded DNA in front of the stalled polymerase is coated by RPA, which recruits Rad6-Rad18. Ubiquitylation then serves to prevent PCNA from being removed by Elg1, thus increasing the chance of TLS polymerase binding or initiation of template switching (Figure 5-11-v).

Previous studies of PCNA ubiquitylation and its role in TLS have hypothesised that the modification is a signal specifically designed to recruit specialised polymerases in response to DNA damage. It has been suggested that this recruitment leads to a disruption of the replicative polymerases in order to replace them with a damage tolerant species. However, data collected in this study and by Dr Daigaku demonstrate that Pol  $\delta$  binds strongly to Ub-PCNA and is enriched on chromatin when PCNA ubiquitylation is induced (Figure 5-11, Figure 5-5B). In the model being proposed here, ubiquitylation arises in the absence of DNA damage. Why then do TLS polymerase specifically interact with Ub-PCNA, if it is arising in the absence of damage? It is an interesting possibility that Ub-PCNA may not be acting as signal for DNA damage, but rather TLS polymerases use this modification as a discriminatory signal for distinguishing DNA-bound vs free PCNA. This becomes apparent when considering the expression levels of PCNA vs TLS polymerases (116,718 PCNA molecules vs 518 Pol  $\eta$  molecules in G2 *S. pombe*, Carpy *et al* 2014). Co-immunoprecipitation experiments in *S. pombe* demonstrated that it is extremely difficult to pull-down TLS polymerases with PCNA, even when PCNA ubiquitylation is upregulated by overexpression of Rhp18 (Y. Daigaku, data not shown). With high levels of freely diffusing PCNA in the nucleus, it would be important for the small number of TLS polymerases to interact specifically with the DNA bound PCNA. Access to PCNA at a stalled polymerase is predicted in this model to be due to dynamic association/disassociation of DNA polymerases at primer-template junctions, presenting the TLS polymerases with a chance to bind and replicate past the damaged base. Such

dynamic behaviour by the DNA polymerases has been previously reported (Hu et al 2012).

Although the recruitment of some TLS polymerases requires the ubiquitylation of PCNA, some studies have suggested that ubiquitylation is not entirely essential and that TLS occurs in its absence, albeit at a reduced efficiency (Acharya 2008, Hendel 2011, Wit 2014). If ubiquitylation of PCNA does prevent Elg1-dependent unloading of the sliding clamp, it would be interesting to see if deletion of *elg1* partially rescues any DNA damage phenotypes associated with lack of Ub-PCNA. The prediction being, in the absence of Ub-PCNA, removal of PCNA from the site of DNA damage could prevent ubiquitin-independent recruitment of TLS polymerases, thus causing a reduced efficiency of repair.

The timing of PCNA unloading by Elg1 during lagging strand synthesis is an interesting area of future study. Ensuring PCNA is not unloaded prematurely is of importance to ensure completion of Okazaki fragments. A recent study in budding yeast has suggested that Elg1-dependent PCNA unloading occurs after Okazaki fragment ligation (Kubota 2015). Degradation of the Cdc9 ligase during DNA replication resulted in retention of PCNA on the DNA to similar levels observed in an *elg1* $\Delta$  background. Although the modification of PCNA in fission yeast and budding yeast seem to differ, it would be interesting to explore whether ubiquitylation plays a role in this mechanism in both *S. pombe* and higher eukaryotes. In human cells, PCNA has been shown to be de-ubiquitinated by USP-1 (ubiquitin specific protease 1) (Huang 2006). More recently, Elg1 has been implicated in USP-1 dependent de-ubiquitylation of PCNA by recruiting USP-1 to Ub-PCNA (Lee 2010). This opens some interesting questions for future projects regarding the role of Ub-PCNA and the dynamics of PCNA unloading during S-phase. Does S-phase dependent PCNA ubiquitylation serve as an inhibitory signal to Elg1? Are its functions similar in humans as in fission yeast?

#### **5.7.4 Species variation**

One potential criticism of this model is the contrasting observations between *S. pombe* data from this collaboration and the previously published data in *S. cerevisiae*. Principally, ubiquitylation of PCNA in budding yeast is almost exclusively reserved for response to DNA damaging agents (Davies 2008). Extremely low levels of Ub-PCNA are

detected in cells undergoing normal S-phase, suggesting that there is no role for the modification during DNA replication. In fission yeast, ubiquitinated PCNA species are robustly detected at the onset of S-phase and is not induced significantly further if damaged DNA is present during replication (Frampton 2006, Figure 5-1A). Mammalian cells exhibit a mixture of the two yeast phenotypes, as Ub-PCNA can be detected during unperturbed S-phase but is induced in response to DNA damage (Figure 5-1B). Thus it appears that the two yeasts represent two ends of spectrum of PCNA ubiquitylation/deubiquitylation dynamics. It remains to be elucidated as to the reason behind the species variation, especially considering the essential nature of PCNA and the conservation of its protein structure. However, we hypothesise that it may be a result of differences in distinct thresholds of ssDNA coated with RPA, which is required to activate the Rad18-Rad6 ubiquitin ligase and/or the dynamics of PCNA deubiquitylation. In order to maintain an appropriate balance between unsuitable use of TLS polymerase during S-phase and their recruitment in response to damage, it is also likely that binding kinetics for the replicative and TLS polymerases may differ between species.

S-phase dependant modification of PCNA does exist in budding yeast, however it arises in the form of SUMOylation (Parker 2008). This SUMOylation occurs when PCNA is bound to DNA in S-phase, almost directly mimicking the ubiquitin observations in this collaboration. SUMO does not seem to prevent Elg1 unloading from the DNA as is predicted for ubiquitin in this project (Kubota 2013). Interestingly, ubiquitylation of PCNA in budding yeast has been reported in cells undergoing DNA replication in the absence of DNA ligase I (Das-Bradoo 2010). This modification arose at lysine 107, not at the well-known lysine 164, and was dependent on Rad5 and Mms2. This modification demonstrates a further link between lagging strand synthesis and PCNA modification.

### **5.7.5 Conclusion**

In conclusion, both data shown in this chapter and that collected by Dr Daigaku highlight the complexities of PCNA modification and the dynamics that occur between PCNA-associating factors during DNA synthesis. More studies must be conducted that investigate the role of ubiquitylation of PCNA in cells, as it may not be as clear as previously thought. From this study, it is apparent that ubiquitinated PCNA does not act solely as a marker of DNA damage, at least in fission yeast and to a certain extent in

human cells. Its purpose may ultimately lie in controlling the DNA loading status of PCNA and the association with the lagging strand polymerase. Differences between model systems obscures the exact role, however it seems that studies in *S. pombe* may yet play a role due to the similarities observed in S-phase dependent ubiquitylation with human cell lines.

# Chapter 6

## Characterisation of factors effecting global chromatin association of the Smc5/6 complex

### 6.1. Introduction

Structural Maintenance of Chromosomes (SMC) complexes play key roles in organising chromosome arrangement and dynamics throughout the cell cycle. Together, they possess an extensive repertoire of functionalities, ranging from sister chromatid cohesion (cohesin), chromosome condensation (condensin) and DNA repair (Smc5/6). Of these three complexes, the role of Smc5/6 is the least understood. Its initial discovery in *S. pombe* was by complementation of a DNA damage sensitive mutant, and further genetic analysis has placed the complex as part of several DNA repair processes that involve homologous recombination (HR) (Lehmann et al 1995, Verkade 1999). In contrast to other genes involved in HR, the complex is essential in the yeasts and deletion of any of its major components renders cells inviable. This suggests that Smc5/6 is required during unperturbed cellular growth in the absence of genotoxic agents, not just in response to DNA damage.

During DNA replication, the replication machinery can encounter obstacles such as DNA damage or protein barriers, which cause it to stall. Homologous recombination proteins are required during S-phase to overcome such perturbations by either protecting stalled forks, bypassing the blockage, or restarting collapsed replication forks (Lambert et al 2005, Branzei et al 2008). The Smc5/6 complex has been implicated in contributing to these processes. Hypomorphic mutants of the complex display catastrophic mitoses following replication perturbation. (Verkade 1999, Miyabe 2006, Ampatzidou 2006). Failure to separate DNA at mitosis is suggestive of unresolved HR intermediates that go undetected by the S-M checkpoint. This implicates the Smc5/6 complex as having a role in processing of late stage HR intermediates during restart of collapsed replication forks. In addition to this role in joint molecule resolution, Smc5/6 has also been shown to play a role in the stabilisation of stalled replication forks (Irmisch et al 2009). The

hypomorphic *smc6-74* mutant presents a defect in recruitment of Rad52 and RPA to HU stalled replication forks, hinting that the complex may act to keep stalled replication forks in a “recombination competent” conformation.

More recently, studies have focussed on understanding the interaction between Smc5/6 and DNA in more detail, and elucidating key factors that are important for the association of the complex with the chromatin. In budding yeast, early ChIP-on-chip experiments demonstrated that Smc5/6 localises to specific regions of the genome at various stages of an unperturbed cell cycle, most notably telomeres (G1), ARS sequences (S) and centromeres (G2) (Lindroos et al 2006). ChIP based studies performed in fission yeast have also reported Smc5/6 localisation at centromeric and sub-telomeric regions, following HU arrest or MMS treatment respectively (Pebernard et al 2008). The recruitment of Smc5/6 to the centromeres was shown to be dependent on heterochromatin, whereas sub-telomeric localisation required Nse2 SUMO ligase activity. Furthermore, accumulation of Smc5/6 at various genomic loci in response to MMS required the Nse1 vRING domain (Tapia-Alveal and O’Connell 2011). The Smc5/6 complex thus appears to be required at difficult to replicate regions in the genome, such as highly repetitive DNA sequences. These data lead to the notion that an important role for Smc5/6 may be required to coordinate events at these loci (reviewed in Murray and Carr 2008). Additionally, Smc5/6 appears to act in response to replication stress, localising to stalled replication forks and the associated NSE subunits may play a role in its recruitment.

Further functionalities for Smc5/6 have been proposed based on similarities in genomic localisation with Cohesin (reviewed in Tapia-Alveal 2014). Cohesin is required to physically link sister chromatids after DNA replication, in order to ensure correct segregation during mitosis. The early ChIP-on-chip data from the Sjorgen lab suggested that Smc5/6 accumulation on chromosomes was linked to Cohesin, as inactivation of the cohesin loader reduced overall Smc5/6 levels (Lindroos 2006). This result could not distinguish whether the Smc5/6 complex required the cohesin loader to associate with the chromatin or whether it was dependent on loaded cohesin itself. More recently, the same group have presented data that proposes Smc5/6 chromosomal association depends on cohesion and is required to facilitate the resolution of sister chromatid intertwinings (Jeppsson 2014a). Thus, the complex is not directly dependant on cohesin, rather the

DNA structures caused by sister chromatid cohesion. In budding yeast, Smc5/6 has been previously implicated in the resolution of sister chromatid linkages caused by topological links or exchange of DNA strands during repair (Bermudez-Lopez et al 2010). Likewise, inactivation of Topoisomerase II (Top2) by Jeppsson *et al* caused elevated levels of Smc5/6 on the DNA, suggesting that Smc5/6 associates with a TopII DNA substrate. However, since depletion of Top2 would lead to replication stress, this recruitment could be indirect. The precise role of Smc5/6 at such DNA structures is yet to be elucidated but recent *in vitro* data suggests that the complex may act as an intermolecular DNA linker, regulating DNA topology during replication (Kanno 2015).

Many of the aforementioned studies have relied on mapping of SMC complexes via ChIP-seq, ChIP-qPCR or ChIP-on-chip. Although this is a useful way of correlating SMC localisation with function, these methodologies have drawbacks, which have been recently reviewed (Jeppsson et al 2014b). Briefly, all these experiments require extensive formaldehyde crosslinking, which will mask any on-off equilibria that may exist and could lead to artefacts caused by linking intra- and inter-chromatid sections of DNA. Secondly, quantification of enrichment/recruitment is difficult in such experiments. qPCR can provide a certain level of quantitative information, however as these experiments are performed on cell populations a high enrichment signal cannot be distinguished between many Smc5/6 complexes at one loci or that more cells have protein at this site. Although these studies are focussing on specific regions in which the complex binds to the genome, in order to elucidate functionality, there is a distinct lack of research around the global chromatin association of Smc5/6. Thus, one interesting question is whether the chromatin association of the Smc5/6 complex is altered on a global scale in response to cell cycle stage, genotoxic agents or genetic backgrounds. Understanding the dynamics of the loading/unloading of the complex onto DNA, which cannot easily be ascertained by ChIP experiments, may provide important insight into how Smc5/6 functions within the cell. Single molecule microscopy is best suited for such experiments, whereby protein dynamics can be studied within cells with minimal disturbance.

This chapter outlines preliminary work performed as part of a collaborative project I initiated with the Murray Lab (University of Sussex). The overall objective of the project is to use PALM-based approaches to characterise the recruitment of Smc5/6 complex to the chromatin in *S. pombe*. This project will provide a basic understanding of the

dynamics of Smc5/6 chromatin association and the factors affecting its loading. Specifically, the preliminary aims were simply to elucidate whether the complex is actively loaded to any significant extent onto the DNA in response to DNA replication or during replication stress. Furthermore, we aimed to study the effect of Nse1 RING domain mutations on the chromatin loading of the complex. Finally, in light of previous findings from the Murray lab, the association of recombination protein Rad52 with chromatin was studied with a view to aid future characterisation of its role and interactions with Smc5/6.

## **6.2. Smc5/6 chromatin association in an unperturbed cell cycle**

To understand more about the overall chromatin association status of Smc5/6, the motion blur based PALM method described in Chapter 4 was employed. We envisaged that using this methodology we could learn more about the recruitment of the complex to the chromatin during DNA replication and in response to replication stress. Previous studies in fission yeast have used the kleisin-like subunit of Smc5/6, Nse4, to study its localisation by fluorescence microscopy and ChIP (Pebernard *et al* 2008). Thus, in order to visualise DNA-associated Smc5/6 we used a strain expressing Nse4 tagged with the mEosFP variant, mEos3.2 (Nse4-mEos3.2) which had been previously made in the Murray Lab (University of Sussex).

As previously mentioned the distribution of Smc5/6 on chromosomes during the cell cycle has been explored by ChIP-based methods. In asynchronously growing *S. pombe* cultures, the complex is distributed along the arms of the chromosomes with no clear patterning (Pebernard *et al* 2008). Synchronisation of cells into S-phase using hydroxyurea led to Smc5/6 enrichment at centromeric repeats and subtelomeric repeats. Similar results had been reported in budding yeast (Lindoos *et al* 2006), and it was thus suggested that the complex is actively loaded on chromatin during replication. However, in such experiments, the use of hydroxyurea results in stalling of replication forks, and since Smc5/6 is known to play a role in stabilising arrested forks (Irmisch 2009), thus this could cause the enrichment observed in such experiments.

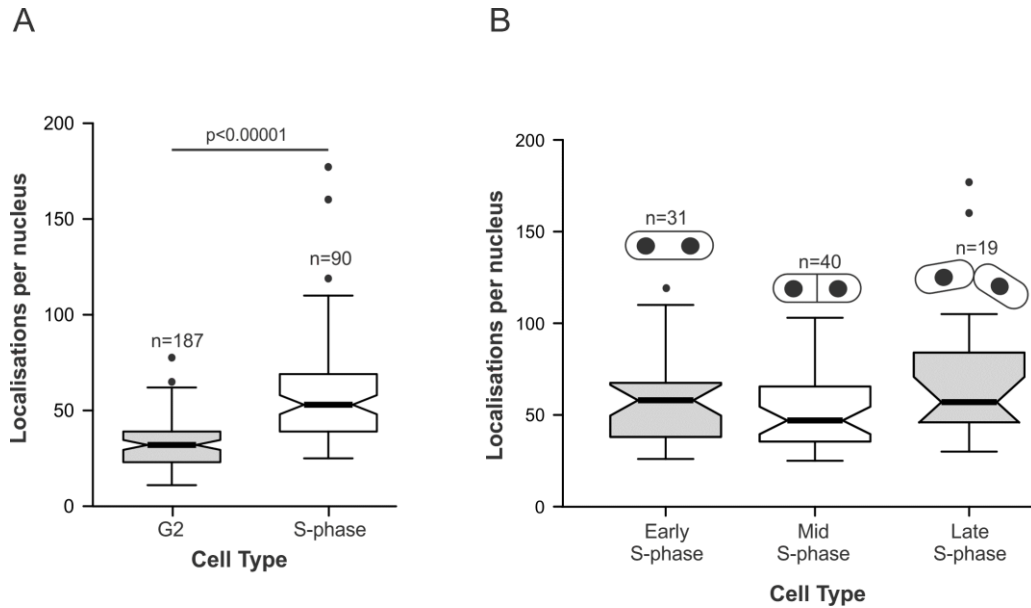


**Figure 6-1. Chromatin association of Smc5/6 is enriched in S-phase.**

**A)** Quantification of nuclear Nse4-mEos3.2 localisations in G2 and S-phase fission yeast cells. P-value determined by two-tailed students T-test. **B)** Data from A) sorted into S-phase stages. Cells were sorted based on morphology depicted.

To assess whether the chromatin association of the complex is indeed increased during unperturbed DNA replication, Nse4-mEos3.2 cells were synchronised by lactose gradient centrifugation and analysed using motion blur PALM microscopy. Lactose gradient synchronisation allows for the analysis of chromatin bound proteins in S-phase cells that are not synchronised by hydroxyurea, preventing compounding factors influencing the result. Nse4-mEos3.2 was imaged in cells in S-phase and compared to cells in G2. The outcome of this experiment highlighted a slight but significant increase in chromatin bound Nse4 in unchallenged S-phase cells compared to early G2 cells (Figure 6-1A). Further *in silico* synchronisation of intermediate S-phase stages yielded no difference between early and mid S-phase cells, however, a slight but significant increase was observed towards the end of S-phase (Figure 6-1B). This data is consistent with the hypothesis that Smc5/6 chromatin association is increased during S-phase. The slight increase in late-S is also consistent with previous findings in both yeasts of a temporal separation between recombination and replication events (Lisby 2004, Meister 2005). As Smc5/6 is required for HR events, this increase in chromatin association of the complex could signify a role in such events towards the end of S-phase into early G2. However, this data is preliminary in status and requires further investigation.

### 6.3. Global levels of Smc5/6 chromatin association are unchanged in response to replication fork stalling or DNA damage

The increase in Smc5/6 chromatin association during DNA replication could reflect the fact that the complex travels with replication forks or it could be due to an increase in HR based processes occurring during replication. To ascertain whether this increase in loaded Smc5/6 was as a result of repair of intrinsic damage or a replication dependent phenomenon, the chromatin association of Smc5/6 was measured in the presence of genotoxic agents. To address this question, cells expressing Nse4-mEos3.2 were synchronised into G2 via lactose gradients and allowed to progress into S-phase in the presence of 10mM hydroxyurea or 0.005% MMS.

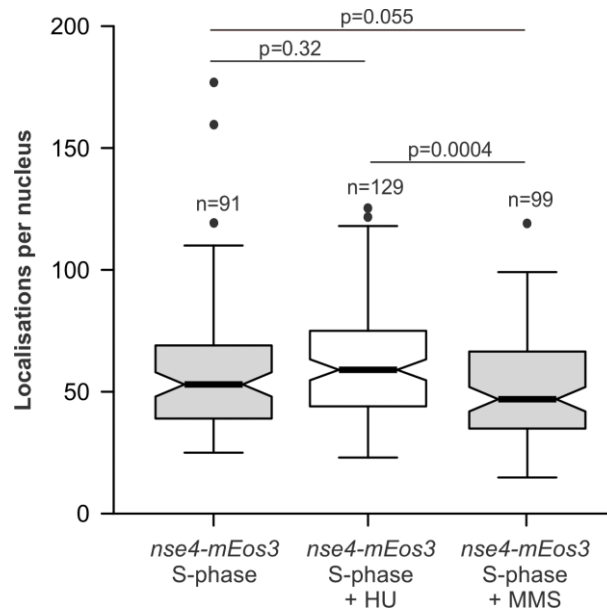


**Figure 6-2. Smc5/6 chromatin association in response to hydroxyurea and MMS treatment.**

Quantification of nuclear localisations of Nse4-mEos3.2 in S-phase fission yeast. G2 cells isolated from lactose gradients were synchronised into S-phase in the presence of 10mM HU, 0.005% MMS and compared to untreated S-phase data set from Figure 6-1A. Significance was determined by two-tailed students T-test.

Smc5/6 is required for maintaining and repairing stalled and collapsed replication forks (Irmisch 2009, Ampatzidou 2006). Previous ChIP data have shown that Smc5/6 is enriched at genomic regions upon exposure to hydroxyurea in *S. pombe* and budding yeast (Pebernard 2008, Bustard *et al* 2012, Jeppsson 2014a). Exposure to the DNA damaging agent methyl methane sulfonate (MMS) which causes purine alkylation, also causes enrichment of Smc5/6 at specific loci (Pebernard 2008, Tapia-Alveal *et al* 2011). It is of particular interest to understand the dynamics and mechanism of this enrichment. Is it a result of increased Smc5/6 loading or re-localisation of loaded molecules? Results from motion blur PALM imaging of cells undergoing DNA synthesis showed no significant

difference in chromatin associated Nse4 in the presence of either chemical, compared to the untreated data set collected in Figure 6-1 (Figure 6-2). This result suggests that in response to replication stress or DNA damage in S-phase, levels of chromatin associated Smc5/6 are not substantially increased, and that enrichment observed in ChIP experiments may be due to re-localisation of the complex.

#### **6.4. Nse1 ubiquitin ligase activity is not required for chromosomal association of Smc5/6 during DNA replication or in response to replication stress**

The Smc5/6 complex contains Non-SMC elements (Nse) Nse1-6, of which Nse1-4 are essential. The role of each individual Nse protein has been the focus of several studies. The Smc5/6 complex is unique compared to other SMC proteins as two of the subunits have catalytic activity. Nse1 possess a variant form of the RING domain (vRING) which contains zinc-coordinating amino acid residues. This domain was suggested to possess E3 ubiquitin ligase activity, which has been the subject of previous studies, but has not yet been categorically demonstrated for the holocomplex (Pebernard 2008b, Doyle 2010).

The role of the vRING domain in Nse1 has however been explored in fission yeast. Alignment and comparative modelling of the vRING domain revealed conserved cysteine and histidine residues arranged in a C<sub>4</sub>HC<sub>4</sub> manner (Figure 6-3A, Pebernard 2008b). Deletion of the entire vRING domain or mutation of a conserved cysteine residue to alanine (C199A) supported cellular growth but resulted in increased DNA damage sensitivity. Deletion of the domain also prevented formation of MMS induced Nse4-GFP foci and destabilised the trimeric Nse1-Nse3-Nse4 sub-complex. These results demonstrated that vRING domain is not required for the essential role of Smc5/6 but is important in the response to DNA damage. More recently, mutation of cysteine 216 to serine (C216S) in the RING domain suppressed hypomorphic alleles of Smc6 and Nse2 and was shown to reduce the MMS and HU-dependent enrichment of Smc5/6 at specific loci by ChIP (Tapia-Alveal and O'Connell 2011). However, this mutant did not display any increased sensitivity to DNA damaging agents. Together, these studies suggest that the RING domain of Nse1 is important to stabilise the Nse1-3-4 sub complex and direct the Smc5/6 complex to DNA damage. Whether any of these phenotypes are due to a lack of ubiquitin ligase activity or due to structural disruption of the protein is yet to be determined.

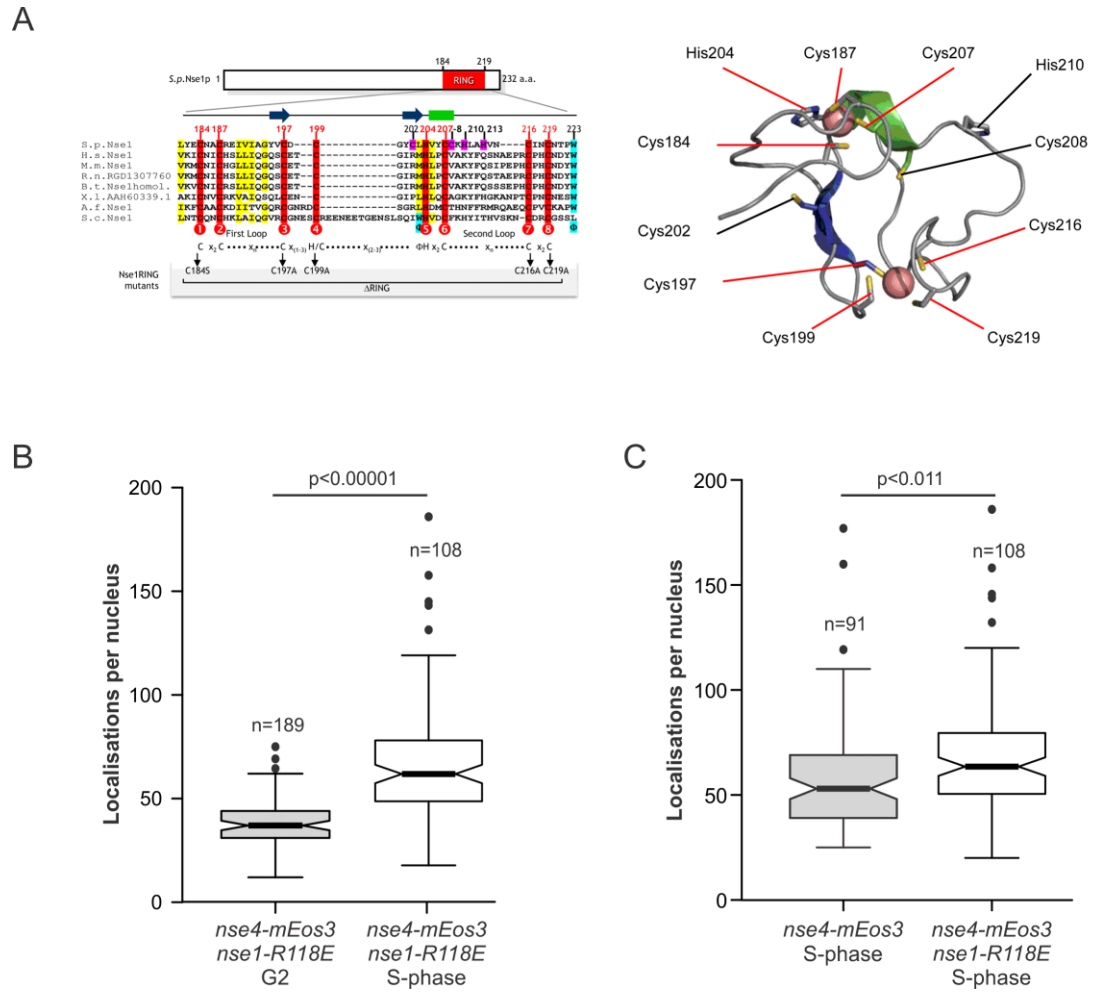


**Figure 6-3. Mutation of Nse1 ubiquitin ligase domain does not impair chromatin association of Smc5/6.** **A)** Cross-species alignment of Nse1 vRING domain amino acid sequences (left) and comparative modelling of *S.pombe* Nse1 based on human Nse1 structure, taken from Pebernard 2008. Cysteine and Histidine residues that chelate  $Zn^{2+}$  are displayed with red lines. **B)** Quantification of nuclear Nse4-mEos3.2 localisations in *nse1-R118E* G2 and S-phase fission yeast cells, and **C)** compared to wild type S-phase data set from Figure 6-1A. Significance was determined by two-tailed students T-test.

Recent data *in vitro* data has suggested that fission yeast Nse1 does indeed possess ubiquitin ligase activity (Unpublished data communication, Palecek Lab). Modelling crystal structures of Nse1 resulted in generation of an arginine to glutamic acid mutant (R188E) that was predicted to abolish any interaction between Nse1 and the required E2 ligase. The Palecek group were able to demonstrate Nse1 functions as an ubiquitin ligase *in vitro* and show that the R188E mutation decreased this activity to <5%. The *nse1-R188E* mutant also displayed sensitivity to HU, MMS and UV exposure. To investigate whether ubiquitin ligase activity of Nse1 is required for efficient Smc5/6 chromatin association, the *nse4-mEos3.2* construct was introduced into an *nse1-R188E* genetic background. Motion blur PALM analysis revealed that *nse1-R188E* cells display increased levels of loaded Smc5/6 in S-phase compared to G2 as seen in wild type cells,

suggesting lack of ubiquitin ligase activity does not affect chromatin loading in S-phase. (Figure 6-3B). When compared to the wild type data set (Figure 6-1A), the *nse1-R188E* mutant displayed a slight increase in localisations per nucleus (Figure 6-3C). This result is most probably due to experimental fluctuation, as the spread of data is very similar and the significance is weak ( $P = 0.0105$ ). However, this phenomenon will be further investigated in the future.

As previously mentioned, mutations in the vRING domain of Nse1 reduced the levels of Smc5/6 detected at lesion containing loci via ChIP (Tapia-Alveal and O'Connell 2011). To assess whether the *nse1-R188E* mutation prevented Smc5/6 chromatin association in response to DNA damage and replication stress, *nse1-R188E nse4-mEos3.2* cells were synchronised into S-phase in the presence of MMS or HU. In the presence of 0.005% MMS, no difference was detected between the wild type and *nse1-R188E* cells (Figure 6-4A). However, *nse1-R188E* cells subjected to MMS displayed significantly less chromatin bound Nse4 than untreated *nse1-R188E* cells. This may be due to the slightly higher values displayed in the untreated *nse1-R188E* S-phase dataset from Figure 6-3D. In response to replication fork stalling in the presence of HU, there was no gross change in the chromatin association of Smc5/6 (Figure 6-4B). These data indicate that the ubiquitin ligase activity of Nse1 is most likely not required for association of Smc5/6 on chromatin in response to HU or MMS treatment.

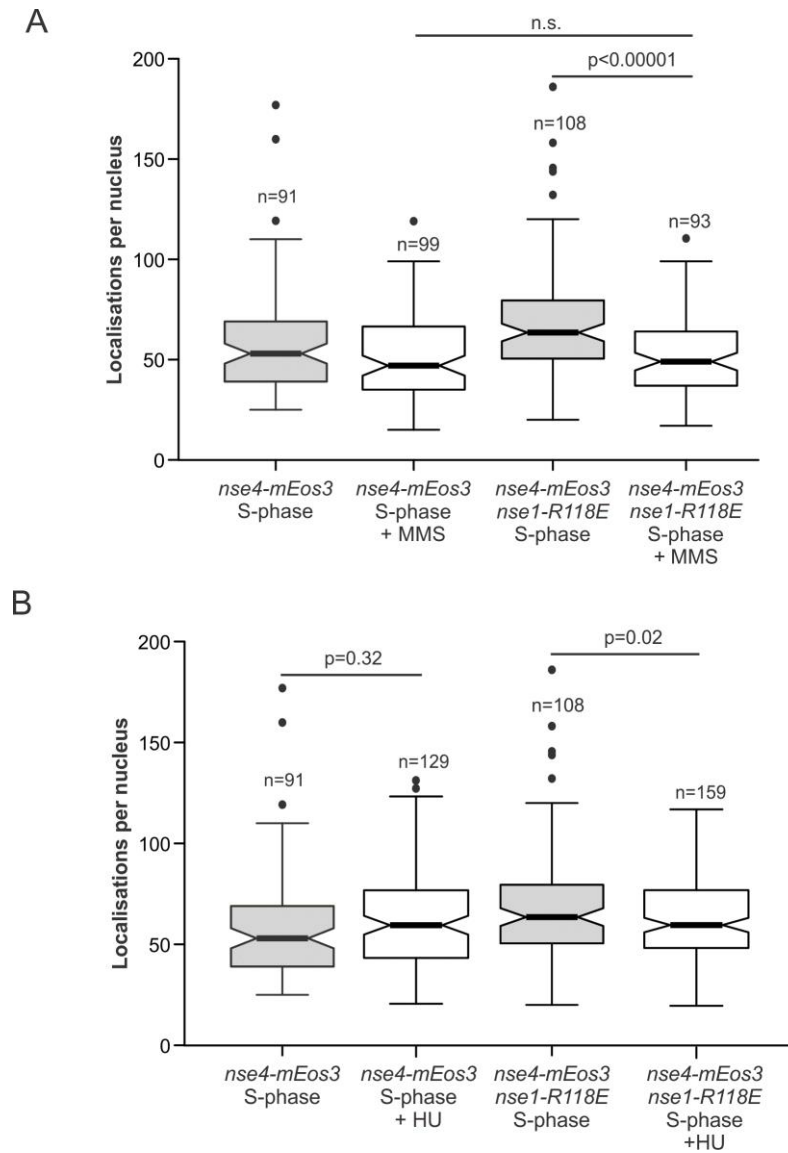


**Figure 6-4. Smc5/6 chromatin association in response to replication stress is independent of Nse1 ubiquitin liage activity.**

Quantification of nuclear Nse4-mEos3 localisations in wild type or *nse1-R188E* genetic backgrounds. G2 cells were isolated from lactose gradients and synchronised into S-phase in the presence of **A**) 0.005% MMS or **B**) 10mM HU and compared to untreated data sets from Figure 6-1 (WT), Figure 6-2 (WT + HU/MMS) and Figure 6-3 (R188E S-phase) Statistical significance was determined by two-tailed students T-test

## 6.5. Rad52 chromatin association is increased during unperturbed DNA replication

The Smc5/6 complex is required to prevent genomic instability during replication stress. Using the two hypomorphic mutants, *smc6-74* and *smc6-X*, studies have shown that the complex functions to both protect stably stalled forks and to ensure proficient HR-dependent repair of collapsed forks (Ampatzidou 2006, Irmisch 2009). The intra-S-phase

checkpoint acts to stabilise stalled replication forks through the actions of the Cds1 kinase in *S. pombe* (Lindsay *et al* 1998), preventing fork collapse and thus the requirement for HR. One surprising finding was that the recombination protein Rad52 was shown via ChIP to be enriched on DNA during replication arrest in checkpoint proficient cells (Irmisch 2009). This enrichment was most notable, but not exclusive to, the genomic region containing the *rDNA* repeats. Further ChIP analysis demonstrated that this enrichment required Smc5/6, as cells harbouring the *smc6-74* allele displayed suppressed levels of Rad52 chromatin association. In the absence of intra-S checkpoint kinase Cds1, the levels of Rad52 detected at the loci tested were unaffected in the *smc6-74* genetic background. The authors hypothesised that Smc5/6 plays an ‘early’ role at stalled replication forks by keeping them primed for restart. They postulated that *smc6-74* allele confers a defect in this early response, resulting in reduced levels of loaded Rad52.

During the above-mentioned study, Rad52 ChIP levels were only enriched in samples treated with HU thus the conclusion reached was that Rad52 binds stalled replication forks. However, replication is a very dynamic process and the possibility exists that Rad52 associates with replication forks during unperturbed S-phase, but ChIP has insufficient sensitivity to detect this. In fact, recent evidence exploring the role of Rad52 in replication has suggested that it binds unperturbed replication forks in order to promote DNA damage tolerance (Gonzalez-Prieto 2013). In light of these studies we began to investigate the chromatin association of Rad52 and its relationship to Smc5/6 function in the context of replication using motion blur PALM.

If Rad52 is indeed playing a role at unperturbed DNA replication forks then one would expect to see an increase in chromatin bound Rad52 during S-phase. To test this hypothesis PALM imaging was performed on S-phase cells expressing Rad52-mEos3.1 (previously made in the Carr lab). The S-phase PALM data set was then compared to cells in G2, which were considered to have completed DNA replication. Comparison of the data show that there is an increase in static Rad52 molecules in S-phase cells compared to those in G2 (Figure 6-5A). Overall, the median number of localisations per nucleus increase 2.3 times and this increase is statistically significant. Rad52 is known to form foci in response to DNA damage and these foci can arise spontaneously in unchallenged cells (Lisby 2001, Lambert 2005). Consistent with previous reports, cells containing Rad52-mEos3.1 foci were observed in G2 cells, and these foci lead to augmented

localisation values which fell as extreme outliers in the box plots (Figure 6-5A). These cells were removed from the statistical calculations.

The data presented in Figure 6-5A suggest that Rad52 is recruited to the chromatin during S-phase. Due to time restrictions the association of Rad52 in response to replication stress or in the *smc6-74/X* alleles was not analysed, however this is the focus of ongoing efforts in the Carr lab.

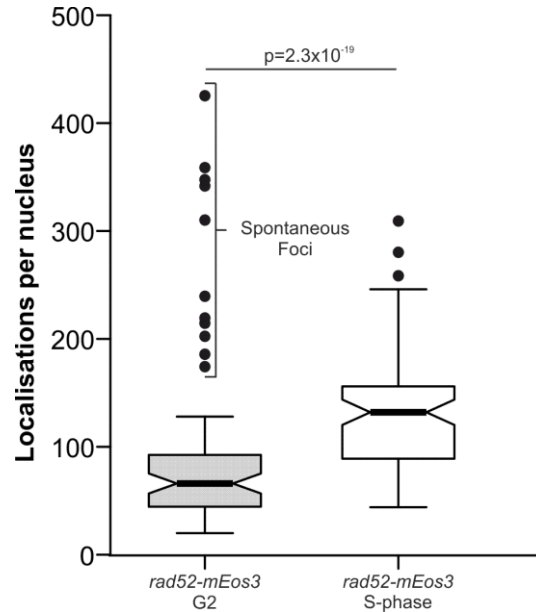


**Figure 6-5. Rad52 chromatin association increases during S-phase.**

Quantification of Rad52-mEos3.1 nuclear localisations detected during motion blur PALM imaging. P-value determined by two-tailed students T-test.

## 6.6. Discussion and conclusion

The data presented in this chapter are the preliminary findings of a long-term project that will help to shed light on the dynamics of Smc5/6 chromatin association in fission yeast. Of particular interest in this project is understanding how global levels of chromatin associated Smc5/6 change within the cell, and whether or not any of the Smc5/6 complex subunits play a role in its loading status. Developing an understanding of how the complex is recruited to the chromatin during DNA replication and in response to damage will help to elucidate its overall function in the cell. Previously, many groups have studied the chromatin association of Smc5/6 during via ChIP based approaches. Using such techniques allows for the detection of enrichment of proteins at specific genomic loci.

However, if the protein of interest is not enriched at specific loci, but rather randomly distributed across the genome, these methods cannot provide accurate information about the overall amount of associated protein. Thus, the motion blur PALM approach provides an excellent alternative to studying such behaviour.

Recent research in budding yeast focussing on the loading of the Smc5/6 complex on to DNA suggests that it increases in S-phase and may require sister chromatid cohesion formed during DNA replication (Jeppsson 2014). Data shown in this chapter show that levels of chromatin associated Smc5/6 also peaks in S-phase in fission yeast, suggesting that complex is recruited to the DNA before or during replication (Figure 6-1A). The role of sister chromatid cohesion has not been explored with the PALM method, but is a potential future question that could be explored. Interesting future experiments can now be performed in the Carr lab to elucidate whether S-phase dependent chromatin binding of the Smc5/6 complex requires a loading factor such is the case for cohesin (Ciosk 2000), or whether it is dependent on structural aspects of DNA.

Many of the ChIP studies previously performed have demonstrated that Smc5/6 accumulates at certain loci in response to replication stress (Pebernard 2008, Tapia-Alveal 2011). During this project, we were interested to know whether this accumulation was a result of an increase in global levels of chromatin associated Smc5/6 when cells are treated with genotoxic agents during DNA replication. The data from the PALM experiments actually suggest that the overall levels of chromatin bound Smc5/6 are unchanged when cells are treated with either HU or MMS (Figure 6-2). This was also the case in the ubiquitin ligase dead *nse1-R188E* genetic background (Figure 6-4). When considered in context of previously published ChIP data, this observation could be explained in two ways.

Firstly, the loci specific increase detected in other studies may be merely a redistribution of the Smc5/6 complex that is deposited during DNA replication. Cohesin is known to move along DNA away from where it was loaded (reviewed in Ocampo-Hafalla and Uhlmann 2011), this may be the case for the Smc5/6 complex as it possess a similar protein structure. One prediction may be that once loaded onto the DNA, Smc5/6 slides along until it encounters a DNA structure (e.g. stalled replication fork) which it recognises. If true, this would lead to a series of interesting questions surrounding how the Smc5/6 is

redistributed and how it recognises stalled fork structures. Future work in this project will be focussing on applying PALM and other biophysical techniques to attempt to monitor the dynamics of chromatin bound Smc5/6 *in vivo*.

A second explanation for the difference between the PALM data and previous observations may be due to differences in the way the experiments were executed. In the motion blur experiments, cells were synchronised by lactose gradients into G2 and then incubated in the presence of HU or MMS for 2 hours. In previous publications from other groups, asynchronous populations were used which resulted in much longer exposure times (4-6hours) (Tapia-Alveal and O'Connell 2011). Furthermore in Pebernard et al (2008) the levels of MMS used were much higher 0.03% (which we consider lethal) compared to 0.005%. In both of the above mentioned studies, Nse4-GFP foci were also detected after incubation with HU and MMS, which was not observed in this study. The recruitment of Smc5/6 in this case could be due to substantial amounts of DNA damage.

As well as monitoring the chromatin association of the Smc5/6 complex itself, the motion blur PALM technique can also be used to observe the effect of mutant Smc5/6 proteins on the DNA binding of other repair factors. Of future interest is the recombination protein Rad52, which was previously shown to be indirectly dependent on the Smc5/6 protein in order to associate with stalled forks. In this study, Rad52 chromatin association was briefly assessed in G2 and S-phase fission yeast cells. PALM analysis demonstrated that the chromatin association of Rad52 peaks in S-phase, similar to Smc5/6 (Figure 6-5). Future experiments will be performed to elucidate whether the levels of loaded Rad52 are changed during replication stress or when Smc5/6 functionality is compromised.

This project also provided the opportunity to further test the motion blur PALM method as a way of investigating chromatin association of proteins. The data collected in this study highlighted a need for further development of final data analysis of such an experiment. In some cases, weak statistical significances are detected between data sets that have very similar median values and data spread. For example, in Figure 6-4B the '*nse4-mEos3 nse1-R188E S-phase*' and '*nse4-mEos3 nse1-R188E S-phase + HU*' sample data sets show a T-test p-value of 0.02, which could be considered significant. Understanding whether such small differences reflect real changes in DNA binding or are due to experimental fluctuations will be important in future studies. The way in which the

data are collected could be improved to help reduce any potential fluctuations in data sets. Currently, due to the length of time it takes to perform PALM imaging on one sample, and the fact the samples are not fixed, it is not possible to perform the synchronisation and imaging at the same time for all samples. Cultures are grown on the same day, but synchronised at different times and imaged on different slides. Data sets are built over consecutive days of imaging and then compared. Thus, running a control experiment at the same time as a mutant or treated sample was not possible. In the future, imaging two samples on one coverslip will be tested by staining one of the samples with fluorescently labelled lectin or concanavalin A. This will allow for synchronisation of samples at the same time and direct comparison of chromatin association between two samples on the same slide.

# Chapter 7

## Discussion

### 7.1. Overview

The development of super-resolution microscopy techniques has provided researchers with another tool to explore the structural and molecular basis of cells. In this thesis, I aimed to establish one such technique, PALM, in the Carr lab and demonstrate its potential for use as a methodology to study DNA replication and repair proteins in *S. pombe*. The work presented here has laid the foundations for future investigations in the lab using PALM. During the initial stages of the project, efforts were directed towards familiarisation with the custom-built equipment, optimisation of sample preparation and development of protocols that could be applied to future investigations in fission yeast. A Desire to visualise only DNA bound proteins led to the development of a protocol that utilises motion blurring of fluorescence to distinguish between freely diffusing and DNA bound proteins. Basic experiments were performed to demonstrate that chromatin associated molecules can be readily detected and quantified, providing a means to measure changes in chromatin binding in different cell types or genetic backgrounds. To further test this application, I initiated two collaborative projects focussing on PCNA and Smc5/6. The technique has shown itself to be a powerful tool that can be used to study changes in the chromatin association of these proteins, in conjunction with other molecular biology techniques.

### 7.2. Motion Blur PALM

Photoactivated localisation microscopy was invented by Eric Betzig and colleagues in order to break the diffraction barrier of light and increase resolution of fluorescence microscopy images. During the initial stages of this project, the aim was to utilise PALM to study DNA replication at the super-resolution level. However, as described in Chapter 4, the use of chemical fixation (plus the incompatibility of extraction protocols) limited the application of PALM in fixed cells. This may not have had been such a limiting factor

if the project had been focussed on cellular components that have known and repetitive structures such as actin fibres. These structures would be easy to distinguish above the background localisations of cytosolic species and could be removed with nearest neighbour subtraction algorithms. However, chromatin associated proteins do not possess such ordered structures making it impossible to differentiate between them and unbound molecules that had become fixed to nuclear components during formaldehyde treatment.

In order to distinguish between the two sub-populations of molecules, we employed motion blurring of fluorescence by increasing the camera exposure time and imaging unfixed cells. This technique has been previously applied by other groups to differentiate between static and diffuse protein species, mostly to study DNA binding kinetics or slow diffusion (Kim et al 2006, Uphoff 2013, Chen 2014). In this study, it was utilised in a quantitative manner, allowing for the relative comparison of chromatin association between different strains by counting the number of nuclear localisations detected during imaging. This application produced results that agree with well-characterised biological phenomena such as S-phase DNA binding characteristics of the MCM helicase and PCNA (Figure 4-8 and Figure 4-10). Thus demonstrating that it is an accurate methodology that can now be used in the future to investigate novel processes.

Unfortunately, the nature of the sample preparation in this technique and the length of time required for imaging precluded a detailed mapping of protein localisation and generation of super-resolution images. This is due to the fact that the chromatin is still mobile during imaging, and thus individual proteins in a cluster may not be localised in the same region. Thus, this is the major limitation to this technique. Future experiments in the Carr lab will be directed towards developing a protocol that allows for the production of super-resolution images of the spatial organisation of replication proteins in fission yeast nuclei. Recently, bimolecular fluorescence complementation (BiFC) has been demonstrated with the photoconvertible protein mEos3.2 (Liu 2014). During this thesis, a project was initiated to assess the potential of using this to observe fluorescence from interacting proteins at the replication fork. Due to time restrictions, this has not yet generated any data but could be a future method that is compatible with chemical fixation procedures. The ideal outcome would be that only chromatin bound proteins interacting at the replication fork would produce fluorescence via BiFC.

Further refinements and improvements of the motion blur technique can be made by imaging multiple strains at the same time and implementing a statistical threshold for accepting or rejecting differences between data sets. Regrettably, this work could not be completed within the duration of this thesis but is a current working progress within the Carr lab. Application of this technique to larger mammalian cells has also not yet been attempted. The basic methodology should still be applicable to such systems; however, the imaging time may be extensive due to larger nuclear volume and protein expression levels.

In conclusion, the technical development presented in this thesis has provided a novel method of visualising fluctuations of chromatin association of proteins within cells. This method will be a powerful technique in the future that can be used alongside existing molecular biology protocols.

### **7.3. S-phase dependant PCNA ubiquitylation**

The focus of PCNA mono-ubiquitylation has been mainly directed towards its induction in the presence of DNA damage and its role in recruitment of TLS polymerases. This is mainly due to a large body of research having been conducted in budding yeast, in which the vast majority of Ub-PCNA is detected after exposure to genotoxic agents. The appearance of Ub-PCNA in unperturbed fission yeast cells was observed almost a decade ago (Frampton 2006), and although its presence was discussed, it has never been fully investigated. Understanding the dynamics of PCNA ubiquitylation and its effect on the major replicative polymerases and other PCNA-associating factors is of importance in order to fully elucidate the mechanisms underlying tolerance of DNA damage during replication. Thus, the project initiated by Dr Daigaku and the work completed thus far provide an important insight into the function of Ub-PCNA at the replication fork.

Deletion of the E3 ligase Rhp18 in *S. pombe* is not lethal and cell cycle progression is not affected in its absence. Therefore, PCNA ubiquitylation is not essential for DNA replication. However, delayed replication at certain genomic loci and increased ssDNA gaps in an *rhp18* $\Delta$  strain suggests that it has an underlying contribution to the timely completion of S-phase. The data collected previously by Dr Daigaku strongly support a

role for Ub-PCNA ubiquitylation in lagging strand synthesis. This hypothesis was tested using the motion blur PALM technique by analysing the chromatin association of both PCNA and the lagging strand polymerase. This work could not disprove the original hypothesis and has thus helped to further our understanding of the role of Ub-PCNA in S-phase. Reduced PCNA chromatin association in an *rhp18* $\Delta$  mutant indicates a stability defect, which may reflect a role for ubiquitylation in preventing PCNA unloading. This role has yet to be confirmed and will require extensive *in vitro* experiments to demonstrate. Increased association of the lagging strand polymerase with the chromatin in response to hydroxyurea also supports a role for PCNA ubiquitylation in stable accumulation of polymerase delta. This increase is not observed in the absence of *rhp18*, and is thus consistent with a role for Ub-PCNA in lagging strand synthesis.

The importance of this project lies in the demonstration that PCNA ubiquitylation is not specifically a response to DNA damage. Furthermore, this collaboration provides important insights into the dynamics of both the replicative and TLS polymerases association with Ub-PCNA. A strengthened association of polymerase delta and Ub-PCNA was unexpected as ubiquitylation was seen as a signal to recruit TLS polymerases to displace the replicative polymerases. This finding will hopefully stimulate discussion and future research on the exact mechanism of polymerase switching and also the contribution of non-canonical polymerases to genome replication. The motion blur PALM technique will be an ideal way to study the recruitment of TLS polymerases to the DNA during unperturbed replication and in response to DNA damage. Furthermore, the PALM microscope is also capable of performing STORM based imaging, which could help provide insights into polymerase localisation in mammalian cells at the super-resolution level.

#### **7.4. Smc5/6 chromatin association**

The Smc5/6 complex is still somewhat of an enigmatic subject of research. The true function of the complex and the activities of the individual subunits have still yet to be elucidated. In this thesis, I collaborated with the Murray lab to begin to characterise the basic changes in chromatin association of the complex during different cell cycle stages and in response to replication stress. Surprisingly, such a study has not been previously reported in the literature, with most groups focussing on the specific distribution of the

complex on the genome by ChIP-seq. Although this approach can provide a detailed insight into aspects of the complexes functionality, it lacks any mechanistic detail on how the complex behaves once loaded onto the chromatin. Previous studies using ChIP-seq have reported localised increases in Smc5/6 localisation at specific genomic loci in response to replicative stress. Therefore it is surprising that experiments presented in Chapter 6 were unable to detect global increases in chromatin associated Smc5/6 in response to HU or MMS. This preliminary characterisation is possibly hinting that loaded Smc5/6 is relocated to stalled replication forks rather than being actively loaded at stalled forks. This would be consistent with the sliding behaviour of Cohesin, a very similarly structured protein. It could however be the case that the dynamics of Smc5/6 unloading and loading are too fast to detect in the motion blur experiments.

The benefit of single-molecule based experiments is the potential for discovering sub-populations of molecular behaviour that would not be observed in an ensemble fluorescence experiment. Future investigations into Smc5/6 behaviour using PALM in live cells may help to answer questions relating to its recruitment to stalled forks and sites of damage. Collaborations between the Carr and Murray labs will be focussing on studying the residency times of the complex once loaded onto the DNA, as well as attempting to detect any evidence of sliding along chromatin. As well as this, the motion blur technique will be used to continue basic characterisation of the loading status of the complex in different genetic backgrounds. Finally, as mentioned previously, the STORM based approach to super-resolution imaging could also be applied to this project. Localisation of Smc5/6 at super-resolution could provide further insights into where Smc5/6 is localised within the cell and its interacting partners. Such a project has very recently been initiated in collaboration with the Murray lab in human cells. Overall the work presented in Chapter 6 of this thesis has provided interesting observations regarding Smc5/6 global chromatin association and a basis in which to pursue further characterisation of the complex and its interactions with DNA.

## References

Abe, T., Sugimura, K., Hosono, Y., Takami, Y., Akita, M., Yoshimura, A., Tada, S., Nakayama, T., Murofushi, H., Okumura, K., Takeda, S., Horikoshi, M., Seki, M. & Enomoto, T. (2011). The Histone Chaperone Facilitates Chromatin Transcription (FACT) Protein Maintains Normal Replication Fork Rates. *Journal of Biological Chemistry*. 286 (35). p.pp. 30504–30512.

Abbe, E (1873). Beitrage zur Theorie des Mikroskops und der mikroskopischen. Archiv fur Mikroskopische Anatomie. F. Cohen. (9) 413

Acharya, N., Johnson, R., Prakash, S. & Prakash, L. (2006). Complex Formation with Rev1 Enhances the Proficiency of *Saccharomyces cerevisiae* DNA Polymerase  $\zeta$  for Mismatch Extension and for Extension Opposite from DNA Lesions. *Molecular and Cellular Biology*. 26 (24). p.pp. 9555–9563.

Acharya, N, Yoon, JH, Gali, H & Unk, I (2008). Roles of PCNA-binding and ubiquitin-binding domains in human DNA polymerase  $\eta$  in translesion DNA synthesis. *Proceedings of the National Academy of Sciences*. 105 (46) p.pp. 1772-17729

Amos, W.B. & White, J.G. (2003). How the Confocal Laser Scanning Microscope entered Biological Research. *Biology of the Cell*. 95 (6). p.pp. 335–342.

Ampatzidou, E., Irmisch, A., O’Connell, M.J. & Murray, J.M. (2006). Smc5/6 is required for repair at collapsed replication forks. *Molecular and Cellular Biology*. 26 (24). p.pp. 9387–401.

Andrews, EA, Palecek, J & Sergeant, J (2005). Nse2, a component of the Smc5-6 complex, is a SUMO ligase required for the response to DNA damage. *Molecular and Cellular Biology*. 25 (1) p.pp 185-96

Ando, R, Hama, H & Yamamoto-Hino, M (2002). An optical marker based on the UV-induced green-to-red photoconversion of a fluorescent protein. *Proceedings of the National Academy of Sciences*. 99 (20) p.pp 12651-12656

Annibale, P., Scarselli, M., Kodiyan, A. & Radenovic, A. (2010). Photoactivatable Fluorescent Protein mEos2 Displays Repeated Photoactivation after a Long-Lived Dark State in the Red Photoconverted Form. *The Journal of Physical Chemistry Letters*. 1 (9). p.pp. 1506–1510.

Arakawa, H., Moldovan, G.-L., Saribasak, H., Saribasak, N., Jentsch, S. & Buerstedde, J.-M. (2006). A Role for PCNA Ubiquitination in Immunoglobulin Hypermutation. *PLoS Biology*. 4 (11). p.pp 1947-1956

Asghar, U., Witkiewicz, A., Turner, N. & Knudsen, E. (2015). The history and future of targeting cyclin-dependent kinases in cancer therapy. *Nature Reviews Drug Discovery*. 14 (2). p.pp. 130–146.

Axelrod, D., Koppel, D.E., Schlessinger, J., Elson, E. & Webb, W.W. (1979). Mobility measurement by analysis of fluorescence photobleaching recovery kinetics. *Biophysical Journal*. 16 (9). p.pp 1055-1069

Axelrod, D. (1981). Cell-substrate contacts illuminated by total internal reflection fluorescence. *The Journal of Cell Biology*. 89 (1). p.pp. 141–145.

Ayyagari, R., Gomes, X., Gordenin, D. & Burgers, P. (2003). Okazaki Fragment Maturation in Yeast I. distribution of functions between Fen1 and Dna2. *Journal of Biological Chemistry*. 278 (3). p.pp. 1618–1625.

Bae, S.-H., Bae, K.-H., Kim, J.-A. & Seo, Y.-S. (2001). RPA governs endonuclease switching during processing of Okazaki fragments in eukaryotes. *Nature*. 412 (6845). p.pp. 456–461.

Bailly, V., Lamb, J., Sung, P., Prakash, S. & Prakash, L. (1994). Specific complex formation between yeast RAD6 and RAD18 proteins: a potential mechanism for targeting RAD6 ubiquitin-conjugating activity to DNA damage sites. *Genes & Development*. 8 (7). p.pp. 811–820.

Bailly, V., Lauder, S., Prakash, S. & Prakash, L. (1997). Yeast DNA Repair Proteins Rad6 and Rad18 Form a Heterodimer That Has Ubiquitin Conjugating, DNA Binding, and ATP Hydrolytic Activities. *Journal of Biological Chemistry*. 272 (37). p.pp. 23360–23365.

Balakrishnan, L. & Bambara, R. (2011). Eukaryotic Lagging Strand DNA Replication Employs a Multi-pathway Mechanism That Protects Genome Integrity. *Journal of Biological Chemistry*. 286 (9). p.pp. 6865–6870.

Ball, H.L., Myers, J.S. & Cortez, D. (2005). ATRIP binding to replication protein A-single-stranded DNA promotes ATR-ATRIP localization but is dispensable for Chk1 phosphorylation. *Molecular biology of the cell*. 16 (5). p.pp. 2372–81.

Barlow, J.H., Faryabi, R.B., Callén, E., Wong, N., Malhowski, A., Chen, H.T., Gutierrez-Cruz, G., Sun, H.-W.W., McKinnon, P., Wright, G., Casellas, R., Robbiani, D.F., Staudt, L., Fernandez-Capetillo, O. & Nussenzweig, A. (2013). Identification of early replicating fragile sites that contribute to genome instability. *Cell*. 152 (3). p.pp. 620–32.

Bartkova, J., Rezaei, N., Lontos, M., Karakaidos, P., Kletsas, D., Issaeva, N., Vassiliou, L.-V., Kolettas, E., Niforou, K., Zoumpourlis, V., Takaoka, M., Nakagawa, H., Tort, F., Fugger, K., Johansson, F., Sehested, M., Andersen, C., Dyrskjot, L., Ørntoft, T., Lukas, J., Kittas, C., Helleday, T., Halazonetis, T., Bartek, J. & Gorgoulis, V. (2006). Oncogene-induced senescence is part of the tumorigenesis barrier imposed by DNA damage checkpoints. *Nature*. 444 (7119). p.pp. 633–637.

Bates, M., Blosser, T.R. & Zhuang, X. (2005). Short-range spectroscopic ruler based on a single-molecule optical switch. *Physical review letters*. 94 (10). p.p. 108101.

Baum, B., Nishitani, H., Yanow, S. & Nurse, P. (1998). Cdc18 transcription and proteolysis couple S phase to passage through mitosis. *The EMBO Journal*. 17 (19). p.pp. 5689–5698.

Ben-Aroya, S., Koren, A., Liefshitz, B., Steinlauf, R. & Kupiec, M. (2003). ELG1, a yeast gene required for genome stability, forms a complex related to replication factor C. *Proceedings of the National Academy of Sciences*. 100 (17). p.pp. 9906–11.

Bell, S.P. & Stillman, B. (1992). ATP-dependent recognition of eukaryotic origins of DNA replication by a multiprotein complex. *Nature*. 357 (6374). p.pp. 128–34.

Bermejo, R., Doksan, Y., Capra, T., Katou, Y.-M., Tanaka, H., Shirahige, K. & Foiani, M. (2007). Top1-and Top2-mediated topological transitions at replication forks ensure fork progression and stability and prevent DNA damage checkpoint activation. *Genes & Development*. 21 (15). p.pp. 1921–1936.

Bermudez, VP, Maniwa, Y & Tappin, I (2003). The alternative Ctf18-Dcc1-Ctf8-replication factor C complex required for sister chromatid cohesion loads proliferating cell nuclear antigen onto DNA. *Proceedings of the National Academy of Sciences*. 100 (18). p.pp 10237–10242

Bermúdez-López, M., Pociño-Merino, I., Sánchez, H., Bueno, A., Guasch, C., Almedawar, S., Bru-Virgili, S., Garí, E., Wyman, C., Reverter, D., Colomina, N. & Torres-Rosell, J. (2015). ATPase-dependent control of the Mms21 SUMO ligase during DNA repair. *PLoS biology*. 13 (3). p.p. e1002089.

Betzig, E., Patterson, G., Sougrat, R., Lindwasser, W., Olenych, S., Bonifacino, J., Davidson, M., Lippincott-Schwartz, J. & Hess, H. (2006). Imaging Intracellular Fluorescent Proteins at Nanometer Resolution. *Science*. 313 (5793). p.pp. 1642–1645.

- Bi, X., Barkley, L.R., Slater, D.M., Tateishi, S., Yamaizumi, M., Ohmori, H. & Vaziri, C. (2006). Rad18 regulates DNA polymerase kappa and is required for recovery from S-phase checkpoint-mediated arrest. *Molecular and Cellular Biology*. 26 (9). p.pp. 3527–40.
- Bieging, K., Mello, S. & Attardi, L. (2014). Unravelling mechanisms of p53-mediated tumour suppression. *Nature Reviews Cancer*. 14 (5). p.pp. 359–370.
- Bienko, M., Green, C., Crosetto, N., Rudolf, F., Zapart, G., Coull, B., Kannouche, P., Wider, G., Peter, M., Lehmann, A., Hofmann, K. & Dikic, I. (2005). Ubiquitin-Binding Domains in Y-Family Polymerases Regulate Translesion Synthesis. *Science*. 310 (5755). p.pp. 1821–1824.
- Bochman, M., Paeschke, K. & Zakian, V. (2012). DNA secondary structures: stability and function of G-quadruplex structures. *Nature Reviews Genetics*. 13 (11). p.pp. 770–780.
- Boddy, Lopez-Girona, Shanahan, Interthal, Heyer & Russell (2000). Damage tolerance protein Mus81 associates with the FHA1 domain of checkpoint kinase Cds1. *Molecular and Cellular Biology*. 20(23). p.pp 8758-66
- Bowers, J.L., Randell, J.C., Chen, S. & Bell, S.P. (2004). ATP hydrolysis by ORC catalyzes reiterative Mcm2-7 assembly at a defined origin of replication. *Molecular cell*. 16 (6). p.pp. 967–78.
- Bowman, G., O'Donnell, M. & Kuriyan, J. (2004). Structural analysis of a eukaryotic sliding DNA clamp–clamp loader complex. *Nature*. 429 (6993). p.pp. 724–730.
- Branzei, D., Vanoli, F. & Foiani, M. (2008). SUMOylation regulates Rad18-mediated template switch. *Nature*. 456 (7224). p.pp. 915–920.
- Branzei, D. & Foiani, M. (2010). Maintaining genome stability at the replication fork. *Nature Reviews Molecular Cell Biology*. 11 (3). p.pp. 208–219.
- Bretschneider, S., Eggeling, C. & Hell, S.W. (2007). Breaking the diffraction barrier in fluorescence microscopy by optical shelving. *Physical review letters*. 98 (21). p.p. 218103.
- Brewer, B.J. & Fangman, W.L. (1988). A replication fork barrier at the 3' end of yeast ribosomal RNA genes. *Cell*. 55 (4). p.pp. 637–643.
- Brusky, J., Zhu, Y. & Xiao, W. (2000). UBC13, a DNA-damage-inducible gene, is a member of the error-free postreplication repair pathway in *Saccharomyces cerevisiae*. *Current genetics*. 37 (3). p.pp. 168–74.

Budd, M., Reis, C., Smith, S., Myung, K. & Campbell, J. (2006). Evidence Suggesting that Pif1 Helicase Functions in DNA Replication with the Dna2 Helicase/Nuclease and DNA Polymerase  $\delta$ . *Molecular and Cellular Biology*. 26 (7). p.pp. 2490–2500.

Burgess, A., Lorca, T. & Castro, A. (2012). Quantitative Live Imaging of Endogenous DNA Replication in Mammalian Cells. *PLoS ONE*. 7 (9). e45726

Bustard, D.E., Menolfi, D., Jeppsson, K., Ball, L.G., Dewey, S.C., Shirahige, K., Sjögren, C., Branzei, D. & Cobb, J.A. (2012). During replication stress, non-SMC element 5 (NSE5) is required for Smc5/6 protein complex functionality at stalled forks. *The Journal of Biological Chemistry*. 287 (14). p.pp. 11374–83.

Byun, T.S., Pacek, M., Yee, M.C., Walter, J.C. & Cimprich, K.A. (2005). Functional uncoupling of MCM helicase and DNA polymerase activities activates the ATR-dependent checkpoint. *Genes & Development*. 19 (9). p.pp. 1040–52.

Cayrou, C., Coulombe, P., Vigneron, A., Stanojcic, S., Ganier, O., Peiffer, I., Rivals, E., Puy, A., Laurent-Chabalier, S., Desprat, R. & Méchali, M. (2011). Genome-scale analysis of metazoan replication origins reveals their organization in specific but flexible sites defined by conserved features. *Genome research*. 21 (9). p.pp. 1438–49.

Calzada, A., Hodgson, B., Kanemaki, M., Bueno, A. & Labib, K. (2005). Molecular anatomy and regulation of a stable replisome at a paused eukaryotic DNA replication fork. *Genes & Development*. 19 (16). p.pp. 1905–1919.

Carpy, A., Krug, K., Graf, S., Koch, A., Popic, S., Hauf, S. & Macek, B. (2014). Absolute proteome and phosphoproteome dynamics during the cell cycle of *Schizosaccharomyces pombe* (Fission Yeast). *Molecular & cellular proteomics*. 13 (8). p.pp. 1925–36.

Carr, A.M. (2002). DNA structure dependent checkpoints as regulators of DNA repair. *DNA repair*. 1 (12). p.pp. 983–94.

Chalfie, M., Tu, Y., Euskirchen, G., Ward, W.W. & Prasher, D.C. (1994). Green fluorescent protein as a marker for gene expression. *Science*. 263 (5148). p.pp. 802–5.

Chang, D.J., Lupardus, P.J. & Cimprich, K.A. (2006). Monoubiquitination of proliferating cell nuclear antigen induced by stalled replication requires uncoupling of DNA polymerase and mini-chromosome maintenance helicase activities. *Journal of Biological Chemistry*. 281 (43). p.pp. 32081–32088.

- Chavez, A, Agrawal, V & Johnson, FB (2011). Homologous recombination-dependent rescue of deficiency in the structural maintenance of chromosomes (Smc) 5/6 complex. *Journal of Biological Chemistry*. 286 (7). p.pp 5119-5125
- Chen, Y.-H., Choi, K., Szakal, B., Arenz, J., Duan, X., Ye, H., Branzei, D. & Zhao, X. (2009). Interplay between the Smc5/6 complex and the Mph1 helicase in recombinational repair. *Proceedings of the National Academy of Sciences*. 106 (50). p.pp. 21252–21257.
- Chen, J., Zhang, Z., Li, L., Chen, B.-C., Revyakin, A., Hajj, B., Legant, W., Dahan, M., Lionnet, T., Betzig, E., Tjian, R. & Liu, Z. (2014). Single-Molecule Dynamics of Enhanceosome Assembly in Embryonic Stem Cells. *Cell*. 156 (6). p.pp 1274-1285
- Cheng, L., Collyer, T. & Hardy, C.F. (1999). Cell cycle regulation of DNA replication initiator factor Dbf4p. *Molecular and Cellular Biology*. 19 (6). p.pp. 4270–8.
- Chilkova, O., Stenlund, P., Isoz, I., Stith, C., Grabowski, P., Lundström, E.-B., Burgers, P. & Johansson, E. (2007). The eukaryotic leading and lagging strand DNA polymerases are loaded onto primer-ends via separate mechanisms but have comparable processivity in the presence of PCNA. *Nucleic Acids Research*. 35 (19). p.pp. 6588–6597.
- Cobb, J.A., Bjergbaek, L., Shimada, K., Frei, C. & Gasser, S.M. (2003). DNA polymerase stabilization at stalled replication forks requires Mec1 and the RecQ helicase Sgs1. *The EMBO Journal*. 22 (16). p.pp. 4325–36.
- Cocker, J., Piatti, S., Santocanale, C., Nasmyth, K. & Diffley, J. (1996). An essential role for the Cdc6 protein in forming the pre-replicative complexes of budding yeast. *Nature*. 379 (6561). p.pp. 180–182.
- Collins, A. (1999). Oxidative DNA damage, antioxidants, and cancer. *BioEssays*. 21 (3). p.pp. 238–246.
- Coons, A.H., Creech, HJ., and Jones, R.N. (1941). Immunological properties of an antibody containing a fluorescent group. *Proceedings of the Society for Experimental Biology and Medicine*. 47 (2). p.pp 200-202
- Coons, A.H. (1961). The beginnings of immunofluorescence. *Journal of immunology*. 87. p.pp. 499–503.
- Correa-Bordes, J. & Nurse, P. (1995). p25rum1 orders S phase and mitosis by acting as an inhibitor of the p34cdc2 mitotic kinase. *Cell*. 83 (6). p.pp. 1001–9.
- Cortez, D., Glick, G. & Elledge, S. (2004). Minichromosome maintenance proteins are direct targets of the ATM and ATR checkpoint kinases. *Proceedings of the National Academy of Sciences*. 101 (27). p.pp. 10078–10083.

Cortez, D. (2015). Preventing replication fork collapse to maintain genome integrity. *DNA Repair*. 32 p.pp 149-157

Cost, G. & Cozzarelli, N. (2006). Smc5p Promotes Faithful Chromosome Transmission and DNA Repair in *Saccharomyces cerevisiae*. *Genetics*. 172 (4). p.pp. 2185–2200.

Coster, G., Frigola, J., Beuron, F., Morris, E. & Diffley, J. (2014). Origin Licensing Requires ATP Binding and Hydrolysis by the MCM Replicative Helicase. *Molecular Cell*. 55 (5). p.pp 666-677

Cotta-Ramusino, C., Fachinetti, D., Lucca, C., Doksani, Y., Lopes, M., Sogo, J. & Foiani, M. (2004). Exo1 Processes Stalled Replication Forks and Counteracts Fork Reversal in Checkpoint-Defective Cells. *Molecular Cell*. 17 (1). 153-159

Ciccio, A. & Elledge, S. (2010). The DNA Damage Response: Making It Safe to Play with Knives. *Molecular Cell*. 40 (2). p.pp 179-204

Ciosk, R., Shirayama, M., Shevchenko, A., Tanaka, T., Toth, A., Shevchenko, A. & Nasmyth, K. (2000). Cohesin's binding to chromosomes depends on a separate complex consisting of Scc2 and Scc4 proteins. *Molecular cell*. 5 (2). p.pp. 243–54.

Daigaku, Y., Davies, A.A. & Ulrich, H.D. (2010). Ubiquitin-dependent DNA damage bypass is separable from genome replication. *Nature*. 465 (7300). p.pp. 951–5.

Daigaku, Y. (2012). Roadworks of DNA Damage Bypass during and after Replication. *Genes and Environment*. 34 (2). p.pp. 77–88.

Daigaku, Y., Keszthelyi, A., Müller, C., Miyabe, I., Brooks, T., Retkute, R., Hubank, M., Nieduszynski, C. & Carr, A. (2015). A global profile of replicative polymerase usage. *Nature Structural & Molecular Biology*. 22 (3). p.pp. 192–198.

Das-Bradoo, S., Nguyen, H.D., Wood, J.L., Ricke, R.M., Haworth, J.C. & Bielinsky, A.-K.K. (2010). Defects in DNA ligase I trigger PCNA ubiquitylation at Lys 107. *Nature cell biology*. 12 (1). p.pp. 74–79

Davey, M., Indiani, C. & O'Donnell, M. (2003). Reconstitution of the Mcm2-7p Heterohexamers, Subunit Arrangement, and ATP Site Architecture. *Journal of Biological Chemistry*. 278 (7). p.pp. 4491–4499.

Davies, A., Huttner, D., Daigaku, Y., Chen, S. & Ulrich, H. (2008). Activation of Ubiquitin-Dependent DNA Damage Bypass Is Mediated by Replication Protein A. *Molecular Cell*. 29 (5). p.pp 625-636

- Davis, A.P. & Symington, L.S. (2004). RAD51-dependent break-induced replication in yeast. *Molecular and Cellular Biology*. 24 (6). p.pp. 2344–51.
- De Piccoli, G., Katou, Y., Itoh, T., Nakato, R., Shirahige, K. & Labib, K. (2012). Replisome Stability at Defective DNA Replication Forks Is Independent of S Phase Checkpoint Kinases. *Molecular Cell*. 45 (5). p.pp 696-704
- Dedecker, P., Schryver, F. & Hofkens, J. (2013). Fluorescent Proteins: Shine on, You Crazy Diamond. *Journal of the American Chemical Society*. 135 (7). p.pp. 2387–2402.
- Delacroix, S., Wagner, J., Kobayashi, M., Yamamoto, K. & Karnitz, L. (2007). The Rad9–Hus1–Rad1 (9–1–1) clamp activates checkpoint signaling via TopBP1. *Genes & Development*. 21 (12). p.pp. 1472–1477.
- Dieckman, L. & Washington, M. (2013). PCNA trimer instability inhibits translesion synthesis by DNA polymerase  $\eta$  and by DNA polymerase  $\delta$ . *DNA Repair*. 12 (5). p.p. 367376.
- Diffley, J., Cocker, J., Dowell, S. & Rowley, A. (1994). Two steps in the assembly of complexes at yeast replication origins in vivo. *Cell*. 78 (2). p.p. 303316.
- Diffley, J. (2004). Regulation of Early Events in Chromosome Replication. *Current Biology*. 14 (18). p.pp 778-786
- Diffley, J. (2011). Quality control in the initiation of eukaryotic DNA replication. *Philosophical Transactions of the Royal Society B: Biological Sciences*. 366 (1584). p.pp. 3545–3553.
- Dion, V & Gasser, SM (2013). Chromatin movement in the maintenance of genome stability. *Cell*. 152 (6) p.pp 1355-1364
- Doré, A., Kilkenny, M., Rzechorzek, N. & Pearl, L. (2009). Crystal Structure of the Rad9–Rad1–Hus1 DNA Damage Checkpoint Complex—Implications for Clamp Loading and Regulation. *Molecular Cell*. 34 (6). p.pp 735-745
- Donovan, S., Harwood, J., Drury, L. & Diffley, J. (1997). Cdc6p-dependent loading of Mcm proteins onto pre-replicative chromatin in budding yeast. *Proceedings of the National Academy of Sciences*. 94 (11). p.pp. 5611–5616.
- Doyle, J., Gao, J., Wang, J., Yang, M. & Potts, P. (2010). MAGE-RING Protein Complexes Comprise a Family of E3 Ubiquitin Ligases. *Molecular Cell*. 39 (6). p.pp 963-974

- Duan, X., Sarangi, P., Liu, X., Rangi, G.K., Zhao, X. & Ye, H. (2009a). Structural and functional insights into the roles of the Mms21 subunit of the Smc5/6 complex. *Molecular Cell*. 35 (5). p.pp. 657–68.
- Duan, X., Yang, Y., Chen, Y.-H., Arenz, J., Rangi, G., Zhao, X. & Ye, H. (2009b). Architecture of the Smc5/6 Complex of *Saccharomyces cerevisiae* Reveals a Unique Interaction between the Nse5-6 Subcomplex and the Hinge Regions of Smc5 and Smc6. *Journal of Biological Chemistry*. 284 (13). p.pp. 8507–8515.
- Dubey, D.D., Zhu, J., Carlson, D.L., Sharma, K. & Huberman, J.A. (1994). Three ARS elements contribute to the *ura4* replication origin region in the fission yeast, *Schizosaccharomyces pombe*. *The EMBO journal*. 13 (15). p.pp. 3638–47.
- Edelstein, A., Amodaj, N., Hoover, K., Vale, R. & Stuurman, N. (2010). Current Protocols in Molecular Biology. *Current protocols in molecular biology* p.pp. 14.20.1–14.20.17.
- Edmunds, C.E., Simpson, L.J. & Sale, J.E. (2008). PCNA ubiquitination and REV1 define temporally distinct mechanisms for controlling translesion synthesis in the avian cell line DT40. *Molecular Cell*. 30 (4). p.pp. 519–29.
- Edwards, RJ, Bentley, NJ & Carr, AM (1999). A Rad3–Rad26 complex responds to DNA damage independently of other checkpoint proteins. *Nature cell biology*. 1, p.pp 393 – 398
- Elf, J., Li, G.-W. & Xie, X. (2007). Probing transcription factor dynamics at the single-molecule level in a living cell. *Science*. 316 (5828). p.pp. 1191–4.
- Erzberger, J., Mott, M. & Berger, J. (2006). Structural basis for ATP-dependent DnaA assembly and replication-origin remodeling. *Nature Structural & Molecular Biology*. 13 (8). p.pp. 676–683.
- Essers, J., Theil, A., Baldeyron, C., van Cappellen, W., Houtsmuller, A., Kanaar, R. & Vermeulen, W. (2005). Nuclear Dynamics of PCNA in DNA Replication and Repair. *Molecular and Cellular Biology*. 25 (21). p.pp. 9350–9359.
- Etheridge, T.J., Boulineau, R.L.L., Herbert, A., Watson, A.T., Daigaku, Y., Tucker, J., George, S., Jönsson, P., Palayret, M., Lando, D., Laue, E., Osborne, M.A., Klenerman, D., Lee, S.F. & Carr, A.M. (2014). Quantification of DNA-associated proteins inside eukaryotic cells using single-molecule localization microscopy. *Nucleic acids research*. 42 (19). p.p. e146.

Evrin, C., Clarke, P., Zech, J., Lurz, R., Sun, J., Uhle, S., Li, H., Stillman, B. & Speck, C. (2009). A double-hexameric MCM2-7 complex is loaded onto origin DNA during licensing of eukaryotic DNA replication. *Proceedings of the National Academy of Sciences*. 106 (48). p.pp. 20240–20245.

Evrin, C., Fernández-Cid, A., Riera, A., Zech, J., Clarke, P., Herrera, C.M., Tognetti, S., Lurz, R. & Speck, C. (2013). The ORC/Cdc6/MCM2-7 complex facilitates MCM2-7 dimerization during prereplicative complex formation. *Nucleic acids research*. 42 (4) p.pp 2257-2269

Falconi, M., Brown, G. & Kelly, T. (1996). cdc18+ regulates initiation of DNA replication in *Schizosaccharomyces pombe*. *Proceedings of the National Academy of Sciences*. 93 (4). p.pp. 1566–1570.

Falck, J., Petrini, J.H., Williams, B.R., Lukas, J. & Bartek, J. (2002). The DNA damage-dependent intra-S phase checkpoint is regulated by parallel pathways. *Nature genetics*. 30 (3). p.pp. 290–4.

Feijoo, C., Hall-Jackson, C., Wu, R., Jenkins, D., Leitch, J., Gilbert, D. & Smythe, C. (2001). Activation of mammalian Chk1 during DNA replication arrest a role for Chk1 in the intra-S phase checkpoint monitoring replication origin firing. *The Journal of Cell Biology*. 154 (5). p.pp. 913–924.

Ferlay J, Soerjomataram I, Ervik M, Dikshit R, Eser S, Mathers C, Rebelo M, Parkin DM, Forman D, Bray,F. GLOBOCAN 2012 v1.0, Cancer Incidence and Mortality Worldwide: IARC CancerBase No. 11 [Internet].Lyon, France: International Agency for Research on Cancer; 2013. Available from: <http://globocan.iarc.fr>, accessed on 22/06/2015.

Fernández-Cid, A., Riera, A., Tognetti, S., Herrera, M., Samel, S., Evrin, C., Winkler, C., Gardenal, E., Uhle, S. & Speck, C. (2013). An ORC/Cdc6/MCM2-7 complex is formed in a multistep reaction to serve as a platform for MCM double-hexamer assembly. *Molecular Cell*. 50 (4). p.pp. 577–88.

Forsburg, SL (1994). Codon usage table for *Schizosaccharomyces pombe*. *Yeast*. 10 (8). p.pp 1045-1047

Frampton, J., Irmisch, A., Green, C.M., Neiss, A., Trickey, M., Ulrich, H.D., Furuya, K., Watts, F.Z., Carr, A.M. & Lehmann, A.R. (2006). Postreplication repair and PCNA modification in *Schizosaccharomyces pombe*. *Molecular Biology of the Cell*. 17 (7). p.pp. 2976–85.

Freudenthal, B., Gakhar, L., Ramaswamy & Washington, T. (2010). Structure of monoubiquitinated PCNA and implications for translesion synthesis and DNA polymerase exchange. *Nature Structural & Molecular Biology*. 17 (4). p.pp. 479–484.

Fu, Y., Yardimci, H., Long, D., Ho, T., Guainazzi, A., Bermudez, V., Hurwitz, J., Oijen, A., Schärer, O. & Walter, J. (2011). Selective Bypass of a Lagging Strand Roadblock by the Eukaryotic Replicative DNA Helicase. *Cell*. 146 (6). p.pp 931-941

Furuya, K., Poitelea, M., Guo, L., Caspari, T. & Carr, A.M. (2004). Chk1 activation requires Rad9 S/TQ-site phosphorylation to promote association with C-terminal BRCT domains of Rad4TOPBP1. *Genes & Development*. 18 (10). p.pp. 1154–64.

Gaillard, H, García-Muse, T & Aguilera, A (2015). Replication stress and cancer. *Nature Reviews Cancer*. 15. p.pp 276-289

Gali, H., Juhasz, S., Morocz, M., Hajdu, I., Fatyol, K., Szukacsov, V., Burkovics, P. & Haracska, L. (2012). Role of SUMO modification of human PCNA at stalled replication fork. *Nucleic Acids Research*. 40 (13). p.pp. 6049–6059.

Gambus, A., Jones, R., Sanchez-Diaz, A., Kanemaki, M., Deursen, F., Edmondson, R. & Labib, K. (2006). GINS maintains association of Cdc45 with MCM in replisome progression complexes at eukaryotic DNA replication forks. *Nature Cell Biology*. 8 (4). p.pp. 358–366.

Gambus, A., van Deursen, F., Polychronopoulos, D., Foltman, M., Jones, R.C., Edmondson, R.D., Calzada, A. & Labib, K. (2009). A key role for Ctf4 in coupling the MCM2-7 helicase to DNA polymerase alpha within the eukaryotic replisome. *The EMBO Journal*. 28 (19). p.pp. 2992–3004.

Gangavarapu, V., Prakash, S. & Prakash, L. (2007). Requirement of RAD52 Group Genes for Postreplication Repair of UV-Damaged DNA in *Saccharomyces cerevisiae*. *Molecular and Cellular Biology*. 27 (21). p.pp. 7758–7764.

Gao, L., Shao, L., Higgins, C.D., Poulton, J.S., Peifer, M., Davidson, M.W., Wu, X., Goldstein, B. & Betzig, E. (2012). Noninvasive imaging beyond the diffraction limit of 3D dynamics in thickly fluorescent specimens. *Cell*. 151 (6). p.pp. 1370–85.

Ge, X., Jackson, D. & Blow, J. (2007). Dormant origins licensed by excess Mcm2–7 are required for human cells to survive replicative stress. *Genes & Development*. 21 (24). p.pp. 3331–3341.

Ge, XQ & Blow, JJ (2010). Chk1 inhibits replication factory activation but allows dormant origin firing in existing factories. *The Journal of cell biology*. 191 (7) p.pp 1285-1297

Georgescu, R., Langston, L., Yao, N., Yurieva, O., Zhang, D., Finkelstein, J., Agarwal, T. & O'Donnell, M. (2014). Mechanism of asymmetric polymerase assembly at the eukaryotic replication fork. *Nature Structural & Molecular Biology*. 21 (8). p.pp. 664–670.

Georgescu, R., Langston, L. & O'Donnell, M. (2015). A proposal: Evolution of PCNA's role as a marker of newly replicated DNA. *DNA repair*. 29. p.pp. 4–15.

Gibbs, P., McDonald, J., Woodgate, R. & Lawrence, C. (2005). The Relative Roles in Vivo of *Saccharomyces cerevisiae* Pol  $\eta$ , Pol  $\zeta$ , Rev1 Protein and Pol32 in the Bypass and Mutation Induction of an Abasic Site, T-T (6-4) Photoadduct and T-T cis-syn Cyclobutane Dimer. *Genetics*. 169 (2). p.pp. 575–582.

Giannattasio, M., Zwicky, K., Follonier, C., Foiani, M., Lopes, M. & Branzei, D. (2014). Visualization of recombination-mediated damage bypass by template switching. *Nature Structural & Molecular Biology*. 21 (10). p.pp. 884–892.

Gloor, J., Balakrishnan, L. & Bambara, R. (2010). Flap Endonuclease 1 Mechanism Analysis Indicates Flap Base Binding Prior to Threading. *Journal of Biological Chemistry*. 285 (45). p.pp. 34922–34931.

González-Prieto, R., Muñoz-Cabello, A., Cabello-Lobato, M. & Prado, F. (2013). Rad51 replication fork recruitment is required for DNA damage tolerance. *The EMBO Journal*. 32 (9). p.pp. 1307–21.

Göttfert, F, Wurm, CA, Mueller, V, Berning, S & Cordes, VC (2013). Coaligned dual-channel STED nanoscopy and molecular diffusion analysis at 20 nm resolution. *Biophysical journal*. 105 (1) p.pp L01-L03

Gomes, X. & Burgers, P. (2001). ATP Utilization by Yeast Replication Factor C. ATP-mediated interaction with DNA and with Proliferating Cell Nuclear Antigen. *Journal of Biological Chemistry*. 276 (37). p.pp. 34768–34775.

Gorgoulis, V., Vassiliou, L.-V., Karakaidos, P., Zacharatos, P., Kotsinas, A., Liloglou, T., Venere, M., DiTullio, R., Kastriakis, N., Levy, B., Kletsas, D., Yoneta, A., Herlyn, M., Kittas, C. & Halazonetis, T. (2005). Activation of the DNA damage checkpoint and genomic instability in human precancerous lesions. *Nature*. 434 (7035). p.pp. 907–913.

Gould, K.L. & Nurse, P. (1989). Tyrosine phosphorylation of the fission yeast cdc2+ protein kinase regulates entry into mitosis. *Nature*. 342 (6245). p.pp. 39–45.

Grallert, A., Patel, A., Tallada, V., Chan, K., Bagley, S., Krapp, A., Simanis, V. & Hagan, I. (2012). Centrosomal MPF triggers the mitotic and morphogenetic switches of fission yeast. *Nature Cell Biology*. 15 (1). p.pp. 88–95.

Guarino, E., Shepherd, M., Salguero, I., Hua, H., Deegan, R. & Kearsley, S. (2011). Cdt1 proteolysis is promoted by dual PIP degrons and is modulated by PCNA ubiquitylation. *Nucleic Acids Research*. 39 (14). p.pp. 5978–5990.

Gustafsson, Agard & Sedat (1999). I5M: 3D widefield light microscopy with better than 100 nm axial resolution. *Journal of Microscopy*. 195 (1). p.pp. 10–16.

Gustafsson, M.G. (2000). Surpassing the lateral resolution limit by a factor of two using structured illumination microscopy. *Journal of microscopy*. 198 (Pt 2). p.pp. 82–7.

Ha, T. & Tinnefeld, P. (2012). Photophysics of fluorescent probes for single-molecule biophysics and super-resolution imaging. *Annual review of physical chemistry*. 63. p.pp. 595–617.

Hajj, B., Wisniewski, J., Beheiry, M., Chen, J., Revyakin, A., Wu, C. & Dahan, M. (2014). Whole-cell, multicolor superresolution imaging using volumetric multifocus microscopy. *Proceedings of the National Academy of Sciences*. 111 (49). p.pp. 17480–17485.

Han, J., Li, Q., McCullough, L., Kettelkamp, C., Formosa, T. & Zhang, Z. (2010). Ubiquitylation of FACT by the Cullin-E3 ligase Rtt101 connects FACT to DNA replication. *Genes & Development*. 24 (14). p.pp. 1485–1490.

Hanahan, D. & Weinberg, R. (2000). The Hallmarks of Cancer. *Cell*. 100 (1). p.pp 57-70

Hanahan, D. & Weinberg, R. (2011). Hallmarks of Cancer: The Next Generation. *Cell*. 144 (5). p.pp 646-674

Haracska, L., Unk, I., Prakash, L. & Prakash, S. (2006). Ubiquitylation of yeast proliferating cell nuclear antigen and its implications for translesion DNA synthesis. *Proceedings of the National Academy of Sciences*. 103 (17). p.pp. 6477–82.

Harrington, J.J. & Lieber, M.R. (1994). The characterization of a mammalian DNA structure-specific endonuclease. *The EMBO journal*. 13 (5). p.pp. 1235–46.

Hartwell, L.H., Culotti, J., Pringle, J.R. & Reid, B.J. (1974). Genetic control of the cell division cycle in yeast. *Science*. 183 (4120). p.pp. 46–51.

Hashimoto, Y, Puddu, F & Costanzo, V (2012). RAD51-and MRE11-dependent reassembly of uncoupled CMG helicase complex at collapsed replication forks. *Nature structural & molecular biology*. 19 (1). p.pp 17-25

Hazbun, T., Malmström, L., Anderson, S., Graczyk, B., Fox, B., Riffle, M., Sundin, B., Aranda, J.D., McDonald, W.H., Chiu, C.-H., Snydsman, B., Bradley, P., Muller, E., Fields, S., Baker, D., III, J. & Davis, T. (2003). Assigning Function to Yeast Proteins by Integration of Technologies. *Molecular Cell*. 12 (6). p.pp 1353-1365

Heilemann, M., van de Linde, S., Schüttelz, M., Kasper, R., Seefeldt, B., Mukherjee, A., Tinnefeld, P. & Sauer, M. (2008). Subdiffraction-Resolution Fluorescence Imaging with Conventional Fluorescent Probes. *Angewandte Chemie International Edition*. 47 (33). p.pp. 6172–6176.

Heim, R, Prasher, DC & Tsien, RY (1994). Wavelength mutations and posttranslational autoxidation of green fluorescent protein. *Proceedings of the National Academy of Sciences*. 91 (26) p.pp 12501-12504

Heimstadt, O. (1911). Das Fluoreszenzmikroskop. *Zeitschr. Wissensch. Mikrosk.* 28, p.pp 330-337

Hell, S & Stelzer, E. (1992). Fundamental improvement of resolution with a 4Pi-confocal fluorescence microscope using two-photon excitation. *Optics Communications*. 93 p.pp 277-282

Hell, S.W. & Wichmann, J. (1994). Breaking the diffraction resolution limit by stimulated emission: stimulated-emission-depletion fluorescence microscopy. *Optics letters*. 19 (11). p.pp. 780–2.

Hell, S. & Kroug, M. (1995). Ground-state-depletion fluorescence microscopy: A concept for breaking the diffraction resolution limit. *Applied Physics B*. 60 (5). p.pp. 495–497.

Hell, S.W. (2007). Far-field optical nanoscopy. *Science*. 316 (5828). p.pp. 1153–8.

Heller, R., Kang, S., Lam, W., Chen, S., Chan, C. & Bell, S. (2011). Eukaryotic Origin-Dependent DNA Replication In Vitro Reveals Sequential Action of DDK and S-CDK Kinases. *Cell*. 146 (1). p.pp 80-91

Helmrich, A., Ballarino, M., Nudler, E. & Tora, L. (2013). Transcription-replication encounters, consequences and genomic instability. *Nature structural & molecular biology*. 20 (4). p.pp. 412–8.

Hendel, A., Krijger, P., Diamant, N., Goren, Z., Langerak, P., Kim, J., Reißner, T., Lee, K., Geacintov, N., Carell, T., Myung, K., Tateishi, S., D'Andrea, A., Jacobs, H. & Livneh, Z. (2011). PCNA Ubiquitination Is Important, But Not Essential for Translesion DNA Synthesis in Mammalian Cells. *PLoS Genetics*. 7 (9). e1002262

Henriques, R., Lelek, M., Fornasiero, E., Valtorta, F., Zimmer, C. & Mhlanga, M. (2010). QuickPALM: 3D real-time photoactivation nanoscopy image processing in ImageJ. *Nature Methods*. 7 (5). p.pp. 339–340.

Hess, S.T., Girirajan, T.P. & Mason, M.D. (2006). Ultra-high resolution imaging by fluorescence photoactivation localization microscopy. *Biophysical journal*. 91 (11). p.pp. 4258–72.

Higgins, NP, Kato, K & Strauss, B (1976). A model for replication repair in mammalian cells. *Journal of molecular biology*. 101 (3). p.pp 417-425

Higgs, M., Reynolds, J., Winczura, A., Blackford, A., Borel, V., Miller, E., Zlatanou, A., Nieminuszczy, J., Ryan, E., Davies, N., Stankovic, T., Boulton, S., Niedzwiedz, W. & Stewart, G. (2015). BOD1L Is Required to Suppress Deleterious Resection of Stressed Replication Forks. *Molecular Cell*. 59 (3). p.pp. 462–77.

Hoegge, C., Pfander, B., Moldovan, G.-L., Pyrowolakis, G. & Jentsch, S. (2002). RAD6-dependent DNA repair is linked to modification of PCNA by ubiquitin and SUMO. *Nature*. 419 (6903). p.pp. 135–141.

Hofmann, JF & Beach, D. (1994). cdt1 is an essential target of the Cdc10/Sct1 transcription factor: requirement for DNA replication and inhibition of mitosis. *The EMBO Journal*. 13 (2). p.pp 425-434

Holden, S., Pengo, T., Meibom, K., Fernandez, C., Collier, J. & Manley, S. (2014). High throughput 3D super-resolution microscopy reveals *Caulobacter crescentus* in vivo Z-ring organization. *Proceedings of the National Academy of Sciences*. 111 (12). p.pp. 4566–4571.

Hsiang, YH, Lihou, MG & Liu, LF (1989). Arrest of replication forks by drug-stabilized topoisomerase I-DNA cleavable complexes as a mechanism of cell killing by camptothecin. *Cancer research*. 49. p.pp 5077-5082

Hu, Z., Perumal, S., Yue, H. & Benkovic, S. (2012). The Human Lagging Strand DNA Polymerase Holoenzyme Is Distributive. *Journal of Biological Chemistry*. 287 (46). p.p. 3844238448.

Hu, J., Sun, L., Shen, F., Chen, Y., Hua, Y., Liu, Y., Zhang, M., Hu, Y., Wang, Q., Xu, W., Sun, F., Ji, J., Murray, J.M., Carr, A.M. & Kong, D. (2012). The intra-S phase checkpoint targets Dna2 to prevent stalled replication forks from reversing. *Cell*. 149 (6). p.pp. 1221–32.

Huang, T., Nijman, S., Mirchandani, K., Galardy, P., Cohn, M., Haas, W., Gygi, S., Ploegh, H., Bernards, R. & D'Andrea, A. (2006). Regulation of monoubiquitinated PCNA by DUB autocleavage. *Nature Cell Biology*. 8 (4). p.pp. 341–347.

Huang, B., Wang, W., Bates, M. & Zhuang, X. (2008a). Three-dimensional super-resolution imaging by stochastic optical reconstruction microscopy. *Science*. 319 (5864). p.pp. 810–3.

Huang, B., Jones, S.A., Brandenburg, B. & Zhuang, X. (2008b). Whole-cell 3D STORM reveals interactions between cellular structures with nanometer-scale resolution. *Nature Methods*. 5 (12). p.pp. 1047–52.

Huang, B., Bates, M. & Zhuang, X. (2009). Super-Resolution Fluorescence Microscopy. *Biochemistry*. 78 (1). p.pp. 993–1016.

Indiani, C. & O'Donnell, M. (2006). The replication clamp-loading machine at work in the three domains of life. *Nature reviews. Molecular cell biology*. 7 (10). p.pp. 751–61.

Iraqi, I., Chekkal, Y., Jmari, N., Pietrobon, V., Fréon, K., Costes, A. & Lambert, S.A. (2012). Recovery of arrested replication forks by homologous recombination is error-prone. *PLoS genetics*. 8 (10). p.p. e1002976.

Irmisch, A., Ampatzidou, E., Mizuno, K., O'Connell, M.J. & Murray, J.M. (2009). Smc5/6 maintains stalled replication forks in a recombination-competent conformation. *The EMBO journal*. 28 (2). p.pp. 144–55.

Jackson, A., Laskey, R. & Coleman, N. (2014). Replication proteins and human disease. *Cold Spring Harbor perspectives in biology*. 6 (1)

Jacob F, Brenner J, Cuzin F. 1963. On the regulation of DNA replication in bacteria. *Cold Spring Harbor Symp Quant Biol* 28. p.pp 329 –348

Jeppsson, K., Carlborg, K., Nakato, R., Berta, D., Lilienthal, I., Kanno, T., Lindqvist, A., Brink, M., Dantuma, N., Katou, Y., Shirahige, K. & Sjögren, C. (2014a). The Chromosomal Association of the Smc5/6 Complex Depends on Cohesion and Predicts the Level of Sister Chromatid Entanglement. *PLoS Genetics*. 10 (10). e1004680

Jeppsson, K., Kanno, T., Shirahige, K. & Sjögren, C. (2014b). The maintenance of chromosome structure: positioning and functioning of SMC complexes. *Nature Reviews Molecular Cell Biology*. 15 (9). p.pp. 601–614.

Jensen, RB, Carreira, A & Kowalczykowski, SC (2010). Purified human BRCA2 stimulates RAD51-mediated recombination. *Nature*. 467 (7316) p.pp 678-683

Jentsch, S., McGrath, J. & Varshavsky, A. (1987). The yeast DNA repair gene RAD6 encodes a ubiquitin-conjugating enzyme. *Nature*. 329 (6135). p.pp. 131–134.

Jia, S., Vaughan, J.C. & Zhuang, X. (2014). Isotropic 3D Super-resolution Imaging with a Self-bending Point Spread Function. *Nature photonics*. 8. p.pp. 302–306.

Johnson, R., Henderson, S., Petes, T., Prakash, S., Bankmann, M. & Prakash, L. (1992). *Saccharomyces cerevisiae* RAD5-encoded DNA repair protein contains DNA helicase and zinc-binding sequence motifs and affects the stability of simple repetitive sequences in the genome. *Molecular and Cellular Biology*. 12 (9). p.pp. 3807–18.

Johnson, R., Washington, M., Haracska, L., Prakash, S. & Prakash, L. (2000). Eukaryotic polymerases  $\iota$  and  $\zeta$  act sequentially to bypass DNA lesions. *Nature*. 406 (6799). p.pp. 1015–1019.

Jónsson, Z., Hindges, R. & Hübscher, U. (1998). Regulation of DNA replication and repair proteins through interaction with the front side of proliferating cell nuclear antigen. *The EMBO Journal*. 17 (8). p.pp. 2412–2425.

Kamimura, Y., Tak, Y., Sugino, A. & Araki, H. (2001). Sld3, which interacts with Cdc45 (Sld4), functions for chromosomal DNA replication in *Saccharomyces cerevisiae*. *The EMBO Journal*. 20 (8). p.pp. 2097–2107.

Kandoth, C., McLellan, M.D., Vandin, F., Ye, K., Niu, B., Lu, C., Xie, M., Zhang, Q., McMichael, J.F., Wyczalkowski, M.A., Leiserson, M.D., Miller, C.A., Welch, J.S., Walter, M.J., Wendl, M.C., Ley, T.J., Wilson, R.K., Raphael, B.J. & Ding, L. (2013). Mutational landscape and significance across 12 major cancer types. *Nature*. 502 (7471). p.pp. 333–9.

Kanke, M., Kodama, Y., Takahashi, T.S., Nakagawa, T. & Masukata, H. (2012). Mcm10 plays an essential role in origin DNA unwinding after loading of the CMG components. *The EMBO Journal*. 31 (9). p.pp. 2182–2194.

Kanno, T., Berta, D.G. & Sjögren, C. (2015). The Smc5/6 Complex Is an ATP-Dependent Intermolecular DNA Linker. *Cell reports*. 12 (9) p.pp 1471-1482

Kannouche, P., Wing, J. & Lehmann, A. (2003). Interaction of Human DNA Polymerase  $\eta$  with Monoubiquitinated PCNA: A Possible Mechanism for the Polymerase Switch in Response to DNA Damage. *Molecular Cell*. 14 (4). p.pp 491-500

Kao, H.-I., Henricksen, L., Liu, Y. & Bambara, R. (2002). Cleavage specificity of *Saccharomyces cerevisiae* flap endonuclease 1 suggests a double-flap structure as the cellular substrate. *Journal of Biological Chemistry*. 277. p.pp 14379-14389

- Karras, G.I. & Jentsch, S. (2010). The RAD6 DNA damage tolerance pathway operates uncoupled from the replication fork and is functional beyond S phase. *Cell*. 141 (2). p.pp. 255–67.
- Kearsey, SE, Montgomery, S & Labib, K (2000). Chromatin binding of the fission yeast replication factor mcm4 occurs during anaphase and requires ORC and cdc18. *The EMBO Journal*. 19 (7) p.pp 681-1690
- Kegel, A., Betts-Lindroos, H., Kanno, T., Jeppsson, K., Ström, L., Katou, Y., Itoh, T., Shirahige, K. & Sjögren, C. (2011). Chromosome length influences replication-induced topological stress. *Nature*. 471 (7338). p.pp. 392–6.
- Kim, S. & Huberman, J. (2001). Regulation of replication timing in fission yeast. *The EMBO Journal*. 20 (21). p.pp. 6115–6126.
- Kim, S., Gitai, Z., Kinkhabwala, A., Shapiro, L. & Moerner, W. (2006). Single molecules of the bacterial actin MreB undergo directed treadmilling motion in *Caulobacter crescentus*. *Proceedings of the National Academy of Sciences*. 103 (29). p.pp. 10929–10934.
- Kiuchi, T., Higuchi, M., Takamura, A., Maruoka, M. & Watanabe, N. (2015). Multitarget super-resolution microscopy with high-density labeling by exchangeable probes. *Nature Methods*. 12 (8). p.pp. 743–746.
- Klar, T.A. & Hell, S.W. (1999). Subdiffraction resolution in far-field fluorescence microscopy. *Optics letters*. 24 (14). p.pp. 954–6.
- Kommajosyula, N. & Rhind, N. (2006). Cdc2 tyrosine phosphorylation is not required for the S-phase DNA damage checkpoint in fission yeast. *Cell cycle*. 5 (21). p.pp. 2495–500.
- Krishna, T.S., Kong, X.P., Gary, S., Burgers, P.M. & Kuriyan, J. (1994). Crystal structure of the eukaryotic DNA polymerase processivity factor PCNA. *Cell*. 79 (7). p.pp. 1233–43.
- Kubota, Y., Takase, Y., Komori, Y., Hashimoto, Y., Arata, T., Kamimura, Y., Araki, H. & Takisawa, H. (2003). A novel ring-like complex of *Xenopus* proteins essential for the initiation of DNA replication. *Genes & Development*. 17 (9). p.pp. 1141–1152.
- Kubota, T., Nishimura, K., Kanemaki, M. & Donaldson, A. (2013). The Elg1 Replication Factor C-like Complex Functions in PCNA Unloading during DNA Replication. *Molecular Cell*. 50 (2). p.pp. 273–80.

- Kubota, T., Katou, Y., Nakato, R., Shirahige, K. & Donaldson, A. (2015). Replication-Coupled PCNA Unloading by the Elg1 Complex Occurs Genome-wide and Requires Okazaki Fragment Ligation. *Cell Reports*. 12 (5) p.pp 774-787
- Kuchta, R. & Stengel, G. (2010). Mechanism and evolution of DNA primases. *Biochimica et Biophysica Acta (BBA) - Proteins and Proteomics*. 1804 (5). p.p. 11801189.
- Kuipers, M., Stasevich, T., Sasaki, T., Wilson, K., Hazelwood, K., McNally, J., Davidson, M. & Gilbert, D. (2011). Highly stable loading of Mcm proteins onto chromatin in living cells requires replication to unload. *The Journal of Cell Biology*. 192 (1). p.pp. 29–41.
- Kumagai, A., Lee, J., Yoo, H. & Dunphy, W. (2005). TopBP1 Activates the ATR-ATRIP Complex. *Cell*. 124(5) p.pp 943-55.
- Kumar, S. & Burgers, P. (2013). Lagging strand maturation factor Dna2 is a component of the replication checkpoint initiation machinery. *Genes & Development*. 27 (3). p.pp. 313–321.
- Lambert, S., Watson, A., Sheedy, D.M., Martin, B. & Carr, A.M. (2005). Gross chromosomal rearrangements and elevated recombination at an inducible site-specific replication fork barrier. *Cell*. 121 (5). p.pp. 689–702.
- Lambert, S., Mizuno, K., Blaisonneau, J., Martineau, S., Chanet, R., Fréon, K., Murray, J.M., Carr, A.M. & Baldacci, G. (2010). Homologous recombination restarts blocked replication forks at the expense of genome rearrangements by template exchange. *Molecular cell*. 39 (3). p.pp. 346–59.
- Lambert, S. & Carr, A.M. (2013). Impediments to replication fork movement: stabilisation, reactivation and genome instability. *Chromosoma*. 122 (1-2). p.pp. 33–45.
- Lando, D., Endesfelder, U., Berger, H., Subramanian, L., Dunne, P.D., McColl, J., Klenerman, D., Carr, A.M., Sauer, M., Allshire, R.C., Heilemann, M. & Laue, E.D. (2012). Quantitative single-molecule microscopy reveals that CENP-A(Cnp1) deposition occurs during G2 in fission yeast. *Open biology*. 2 (7). p.p. 120078.
- Langston, L. & O'Donnell, M. (2008). DNA Polymerase  $\delta$  Is Highly Processive with Proliferating Cell Nuclear Antigen and Undergoes Collision Release upon Completing DNA. *Journal of Biological Chemistry*. 283 (43). p.pp. 29522–29531.
- Lazzaro, F., Novarina, D., Amara, F., Watt, D.L., Stone, J.E., Costanzo, V., Burgers, P.M., Kunkel, T.A., Plevani, P. & Muzi-Falconi, M. (2012). RNase H and postreplication repair protect cells from ribonucleotides incorporated in DNA. *Molecular Cell*. 45 (1). p.pp. 99–110.

- Leach, C.A. & Michael, W.M. (2005). Ubiquitin/SUMO modification of PCNA promotes replication fork progression in *Xenopus laevis* egg extracts. *The Journal of Cell Biology*. 171 (6). p.pp. 947–54.
- Lee, C., Hong, B., Choi, J., Kim, Y., Watanabe, S., Ishimi, Y., Enomoto, T., Tada, S., Kim, Y. & Cho, Y. (2004). Structural basis for inhibition of the replication licensing factor Cdt1 by geminin. *Nature*. 430 (7002). p.pp. 913–917.
- Lee, J.-B., Hite, R., Hamdan, S., Xie, X., Richardson, C. & Oijen, A. (2006). DNA primase acts as a molecular brake in DNA replication. *Nature*. 439 (7076). p.pp. 621–624.
- Lee, K., Yang, K., Cohn, M., Sikdar, N., D'Andrea, A. & Myung, K. (2010). Human ELG1 Regulates the Level of Ubiquitinated Proliferating Cell Nuclear Antigen (PCNA) through Its Interactions with PCNA and USP1. *Journal of Biological Chemistry*. 285 (14). p.pp. 10362–10369.
- Lee, S.-H., Shin, J., Lee, A. & Bustamante, C. (2012). Counting single photoactivatable fluorescent molecules by photoactivated localization microscopy (PALM). *Proceedings of the National Academy of Sciences*. 109 (43). p.pp. 17436–17441.
- Lehmann, H. (1913). Das Lumineszenz-Mikroskop, seine Grundlagen und seine Anwendungen. *Zeitschr. Wissensch. Mikrosk.* 30, p.pp 418–470
- Lehmann, A.R., Walicka, M., Griffiths, D.J., Murray, J.M., Watts, F.Z., McCready, S. & Carr, A.M. (1995). The rad18 gene of *Schizosaccharomyces pombe* defines a new subgroup of the SMC superfamily involved in DNA repair. *Molecular and Cellular Biology*. 15 (12). p.pp. 7067–80.
- Lehmann, A., Niimi, A., Ogi, T., Brown, S., Sabbioneda, S., Wing, J., Kannouche, P. & Green, C. (2007). Translesion synthesis: Y-family polymerases and the polymerase switch. *DNA Repair*. 6 (7). p.p. 891899.
- Lei, M., Kawasaki, Y, Young, MR & Kihara, M (1997). Mcm2 is a target of regulation by Cdc7–Dbf4 during the initiation of DNA synthesis. *Genes & Development*. 11 (24), p.pp 3365–3374
- Leonhardt, H., Rahn, H.-P., Weinzierl, P., Sporbert, A., Cremer, T., Zink, D. & Cardoso, M. (2000). Dynamics of DNA Replication Factories in Living Cells. *The Journal of Cell Biology*. 149 (2). p.pp. 271–280.

- Leung, G., Lee, L., Schmidt, T., Shirahige, K. & Kobor, M. (2011). Rtt107 Is Required for Recruitment of the SMC5/6 Complex to DNA Double Strand Breaks. *Journal of Biological Chemistry*. 286 (29). p.pp. 26250–26257.
- Li, X., Li, J., Harrington, J., Lieber, M.R. & Burgers, P.M. (1995). Lagging strand DNA synthesis at the eukaryotic replication fork involves binding and stimulation of FEN-1 by proliferating cell nuclear antigen. *The Journal of Biological Chemistry*. 270 (38). p.pp. 22109–12.
- Lin, S.-J., Wardlaw, C., Morishita, T., Miyabe, I., Chahwan, C., Caspari, T., Schmidt, U., Carr, A. & Garcia, V. (2012). The Rad4TopBP1 ATR-Activation Domain Functions in G1/S Phase in a Chromatin-Dependent Manner. *PLoS Genetics*. 8 (6). e1002801
- Lindsay, H., Griffiths, D., Edwards, R., Christensen, P., Murray, J., Osman, F., Walworth, N. & Carr, A. (1998). S-phase-specific activation of Cds1 kinase defines a subpathway of the checkpoint response in *Schizosaccharomyces pombe*. *Genes & Development*. 12 (3). p.pp. 382–395.
- Liontos, M., Koutsami, M., Sideridou, M., Evangelou, K., Kletsas, D., Levy, B., Kotsinas, A., Nahum, O., Zoumpourlis, V., Kouloukoussa, M., Lygerou, Z., Taraviras, S., Kittas, C., Bartkova, J., Papavassiliou, A., Bartek, J., Halazonetis, T. & Gorgoulis, V. (2007). Deregulated Overexpression of hCdt1 and hCdc6 Promotes Malignant Behavior. *Cancer Research*. 67 (22). p.pp. 10899–10909.
- Lippincott-Schwartz, J & Patterson, GH (2003). Development and use of fluorescent protein markers in living cells. *Science*. 300 (5616). p.pp 87-91
- Lisby, M., Rothstein, R. & Mortensen, U. (2001). Rad52 forms DNA repair and recombination centers during S phase. *Proceedings of the National Academy of Sciences*. 98 (15). p.pp. 8276–8282.
- Loeb, L., Bielas, J., Beckman, R. & Bodmer, I. (2008). Cancers Exhibit a Mutator Phenotype: Clinical Implications. *Cancer Research*. 68 (10). p.pp. 3551–3557.
- Lopes, M., Cotta-Ramusino, C., Pelliccioli, A., Liberi, G., Plevani, P., Muzi-Falconi, M., Newlon, C. & Foiani, M. (2001). The DNA replication checkpoint response stabilizes stalled replication forks. *Nature*. 412 (6846). p.pp. 557–561.
- Lopes, M., Foiani, M. & Sogo, J. (2006). Multiple Mechanisms Control Chromosome Integrity after Replication Fork Uncoupling and Restart at Irreparable UV Lesions. *Molecular Cell*. 21 (1). p.pp 15-27

- Lossaint, G., Larroque, M., Ribeyre, C., Bec, N., Larroque, C., Décaillet, C., Gari, K. & Constantinou, A. (2013). FANCD2 binds MCM proteins and controls replisome function upon activation of S phase checkpoint signalling. *Molecular Cell*. 51 (5). p.pp. 678–90.
- Lou, H., Komata, M., Katou, Y., Guan, Z., Reis, C.C., Budd, M., Shirahige, K. & Campbell, J.L. (2008). Mrc1 and DNA polymerase epsilon function together in linking DNA replication and the S phase checkpoint. *Molecular Cell*. 32 (1). p.pp. 106–17.
- Lucca, C., Vanoli, F., Cotta-Ramusino, C., Pelliccioli, A., Liberi, G., Haber, J. & Foiani, M. (2004). Checkpoint-mediated control of replisome–fork association and signalling in response to replication pausing. *Oncogene*. 23 (6). p.pp. 1206–1213.
- Lindroos, H.B., Ström, L., Itoh, T., Katou, Y., Shirahige, K. & Sjögren, C. (2006). Chromosomal association of the Smc5/6 complex reveals that it functions in differently regulated pathways. *Molecular Cell*. 22 (6). p.pp. 755–67.
- Liu, J., Doty, T., Gibson, B. & Heyer, W.-D. (2010). Human BRCA2 protein promotes RAD51 filament formation on RPA-covered single-stranded DNA. *Nature structural & molecular biology*. 17 (10). p.pp. 1260–1262.
- Liu, Z., Xing, D., Su, Q., Zhu, Y., Zhang, J., Kong, X., Xue, B., Wang, S., Sun, H., Tao, Y. & Sun, Y. (2014). Super-resolution imaging and tracking of protein–protein interactions in sub-diffraction cellular space. *Nature Communications*. 5. doi:10.1038/ncomms5443
- Lydeard, J.R., Jain, S., Yamaguchi, M. & Haber, J.E. (2007). Break-induced replication and telomerase-independent telomere maintenance require Pol32. *Nature*. 448 (7155). p.pp. 820–3.
- Macheret, M. & Halazonetis, T.D. (2015). DNA replication stress as a hallmark of cancer. *Annual review of pathology*. 10. p.pp. 425–48.
- Messer, W. (2002). The bacterial replication initiator DnaA. DnaA and oriC, the bacterial mode to initiate DNA replication. *FEMS Microbiology Reviews*. 26 (4). p.pp. 355–374.
- MacDougall, C., Byun, T., Van, C., Yee, M. & Cimprich, K. (2007). The structural determinants of checkpoint activation. *Genes & Development*. 21 (8). p.pp. 898–903.
- Maga, G., Villani, G., Tillement, V., Stucki, M., Locatelli, G., Frouin, I., Spadari, S. & Hübscher, U. (2001). Okazaki fragment processing: Modulation of the strand displacement activity of DNA polymerase  $\delta$  by the concerted action of replication protein A, proliferating cell nuclear antigen, and flap endonuclease-1. *Proceedings of the National Academy of Sciences*. 98 (25). p.pp. 14298–14303.

- Maiorano, D., Moreau, J. & Méchali, M. (2000). XCDT1 is required for the assembly of pre-replicative complexes in *Xenopus laevis*. *Nature*. 404 (6778). p.pp. 622–625.
- Mailand, N., Falck, J., Lukas, C., Syljuåsen, R., Welcker, M., Bartek, J. & Lukas, J. (2000). Rapid Destruction of Human Cdc25A in Response to DNA Damage. *Science*. 288 (5470). p.pp. 1425–1429.
- Majka, J., Binz, S., Wold, M. & Burgers, P. (2006). Replication Protein A Directs Loading of the DNA Damage Checkpoint Clamp to 5'-DNA Junctions. *Journal of Biological Chemistry*. 281 (38). p.pp. 27855–27861.
- Manley, S., Gillette, J., Patterson, G., Shroff, H., Hess, H., Betzig, E. & Lippincott-Schwartz, J. (2008). High-density mapping of single-molecule trajectories with photoactivated localization microscopy. *Nature Methods*. 5 (2). p.pp. 155–157.
- Mantiero, D., Mackenzie, A., Donaldson, A. & Zegerman, P. (2011). Limiting replication initiation factors execute the temporal programme of origin firing in budding yeast. *The EMBO Journal*. 30 (23). p.pp. 4805–4814.
- Marguerat, S, Schmidt, A, Codlin, S & Chen, W (2012). Quantitative analysis of fission yeast transcriptomes and proteomes in proliferating and quiescent cells. *Cell*. 151 (3) p.pp 671-683
- Maric, M., Maculins, T., Piccoli, G. & Labib, K. (2014). Cdc48 and a ubiquitin ligase drive disassembly of the CMG helicase at the end of DNA replication. *Science*. 346 (6208). p.p. 1253596.
- Masuda, Y., Piao, J. & Kamiya, K. (2010). DNA replication-coupled PCNA mono-ubiquitination and polymerase switching in a human in vitro system. *Journal of molecular biology*. 396 (3). p.pp. 487–500.
- Masumoto, H., Muramatsu, S., Kamimura, Y. & Araki, H. (2002). S-Cdk-dependent phosphorylation of Sld2 essential for chromosomal DNA replication in budding yeast. *Nature*. 415 (6872). p.pp. 651–5.
- Masutani, C., Kusumoto, R., Iwai, S. & Hanaoka, F. (2000). Mechanisms of accurate translesion synthesis by human DNA polymerase  $\eta$ . *The EMBO Journal*. 19 (12). p.pp. 3100–3109.
- Matsuyama, A., Shirai, A. & Yoshida, M. (2008). A novel series of vectors for chromosomal integration in fission yeast. *Biochemical and biophysical research communications*. 374 (2). p.pp. 315–9.

- McDonald, H.W., Pavlova, Y., Yates, J.R. & Boddy, M.N. (2003). Novel essential DNA repair proteins Nse1 and Nse2 are subunits of the fission yeast Smc5-Smc6 complex. *Journal of Biological Chemistry*. 278 (46). p.pp. 45460–45467.
- McElhinny, S., Gordenin, D., Stith, C., Burgers, P. & Kunkel, T. (2007). Division of Labor at the Eukaryotic Replication Fork. *Molecular Cell*. 30 (2). p.pp 137-144
- McKinney, S., Murphy, C., Hazelwood, K., Davidson, M. & Looger, L. (2009). A bright and photostable photoconvertible fluorescent protein. *Nature Methods*. 6 (2). p.pp. 131–133.
- Meister, P., Taddei, A., Vernis, L., Poidevin, M., Gasser, S. & Baldacci, G. (2005). Temporal separation of replication and recombination requires the intra-S checkpoint. *The Journal of Cell Biology*. 168 (4). p.pp. 537–544.
- Meister, P., Taddei, A., Ponti, A., Baldacci, G. & Gasser, S. (2007). Replication foci dynamics: replication patterns are modulated by S-phase checkpoint kinases in fission yeast. *The EMBO Journal*. 26 (5). p.pp. 1315–1326.
- Méndez, J. & Stillman, B. (2000). Chromatin Association of Human Origin Recognition Complex, Cdc6, and Minichromosome Maintenance Proteins during the Cell Cycle: Assembly of Prereplication Complexes in Late Mitosis. *Molecular and Cellular Biology*. 20 (22). p.pp. 8602–8612.
- Micco, R., Fumagalli, M., Cicalese, A., Piccinin, S., Gasparini, P., Luise, C., Schurra, C., Garre', M., Nuciforo, P., Bensimon, A., Maestro, R., Pelicci, P. & di Fagagna, F. (2006). Oncogene-induced senescence is a DNA damage response triggered by DNA hyper-replication. *Nature*. 444 (7119). p.pp. 638–642.
- Michalet, X. & Berglund, A. (2012). Optimal diffusion coefficient estimation in single-particle tracking. *Physical Review E*. 85 p.pp 061916
- Michel, B., Boubakri, H., Baharoglu, Z., LeMasson, M. & Lestini, R. (2007). Recombination proteins and rescue of arrested replication forks. *DNA repair*. 6 (7). p.pp. 967–980.
- Miyabe, I., Morishita, T., Hishida, T., Yonei, S. & Shinagawa, H. (2006). Rhp51-dependent recombination intermediates that do not generate checkpoint signal are accumulated in *Schizosaccharomyces pombe* rad60 and smc5/6 mutants after release from replication arrest. *Molecular and Cellular Biology*. 26 (1). p.pp. 343–53.

- Miyabe, I., Morishita, T., Shinagawa, H. & Carr, A.M. (2009). Schizosaccharomyces pombe Cds1Chk2 regulates homologous recombination at stalled replication forks through the phosphorylation of recombination protein Rad60. *Journal of cell science*. 122 (20). p.pp. 3638–43.
- Miyabe, I., Kunkel, T. & Carr, A. (2011). The Major Roles of DNA Polymerases Epsilon and Delta at the Eukaryotic Replication Fork Are Evolutionarily Conserved. *PLoS Genetics*. 7 (12). e1002407
- Mizuno, K., Lambert, S., Baldacci, G., Murray, J.M. & Carr, A.M. (2009). Nearby inverted repeats fuse to generate acentric and dicentric palindromic chromosomes by a replication template exchange mechanism. *Genes & development*. 23 (24). p.pp. 2876–86.
- Mizuno, K., Miyabe, I., Schalbetter, S.A., Carr, A.M. & Murray, J.M. (2013). Recombination-restarted replication makes inverted chromosome fusions at inverted repeats. *Nature*. 493 (7431). p.pp. 246–9.
- Moerner, WE & Kador, L (1989). Optical detection and spectroscopy of single molecules in a solid. *Physical Review Letters*. 62 (21) p.pp 2535-2538
- Moerner, W. (2007). New directions in single-molecule imaging and analysis. *Proceedings of the National Academy of Sciences*. 104 (31). p.pp. 12596–12602.
- Moldovan, G.-L., Pfander, B. & Jentsch, S. (2007). PCNA, the Maestro of the Replication Fork. *Cell*. 129 (4). p.pp 665-679
- Mortensen, K., Churchman, L., Spudich, J. & Flyvbjerg, H. (2010). Optimized localization analysis for single-molecule tracking and super-resolution microscopy. *Nature Methods*. 7 (5). p.pp. 377–81.
- Moyer, S., Lewis, P. & Botchan, M. (2006). Isolation of the Cdc45/Mcm2–7/GINS (CMG) complex, a candidate for the eukaryotic DNA replication fork helicase. *Proceedings of the National Academy of Sciences*. 103 (27). p.pp. 10236–10241.
- Muramatsu, S., Hirai, K., Tak, Y.-S., Kamimura, Y. & Araki, H. (2010). CDK-dependent complex formation between replication proteins Dpb11, Sld2, Pol  $\epsilon$ , and GINS in budding yeast. *Genes & Development*. 24 (6). p.pp. 602–612.
- Murray, J.M. & Carr, A.M. (2008). Smc5/6: a link between DNA repair and unidirectional replication? *Nature reviews: Molecular cell biology*. 9 (2). p.pp. 177–82.

Naim, V., Wilhelm, T., Debatisse, M. & Rosselli, F. (2013). ERCC1 and MUS81-EME1 promote sister chromatid separation by processing late replication intermediates at common fragile sites during mitosis. *Nature cell biology*. 15 (8). p.pp. 1008–15.

Nash, P, Tang, X, Orlicky, S, Chen, Q & Gertler, FB (2001). Multisite phosphorylation of a CDK inhibitor sets a threshold for the onset of DNA replication. *Nature*. 414 (6863) 514-521

Nasheuer, H.P., von Winkler, D., Schneider, C., Dornreiter, I., Gilbert, I. & Fanning, E. (1992). Purification and functional characterization of bovine RP-A in an in vitro SV40 DNA replication system. *Chromosoma*. 102. p.pp. S52–9.

Neelsen, K.J. & Lopes, M. (2015). Replication fork reversal in eukaryotes: from dead end to dynamic response. *Nature reviews: Molecular cell biology*. 16 (4). p.pp. 207–20.

Nestoras, K, Mohammed, AH & Schreurs, AS (2010). Regulation of ribonucleotide reductase by Spd1 involves multiple mechanisms. *Genes & Development*. 24. p.pp 1145-1159

Nick McElhinny, S.A., Kumar, D., Clark, A.B., Watt, D.L., Watts, B.E., Lundström, E.-B.B., Johansson, E., Chabes, A. & Kunkel, T.A. (2010). Genome instability due to ribonucleotide incorporation into DNA. *Nature chemical biology*. 6 (10). p.pp. 774–81.

Niimi, A., Brown, S., Sabbioneda, S., Kannouche, P., Scott, A., Yasui, A., Green, C. & Lehmann, A. (2008). Regulation of proliferating cell nuclear antigen ubiquitination in mammalian cells. *Proceedings of the National Academy of Sciences*. 105 (42). p.pp. 16125–16130.

Nishida, H., Mayanagi, K., Kiyonari, S., Sato, Y., Oyama, T., Ishino, Y. & Morikawa, K. (2009). Structural determinant for switching between the polymerase and exonuclease modes in the PCNA-replicative DNA polymerase complex. *Proceedings of the National Academy of Sciences*. 106 (49). p.pp. 20693–20698.

Nishitani, H., Lygerou, Z., Nishimoto, T. & Nurse, P. (2000). The Cdt1 protein is required to license DNA for replication in fission yeast. *Nature*. 404 (6778). p.pp. 625–628.

Noguchi E, Noguchi C, Du LL, Russell P (2003). Swi1 Prevents Replication Fork Collapse and Controls Checkpoint Kinase Cds1. *Molecular Cell Biology*. 23 (21). p.pp 7861-7874

Noguchi, E., Noguchi, C., McDonald, H., Yates, J. & Russell, P. (2004). Swi1 and Swi3 Are Components of a Replication Fork Protection Complex in Fission Yeast. *Molecular and Cellular Biology*. 24 (19). p.pp. 8342–8355.

- Ocampo-Hafalla & Uhlmann (2011). Cohesin loading and sliding. *Journal of Cell Science*. 124 (5) p.pp 685-691
- Ogiwara, H., Ui, A., Enomoto, T. & Seki, M. (2007). Role of Elg1 protein in double strand break repair. *Nucleic Acids Research*. 35 (2). p.pp. 353–62.
- Okazaki, R., Okazaki, T., Sakabe, K., Sugimoto, K. & Sugino, A. (1968). Mechanism of DNA chain growth. I. Possible discontinuity and unusual secondary structure of newly synthesized chains. *Proceedings of the National Academy of Sciences*. 59 (2). p.pp. 598–605.
- On, K.F., Beuron, F., Frith, D., Snijders, A.P., Morris, E.P. & Diffley, J.F. (2014). Prereplicative complexes assembled in vitro support origin-dependent and independent DNA replication. *The EMBO Journal*. 33 (6). p.pp. 605–20.
- Otsuka, C., Kunitomi, N., Iwai, S., Loakes, D. & Negishi, K. (2005). Roles of the polymerase and BRCT domains of Rev1 protein in translesion DNA synthesis in yeast in vivo. *Mutation Research/Fundamental and Molecular Mechanisms of Mutagenesis*. 578 (1-2). p.p. 7987.
- Paciotti, V., Clerici, M., Lucchini, G. & Longhese, M. (2000). The checkpoint protein Ddc2, functionally related to *S. pombe* Rad26, interacts with Mec1 and is regulated by Mec1-dependent phosphorylation in budding yeast. *Genes & Development*. 14 (16). p.pp. 2046–2059.
- Palecek, J., Vidot, S., Feng, M., Doherty, A. & Lehmann, A. (2006). The Smc5-Smc6 DNA Repair Complex Bridging of the Smc5-Smc6 Heads by the Kleisin, Nse4, and Non-Kleisin Subunits. *Journal of Biological Chemistry*. 281 (48). p.pp. 36952–36959.
- Palzkill, T. & Newlon, C. (1988). A yeast replication origin consists of multiple copies of a small conserved sequence. *Cell*. 53 (3). p.p. 441-450.
- Paeschke, K., Bochman, M.L., Garcia, P.D., Cejka, P., Friedman, K.L., Kowalczykowski, S.C. & Zakian, V.A. (2013). Pif1 family helicases suppress genome instability at G-quadruplex motifs. *Nature*. 497 (7450). p.pp. 458–62.
- Parker, J., Bucceri, A., Davies, A., Heidrich, K., Windecker, H. & Ulrich, H. (2008). SUMO modification of PCNA is controlled by DNA. *The EMBO Journal*. 27 (18). p.pp. 2422–2431.
- Patterson, GH & Lippincott-Schwartz, J (2002). A photoactivatable GFP for selective photolabeling of proteins and cells. *Science*. 297 p.pp 1873-1877

- Pavani, S., Thompson, M., Biteen, J., Lord, S., Liu, N., Twieg, R., Piestun, R. & Moerner, W. (2009). Three-dimensional, single-molecule fluorescence imaging beyond the diffraction limit by using a double-helix point spread function. *Proceedings of the National Academy of Sciences*. 106 (9). p.pp. 2995–2999.
- Pebernard, S., Wohlschlegel, J., McDonald, W.H., Yates, J.R. & Boddy, M.N. (2006). The Nse5-Nse6 dimer mediates DNA repair roles of the Smc5-Smc6 complex. *Molecular and Cellular Biology*. 26 (5). p.pp. 1617–30.
- Pebernard, S., Perry, J.J., Tainer, J.A. & Boddy, M.N. (2008a). Nse1 RING-like domain supports functions of the Smc5-Smc6 holocomplex in genome stability. *Molecular biology of the cell*. 19 (10). p.pp. 4099–109.
- Pebernard, S., Schaffer, L., Campbell, D., Head, S.R. & Boddy, M.N. (2008b). Localization of Smc5/6 to centromeres and telomeres requires heterochromatin and SUMO, respectively. *The EMBO Journal*. 27 (22). p.pp. 3011–23.
- Perkins, G. & Diffley, J.F. (1998). Nucleotide-dependent prereplicative complex assembly by Cdc6p, a homolog of eukaryotic and prokaryotic clamp-loaders. *Molecular Cell*. 2 (1). p.pp. 23–32.
- Peters, J.-M. (2006). The anaphase promoting complex/cyclosome: a machine designed to destroy. *Nature Reviews Molecular Cell Biology*. 7 (9). p.pp. 644–656.
- Petermann, E., Orta, M., Issaeva, N., Schultz, N. & Helleday, T. (2010). Hydroxyurea-Stalled Replication Forks Become Progressively Inactivated and Require Two Different RAD51-Mediated Pathways for Restart and Repair. *Molecular Cell*. 37 (4).
- Pike, J., Henry, R., Burgers, P., Campbell, J. & Bambara, R. (2010). An Alternative Pathway for Okazaki Fragment Processing resolution of fold-back flaps by Pif1 helicase. *Journal of Biological Chemistry*. 285 (53). p.pp. 41712–41723.
- Possoz, C., Filipe, S., Grainge, I. & Sherratt, D. (2006). Tracking of controlled Escherichia coli replication fork stalling and restart at repressor-bound DNA in vivo. *The EMBO Journal*. 25 (11). p.pp. 2596–2604.
- Puddu, F., Granata, M., Di Nola, L., Balestrini, A., Piergiovanni, G., Lazzaro, F., Giannattasio, M., Plevani, P. & Muzi-Falconi, M. (2008). Phosphorylation of the budding yeast 9-1-1 complex is required for Dpb11 function in the full activation of the UV-induced DNA damage checkpoint. *Molecular and cellular biology*. 28 (15). p.pp. 4782–93.

Pursell, Z.F., Isoz, I., Lundström, E.-B.B., Johansson, E. & Kunkel, T.A. (2007). Yeast DNA polymerase epsilon participates in leading-strand DNA replication. *Science*. 317 (5834). p.pp. 127–30.

Randell, J.C., Bowers, J.L., Rodríguez, H.K. & Bell, S.P. (2006). Sequential ATP hydrolysis by Cdc6 and ORC directs loading of the Mcm2-7 helicase. *Molecular Cell*. 21 (1). p.pp. 29–39.

Randell, J.C., Fan, A., Chan, C., Francis, L.I., Heller, R.C., Galani, K. & Bell, S.P. (2010). Mec1 is one of multiple kinases that prime the Mcm2-7 helicase for phosphorylation by Cdc7. *Molecular Cell*. 40 (3). p.pp. 353–63.

Räschle, M., Smeenk, G., Hansen, R.K., Temu, T., Oka, Y., Hein, M.Y., Nagaraj, N., Long, D.T., Walter, J.C., Hofmann, K., Storchova, Z., Cox, J., Bekker-Jensen, S., Mailand, N. & Mann, M. (2015). DNA repair. Proteomics reveals dynamic assembly of repair complexes during bypass of DNA cross-links. *Science*. 348 (6234). p.p. 1253671.

Rasnik, I., McKinney, S.A. & Ha, T. (2006). Nonblinking and long-lasting single-molecule fluorescence imaging. *Nature Methods*. 3 (11). p.pp. 891–3.

Rayleigh L (1896) On the theory of optical images with special reference to the microscope. *Philosophical Magazine*. 42, p 167-195

Remus, D., Beall, E. & Botchan, M. (2004). DNA topology, not DNA sequence, is a critical determinant for Drosophila ORC–DNA binding. *The EMBO Journal*. 23 (4). p.pp. 897–907.

Remus, D., Beuron, F., Tolun, G., Griffith, J.D., Morris, E.P. & Diffley, J.F. (2009). Concerted loading of Mcm2-7 double hexamers around DNA during DNA replication origin licensing. *Cell*. 139 (4). p.pp. 719–30.

Reyes-Lamothe, R., Sherratt, D.J. & Leake, M.C. (2010). Stoichiometry and architecture of active DNA replication machinery in Escherichia coli. *Science*. 328 (5977). p.pp. 498–501.

Rossi, M. & Bambara, R. (2006). Reconstituted Okazaki Fragment Processing Indicates Two Pathways of Primer Removal. *Journal of Biological Chemistry*. 281 (36). p.pp. 26051–26061.

Rossi, M., Pike, J., Wang, W., Burgers, P., Campbell, J. & Bambara, R. (2008). Pif1 Helicase Directs Eukaryotic Okazaki Fragments toward the Two-nuclease Cleavage Pathway for Primer Removal. *Journal of Biological Chemistry*. 283 (41). p.pp. 27483–27493.

- Rothbauer, U., Zolghadr, K., Tillib, S., Nowak, D., Schermelleh, L., Gahl, A., Backmann, N., Conrath, K., Muyldermans, S., Cardoso, M. & Leonhardt, H. (2006). Targeting and tracing antigens in live cells with fluorescent nanobodies. *Nature Methods*. 3 (11). p.pp. 887–889.
- Russell, P. & Nurse, P. (1986). *cdc25+* functions as an inducer in the mitotic control of fission yeast. *Cell*. 45 (1). p.pp. 145–53.
- Rust, M., Bates, M. & Zhuang, X. (2006). Sub-diffraction-limit imaging by stochastic optical reconstruction microscopy (STORM). *Nature Methods*. 3 (10). p.pp. 793–796.
- Sabatinos, S., Green, M. & Forsburg, S. (2012). Continued DNA synthesis in replication checkpoint mutants leads to fork collapse. *Molecular and cellular biology*. 32 (24). p.pp. 4986–97.
- Sage, D., Kirshner, H., Pengo, T., Stuurman, N., Min, J., Manley, S. & Unser, M. (2015). Quantitative evaluation of software packages for single-molecule localization microscopy. *Nature Methods*. 12 (8). p.pp 717-724
- Saini, N., Ramakrishnan, S., Elango, R., Ayyar, S., Zhang, Y., Deem, A., Ira, G., Haber, J., Lobachev, K. & Malkova, A. (2013). Migrating bubble during break-induced replication drives conservative DNA synthesis. *Nature*. 502 (7471). p.pp. 389–92.
- Salk, J., Fox, E. & Loeb, L. (2010). Mutational Heterogeneity in Human Cancers: Origin and Consequences. *Pathology: Mechanisms of Disease*. 5 (1). p.pp. 51–75.
- Sakabe & Okazaki (1966). A unique property of the replicating region of chromosomal DNA. *Biochimica et biophysica acta*. 129 (3). p.pp 651-654
- Samel, S.A., Fernández-Cid, A., Sun, J., Riera, A., Tognetti, S., Herrera, M.C., Li, H. & Speck, C. (2014). A unique DNA entry gate serves for regulated loading of the eukaryotic replicative helicase MCM2-7 onto DNA. *Genes & Development*. 28 (15). p.pp. 1653–66.
- Santocanale, C. & Diffley, J. (1998). A Mec1- and Rad53-dependent checkpoint controls late-firing origins of DNA replication. *Nature*. 395 (6702). p.pp. 615–618.
- Schalbetter, S., Mansoubi, S., Chambers, A., Downs, J. & Baxter, J. (2015). Fork rotation and DNA precatenation are restricted during DNA replication to prevent chromosomal instability. *Proceedings of the National Academy of Sciences*. 112 (33). p.pp. E4565–70.
- Schlacher, K., Christ, N., Siaud, N., Egashira, A & Wu, H (2011). Double-strand break repair-independent role for BRCA2 in blocking stalled replication fork degradation by MRE11. *Cell*. 145, p.pp 529–542

- Schlacher, K., Wu, H. & Jasin, M. (2012). A distinct replication fork protection pathway connects Fanconi anemia tumor suppressors to RAD51-BRCA1/2. *Cancer cell*. 22 (1). p.pp. 106–116.
- Schermelleh, L., Carlton, P., Haase, S., Shao, L., Winoto, L., Kner, P., Burke, B., Cardoso, M., Agard, D., Gustafsson, M., Leonhardt, H. & Sedat, J. (2008). Subdiffraction Multicolor Imaging of the Nuclear Periphery with 3D Structured Illumination Microscopy. *Science*. 320 (5881). p.pp. 1332–1336.
- Schwab, M., Lutum, A.S. & Seufert, W. (1997). Yeast Hct1 is a regulator of Clb2 cyclin proteolysis. *Cell*. 90 (4). p.pp. 683–93.
- Segurado, M. & Diffley, J. (2008). Separate roles for the DNA damage checkpoint protein kinases in stabilizing DNA replication forks. *Genes & Development*. 22 (13). p.pp. 1816–1827.
- Sengupta, S., van Deursen, F., de Piccoli, G. & Labib, K. (2013). Dpb2 integrates the leading-strand DNA polymerase into the eukaryotic replisome. *Current biology*. 23 (7). p.pp. 543–52.
- Sergeant, J., Taylor, E., Palecek, J., Fousteri, M., Andrews, E., Sweeney, S., Shinagawa, H., Watts, F. & Lehmann, A. (2005). Composition and Architecture of the *Schizosaccharomyces pombe* Rad18 (Smc5-6) Complex. *Molecular and Cellular Biology*. 25 (1). p.pp. 172–184.
- Sequeira-Mendes, J., Díaz-Uriarte, R., Apedaile, A., Huntley, D., Brockdorff, N. & Gómez, M. (2009). Transcription initiation activity sets replication origin efficiency in mammalian cells. *PLoS genetics*. 5 (4). p.p. e1000446.
- Shachar, S., Ziv, O., Avkin, S., Adar, S., Wittschieben, J., Reißner, T., Chaney, S., Friedberg, E., Wang, Z., Carell, T., Geacintov, N. & Livneh, Z. (2009). Two-polymerase mechanisms dictate error-free and error-prone translesion DNA synthesis in mammals. *The EMBO Journal*. 28 (4). p.pp. 383–393.
- Shao, L., Kner, P., Rego, E. & Gustafsson, M. (2011). Super-resolution 3D microscopy of live whole cells using structured illumination. *Nature Methods*. 8 (12). p.pp. 1044–1046.
- Shechter, D., Costanzo, V. & Gautier, J. (2004). ATR and ATM regulate the timing of DNA replication origin firing. *Nature Cell Biology*. 6 (7). p.pp. 648–655.
- Shimada, K., Pasero, P. & Gasser, S. (2002). ORC and the intra-S-phase checkpoint: a threshold regulates Rad53p activation in S phase. *Genes & Development*. 16 (24). p.pp. 3236–3252.

Shimomura, O., Johnson, F.H. & Saiga, Y. (1962). Extraction, purification and properties of aequorin, a bioluminescent protein from the luminous hydromedusan, *Aequorea*. *Journal of cellular and comparative physiology*. 59. p.pp. 223–39.

Shiomi, Y. & Nishitani, H. (2013). Alternative replication factor C protein, Elg1, maintains chromosome stability by regulating PCNA levels on chromatin. *Genes to cells : devoted to molecular & cellular mechanisms*. 18 (11). p.pp. 946–59.

Shtengel, G., Galbraith, J.A., Galbraith, C.G., Lippincott-Schwartz, J., Gillette, J.M., Manley, S., Sougrat, R., Waterman, C.M., Kanchanawong, P., Davidson, M.W., Fetter, R.D. & Hess, H.F. (2009). Interferometric fluorescent super-resolution microscopy resolves 3D cellular ultrastructure. *Proceedings of the National Academy of Sciences*. 106 (9). p.pp. 3125–30.

Simpson, L.J., Ross, A.-L.L., Szüts, D., Alviani, C.A., Oestergaard, V.H., Patel, K.J. & Sale, J.E. (2006). RAD18-independent ubiquitination of proliferating-cell nuclear antigen in the avian cell line DT40. *EMBO reports*. 7 (9). p.pp. 927–32.

Sogo, J.M.M., Lopes, M. & Foiani, M. (2002). Fork reversal and ssDNA accumulation at stalled replication forks owing to checkpoint defects. *Science*. 297 (5581). p.pp. 599–602.

Speck, C., Chen, Z., Li, H. & Stillman, B. (2005). ATPase-dependent cooperative binding of ORC and Cdc6 to origin DNA. *Nature Structural & Molecular Biology*. 12 (11). p.pp. 965–971.

Srinivasan, S.V., Dominguez-Sola, D., Wang, L.C., Hyrien, O. & Gautier, J. (2013). Cdc45 is a critical effector of myc-dependent DNA replication stress. *Cell reports*. 3 (5). p.pp. 1629–39.

Stelter, P. & Ulrich, H. (2003). Control of spontaneous and damage-induced mutagenesis by SUMO and ubiquitin conjugation. *Nature*. 425 (6954). p.pp. 188–191.

Stinchcomb, D., Struhl, K. & Davis, R. (1979). Isolation and characterisation of a yeast chromosomal replicator. *Nature*. 282 (5734). p.pp. 39–43.

Stracy, M., Uphoff, S., Leon, F. & Kapanidis, A. (2014). In vivo single-molecule imaging of bacterial DNA replication, transcription, and repair. *FEBS Letters*. 588 (19). p.p. 35853594.

Sudakin, V., Ganoth, D., Dahan, A., Heller, H., Hershko, J., Luca, F., Ruderman, J. & Hershko, A. (1995). The cyclosome, a large complex containing cyclin-selective ubiquitin ligase activity, targets cyclins for destruction at the end of mitosis. *Molecular Biology of the Cell*. 6 (2). p.p. 185197.

- Su'etsugu, M. & Errington, J. (2011). The replicase sliding clamp dynamically accumulates behind progressing replication forks in *Bacillus subtilis* cells. *Molecular Cell*. 41 (6). p.pp. 720–32.
- Szymborska, A., Marco, A., Daigle, N., Cordes, V., Briggs, J. & Ellenberg, J. (2013). Nuclear pore scaffold structure analyzed by super-resolution microscopy and particle averaging. *Science*. 341 (6146). p.pp. 655–8.
- Szyjka, S.J., Viggiani, C.J. & Aparicio, O.M. (2005). Mrc1 is required for normal progression of replication forks throughout chromatin in *S. cerevisiae*. *Molecular Cell*. 19 (5). p.pp. 691–697.
- Takeishi, Y., Ohashi, E., Ogawa, K., Masai, H., Obuse, C. & Tsurimoto, T. (2010). Casein kinase 2-dependent phosphorylation of human Rad9 mediates the interaction between human Rad9-Hus1-Rad1 complex and TopBP1. *Genes to cells : devoted to molecular & cellular mechanisms*. 15 (7). p.pp. 761–71.
- Tan, B., Chien, C., Hirose, S. & Lee, S. (2006). Functional cooperation between FACT and MCM helicase facilitates initiation of chromatin DNA replication. *The EMBO Journal*. 25 (17). p.pp. 3975–3985.
- Tanaka, S. & Diffley, J. (2002). Deregulated G1-cyclin expression induces genomic instability by preventing efficient pre-RC formation. *Genes & Development*. 16 (20). p.p. 26392649.
- Tanaka, S., Umemori, T., Hirai, K., Muramatsu, S., Kamimura, Y. & Araki, H. (2007). CDK-dependent phosphorylation of Sld2 and Sld3 initiates DNA replication in budding yeast. *Nature*. 445 (7125). p.pp. 328–32.
- Tanaka, T., Umemori, T., Endo, S., Muramatsu, S., Kanemaki, M., Kamimura, Y., Obuse, C. & Araki, H. (2011a). Sld7, an Sld3-associated protein required for efficient chromosomal DNA replication in budding yeast. *The EMBO Journal*. 30 (10). p.pp. 2019–2030.
- Tanaka, S., Nakato, R., Katou, Y., Shirahige, K. & Araki, H. (2011b). Origin Association of Sld3, Sld7, and Cdc45 Proteins Is a Key Step for Determination of Origin-Firing Timing. *Current Biology*. 21 (24). p.pp 2055-2063
- Tapia-Alveal, C. & O'Connell, M. (2011). Nse1-dependent recruitment of Smc5/6 to lesion-containing loci contributes to the repair defects of mutant complexes. *Molecular biology of the cell*. 22 (23). p.pp. 4669–82.

Tapia-Alveal, C., Lin, S.-J. & O'Connell, M. (2014). Functional interplay between cohesin and Smc5/6 complexes. *Chromosoma*. 123 (5). p.pp. 437–445.

Tercero, J. & Diffley, J. (2001). Regulation of DNA replication fork progression through damaged DNA by the Mec1/Rad53 checkpoint. *Nature*. 412 (6846). p.pp. 553–557.

Thangavel, S., Berti, M., Levikova, M., Pinto, C., Gomathinayagam, S., Vujanovic, M., Zellweger, R., Moore, H., Lee, E., Hendrickson, E., Cejka, P., Stewart, S., Lopes, M. & Vindigni, A. (2015). DNA2 drives processing and restart of reversed replication forks in human cells. *The Journal of Cell Biology*. 208 (5). p.pp 545-562

Thompson, R., Larson, D. & Webb, W. (2002). Precise Nanometer Localization Analysis for Individual Fluorescent Probes. *Biophysical Journal*. 82 (5). p.pp 2775-2783

Thompson, MA & Lew, MD (2012). Extending microscopic resolution with single-molecule imaging and active control. *Annual review of biophysics*. 41. p.pp 321-342

Tokunaga, M., Imamoto, N. & Sakata-Sogawa, K. (2008). Highly inclined thin illumination enables clear single-molecule imaging in cells. *Nature Methods*. 5 (2). p.pp. 159–161.

Toledo, L.I., Altmeyer, M., Rask, M.-B.B., Lukas, C., Larsen, D.H., Povlsen, L.K., Bekker-Jensen, S., Mailand, N., Bartek, J. & Lukas, J. (2013). ATR prohibits replication catastrophe by preventing global exhaustion of RPA. *Cell*. 155 (5). p.pp. 1088–103.

Tom, S., Henricksen, L., Park, M. & Bambara, R. (2001). DNA Ligase I and Proliferating Cell Nuclear Antigen Form a Functional Complex. *Journal of Biological Chemistry*. 276 (27). p.pp. 24817–24825.

Torres-Ramos, C.A., Prakash, S. & Prakash, L. (2002). Requirement of RAD5 and MMS2 for postreplication repair of UV-damaged DNA in *Saccharomyces cerevisiae*. *Molecular and cellular biology*. 22 (7). p.pp. 2419–26.

Torres-Rosell, J., Sunjevaric, I., Piccoli, G., Sacher, M., Eckert-Boulet, N., Reid, R., Jentsch, S., Rothstein, R., Aragón, L. & Lisby, M. (2007). The Smc5–Smc6 complex and SUMO modification of Rad52 regulates recombinational repair at the ribosomal gene locus. *Nature Cell Biology*. 9 (8). p.pp. 923–931.

Tourrière, H., Versini, G., Cerdón-Preciado, V., Alabert, C. & Pasero, P. (2005). Mrc1 and Tof1 Promote Replication Fork Progression and Recovery Independently of Rad53. *Molecular Cell*. 19 (5). p.pp 699-706

- Ulrich, H. & Jentsch, S. (2000). Two RING finger proteins mediate cooperation between ubiquitin-conjugating enzymes in DNA repair. *The EMBO Journal*. 19 (13). p.pp. 3388–3397.
- Ulrich, H. (2009). Regulating post-translational modifications of the eukaryotic replication clamp PCNA. *DNA repair*. 8 (4). p.pp. 461–9.
- Uphoff, S, Reyes-Lamothe, R, Garza de Leon, F, Sherratt, D, & Kapanidis, A (2013). Single-molecule DNA repair in live bacteria. *Proceedings of the National Academy of Sciences*. 110 (20). p.pp 8063-8068
- Van de Linde, S., Löschberger, A., Klein, T., Heidebreder, M., Wolter, S., Heilemann, M. & Sauer, M. (2011). Direct stochastic optical reconstruction microscopy with standard fluorescent probes. *Nature Protocols*. 6 (7). p.pp. 991–1009.
- Van Deursen, F., Sengupta, S., De Piccoli, G., Sanchez-Diaz, A. & Labib, K. (2012). Mcm10 associates with the loaded DNA helicase at replication origins and defines a novel step in its activation. *The EMBO Journal*. 31 (9). p.pp. 2195–206.
- Vashee, S., Cvetic, C., Lu, W., Simancek, P., Kelly, T. & Walter, J. (2003). Sequence-independent DNA binding and replication initiation by the human origin recognition complex. *Genes & Development*. 17 (15). p.pp. 1894–1908.
- Venclovas, C. & Thelen, M. (2000). Structure-based predictions of Rad1, Rad9, Hus1 and Rad17 participation in sliding clamp and clamp-loading complexes. *Nucleic Acids Research*. 28 (13). p.pp. 2481–2493.
- Verkade, H.M., Bugg, S.J., Lindsay, H.D., Carr, A.M. & O’Connell, M.J. (1999). Rad18 is required for DNA repair and checkpoint responses in fission yeast. *Molecular biology of the cell*. 10 (9). p.pp. 2905–18.
- Verkade, H., Teli, T., Laursen, L., Murray, J. & O’Connell, M. (2001). A homologue of the Rad18 postreplication repair gene is required for DNA damage responses throughout the fission yeast cell cycle. *Molecular Genetics and Genomics*. 265 (6). p.pp. 993–1003.
- Wardlaw, C., Carr, A. & Oliver, A. (2014). TopBP1: A BRCT-scaffold protein functioning in multiple cellular pathways. *DNA Repair*. 22. p.pp 165-174
- Warren, C.D., Eckley, D.M., Lee, M.S., Hanna, J.S., Hughes, A., Peyser, B., Jie, C., Irizarry, R. & Spencer, F.A. (2004). S-phase checkpoint genes safeguard high-fidelity sister chromatid cohesion. *Molecular biology of the cell*. 15 (4). p.pp. 1724–35.

- Watanabe, K., Tateishi, S., Kawasuji, M., Tsurimoto, T., Inoue, H. & Yamaizumi, M. (2004). Rad18 guides pol $\eta$  to replication stalling sites through physical interaction and PCNA monoubiquitination. *The EMBO Journal*. 23 (19). p.pp. 3886–3896.
- Watase, G., Takisawa, H. & Kanemaki, M.T. (2012). Mcm10 plays a role in functioning of the eukaryotic replicative DNA helicase, Cdc45-Mcm-GINS. *Current biology : CB*. 22 (4). p.pp. 343–9.
- Waters, L., Minesinger, B., Wiltrout, M., D'Souza, S., Woodruff, R. & Walker, G. (2009). Eukaryotic Translesion Polymerases and Their Roles and Regulation in DNA Damage Tolerance. *Microbiology and Molecular Biology Reviews*. 73 (1). p.pp. 134–154.
- Watson, A.T., Garcia, V., Bone, N., Carr, A.M. & Armstrong, J. (2008). Gene tagging and gene replacement using recombinase-mediated cassette exchange in *Schizosaccharomyces pombe*. *Gene*. 407 (1-2). p.pp. 63–74.
- Watson, A.T., Werler, P. & Carr, A.M. (2011). Regulation of gene expression at the fission yeast *Schizosaccharomyces pombe* *urg1* locus. *Gene*. 484 (1-2). p.pp. 75–85.
- Watson, A.T., Daigaku, Y., Mohebi, S., Etheridge, T.J., Chahwan, C., Murray, J.M. & Carr, A.M. (2013). Optimisation of the *Schizosaccharomyces pombe* *urg1* expression system. *PloS one*. 8 (12). p.p. e83800.
- Weinert, T., Kaochar, S., Jones, H., Paek, A. & Clark, A. (2009). The replication fork's five degrees of freedom, their failure and genome rearrangements. *Current Opinion in Cell Biology*. 21 (6). p.p. 778784.
- Wehrkamp-Richter, S., Hyppa, R., Prudden, J., Smith, G. & Boddy, M. (2012). Meiotic DNA joint molecule resolution depends on Nse5–Nse6 of the Smc5–Smc6 holocomplex. *Nucleic Acids Research*. 40 (19). p.pp. 9633–9646.
- Willis, N., Chandramouly, G., Huang, B., Kwok, A., Follonier, C., Deng, C. & Scully, R. (2014). BRCA1 controls homologous recombination at Tus/Ter-stalled mammalian replication forks. *Nature*. 510 (7506). p.pp. 556–559.
- Wilson, M., Kwon, Y., Xu, Y., Chung, W.-H., Chi, P., Niu, H., Mayle, R., Chen, X., Malkova, A., Sung, P. & Ira, G. (2013). Pif1 helicase and Pol delta promote recombination-coupled DNA synthesis via bubble migration. *Nature*. 502 (7471). p.pp. 393–6.
- Wit, N, Buoninfante, OA & van den Berk, P. (2014). Roles of PCNA ubiquitination and TLS polymerases  $\kappa$  and  $\eta$  in the bypass of methyl methanesulfonate-induced DNA damage. *Nucleic Acids Research*. 43 (1) p.pp 282-294

Wohlgenuth, J., Bulboaca, G., Moghadam, M., Caddle, M. & Calos, M. (1994). Physical mapping of origins of replication in the fission yeast *Schizosaccharomyces pombe*. *Molecular biology of the cell*. 5 (8). p.pp. 839–49.

Wohlschlegel, JA, Dwyer, BT, Dhar, SK & Cvetic, C (2000). Inhibition of eukaryotic DNA replication by geminin binding to Cdt1. *Science*. 290 p.pp 2309-2312

Wolter, S., Löschberger, A., Holm, T., Aufmkolk, S., Dabauvalle, M.-C., Linde, S. & Sauer, M. (2012). rapidSTORM: accurate, fast open-source software for localization microscopy. *Nature Methods*. 9 (11). p.pp. 1040–1041.

Xu, Y., Davenport, M. & Kelly, T. (2006). Two-stage mechanism for activation of the DNA replication checkpoint kinase Cds1 in fission yeast. *Genes & Development*. 20 (8). p.pp. 990–1003.

Xue, X., Choi, K., Bonner, J., Chiba, T., Kwon, Y., Xu, Y., Sanchez, H., Wyman, C., Niu, H., Zhao, X. & Sung, P. (2014). Restriction of Replication Fork Regression Activities by a Conserved SMC Complex. *Molecular Cell*. 56 (3). p.pp 436-445

Yanow, S., Lygerou, Z. & Nurse, P. (2001). Expression of Cdc18/Cdc6 and Cdt1 during G2 phase induces initiation of DNA replication. *The EMBO Journal*. 20 (17). p.pp. 4648–4656.

Yang, X., Shiotani, B., Classon, M. & Zou, L. (2008). Chk1 and Claspin potentiate PCNA ubiquitination. *Genes & Development*. 22 (9). p.pp. 1147–1152.

Yeeles, J., Poli, J., Mariani, K. & Pasero, P. (2013). Rescuing Stalled or Damaged Replication Forks. *Cold Spring Harbor Perspectives in Biology*. 5 (5). p.p. a012815a012815.

Yeeles, J., Deegan, T., Janska, A., Early, A. & Diffley, J. (2015). Regulated eukaryotic DNA replication origin firing with purified proteins. *Nature*. 519, p.pp 431-435

Yildiz, A, Forkey, JN, McKinney, SA, Ha, T & Goldman, YE (2003). Myosin V walks hand-over-hand: single fluorophore imaging with 1.5-nm localization. *Science*. 300. p.pp 2061-2065

Ying, S., Minocherhomji, S., Chan, K.L., Palmari-Pallag, T., Chu, W.K., Wass, T., Mankouri, H.W., Liu, Y. & Hickson, I.D. (2013). MUS81 promotes common fragile site expression. *Nature cell biology*. 15 (8). p.pp. 1001–7.

Yu, C., Gan, H., Han, J., Zhou, Z.-X., Jia, S., Chabes, A., Farrugia, G., Ordog, T. & Zhang, Z. (2014). Strand-Specific Analysis Shows Protein Binding at Replication Forks and PCNA Unloading from Lagging Strands when Forks Stall. *Molecular Cell*. 56 (4). p.pp 551-563

Yue, M., Singh, A., Wang, Z. & Xu, Y. (2011). The Phosphorylation Network for Efficient Activation of the DNA Replication Checkpoint in Fission Yeast. *Journal of Biological Chemistry*. 286 (26). p.pp. 22864–22874.

Yoo, H., Shevchenko, A., Shevchenko, A. & Dunphy, W. (2004). Mcm2 Is a Direct Substrate of ATM and ATR during DNA Damage and DNA Replication Checkpoint Responses. *Journal of Biological Chemistry*. 279 (51). p.pp. 53353–53364.

York, A.G., Ghitani, A., Vaziri, A., Davidson, M.W. & Shroff, H. (2011). Confined activation and subdiffractional localization enables whole-cell PALM with genetically expressed probes. *Nature Methods*. 8 (4). p.pp. 327–333.

You, Z. & Masai, H. (2008). Cdt1 Forms a Complex with the Minichromosome Maintenance Protein (MCM) and Activates Its Helicase Activity. *Journal of Biological Chemistry*. 283 (36). p.pp. 24469–24477.

Zegerman, P. & Diffley, J.F. (2007). Phosphorylation of Sld2 and Sld3 by cyclin-dependent kinases promotes DNA replication in budding yeast. *Nature*. 445 (7125). p.pp. 281–5.

Zellweger, R., Dalcher, D., Mutreja, K., Berti, M., Schmid, J., Herrador, R., Vindigni, A. & Lopes, M. (2015). Rad51-mediated replication fork reversal is a global response to genotoxic treatments in human cells. *The Journal of Cell Biology*. 208 (5). p.pp. 563–579.

Zhang, H. & Lawrence, C. (2005). The error-free component of the RAD6/RAD18 DNA damage tolerance pathway of budding yeast employs sister-strand recombination. *Proceedings of the National Academy of Sciences*. 102 (44). p.pp. 15954–15959.

Zhang, M, Chang, H, Zhang, Y, Yu, J, Wu, L & Ji, W (2012). Rational design of true monomeric and bright photoactivatable fluorescent proteins. *Nature Methods*. 9. p.pp 727-729

Zhao, H., Tanaka, K., Nogochi, E., Nogochi, C. & Russell, P. (2003). Replication Checkpoint Protein Mrc1 Is Regulated by Rad3 and Tel1 in Fission Yeast. *Molecular and Cellular Biology*. 23 (22). p.pp. 8395–8403.

Zhu, W., Ukomadu, C., Jha, S., Senga, T., Dhar, S., Wohlschlegel, J., Nutt, L., Kornbluth, S. & Dutta, A. (2007). Mcm10 and And-1/CTF4 recruit DNA polymerase  $\alpha$  to chromatin for initiation of DNA replication. *Genes & Development*. 21 (18). p.pp. 2288–2299.

Zou, L & Stillman, B (1998). Formation of a preinitiation complex by S-phase cyclin CDK-dependent loading of Cdc45p onto chromatin. *Science*. 280 (5363) p.pp. 593-596

Zou, L & Elledge, SJ (2003). Sensing DNA damage through ATRIP recognition of RPA-ssDNA complexes. *Science*. 300 (5625) pp. 1542-1548